THESIS

Submitted for the degree of

Doctor of Philosophy

Awarded by : *Universidad del Norte (Barranquilla, Colombia)*

Presented at *Defense date (02/08/2018)* **by:**

DAVID SERJE

A Micro-milling cutting force and chip formation modeling approach for optimal process parameters selection

JURY

Ph.D. Jorge Bris	Professor	Universidad del Norte
Ph.D. Carlos Cortés	Professor	Universidad Nacional
Ph.D. Eduardo Diez	Professor	Universidad de La Frontera
Ph.D. Ciro Rodríguez	Professor	ITESM Campus Monterrey

Program :
Mechanical Engineering
Research Group :
GIMYP
Director :
Ph.D. Jovanny Pacheco

Acknowledgements

First and foremost, my praises and thanks to God for giving me the strength, knowledge and opportunity to undertake this challenge and persevere to successfully complete it. I would like to express my deepest gratitude to my family: My father Federman, my mother Elvira, my brother Ricardo and my sister María for their faith, motivation, understanding and patience. Their encouragement and support have been always the motivation for me to keep looking towards a higher goal. I want to thank Estefany Acuña for her love and support through all these years and more to come!

I wish to thank my advisor Jovanny Pacheco in Colombia and Eduardo Diez in Chile, for their guidance and scientific support through the course of this research. I also would like to thank my committee members, Jorge Bris, Carlos Cortés, Ciro Rodríguez for the sound advice and constructive suggestions.

Personal appreciation is given to my colleagues Hugo Alvarez, Wilmer Velilla, Javier Sanjuan, Victor Fontalvo, Danny Illera, Javier Vargas, Michael Miranda and Enrique Niebles for their invaluable discussions and sharing experiences, classrooms and seminars. Also thanks to all the team at UFRO, which I had the privilege of knowing: Arturo Padilla, Victor Tuninetti, Ricardo Alzugaray, Jorge González and Robert.

Special thanks to Colciencias-Colfuturo for the financial support on living expenses through these years with the research fund for doctoral program No. 6172. I would also like to extend my thanks to Universidad del Norte for financing the tuition fees.

Finally, my thanks go to all the people who have supported me to complete the research work directly or indirectly.

Contents

List of Figures

List of Tables

Acronyms

2-D	Two-Dimensional
3-D	Three-Dimensional
ACF	Atomization based Cutting Fluid
AISI	American Iron and Steel Institute
AE	Acoustic Emissions
ALE	Arbitrarian Lagrangian-Eulerian
AlTiN	Aluminum Titanium Nitride
ANOVA	ANalysis Of VAriance
ASTM	American Society of Testing Materials
BCC	Body-Centered Cubic
BI	Burr Index
BIOMEMS	Biomedical Micro Electro Mechanical Systems
BUE	Built-Up Edge
CBN	Cubic Boron Nitride
CCD	Central Composite Design
CEL	Coupled Eulerian-Lagrangian
CNC	Computer Numerical Control
DIN	Deutsches Institut für Normung
DOC	Depth of Cut
DOE	Design of Experiment
DSA	Dynamic Signal Acquisition
EA	Effective Area
EDM	Electrical Discharge Machining
EMA	Experimental Modal Analysis
FEA	Finite Element Analysis

FEM/A	Finite Element Method or Analysis
FFT	Fast Fourier Transform
FIB	Focused Ion Beam
GIMYP	Grupo de Investigación en Materiales Procesos y Diseño
GTN	Gurson–Tvergaard–Needelman
HCP	Hexagonal Closed-Packed
HRC	Rockwell C Hardness
HSS	High-Speed Steel
IOL	IntraOcular Lens
ISO	International Organization for Standardization
JC	Johnson-Cook
LAMM	Laser Assisted Micro-Milling
LIGA	Litography, electroplating and molding
LBM	Laser Beam Micro-machining
MDS	Molecular Dynamics Simulation
MEMS	Micro Electro Mechanical Systems
MQL	Minimum Quantity Lubrication
MRR	Material Removal Rate
MS	Multi-Scale Simulation
MSE	Mean Squared Error
MUCT	Minimum Uncut Chip Thickness
OFHC	Oxygen-Free High Thermal Conductivity
PCD	PolyCrystalline Diamond
PMMA	PolyMethyl MethacrylAte
RC	Receptance Coupling
RMS	Root Mean Square
RPM	Revolution Per Minute
RSM	Response Surface Methodology

SAE	Society of Automotive Engineers
SEM	Scanning Electron Microscope
SPH	Smoothed Particle Hydrodynamics
SPHB	Split Hopkinson Pressure Bar
VAMM	Vibration Assisted Micro-Milling
WC	Tungsten carbide
WHO	World Health Organization

Nomenclature

Material properties

ρ	Density
υ	Poisson's ratio
E	Young's modulus
A	Yield stress of the material (JC constitutive)
B	Strain hardening constant (JC constitutive)
n	Strain hardening coefficient (JC constitutive)
C	Strain rate strengthening (JC constitutive)
m	Thermal softening coefficient (JC constitutive)
T	Deformation temperature (JC constitutive)
T_r	Room temperature (JC constitutive)
T_m	Melting temperature (JC constitutive)
D_1	Initial fracture strain (JC fracture)
D_2	Exponential factor (JC fracture)
D_3	Triaxiality factor (JC fracture)
D_4	Strain rate constant (JC fracture)
D_5	Temperature constant (JC fracture)
G_f	Fracture energy
K_t	Fracture toughness
λ	Thermal conductivity
C_p	Specific heat

Cutting parameters

f, f_t	Feed per tooth

f_r	Feed rate
a_p	Axial depth of cut
a_e	Radial depth of cut
ω	Spindle angular speed
V_c	Cutting speed

Numerical model

h	Uncut chip thickness
h_m	Minimum uncut chip thickness
w_l, w_h	Workpiece length and height
θ	Position angle of each tooth (tool rotation angle)
μ	Coulomb friction coefficient
ε	Effective strain of workpiece material
$\dot{\varepsilon}$	Effective strain rate of workpiece material
σ	Flow stress of workpiece material
σ_n	Normal stress
σ^*	Stress triaxiality
τ	Frictional shear stress
ε_f	Fracture strain
α	Tool rake angle
γ	Tool clearance angle
r	Tool radius
ϕ	Tool diameter
r_e	Tool edge radius
k	Tool tooth number
x_{ci}, y_{ci}	Tool center coordinates
ρ_e	Tool parallel axis offset distance (runout)

β	Tool helix angle

Design of experiments

n, n_f	Number of factors, factorial points
N	Number of experiments
α	Distance from center points
DOF	Degree of freedom
SS	Sum of squares
MS	Mean square
S/N	Signal-to-noise
$x_i^*(k)$	Grey normalized response
$\xi_i(k)$	Grey relational coefficient
$\Delta_i(k)$	Grey deviation of reference
α_i	Grey relational grade of response "i"
β_k	Grey coefficient relative weight (for response "k")

Cutting forces

F_c, F_t	Force in cutting and tangential direction (orthogonal model)
F_x, F_y	Cutting force in X and Y direction
F_r	Resultant cutting force
F_{pred}, F_{real}	Predicted and real resultant cutting forces

Tool wear

V_{Bax}	Average flank wear (x stands for initial (i) or final (f))
V_{Bx}	Flank wear of tooth x.

r_{eax}	Average tool edge radius (x stands for initial (i) or final (f))
r_{ex}	Tool edge radius of tooth x.
BI_i	Burr index for slot i

Burr formation

A_{bc}	Burr and clogged chip area
$A_{bc.xx}$	Burr and clogged chip area (xx stands for average value (av) or standard deviation (sd))
A_s	Reference slot area
EA_{bc}	Burr and clogged chip equivalent area

Abstract

The last decade's evidence an increased demand for micro and miniature components with tightly specified dimensions and accuracies, that has driven to the development of micro and nanotechnology. Micro-milling, among the micro-machining processes, has the potential to be one of the key processes allows manufacturing micro-components in a wide range of materials with high aspect ratio and geometric complexity with improved flexibility and efficiency at reduced costs while compared with other methods. Compared to other micro-machining techniques, micro-milling allows the production of three-dimensional components in a broader range of materials such as metallic alloys, ceramics, and polymers. Although these techniques are similar to conventionally applied on macro-scale, simple parameters scaling or process models can't be used due to several factors that have a significant influence on the cutting mechanics, thereby resulting in variations in forces, burr formation, vibrations, machining accuracy, tool failure and others.

Complex challenges need to be addressed appropriately to successfully exploiting maximum potential of this technology on different applications. New physical effects (abrasion, adhesion forces), complex cause and effect coherence, unknown material properties and limited knowledge about the process parameters are some of the issues that need to be studied in the micro-cutting mechanics. The principal aim of this research is to develop a better understanding of micro-cutting mechanics to apply to process parameter optimization in micro-milling, considering most significant factors. The applied methodology started with a comprehensive state-of-the-art and a scientometric mapping of research in this area that was further employed for analysis, modeling, simulation, experimentation and optimization of the micro-milling process.

The development of a novel hybrid (numerical-experimental) cutting force approach is shown consisting of three stages: Definition of inputs, whereas material parameters (constitutive and fracture models), cutting parameters, uncut chip thickness models and machine-tool parameters are defined; FE simulations are developed through different cutting conditions; then the simulation results are used with a knowledge database to conduct experimental tests and obtain fundamental and industry-relevant responses. Several instantaneous chip models are studied to include the effect of run-out in micro-cutting. Material properties of the selected material (Commercially pure titanium) were obtained, also calibrating constitutive and fracture models required for numerical simulation. With numerical simulations results, mathematical relationships are established between forces and uncut chip thicknesses that allowed a prediction of resultant cutting forces.

Micro-milling experiments using AlTiN coated tools are conducted measuring cutting forces, tool wear, and burr formation. Frequency analysis by Fast Fourier Transform on the force signals was performed coupled with FE modal analysis of the tool and workpiece as an approach to process stability. The tool wear is investigated by measuring percentual changes in geometrical parameters of the end-mill without removing the tool from the spindle (online

measurement). Besides, simulations are performed to some extent by considering variations in tool edge radius and studying its influence on cutting forces. The burr formation is also studied measuring top burrs during machining of different slots with defined cutting conditions.

All the measured process responses are optimized to identify adequate cutting conditions. The recommended methodology is shown to provide a guide for further studies into different micro-machining processes, workpiece materials, and geometries to select optimum cutting regions.

Chapter 1

Introduction

Contents

1.1 Micro-milling background

The last decades evidence an increased demand for micro and miniature components with tightly specified dimensions and accuracies, have lead to the development of micro and nanotechnology [34, 164]. Micro-machining have proven to be one of the key technologies that can enable the realization of most common features required by such products through material removal with many advantages in terms of material choices, relative accuracy and complexity of produced geometry [132, 159]. The term micro-machining emerged, and now it's used to define the practice of material removal for production of parts having dimensions that lie between 1 and 500μm [135]. Many types of machining techniques can be performed to realize micro-machining, but among them, micro-milling allows to manufacture micro-components through the use of geometrically defined rotating cutting tools that lead to the removal of material from the workpiece in the form of chips [3, 164].

Micro-milling allows the production of three dimensional components in a range of materials such as metallic alloys, ceramics and polymeric materials. It's applications can be seen in several industries and are directly related to micro-components market. For example, Micro Electro Mechanical Systems (MEMS) market is expected to grow over $10 billion dollars with an expected increase close to 20% between 2013 and 2019 [41]. Applications as micro-pumps, micro-molds, micro-channels, micro-nozzles for high temperature jets and others are possible thanks to micro-manufacturing techniques [34]. These applications require tight tolerances and strict functional and structural specifications, but the trend points towards micro-components to improve performance, product diversity, new designs and disruptive technologies that will also to aid industrial growth. Industrial and defense, medical, automotive and electronics applications still offer pockets of growth and profitability.

In Barranquilla city, located in northern Colombia, some developments have been made based on micro-milling application for medical purposes, mainly for eye implants on biocompatible polymers where accuracy and burr reduction are critical factors [156]. Through an agreement of GIMYP research group from Universidad del Norte with Centro Oftalmológico Carriazo under financial support from Department of Science, Technology and Innovation (Colciencias), a significant advance on biomedical engineering and precision manufacturing has been achieved [29]. Only this type of development could benefit more than 246 million people that according to World Health Organization (WHO) suffer from low vision caused by reduced curvature and corneal transparency that in further stages could require a surgery [206].

Although micro-machining techniques are similar to conventionally applied on macro-scale, simple parameters scaling or process models can't be used due to several factors that may have a significant influence on cutting mechanics resulting in variations in burr formation, vibrations, machining accuracy, tool failure, surface integrity and others [119, 34]. Tool geometrical features size is comparable to features to cut; in addition, cutting depths are usually within a range that goes from a few thousandths of millimeter to 100μm and are very close to grain size of workpiece. As a result, while cutting different materials as steel, process response could exhibit some variations, for example, an increased "spring back" effect of the ferrite grains compared to pearlite grains is able to modify cutting forces, achievable accuracy and surface roughness [137]. Effects as tool run-out, deflection or tool wear have a significant impact on precision, chip/burr formation and surface quality.

Micro-milling as one of the micro-machining processes, represents an emerging manufacturing technology with a prominent future for micro-component production. This area involves some practical challenges that could limit this technology on its way towards exploiting maximum potential on medical, industrial and automotive applications. Some of these challenges are:

- *Tool run-out:* Occurs between the spindle (or tool holder) rotational axis and tool symmetry axis, generating drastic periodical changes in chip load and cutting forces. This contributes to non-uniform wear of cutting edges, lower surface quality, and an increase in tool breakage probability. It's critical to control or reduce this issue and often is a very complex task to assess due to tool dimensions [16, 218].

- *Tool wear and tool life:* In extreme cases, an early tool failure can be observed due to an inadequate process parameter selection (leading to cutting forces beyond the tool strength or increased cutting temperatures). A reduced stiffness due to geometrical factors, generates fast wear that is very complex to monitor and makes it difficult to predict tool breakage [53, 17, 151].

  Limited results have been reported about the influence of cutting conditions (machining parameters and tool paths) on performance of micro-endmills and some results make use of one factor at a time method with few investigation on the interaction among the cutting conditions.

- *Micro-burr formation:* Burr presence not only reduces precision and component quality, but it also affects assembly and functionality. Burr formation must be controlled and minimized during process through an optimal tool, refrigerant, parameters selection coupled with an adequate process sequence and machining strategies. Burr reduction practices must be done from design towards to manufacturing process [34, 111].

- *Process parameter optimization:* In conventional macro-milling, adequate process parameters and conditions are adopted mainly from tool suppliers recommendations and trial-and-error practice based on machinist's experiences. Their validity is not fully evaluated due to the fact that limited results are published in this aspect.

  In micro-milling existent knowledge and experiences are limited. As a result, cutting conditions applied are very conservative due to high costs and fragile tools. Critical factors may come from material (micro-structure, anisotropic properties, elastic recovery), tool (material, sharpness, coatings), machine tool (accuracy, stiffness, damping, error compensation) and cutting parameters (feeds, speeds, cutting depth) are fundamental on this scale [26]. It's necessary an optimization of process parameters and most appropriate machining strategy for good relation between performance and productivity [42, 46].

Is in this last group where a different cutting dynamics is recognized and size effect on underlaying mechanism has a significant impact on chip formation, surface quality, cutting forces and vibrations still not fully comprehended [119]. Models considering micro-cutting mechanics, dynamics, and thermal aspects are required.

1.2 Motivation

This thesis arises, using the joint-venture in the knowledge already developed in the GIMYP research group and the need to increase it to try to answer the growing demand for micro-components.

Based on aforementioned purposes, this research aims to a new approach towards cutting force models to improve the micro-cutting comprehension, increasing the scientific and experimental knowledge, therefore offering an important instrument for cutting parameters optimization to improve tool life or production under expected surface quality and efficiency on different materials.

For industrial applications, knowledge that allows to consider main factors including, machines, tool, material and cutting parameters into machining quality and efficiency could aid to compete successfully in the new market trends to meet the needs of different sectors like electronics, medical, bio-technology, energy and others.

1.3 Objectives

The principal aim of this thesis is to develop a better understanding of micro-cutting mechanics to apply into process parameter optimization in micro-milling, considering most significant factors.

The different objectives of the research are:

- Development of the state-of-the-art on cutting force models, burr formation, and micro-milling process parameter optimization.
- Establish a minimum set of parameters to consider and study their effect on micro-cutting through simulations and experimentation.
- Develop and evaluate a model to predict cutting forces considering critical factors like cutting conditions, workpiece material constitutive model, tool edge geometry and tool run-out.
- Develop a process parameter optimization scheme integrating force prediction with tool wear monitoring and burr formation.

1.4 Methodology

Based on previously stated objectives, following methodological phases will aid to accomplish the expected goals:

1. Literature review: In this phase, a deep bibliographic exploration and a review of the state-of-art it's made to consolidate a solid base for the research thereby considering most relevant advances in the area.
2. Parameter analysis and selection: Critical process parameters are selected for micro-milling process optimization based on literature review, simulations and experimentation.
3. Model formulation: Proposed models are developed for cutting forces prediction and its relation with other factors as tool wear is studied.
4. Experimental studies and results: Experimental work is done to evaluate model predictions and performance.
5. Parameter optimization: Knowledge obtained from previous stages is used to propose optimum process parameters through the application of statistical techniques for studied conditions. Results are then analyzed to generate recommendations, conclusions and future work research topics.

1.5 Thesis structure

The research content is divided into seven chapters as shown in Figure 1.1 and the outline is given as follows:

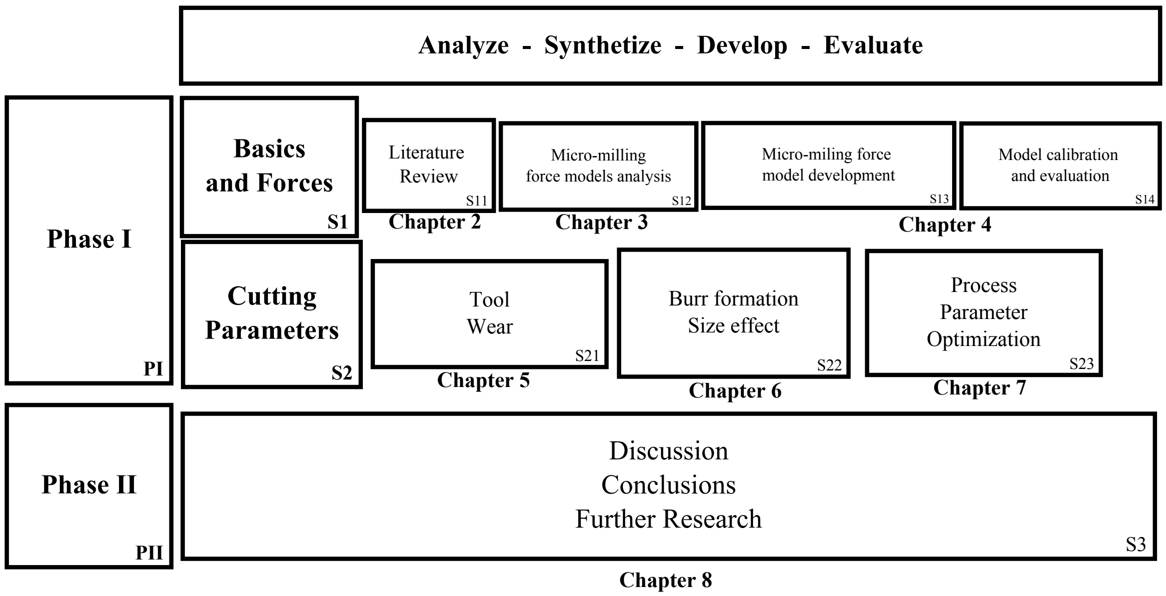

Figure 1.1: Thesis structure.

Chapter 1 introduces the general domain of the micro-milling process and the scientific and technological challenges (background). Motivation, objectives and thesis outline are also presented.

Chapter 2 illustrates a literature review and the state-of-art in the micro-milling community. A brief introduction of the micro-milling process is presented and cutting parameters and other factors that impact on process performance are discussed. An extensive study is condensed as a scientometric analysis of current topic trends, authors, and studies, also finding gaps in the current body of knowledge.

Chapter 3 investigates micro-cutting mechanics and cutting force models with particular application to micro-milling. Several approaches are considered to analyze multiple factors as forces, minimum chip thickness, tool life and surface finish.

Chapter 4 details the development of proposed model and numerically simulates forces using different methods. The simulated results are compared against experimental measurements to evaluate performance and prediction capability through the application of proper design of experiment (DOE) techniques.

Chapter 5 studies tool wear process based on experiments. Cutting forces are used to monitor its progress as well as tool wear measurements.

Chapter 6 chip and burr formation is analyzed.

Chapter 7 partial contributions of different sections of the micro-mill to the total tool deflection are analyzed. Validation of the proposed model through numerical analysis with FEA is presented.

Chapter 8 summarizes the main conclusions derived from this research, and highlights the principal contributions of the thesis. Recommendations for future work in the area are proposed.

Thesis schedule is shown in Figure 1.2:

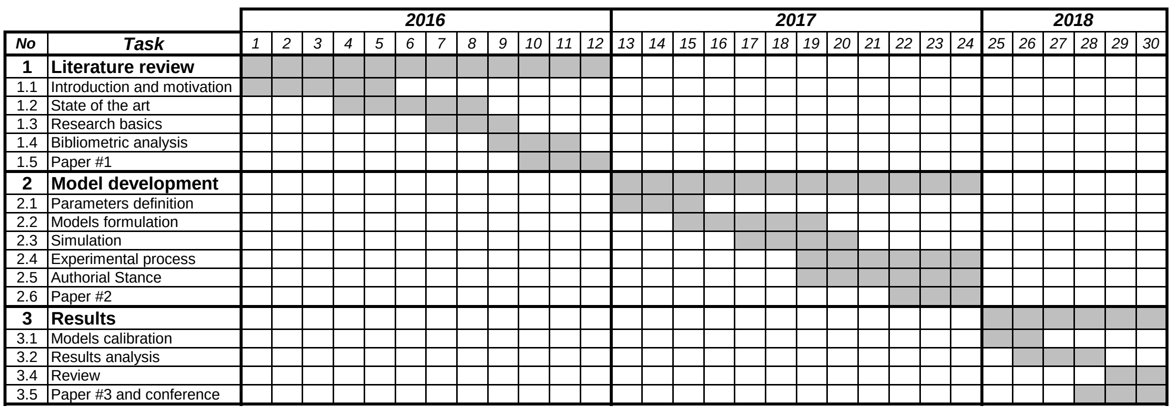

Figure 1.2: Thesis schedule.

1.6 Contributions

The important contributions of this work will be:

- Scientometric mapping of research on micro-milling.
- Advances in the knowledge of the micro-milling process and adequate parameter selection for reduced forces, tool wear, burrs.
- Establish a base study to promote research towards micro-milling process parameter optimization.
- A scheme to increase quality and productivity of micro-milled components.

Chapter 2

Literature review

Contents

2.1 Introduction

Miniaturization has become an important measure of technological advancement in the modern-day world. Minimizing the size of electronics and mechanical components is the key requirement to embed multiple operational features into a small device and functional platform [74]. Low energy and material consumption, lightweight, compact, high sensitivity (less power requirement for actuation of a micro-component/product) and comparatively low cost-to-performance ratio are among the various merits of miniaturized products that are increasingly demanded in the fields of medical, transportation, and communication industries [79, 132, 34, 164].

Miniaturized components/features, with dimensions within the 1-100μm range, demand great accuracy, higher surface quality, while at the same time decreasing component costs and reduced batch sizes [46]. Micro-machining is one of the key technologies that can enable the realization of all of the above requirements for micro-products and fields with such conditions that are rapidly expanding [132].

Figure 2.1 shows the capability of micro-machining relative to other processes where can be seen that Ra values in the range down to almost 5nm can be attained for features with accuracy down to 1μm: it is a critical technology in bridging the gap between macro and nano domain [34, 30].

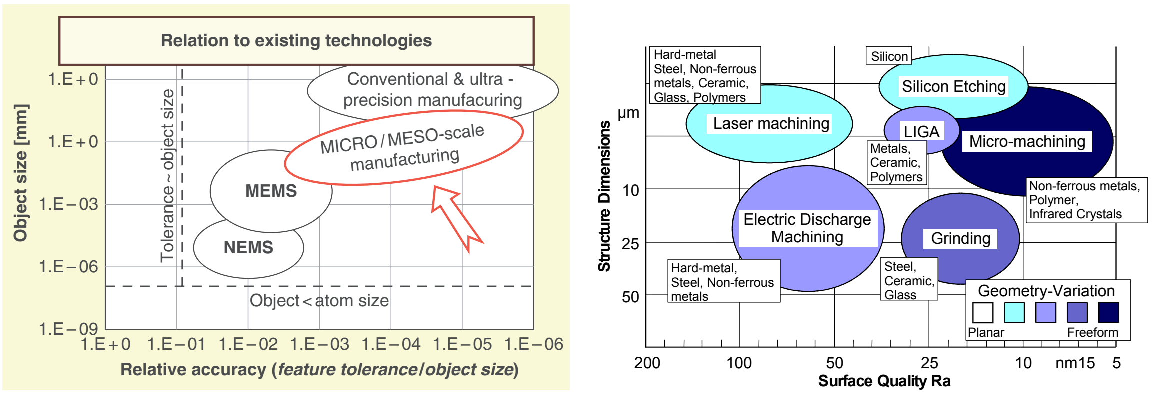

(a) Size/precision [34]. (b) Surface quality [23].

Figure 2.1: Micro-manufacturing domains.

Micro-manufacturing processes include material removal (subtraction), addition (layered manufacturing), joining and mass containing (as micro-forming and micro-casting) processes for fabrication of micro-components, or for the creation of micro-features. Based on this criteria, Figure 2.2 illustrates a general classification of micro-manufacturing processes [79].

Other classification methods can be based on different processes origins as mechanicals (based on material removal), thermal, replication, MEMS, LIGA, and others [3]. Figure 2.3 illustrates a recently developed category (in last two decades), known as non-MEMS or non-lithography-based micro-manufacturing that includes techniques such as micro-EDM, micro-mechanical cutting, micro-extrusion, etc [159].

Table 2.1 highlights the difference between MEMS and non-MEMS micro-manufacturing techniques (using mechanical micro-machining as an example) to compare the fundamental variations between the two category micro-manufacturing processes. It can be found that micro-mechanical machining has many advantages over MEMS-based process such as wider materials choices, higher accuracy, and capability of producing complex 3-D geometry micro parts [34, 30]. Several laboratories and universities have active research programs in micro-machining technology [132, 3, 46, 159]. A report published by the WTEC Panel on Micro-manufacturing, offers a detailed view of the drivers for micro-manufacturing and the opportunities and requirements for further development of the technology from a US viewpoint [52].

Among the subtractive micro-manufacturing processes, micro-cutting processes are characterized by the mechanical interaction of a sharp tool with the workpiece material, causing breakage inside the material along defined paths, eventually leading to the removal of the useless part of the workpiece in the form of chips [3]. According to desired geometrical fea-

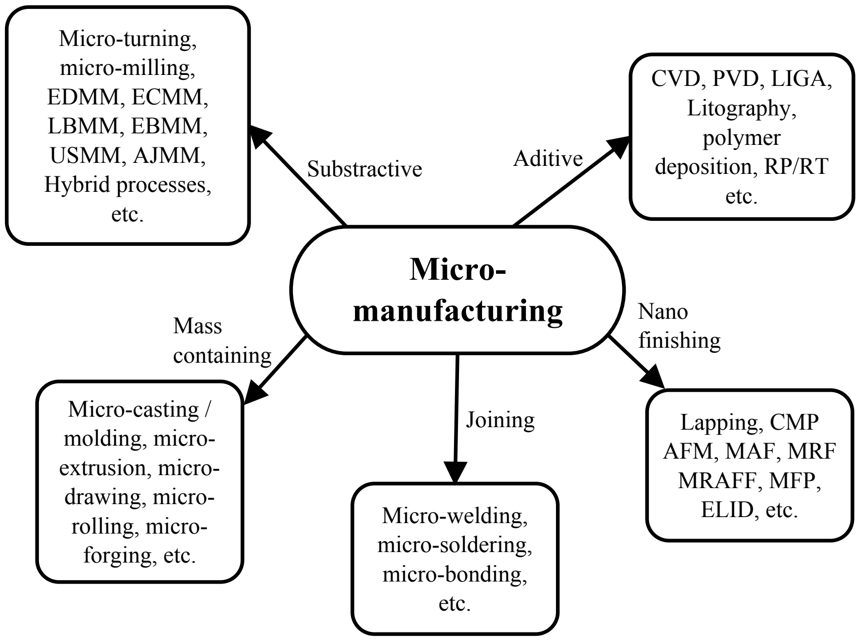

EDMM: electric discharge micromachining; ECMM: electrochemical micromachining; LBMM: laser beam micromachining; EBMM: electron beam micromachining; USMM: ultrasonic micromachining; AJMM: abrasive jet micromachining; CVD: chemical vapor deposition; PVD: physical vapor deposition; LIGA: lithography, electro-deposition and molding; CMP: chemo-mechanical polishing; AFM: abrasive flow machining; MAF: magnetic abrasive finishing; MRF: magneto rheological finishing; MRAFF: magneto rheological abrasive flow finishing; MFP: magnetic float polishing; ELID: electrolytic in-process dressing; RP: Rapid Prototyping; RT: Rapid Tooling.

Figure 2.2: Classification of micro-manufacturing processes [79].

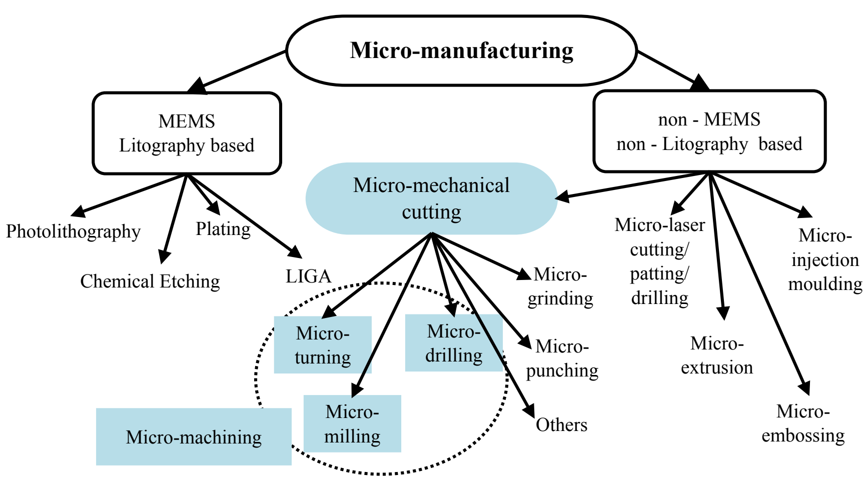

Figure 2.3: Classification of micro manufacturing techniques [159].

Feature	MEMS based	Micro-machining
Workpiece material	Silicon and some metals	Metals, alloys, polymers, composites, ceramics
Component geometry	Planar or 2.5-D	Complex 3-D
Assembly methods	None or bonding	Fastening, welding, bonding
Relative accuracy	10^{-1} to 10^{-3}	10^{-3} to 10^{-5}
Process control	Feed-forward	Feed-back
Production rate	High	Low
Investment	High	Intermediate or low

Table 2.1: Comparisons between MEMS-based process and micro-machining [34].

tures, drilling, turning, grinding or milling could be applied. For example, micro-milling can allow the production of three-dimensional components in a range of materials such as metallic alloys, ceramics and polymeric materials with high aspect ratio and geometric complexity [26, 66]. Table 2.2 illustrates a summary of geometric features, surface roughness and some applications of micro-cutting processes.

	Micro-turning	Micro-milling	Micro-drilling	Micro-grinding
Workpiece shape	Rotational convex shape with large aspect ratio, such as micro-shafts, micro-pins, etc.	3-D shape both convex and concave with high aspect ratios and high geometric complexity	Round holes through or blind	Hard and brittle materials: 3-D convex and concave shape using micro-grinding tips
Typical size	From $\phi5\mu m$ up to $\phi100\mu m$	$\phi50\mu m$ slots are practical applicable	$\phi50\mu m$ holes are practical applicable	Micro-structures down to $20\mu m$
Achievable surface roughness	$0.1\mu m$ Ra	Optical surface ($< 10nm$ Ra)	$0.1\mu m$ Ra	Optical surface ($< 10nm$ Ra)
Applications	Micro-shafts, micro-pins, micro-screws	Micro-gears, micro-molds, 3-D shaped dies	Micro-holes	Surface finish in hard materials

Table 2.2: Geometric characteristics of typical micro-cutting operations and applications (adapted from [34, 164]).

2.1.1 Applications

Currently, mechanical micro-machining is capable of fabricating miniature parts as small as tens of micrometers to a few millimeters with very complex features and close tolerances, using energy-efficient small machine tools [98]. It's flexibility, allow this group of processes to be employed in a large variety of applications. For instance, MEMS, as shown in Figure 2.4, is and will remain one of the main driving forces for micro-cutting [164]. It expected to grow over $10 billion dollars with an expected increase close to 20% between 2013 and 2019 [41]. More products are included everyday in this category and often link micro-cutting with other processing types, measurement devices, etc.

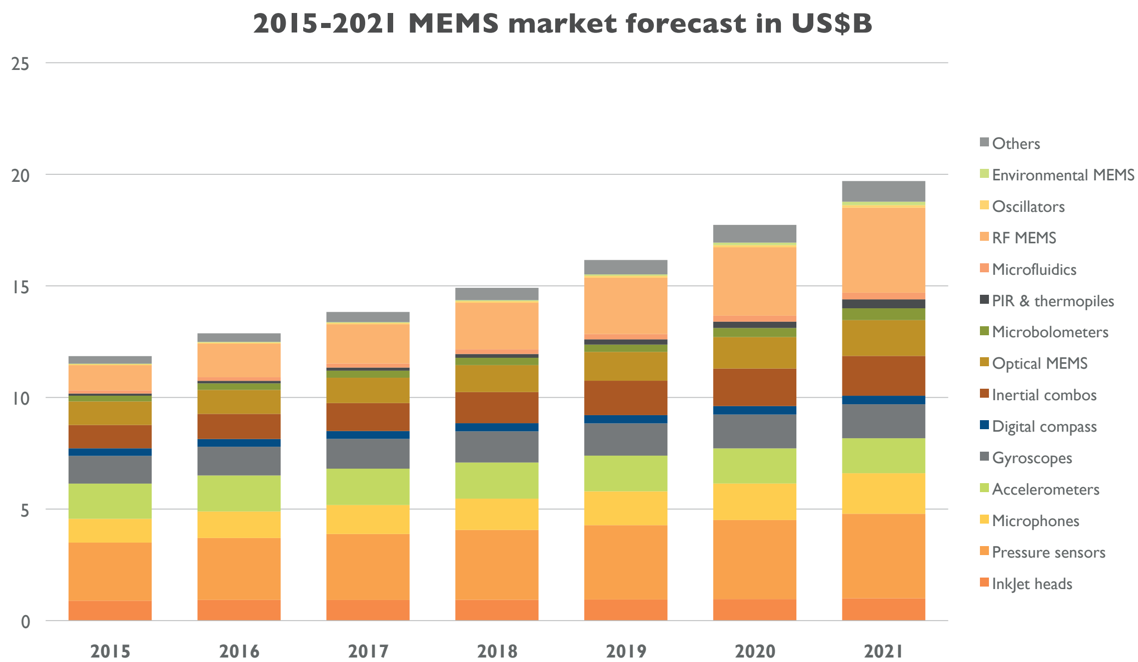

Figure 2.4: MEMS market forecast 2015-2021 [41].

The European FP6 Network of Excellence in Multi-Material Micro Manufacture (4M) has organized the major applications into three areas [43]:

1. *Micro-fluidics:* Biological, medical, pharmaceutical and chemical engineering applications.
2. *Micro-optics:* Telecommunication, bio-technological, instrumentation and medical applications.
3. *Micro-sensors and actuators:* Applications in medicine, biomedical field, health and safety, environment and process control.

Top sectors overall in order of their perceived importance are medical/surgical, automotive and transport, biotechnology, and consumer products. Second level areas are information and communication technology, energy/chemical, academic/scientific, and pharmaceutical [43]. Some of the current applications for micro-milling process in different sectors are [66, 164, 34]:

- *Automotive:* Electrodes for cutting inserts, fuel injection nozzles, diesel injection nozzles, sensors, parts with tight tolerances for micro-drilling.

- *Aerospace:* Instrumentation and electronic connectors and hydraulics, miniature devices for rockets, moulds for miniature planetary gear wheels attached to a turbine.

- *Biomedical:* Cochlear implants, micro-tools for surgery, moulds in micro-dosage application, lab-on-a-chip, in orthodontics (such as dental brackets and implants), replication moulds for cells, moulds in biotechnology applications (microchip electrophoresis devices, polymeric BIOMEMS (biomedical micro-electromechanical systems) devices, accelerating polymerase chain reaction for modular lab-on-a-chip systems), cataract lenses, retinal micro-tacks, etc.

- *Jewerly:* Precision watch cases, tools for watch making, detailing and/or engraving of watch parts, and so on.

- *Others:* Direct machining of optics either ceramic lenses or metallic mirrors, scientific instrumentation, components for measuring devices, electrodes for toy industry, electrodes for manufacturing shaving head of electric razors, crack detection (creating a micro-crack on a helix for turbines/drive shafts), gas leak detection (micro-feature with a special shape—different shapes for different gases).

Often in micro-milling, additional requirements on functional properties (physical, chemical, and biological, etc.) are attached to the products [3]. The micro-milling process attracts most intense interest as its inherent flexibility in manufacturing 3-D complex-shape/forms on a variety of materials. Specific micro-component samples are shown in Figure 2.5 and some micro-products illustrated in Figure 2.6.

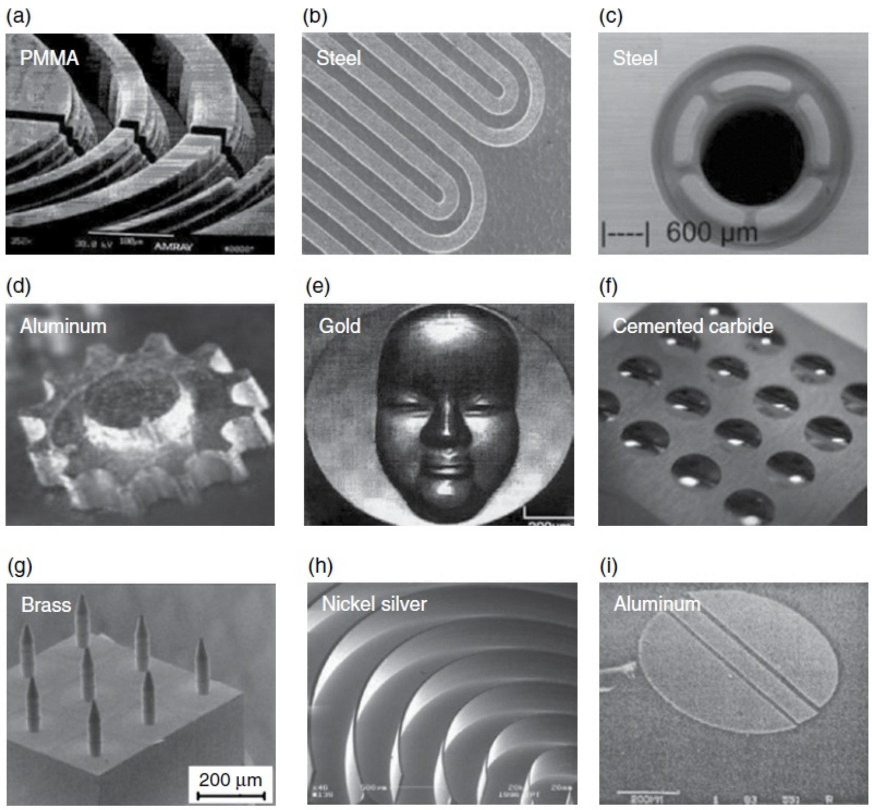

Figure 2.5: Examples of high accuracy micro components and micro structures by micro-cutting [34].
(a) Micro-trenches; (b) Micro-reactor; (c) Micro mould; (d) Micro-gear; (e) 3-D micro-machined part; (f) Micro-projection array; (g) Micro-needles array; (h) Micro-wall; (i) Target foil for nuclear fusion.

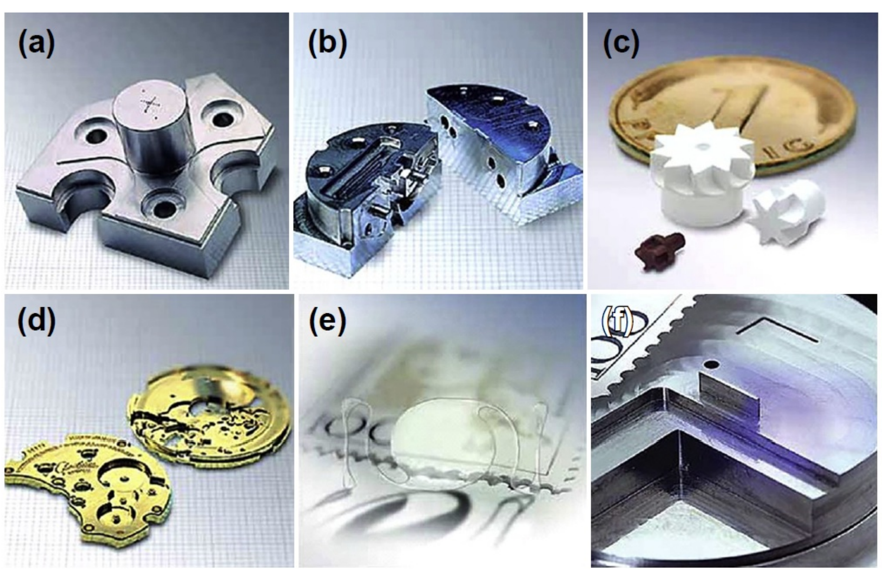

Figure 2.6: Micro-product samples [164].
(a) Joint for optical fiber; (b) Mixing disc (rocket motor); (c) Turbine wheels; (d) Watch base-plates; (e) Cataract lens; (f) Injection molding tool

2.1.2 Manufacturing systems/machine tools

The size and quality of manufactured micro-products depend on the quality and capabilities of the machine tools used to produce them, including factors as their overall accuracy, and their dynamic performance [30]. To achieve requirements like high dimensional accuracy, repeatability, and excellent surface finish often requires machines with high stiffness, good thermal stability, high damping among others [34]. Additionally, a high cutting speed is necessary to achieve a good tooling performance and high material removal rate (or productivity) [30]. This indicates the need for spindles with high rotational speeds, low thermal expansion, and low run-out.

There are some industrial ultra-precision turning and milling machines commercially available for precision components manufacturing (Figure 2.7). These machines can provide rotational speeds up to 160,000 RPM with a positioning resolution close to 10 nm. Examples depicted in Figure 2.7g and h are designed as diamond turning machine tools with a milling or grinding spindle to improve their capabilities towards optical components manufacturing. They require higher floor space (more than 5 m^2) and higher investment costs, but for different purposes, several machine tools have emerged from various manufacturers like Kern, Makino, Fanuc, etc. Main specifications of some mentioned ultra-precision machine tools are summarized in Table 2.3, which provides a comprehensive comparison of characteristics and the state of the art of micro-milling machines. As an alternative, existing machine tools can be retrofitted with high-speed spindles that fit in the conventional tool holder interfaces with rotational speeds near 80,000 RPM and run-out less than 1 μm; in such cases, the maximum positioning accuracy is limited by machine tool capabilities.

Machine tool price is dependent on specifications and additional requirements such as the number of controllable axes, metrology systems, workpiece probing and others that may ensure greater process flexibility and productivity. The accuracy and speed are the characteristics that usually impact cost the most. For example, a basic milling machine (with an accuracy of <25 μm) can be obtained for USD$15,000, whereas, a milling machine with automated tool alignment (with an accuracy of <3 μm) may cost over USD$200,000 [70].

Several types of research have been conducted to develop in-house miniature precision machines or micro-factories for custom applications or to manufacture micro-components [64]. Smaller machines with a reduction in energy, space, materials and costs have been developed allowing a higher portability of such systems [46, 164]. Figure 2.8 illustrates some examples of miniature micro-machine tools. The reduced cost potential of micro-factories holds a promising future for research; further studies are needed to improve the stiffness and their performance to make their way into industrial applications [30, 34].

2.1.3 Micro-tools

An important factor in micro machining processes is the cutting tool. It determines the feature sizes and surface quality of the miniature and micro-components machined [164].

Figure 2.7: Industrial precision machine tools with micro cutting capability [34].
(a) Kern Evo; (b) Sodick AZ150; (c) Fraunhofer IPT Minimill; (d) Makino Hyper2J; (e) Kugler MicroMaster MM2; (f) Fanuc Robonano $\alpha - 0iB$; (g) Precitech freeform 700 Ultra; (h) Nanotech 350FG.

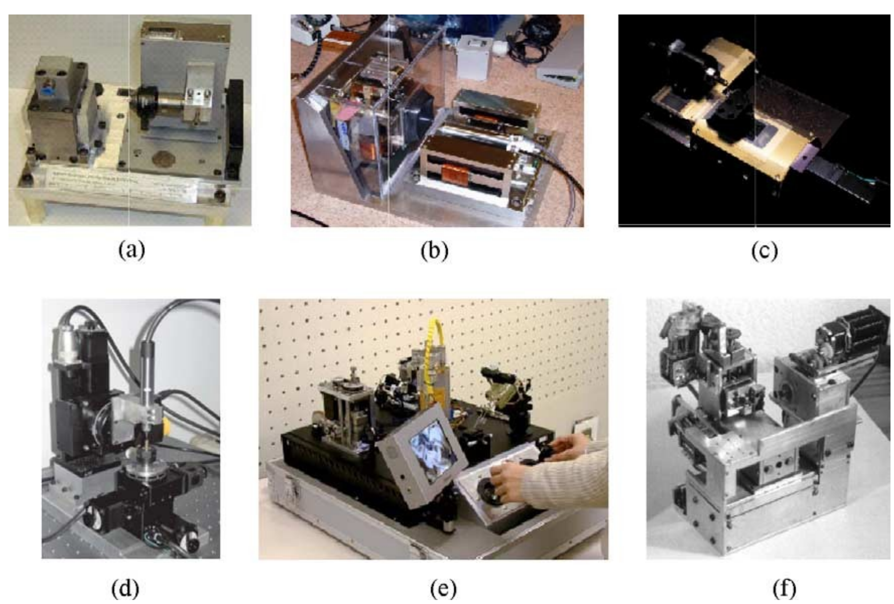

Figure 2.8: Micro-machines [30].
(a) Micro-factory; (b) Miniature machine; (c) Miniature machine; (d) Nanowave; (e) Micro-factory; (f) Micro-machine tool.

Equipment Feature	**Kern** Evo [95]	**Sodick** AZ250L [182]	**Makino** Hyper 2J [125]	**Kugler** Micromaster 5X [99]	**Fanuc** Robonano $\alpha - 0iB$ [59]	**Nanotech** 350UPM [146]
Machine size (m)	2.8/2.5/2.2	1.4/3.0/2.1	N/A	N/A	1.3/1.5/1.5	1.9/1.9/2.1
Weight (kg)	3,000	5,500		N/A	1,700	N/A
Travel X/Y/Z (mm)	300/280/250	250/150/100	200/150/150	300/300/200	280/150/40	350/350/150
Travel A/B/C	-/-/-	-/-/-	-/-/-	130°/ −/360°	−/360°/360°	-/-/-
Base structure	Polymer concrete	Cast iron	Granite base	Solid granite	Cast iron base with concrete	Epoxy-granite composite
Max. Speed (RPM)	160,000	120,000	40,000	200,000	50,000	60,000
Feed rate (mm/min)	16,000	5,000		6,000	500 (XZ) 50 (Y)	N/A
Linear acceleration (m/s^2)	8	5		10	N/A	N/A
Accuracy (μm)	<0.1	N/A	±0.3	± 0.5	<0.2	<0.05

Table 2.3: Specifications of micro-milling machines.

Smaller tools have reduced thermal expansion relative to their size, increased static stiffness from their compact structure, increased dynamic stability from their higher natural frequency, and the potential for decreased cost due to smaller quantities of material utilized [30].

Tool materials The performance of the micro-machining operation is significantly affected by the properties of the tool material. A lot of tool materials including metals, alloys, ceramics, cermets, composites, diamond, etc., have been used in micro-machining operations and have been reported in the literature [199]. An ideal tool material would combine properties like high hardness, good toughness, and chemical stability. However, these requirements indicate opposing properties so that a universal cutting material is not feasible technologically [204]. Many types of materials including high-speed steels, carbides, ceramics, and diamond could be used to fabricate micro-tools [77]. Figure 2.9 compares the capability of the major families of cutting tools and their behavior as a function of the temperature.

High-speed steel (HSS) tools are very common and can be categorized in three principal

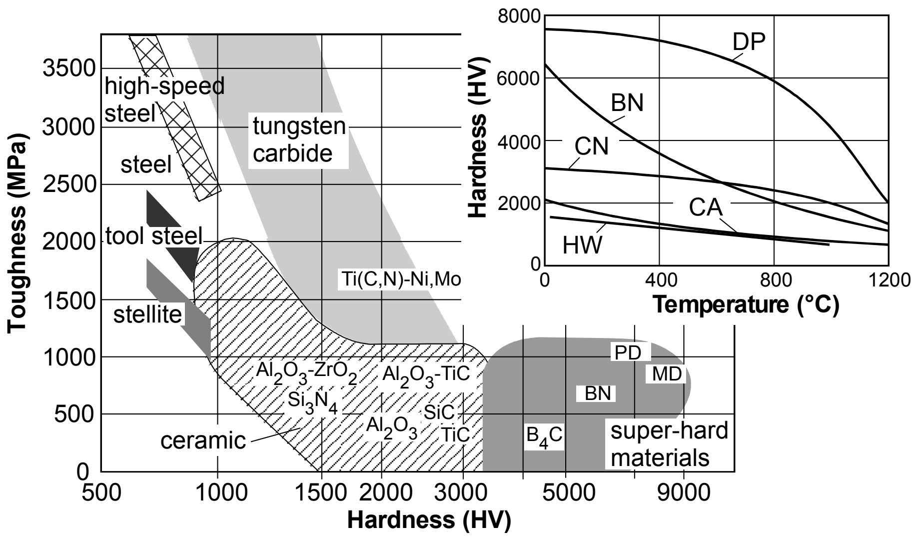

Figure 2.9: Toughness and hardness of cutting materials [23].

classifications: molybdenum based grades (M series), tungsten based grades (T series), and molybdenum-cobalt based grades. Among these grades, M and T series are the most commonly used HSS tools in industry [75]. These materials allowed higher cutting speeds and better tool life than steel, and the application of coatings can further increase their performance. Stellite is a non-magnetic, wear and corrosion resistant alloy of cobalt and chromium introduced in early 20th century. These materials led to the development of more advanced materials like cemented carbide and ceramic inserts.

In the 1930s, carbide tools were developed comprising a high modulus of elasticity, high thermal conductivity, and ultimately high hardness over a wide range of temperatures. Carbide tools, either uncoated or coated, are capable of reaching a cutting speed of three to five times higher than their HSS counterparts. Tungsten carbide (WC), titanium carbide (TiC), tantalum carbide (TaC_x) niobium carbide (NbC and Nb_2C) are the most recognized hard carbides that can be used for making carbide tools in industry [75]. The characteristics and performance of carbide tools are greatly affected by the type of carbide and its grain size. Unlike standard materials, all the fine powder particles have more or less a round shape which has a favorable influence not only on the uniformity of the sintered micro-structure but also on compactability [23].

The ceramic composite materials can be differentiated according to the matrix materials: Aluminum oxide or alumina (Al_2O_3), silicon nitride (Si_3N_4) and sialon (combination of Si, Al, O and N). In general, they offer good high-temperature strength, creep resistance and oxidation resistance. Furthermore, their low thermal expansion coefficient gives them a good thermal shock resistance [23]. Despite these benefits, ceramic tools suffer from lack of toughness; as a result, any shocks or impact during machining must be avoided to prevent chipping or breakage [75].

Cubic boron nitride (CBN) is the second hardest material next to diamond and offers excellent features as high hardness and less chemical wear resistance up to temperatures of $1400°C$. Diamond is the hardest material that combines extreme hardness, highest thermal conductivity at room temperature and low coefficient of friction. It can be manufactured by synthesis under extreme high pressure and temperature and for cutting applications polycrystalline diamond (PCD) tools are preferred [23].

The different tool-workpiece materials used in micro-milling operations along with their share are shown in Figure 2.10. Two significant tool materials used are hardened tool steels and cemented carbides. The ability to withstand high temperatures without losing hardness makes tool steel as one of the most indispensable materials used in micro-machining. Also, from Figure 2.10 it can be noted that most of the work materials studied in literature are considered as easy to cut, such as low hardness carbon steels as well as aluminum and copper alloys [26].

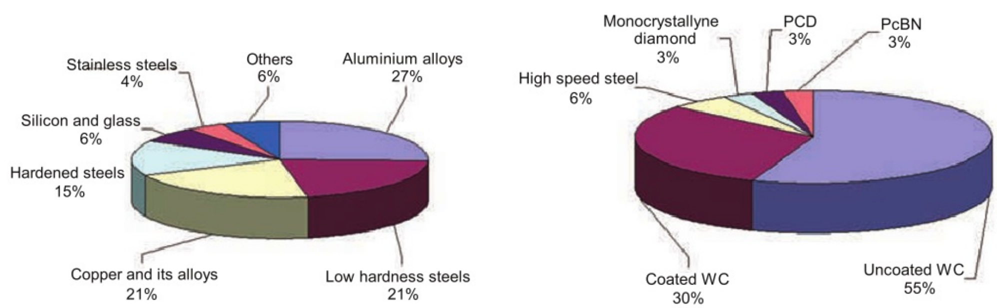

(a) Workpiece. (b) Tool.

Figure 2.10: Main materials used in micro-milling [26].

There are numerous cutting tool manufacturers like as Kyocera, Mitsubishi, Sandvik, Fraisa, Union Carbide, etc. that offer carbide micro-end-mills typically down to 100 μm diameter as standard products, with even smaller cutters for different applications. Smaller size cutters can also be manufactured, as shown in Figure 2.11. The mass fabrication of such micro-tools involves processes like focused ion beam (FIB), electrical discharge machining (EDM), wire electro-discharge grinding (WEDG) and grinding to detail different cross sectional shapes with high surface quality [46]. A comprehensive review of micro-tool manufacturing methods and properties of coated tools can be found in [23, 204].

Tool geometries For most applications, the micro-milling operation uses either flat end mills or ball end mills, both with two flutes [26]. Figure 2.12 a micro-end-mill with a diameter of 200 μm with flat (or square) tip. These tools are always of solid construction with shank sufficiently larger than the end portion on which necessary cutting elements are provided. Cutting edge radius is very important for manufacturers as it becomes comparable to tool size. For example, for end mills with sizes varying from 100 to 500 μm, the edge radius typically varies from 1 to 10 μm [180].

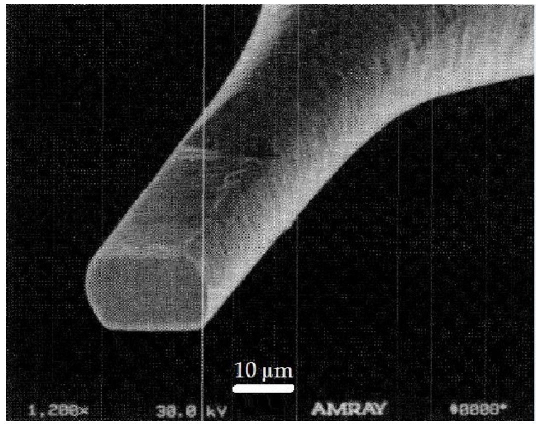

Figure 2.11: Two-fluted micro-milling tool made of HSS by FIB [63].
Tool is 22 μm in diameter with 77 μm long cutting edges.

Micro-tools are designed and developed to machine various materials and different workpiece geometries. Fang et al. [56] and Aramcharoen et al. [7] developed different geometries to improve tool life and surface quality. Milling cutter diameters near to 50 μm have been reported in the literature and also some smaller ones but with unpredictable performance [26]. This effect is produced because a decreasing tool diameter leads to increasing deviation in tool geometry like tool edge radius, rake angle, and clearance angle from the tool design due to difficulty in controlling dimensional tolerance which then turns into modified forces, tool life and tolerances. As these tools are tiny and slender, research has also been carried out to study the dynamic characteristics and vibrations of micro end mills to have a greater insight into their performance [61, 85]. Also, setup faults and unbalance are critical factors that cause the tool to resonate at the spindle frequency affecting the process dynamics.

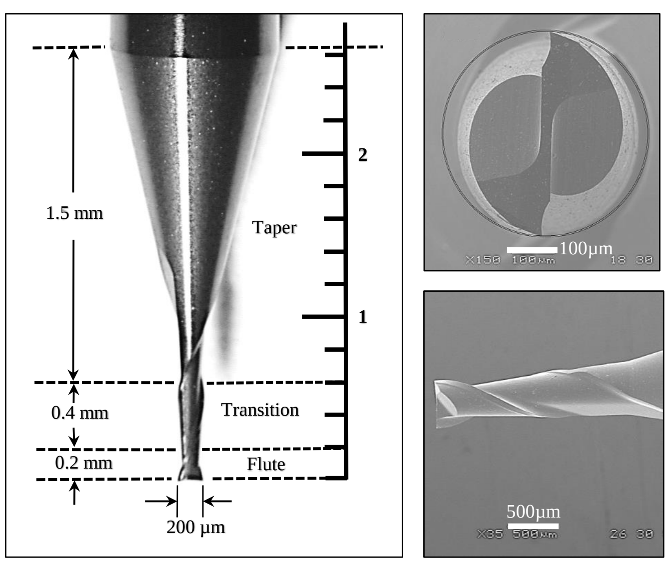

Figure 2.12: Micro-end-mill photographs (two flutes).

2.2 Material removal at micro-scale

2.2.1 Size effect

Micro-machining is a scaled down version of the macro-machining process. Based on this an initial approach, researchers used to assume that the underlying mechanism for chip formation and removal had no significant difference between the micro-scale and the micro-scale. Later studies confirmed that such assumption could not be guaranteed due to a phenomenon called size effect and minimum chip thickness [49, 34, 7]. At small chip thicknesses, the specific energy required to remove a unit amount of material increases, that is often referred as the size effect [34]. During a micro-milling operation, the cutting edge radius of a micro-tool is comparable to the uncut chip thickness, resulting in a possible cutting at negative rake angles. Then, the relationship between the cutting thickness and tool edge radius will set the dominant chip removal mechanism [152]. Figure 2.13 shows the geometric arrangements for conventional and micro-scale machining. The chip will not form unless the cutting depth is greater than a critical value called the minimum uncut chip thickness (h_{min}). Below this value, the material is subjected to an elastic-plastic deformation (plowing/rubbing) without efficient material removal (Figure 2.14), where the actual depth of cut is less than the theoretical depth [199]. Higher cutting thickness (exceeding h_{min} value) plowing effect decreases considerably, and chips are formed efficiently due to the shearing of the workpiece [164].

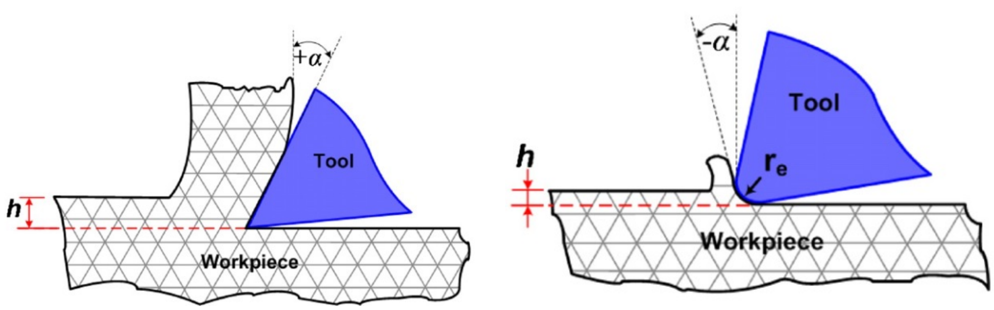

(a) Macro-scale. (b) Micro-scale.

Figure 2.13: Cutting edge size comparison [7].

Plowing effect and the nature of the micro-deformation leads to increased cutting forces, burr formation, and increased surface roughness. Therefore, knowledge of the minimum chip thickness is essential in the selection of appropriate cutting conditions. Its value depends on several factors as the cutting edge radius, workpiece material, micro-structure and other operating parameters.

Some researchers like L'vov [122] and others indicate a minimum cutting depth were the chip separation from the material occurs and its dependency upon the cutting edge sharpness and material properties. Weule et al. [205], then established a relationship to find the

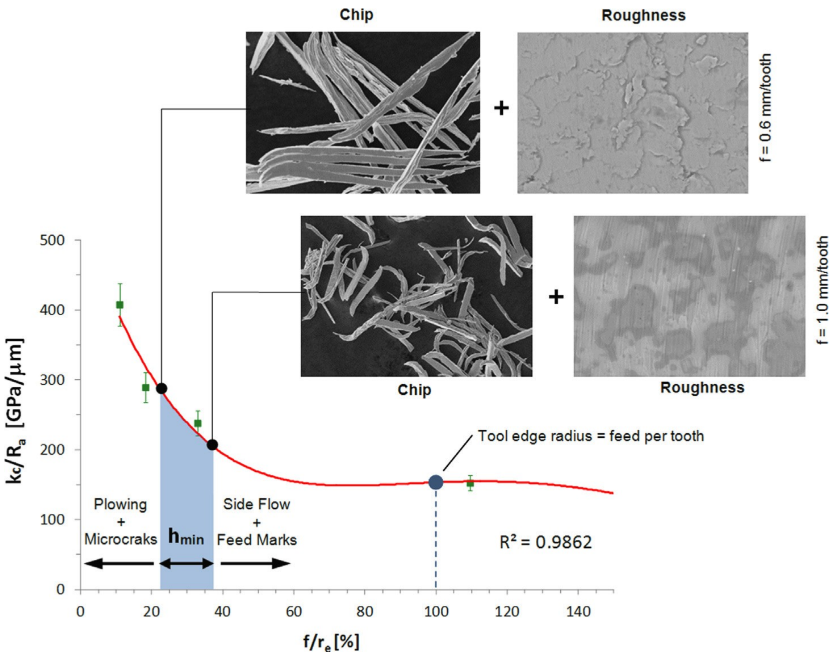

Figure 2.14: Minimum uncut chip thickness determination [153].

achievable surface roughness in terms of h for AISI 1045 Tempered Steel. A saw-tooth-like profile was observed while analyzing the cross section of the machined surface, explained by the minimum chip thickness relationship. Several studies propose various methods to find h_{min}, some recent results concerning its determination for different materials, tools and methods are listed in Table 2.4. It can be seen that in general, h_{min} value is between 1/4 to 1/3 of the tool edge radius. The chip flow stagnation region varies depending on the material and the friction angle and thereby generating a variation on minimum uncut chip thickness.

Cutting edge radius (sharpness) and its effect on other parameters as forces [20, 183], surface roughness [183, 201, 213], burr formation [72] and acoustic emissions (AE) [179] have also been studied. This indicates the relevance of this parameter to guarantee a complete chip formation and to predict other process responses. The minimum uncut chip thickness does not necessarily implies an adequate chip formation, surface integrity or productivity, so to improve productivity some techniques like the use of coolants/lubricants can be considered for an existing machine-tool-workpiece material combination.

Additionally, workpiece micro-structure also involves a critical effect in micro-milling, as features dimensions could range within the same size scale as the grain size. In such cases, the material composition could not be assimilated as homogeneous, and the cutting mechanism differs from conventional macro-machining [46]. Several studies analyze the effect of micro-structure of multi-phase materials as carbon steels and aluminum alloys on the cutting forces [200], tool wear [161] and surface finish [53].

Experimental studies related with micro-milling different materials, are reviewed in [46]. Cutting mechanism varies on monocrystalline, polycrystalline or ductile or fragile materials.

Author (year)	Material (Method)	Tool	h_{min}/r_e
Shi et al. (2017) [179]	Inconel 718 (Experimental)	$\phi = 0.35mm$ $r_e = 6\mu m$	0.23
Oliveira et al. (2015) [153]	AISI 1045 (Experimental)	Carbide w/ TiNAl coat $\phi = 0.8mm$ $r_e = 2.7\mu m$	0.22-0.36
Malekian et al. (2012) [126]	Aluminum 6061 (Analytical)	Non-coated WC, rake 0°	0.23
Shi and Liu (2011) [178]	OFHC Copper (Finite Element)	$r_e = 2.7\mu m$ Different rake angles	0.17
Lai et al. (2008) [104]	OFHC Copper (Finite Element)	Carbide, Rake 10° $\phi = 0.1mm$ $r_e = 2\mu m$	0.25
Son, Lim, and Ahn (2005) [183]	Aluminum, Brass, OFHC Copper (Analytical)	Square diamond $r_e = 0.5\mu m$	0.2, 0.24, 0.18

ϕ: Tool diameter, r_e: Tool edge radius.

Table 2.4: Some minimum uncut chip thickness related research.

A variation in cutting forces is generated while passing through grain boundaries as seen in Figure 2.15, suggesting a higher depth of cut (compared to grain size) to avoid the effects of crystallographic orientation and grain morphology.

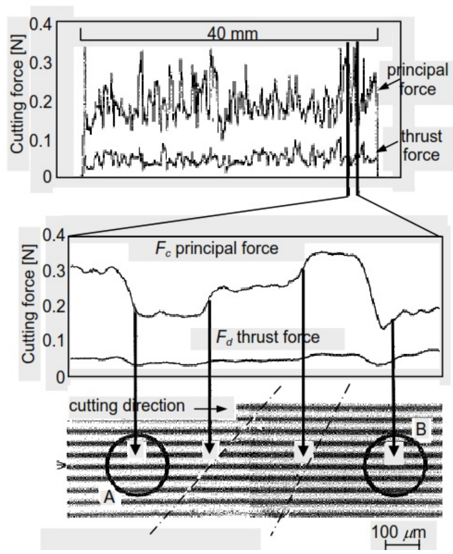

Figure 2.15: Cutting force variation corresponding with the grain boundary of Al alloy [46].

2.2.2 Burr formation

According to the DIN ISO 13715, the burr is a *"material overhang outside of the ideal geometrical shape of the workpiece edge, which remains after the machining"*. A burr is unavoidable, and it may be critical or not based on application requirements. The only solution is to reduce it to an acceptable degree. Often, they hold micro-cracks and generate subsequent problems during assembly, inspection or product operation due to its dimensions and bonding with the rest of the workpiece. Milling burrs can be classified according to the location as shown in Figure 2.16, shape and formation mechanism [73]. In some cases, burrs can be relatively large while compared to the feature size and the amount of time taken to remove them may be over 35% of the time required to machine a part [199].

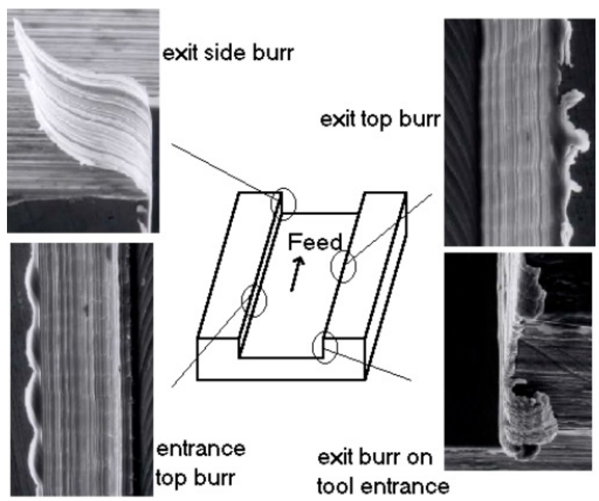

Figure 2.16: Burrs in micro-milling [108].

Chern [35] studied the burr formation while face milling aluminum alloys, reporting the occurrence of five burr types dependent on cutting conditions. Knife-type, curl-type, edge breakout and secondary burr were generated and classified.

The standard ISO 13715 defines a corner with a burr, where it is assessed by measuring the perpendicular distance between the burr tip and the surface from which it is protruding. Schäfer [174] defined the burr value (g), composed by parameters as burr root thickness (b_f), burr root radius (r_f), burr thickness (b_g), burr height (h_0) (Figure 2.17). Burr geometry in the case of micro-machining could not be easily quantified; that is, geometrical parameters like burr height and burr width could not be measured without a lack of repeatability.

In ductile materials, a burr is more likely to be formed due to high elastic-plastic deformation during machining [174], and in brittle or hard materials it is mainly affected by the tool wear progress [205]. In the micro-milling of ductile materials like Aluminum (Al2124), Lekkala et al. [111] observed that up micro-milling produces more side exit burrs and rougher wall surface as compared to down milling. This result is consistent with findings of Schueler et al. [175] while micro-milling Ti-6Al-7Nb alloy. In SAE 1045 Steel, Weule et al. [205] showed that an increase in micro-milling cutting velocities led to less burr formation. Aramcharoen et al. [7] noted that burr size is significantly affected by tool geometry and coatings with favorable rounded cutting edges or chamfered geometries for better quality.

Instead of measuring techniques, research is focused on burr reduction for micro-milling, through experimentation [54, 111, 108, 172] or simulation [112, 31, 210] by varying the process parameters or deburring after machining. The formation of burrs in the macro-milling process has been studied extensively through experimental and predictive analytical modeling, but in the micro-scale, very little work has been reported in the literature.

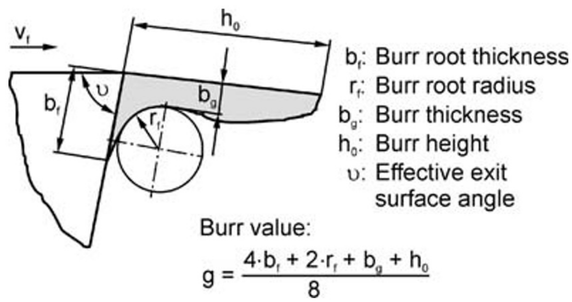

Figure 2.17: Burr measurement according to Schäfer [174].

Although deburring techniques such as electrochemical polishing and others, can be applied to remove burrs, they require additional time and are costly [111]. Burr prevention must consider from design to manufacturing and use proper cutting fluid through strategies such as machining with minimum quantity lubrication coupled with hard coated tools [108].

2.3 Micro-machining modeling and simulation

In the past, intensive cutting tests were realized to develop a better understanding of cutting mechanics and optimize different variables involved in the cutting process. This kind of studies that rely only on experimentation demands considerable time and resources [164]. Diverse modeling and simulation techniques have been developed to aid engineers and scientists to significantly reduce time and resources associated with experimentation, while increasing the available knowledge, exploring possibilities and decrease the learning process cycles [34, 39].

2.3.1 Cutting forces

The micro-cutting process is very complex and involves elastic/plastic deformation, fracture at high strain rates and temperatures generating material properties variations during the process. Micro-milling forces have been studied by several researchers to understand and control process variables to improve the quality of manufactured components. Early approaches by Zvorykin in 1893, Martellotti in 1941, Merchant in 1944 and others established the first analytical studies and basic theories regarding surface finish, cutting power and chip formation. Based on further research, a general classification for cutting forces models was established based on different principles:

- *Analytical models:* Based on a theoretical approach to relations derived from mechanics, materials science or physics. The analysis is done based on process variables as friction coefficient, material behavior parameters (for workpiece and tool), cutting conditions, etc. Complexity varies according to scale [65] and its advantages yield on its capability to predict multiple physical variables as cutting forces, chip length and geometry. Stress and strain rates can also be evaluated due to its global consideration upon the phenomenon; that's why they are known as unified cutting models.

- *Mechanistic models* are sometimes referred as semi-empirical models, as they are not purely analytic, and their capabilities are dependent on empirical data. This results in a mixture of analytic analysis and experimental studies. Additionally, these models offer a significant advantage of not requiring complex mechanical properties, as they are based on the concept of chip load (with forces proportional to chip section).

- *Empirical models:* Often are based on Taylor equation or modifications that include different parameters like depth of cut, feed, or material properties. They offer practical, fast and direct estimation by using curve fitting techniques on data obtained through numerous experiments.

- *Numerical models:* Through the application of continuum mechanics or potential functions, they simulate the cutting process, allowing to model multiple effects and observe stress/strain distribution, chip formation, and others. The significant improvement of algorithms and computer processing power have allowed them to gain a wide popularity.

Table 2.5 shows the principal characteristics of the different modeling techniques. Analytical and numerical models are continuously being developed and updated by researchers for predicting major fundamental variables as stresses, strains, and temperatures. It's still a challenge to develop applied models for predicting machining performance measures such as tool life, surface integrity, chip formation, that would be necessary by industry for immediate use [11]. Hybrid modeling (analytical/numerical, and empirical/numerical), also brings an interesting alternative, as it is recommended to cut down computational time and produce a more reliable result. Jing et al. [83] illustrate an example of a numerical/mechanistic approach, where the cutting forces coefficients are determined based on FE modeling. This method allows then to predict forces under different cutting conditions within a very short computational time while compared to numerical models.

According to previously mentioned classification, Table 2.6 reviews some of the cutting force models applied to micro-milling with a short description of innovations in every proposal and their focus. It can be seen that most of the analytical models are based on slip-line field principle and often consider the size effect and tool tip trajectory. Numerical methods allow investigating different tool geometries and trajectories, temperatures distribution, chip formation, etc. Additionally, common materials like Copper, Aluminum, Steel and their alloys are frequent.

	Analytical	Numerical	Empirical	Hybrid
Principle	Slip-line theory or minimum energy principle	Continuum mechanics using FEM, FDM & meshless FEM	Curve fitting of experimental data	Combines the strengths of other approaches
Capabilities	Predicts cutting forces, chip geometry, tool–chip contact length, average stresses, strains, strain-rates and temperatures	Predicts forces, chip geometry, stresses, strain, strain-rates and temperatures	Applicable to most machining operations for measurable process variables only	Provides meta-models for a family of models to be integrated
Limitations	Usually limited to 2-D analysis with single and multiple cutting edge, but some 3-D models exist	Material model, friction as input, computational limitations: e.g., meshing	Valid only for the range of experimentation	Limited to the strength of the base model: i.e., analytical, numerical, empirical, etc.
Advantages	Ability to develop fast practical tools	Opportunities to connect to industry-relevant parameters	Practical, fast and direct estimation of industry-relevant parameters	Improves the capabilities and accuracies of the base models
Disadvantages	Unique to each machining problem	Long computation time	Extensive experimentation, time-consuming and costly	Need for extensive data from experiments and/or simulations

Table 2.5: Capabilities and limitations of modeling approaches [11].

Micro-milling involves a complex dynamics with multiple parameters and characteristics that affect the evolution of cutting forces. Different approaches made by researchers according to modeling as mentioned above techniques may include or not some of the following relevant factors:

- *Tool trajectory and run-out:* Occurs between the spindle (or tool holder) rotational axis and tool symmetry axis, generating drastic periodical changes in cutting forces and chip load. This contributes to non-uniform wear of cutting edges, lower surface quality, and an increase in tool breakage probability. It's critical to control or reduce this issue and often is a very complex task to assess due to tool dimensions [16, 218].

- *Tool wear and tool geometry:* Tool cutting edge radius (sharpness) have a significant effect on forces [20, 183] and other parameters like dimensional tolerances and surface quality. Micro-tools rapidly wear out losing their sharpness and their effective diameter affecting radial and tangential forces acting on the cutting edge [151]. This can be explained by the fact that the contacting length at larger radii is longer which creates more friction [2].

- *Tool deflection:* Tools used in micro-milling often have geometrical features that cause them to exhibit a light resistance to deflection. In some cases, tool flexibility influence more than 85% of machine-tool-workpiece system compliance [198]. The action of

Author (year)	Model	Principle	Remarks
Bao and Tansel (2000) [15]	Analytical	Material Properties	Investigates cutting forces, considering instantaneous chip thickness and tool tip trajectory. WM: Aluminum, Copper, NAK-55 Steel.
Jun et al. (2006) [86]	Analytical	Slip-line field	Develops a cutting force model that accounts for variations in effective rake angle an dead metal cap. Considers tool vibration and deflection. WM: Carbon Steel.
Annoni et al. (2013) [6]	Analytical	Slip-line field	Waldorf model for macro-scale that allows to evaluate shearing and ploughing force, a modified version is proposed to consider the partial effective rake angle. WM: Brass.
Zhang, Liu, and Xu (2015) [216]	Analytical	Slip-line field	A force model is established based on size effect of specific cutting force. Ratio between uncut chip thickness to cutting edge radius, milling and tool parameters are included. WM: Steel 1045.
Pérez et al. (2007) [163]	Analytical	Mechanistic	A model based on specific cutting pressure, considering uncut chip thickness and run-out for forces calculation. WM: Aluminum, Steel Alloys.
Uriarte et al. (2008) [197]	Analytical	Mechanistic	A conventional milling cutting force model based on six coefficients is adapted to predict micro-milling force, including tool edge radius and tool deflection. WM: Steel H13.
Malekian, Park, and Jun (2009) [127]	Analytical	Mechanistic	Mechanistic model that considers elastic recovery, tool run-out and dynamic effects on forces. WM: Aluminum Al6061-T6.
Liu, Li, and Xu (2013) [118]	Analytical	Mechanistic	Investigates elastic recovery zones and considers material properties, particle size and volume fraction on reinforced material. WM: Mg-MMC reinforced with SiC.
Aly et al. (2006) [4]	Numerical	MD-FEM	Material properties such as yield stress, and modulus of elasticity are extracted from a MD model. Then a FEM model evaluates forces at different speeds and depths of cut. WM: Silicon.
Afazov, Ratchev, and Segal (2010) [2]	Numerical	FEM	Force model that considers run-out effect, tool geometry, uncut chip thickness and machining parameters. WM: Steel 4340.
Jin and Altintas (2012) [81]	Numerical	FEM	Using cutting force coefficients identified from a series of FE simulations, forces are calculated considering tool trajectory, run-out and dynamometer dynamics. WM: Brass 260.
Guo et al. (2014) [72]	Numerical	SPH	Investigates the effects of tool edge radius on micro-machining. Evaluates temperature distribution and chip formation. WM: Oxygen-free copper.

WM: Workpiece Material.

Table 2.6: Cutting force models for micro-milling.

cutting forces causes a deviation of the tool from its theoretical position [167]. Tool deflection is one of the main error sources in a final milled micro-part [197], also generates tool wear and breakage [198].

- *Micro-structure:* It's important to realize that materials used in micro-machining are not homogeneous and isotropic (particularly in dual-phase or multi-phase alloys). Grain size in the workpiece may be comparable to tool edge radius and depth of micro-cuts. This fact indicates that the workpiece material plays a significant role in forces and tool wear [200, 20, 53], surface quality [205] and general performance.

- *Temperature:* The material undergoing micro-cutting is subject to high strain, large strain rates, and temperatures, thereby leading to a complex thermo-mechanical problem [34]. The high temperature has a thermal softening effect on the material flow stress [199]. Some material constitutive models as given by Johnson and Cook consider a flow stress variation with temperature.

- *Minimum Uncut Chip Thickness (MUCT):* In micro-milling, the tool describes a trochoidal trajectory and its cutting edge radius becomes comparable to the chip thickness, resulting in a possible cutting at negative rake angles. A minimum uncut chip thickness is then required to set the dominant removal mechanism in a positive rake angle zone, where plowing effect decreases considerably, and chips are removed efficiently [164]. Below MUCT, the forces and specific energy required to remove a unit amount of material increases with higher plowing/rubbing effect [34].

Figure 2.18 depicts some recent studies and indicates whether if one of the mentioned factors is included or not. It can be noted that almost all the approaches include tool wear or tool geometry effects. Most of the publications consider at least one change in tool edge radius and evaluate its effects; few studies examined variations in geometry due to tool wear (flank wear, rake angle modifications, etc.). Also, MUCT is frequently considered with analytical formulas or through simulation to study plowing effects during cutting. Tool trajectory and run-out are not available in every model type, and often it's not coupled with tool tip deflection. Material micro-structure effects are included in some analytical and mechanistic studies were multi-phase metals like Steel (with ferrite and pearlite phases), or composite materials are considered. Finally, the thermo-mechanical coupling of factors high strain, large strain rates and temperatures are often exclusive of numerical modeling [34], as other methods can not capture this effects efficiently.

Figure 2.18 also illustrates that most of the previous studies analyze their force models on Aluminum, Copper, Steel and their alloys. Few studies analyze micro-cutting forces during processing hard to cut materials like Titanium and its alloys, polymers, and composites. Hybrid models that combine the strengths of other approaches that consider factors above like run-out, tool wear, temperature distribution, etc. while micro-milling materials like Titanium and its alloys are still required.

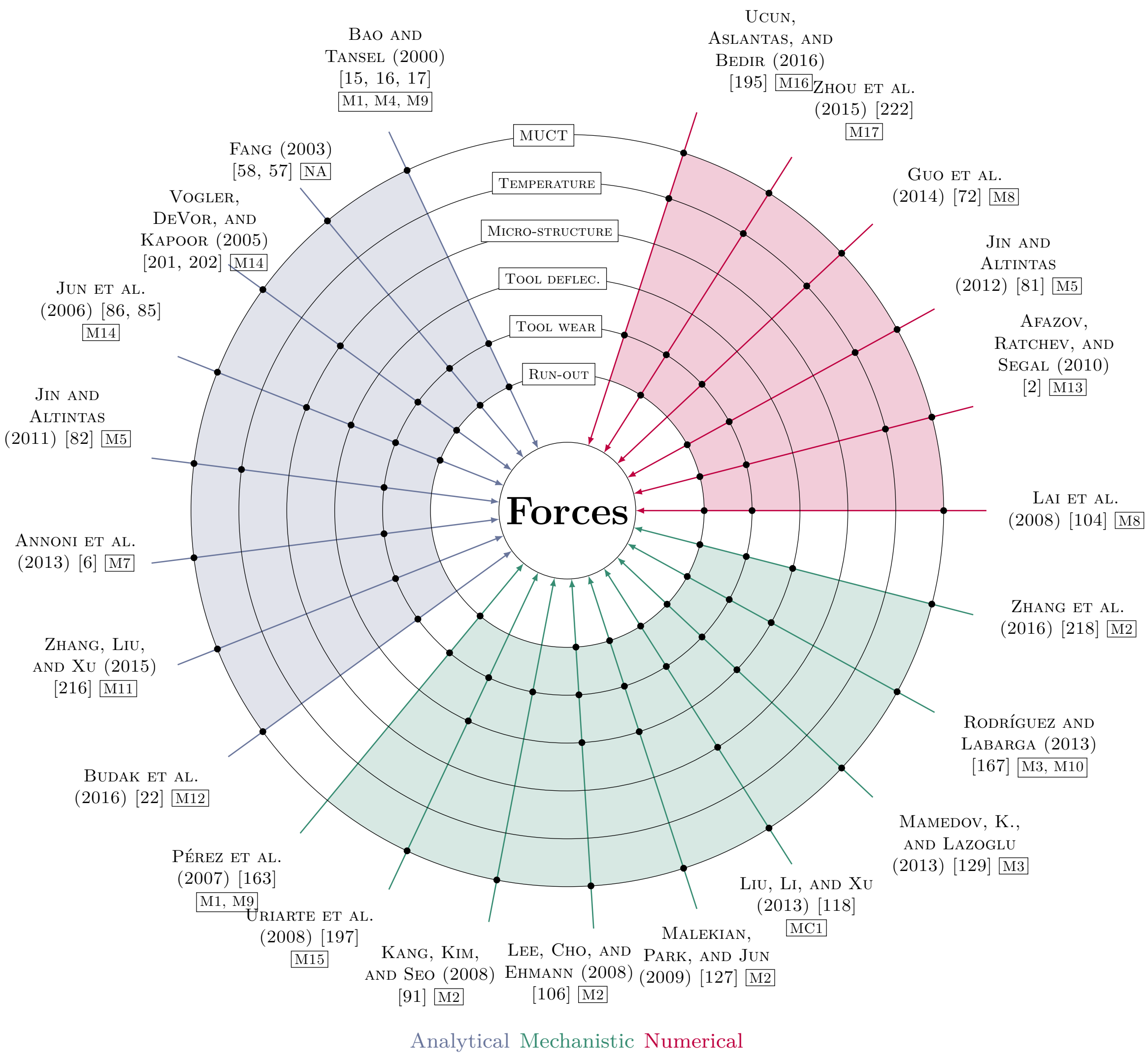

No	Type	Material
M1		Aluminum
M2		Aluminum (6061-T6)
M3		Aluminum (7075)
M4		Copper
M5		Copper (Brass 260)
M6		Copper (Brass 260)
M7		Copper (Brass C38500)
M8		Copper (OFHC)
M9	Metal	Steel
M10		Steel (AISI 1015)
M11		Steel (AISI 1045)
M12		Steel (AISI 1050)
M13		Steel (AISI 4340)
M14		Steel (Ferrite, pearlite phases)
M15		Steel (H13)
M16		Steel (Inconel 718)
M17		Steel (NAK80)
MC1	Composite	Mg-MMCs reinforced with SiC

Figure 2.18: Recent cutting force models for micro-milling.

Some numerical techniques that have been applied to simulate this process response are: Finite Element Method (FEM), Smooth Particle Hydrodynamics (SPH), Molecular Dynamics (MD) and Multi-Scale (MS). Table 2.7 shows different simulation techniques developed for modeling and simulation of micro-cutting.

	Technique			
Feature	**FEM**	**SPH**	**MD**	**MS**
Scale	Big	Medium	Small	Medium
Basic Unit	Node	Particle	Atom	Atom
Beginnings	1940s	1970s 1990s in strength of materials	1950s	1990s
	1970s in machining		1990s in micro-manufacturing	
Basic Principle	Constitutive Equations (Continuum Mechanics)	Constitutive Equations (Continuum Mechanics)	Potential function and Newton second law	Mixed
Software	Ansys, Abaqus, Deform 3D, AdvantEdge	LS-Dyna, Pasimodo	Lammps, Gromos, MDynaMix	QC, MAAD, CADD, CGMD,...

Table 2.7: Simulation techniques for micro-milling (adapted from [34, 164]).

- *Finite Element Method (FEM):* FEM is based in continuum mechanics, material is discretized through finite elements and effects as crystal structures, grain size and inter-atomic distances are ignored. The problem variables and properties, are determined exactly only at node locations; for intermediate locations interpolations are used [39, 164]. It has been successfully applied to analyze chip and burr formation, cutting forces, vibrations, temperature distribution [34]. Numerical formulations as Arbitrary Lagrange Euler (ALE) allow high plastic deformation and apply proper chip separation criterion and adaptative meshing [39].

- *Smooth Particle Hydrodynamics (SPH):* A discrete set of points (particles) is used to approximate material properties and state variables, allowing to analyze processes with high dynamic behavior and large deformations [185]. This avoids severe problems encountered while dealing with large deformations [116] and material removal/fracture [72]. This method has been applied to study multi-materials interfaces, chip formation and material removal [209], tool wear and tool geometry effects [24], stress/strain and temperature distributions.

- *Molecular Dynamics (MD):* Generally this method its used for microscopic modeling at molecular scale [39]. Based on the atomic interaction potentials, forces that can be derived from a potential function (like Lennard-Jones and Morse functions). Crystal orientation effect, chip formation, minimum uncut chip thickness on nanometric cutting, cutting forces and temperatures, surface integrity and friction, wear and scratching mechanisms can be studied through MD [66].

- *Multi-Scale (MS):* Due to the varying size scales during micro-cutting, different methods have been developed like FEAt (Finite Element Atomistic), QC (Quasicontinuum), MAAD (Macroscopic Atomistic Ab initio Dynamics), CGMD (Coarse Grained Molecular Dynamics) and CADD (Coupled Atomistic and Discrete Dislocation). QC, FEAt and CADD method have gained extensive applications in materials science to explain micro/macro mechanisms and solve several scientific issues [34]. Combined techniques as MD-FEM can be applied to predict temperatures in the cutting zone, stress/strain distribution, cutting forces while explaining the phenomena occurring at nanometric scale including surface roughness, residual stress, micro-hardness and fatigue [188].

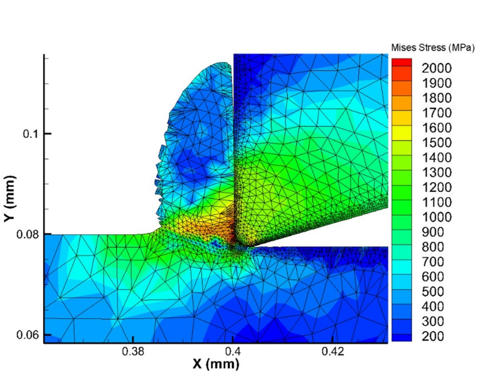

(a) FEM-Stress [222].

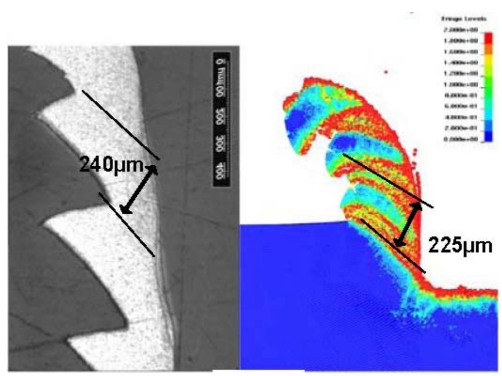

(b) SPH-Chip formation[116].

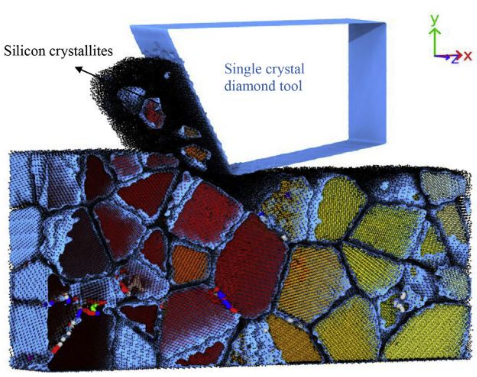

(c) MD-Polycrystalline material cutting [68].

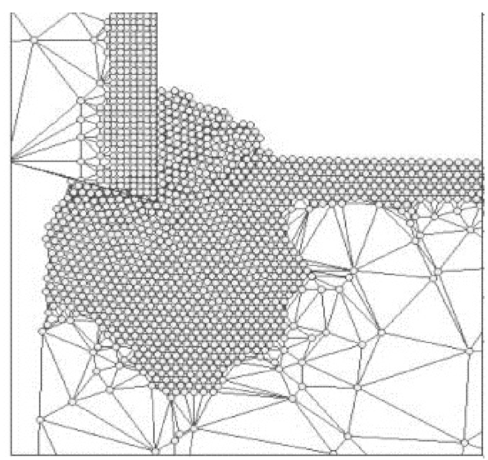

(d) MS-Copper nanometric cutting (1nm) [188].

Figure 2.19: Micro-cutting simulations.

Many analytic models are based on initial approaches made by Tlusty and McNeil or Armarego for mechanistic models. Numerical models are mainly formulated through FEM with some few cases through the application of MD or SPH. Several considerations need to be included due to severe conditions present in the micro-cutting mechanics.

2.3.2 Cutting temperature

During a chip formation process, some of the energy is released in the form of heat. This heat raises both tool and workpiece temperature. Such temperatures generated in metal cutting are widely recognized as a major factor affecting several aspects such as tool wear/life, surface quality, part dimensional accuracy and workpiece residual stress. Its effects may be positive (like material softening) and negative (like promoting tool wear) on the macro-machining process. In case of micro-machining, it is still doubtful about the benefit of heat, since heat may encourage even more elastic deformation in the micro-machining process. An example of possible benefits is shown by Laser-assisted micro-milling (LAMM) that is a process which uses a low-power laser to locally preheat the material that is then removed by the tool immediately behind it. Some results point to increased dimensional accuracy, reduction in resultant peak forces [142] and better machining quality [196].

The determination of temperatures and their distribution in the cutting area is technically a difficult task. Some tools and methods that are used to measure the cutting temperature are through thermocouples (direct conduction), infrared thermometers and thermographic cameras (indirect radiation). Often, cutting metal process simulation is an alternative technique to extend the tool life predicting the temperature and stress in the tool without spending time and money on experimental procedures [38]. Simulations results are affected by several parameters such as constitutive model constants and friction coefficients, but they can show the effects of cutting parameters on temperatures [222].

Karpat and Ozel [93] introduced a modeling technique to determine forces, stresses, and temperature distributions while considering the influence of tool flank wear. While applying their method to machining of AISI 1045 steel, Al-6082-T6, and Al-6061-T6 aluminum alloys, their results explain the heat partition behavior of the tool-chip and tool-workpiece interfaces. Ucun et al. [195] performed finite element modeling to study the cutting forces, tool stresses and cutting temperature during micro-milling of Inconel 718 steel finding a real coherence between numerical and experimental results. Figure 2.21 illustrates temperature distribution through FEM and thermal camera images for such case. Also, they found from the numerical results that different cutting edge geometries also affect the temperature. In the cutting process performed with the tool with a negative edge angle, a higher cutting temperature was observed.

Experimental research on cutting temperature of macro-cutting is another area that has been extensively investigated. Kadirgama et al. [88] determined temperature distribution on the cutting tool when macro-machining Hastelloy with carbide coated tools. Through the application of response surface method (RSM) and FEM, their results indicate that the feed rate has the most dominant parameter on the temperature, followed by the axial depth and cutting speed. The tool tip temperature was measured with an infrared thermometer. The cutting temperature and heat partition remains a challenge for micro-milling process and needs further research [11].

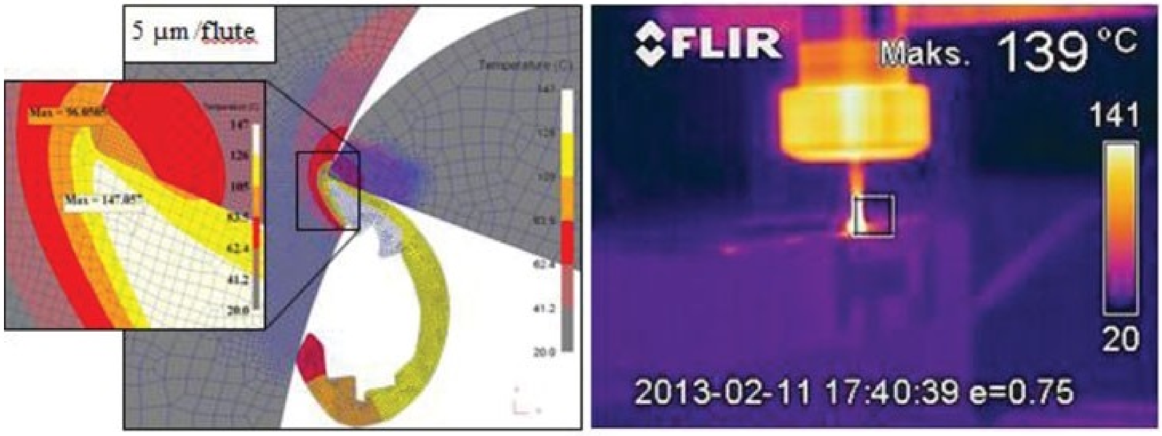

Figure 2.20: Temperature distribution and thermal camera images obtained from the cutting zone (adapted from [195]).

2.3.3 Tool wear

During operational conditions, micro-tools rapidly wear out and they lose their sharpness, which influences the surface quality and the cutting forces. The machining force is the primary measurable quantity leading to tool wear and breakage. It's related to several parameters like vibrations, stress, temperature and others that are causes of tool wear (Figure 2.21). Also, the variation in the cutting mechanics between macro and micro-scale, makes the tool condition monitoring in the micro-machining draws much more challenging than in the conventional cutting [130].

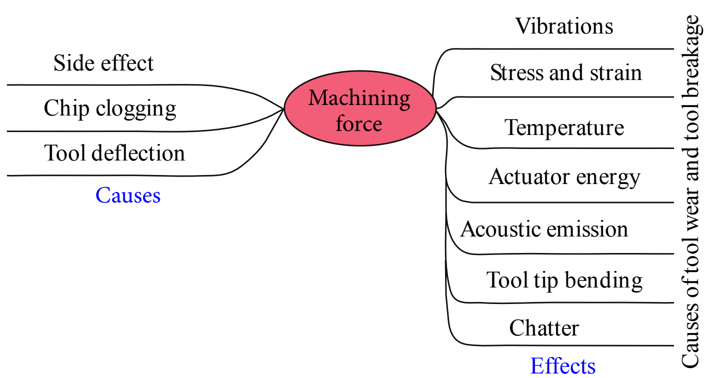

Figure 2.21: Primary causes and effects of machining forces (adapted from [130]).

Many types of research focus on different variables and sensors to detect tool wear process. The proposed methods for tool condition monitoring in micro-milling include use of acoustic emission (AE) sensors and related signal processing approaches, measurement of dynamic cutting force and its classification, use of vibration sensors, use of the motor current signature, machine vision, a combination of the preceding approaches, and sensor fusion [130]. Lee et al. [105] presented different requirements and the suitability of AE as a monitoring technique at the precision scale. Results indicate that with appropriate sensor technology, AE could be used as a mean to link the manufacturing and quality control stages together closely. Studies by Lee et al. [109] indicate that for micro-milling AE could classify tool wear levels depending on the feature bandwidth size. Lu and Wan [120] studied high-frequency sound signals for monitoring tool wear while micro-milling Sk2 steel with a 0.7 mm tool. By using a single microphone with a frequency range between 20 and 80kHz their measurements in the time domain signals, indicated a slight change in amplitude, as depicted in Figure 2.22. Also, this method proves to be a superior approach to distinguish a worn tool from a sharp tool with the proper selection of feature bandwidth and other parameters. Often, cutting force measurement is known as the most effective method for monitoring tool wear conditions since it provides higher signal-to-noise ratios, and best represents the state of machine tools and operations. The most common direct method to measure cutting forces in micro-milling through dynamometers or piezoelectric load cells.

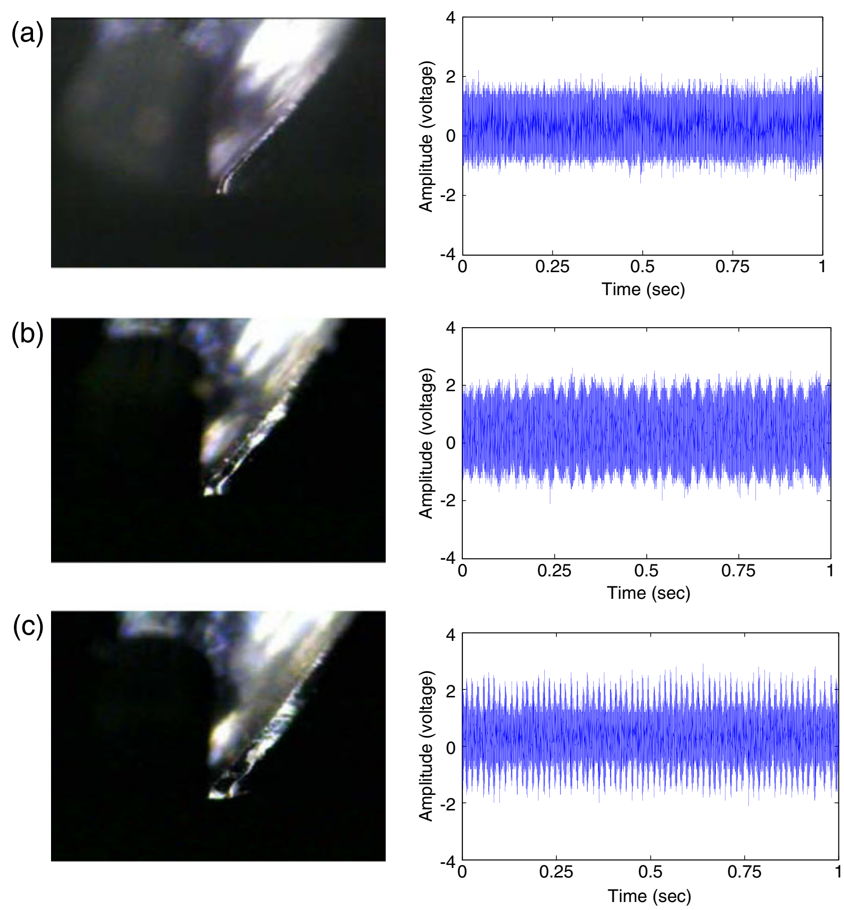

Figure 2.22: Tool wear level and corresponding time domain sound signal for tool condition [120].
(a) Sharp tool; (b) Fourth cutting pass (VB: 0.026 mm); (c) Fifth cutting pass (VB: 0.038 mm; spindle speed, 50,000 RPM; feed rate, 0.6 μm; depth of cut, 0.2 mm).

However, another group of investigations is more focused on tool wear effects on different parameters. Bao et al. [17] modified the cutting force model under the effect of tool wear during the micro-milling process. Their study indicates that unlike progressive tool wear in conventional milling, tool wear in micro-cutting could easily lead to tool breakage due to induced increasing cutting forces that exceed the tool strength. Therefore, micro-milling tool monitoring is critical and practical to optimise cutting parameters and ensure meeting machining quality standards. Karpat and Ozel [93] introduced a modeling technique to determine forces, stresses, and temperature distributions while considering the influence of tool flank wear. Their results illustrate an increase in the tool-workpiece interface, changes in shear angle and higher cutting forces with increased flank length.

Filiz et al. [62] in micro-milling experiments in OFHC copper demonstrate a greater tool wear at low un-deformed chip thickness. Uriarte et al. [197] used 300 μm diameter end-mills with TiAlN coating to micro-mill tool steel (H13 hardened up to 60HRC). They concluded that tool wear is one of the main error sources in a final milled component, affecting the accuracy and roughness of the micro-part. Additionally, they noted that wearing appears not only in the cutting edge area, but also in the opposite zone due to high tool deflection effects. The effect of wearing can also be seen in the rounding of the tool tip corner as seen in Figure 2.23.

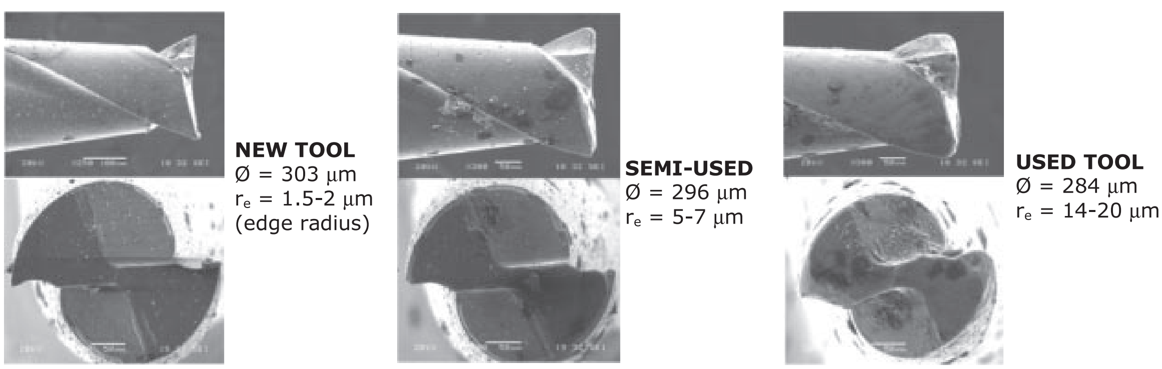

(a) (b) (c)

Figure 2.23: SEM image of wear in micro-tool [197].

Oliaei and Karpat [151] studied the influence of tool wear on milling forces, surface roughness, and tool deflections through different techniques. Their results indicate that during micro-milling operation, tool wear is observed to evolve as edge rounding, flank wear and also tool diameter reduction as an easy option to monitor during the process. Lu et al. [121] developed a three-dimensional cutting force prediction model to include flank wear effect while micro-milling a Nickel-based super-alloy.

Experimental based studies have also been reported in the literature. Saedon et al. [168] considered micro-milling of AISI D2 steel and formulated a tool life equation by applying response surface methodology. Their results showed that cutting speed is the most important factor, followed by feed and axial depth of cut.

In spite of the extensive research carried out on this issue, however, tool wear predictions to accurately represent its status with high resolution is still not yet accomplished. More research and new strategies need to be developed to monitor its development and its effects at the micro-scale effectively.

2.3.4 Cutting fluids

Cutting fluid is applied during machining to increase tool life, enhance surface finish, decrease burr, and avoid build-up edge formation [34, 199]. Traditionally coolants promote a friction and temperature reduction, to remove chips from the cutting zone, to limit chemical diffusion and to protect the machined surface from corrosion [18].

- *Flood (wet) cooling:* Flood cooling (wet cooling) with jets or nozzles sprays large quantities of fluid to the workpiece. Cooling reduces friction, aid to dissipate heat, remove chips and other secondary functions [204]. Coolants/Lubricants also allow to increase the cutting speeds, extend tool life, reduce the workpiece damage, and improve the surface quality while aiding to meet the expected dimensions and tolerances [18]. Therefore, cutting fluids increase productivity, improve efficiency by reducing the number of defects, help to ensure the process safety and guarantee and enhance the machining quality.

  Flood cooling also involves some drawbacks such as their high costs, environmental concerns, and human health risks. Also, in micro-milling, the application of flood cooling may not be very effective due to poor penetration based liquid tension at small surfaces (in magnitudes of micrometers) rotating at very high speeds. The impact created by these fluids may be greater than the cutting forces observed during micro-machining [199]. These issues make necessary to develop and apply novel lubrication/cooling systems like dry machining, minimum quantity lubrication (MQL), cryogenic refrigeration, and gaseous refrigeration.

- *Dry machining:* To manufacture without using any cutting fluid, also referred to as dry machining, is being very popular among researchers in recent years [204]. An economical and environmentally friendly process like dry machining must incorporate some changes to overcome the absence of coolant and its benefits like cooling, lubrication and chip removal. Tool material with high hardness, thermal fatigue limit and chemical stability, and proper cutting parameters must be carefully selected for a successful implementation [18]. This technique has been applied in numerous machining processes mainly in the automotive industry with materials like gray cast iron and aluminum cast alloys which yield low cutting forces and temperatures [204]. Interrupted machining processes such as milling, turning and sawing with short breaking chips (Figure 2.24) are suited for a coolant/lubricant reduction [18]. Several challenges still exist for machining some materials, and near dry machining or minimum quantity lubrication have evolved to address some of this issues.

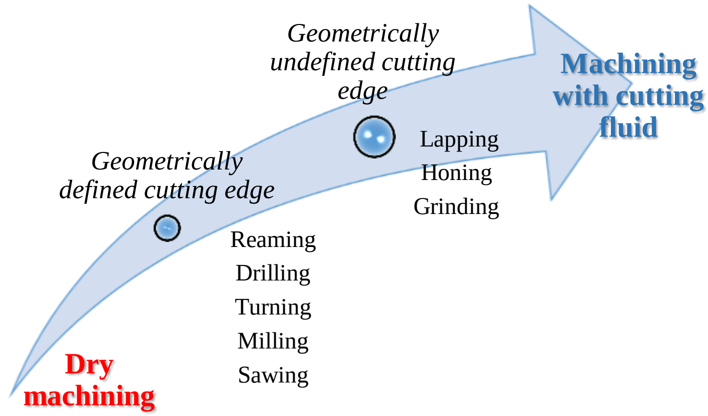

Figure 2.24: Machining process influence on cooling lubricant supply.

- *Minimum quantity lubrication:* Minimum quantity lubrication (MQL) uses a mix of compressed air with a reduced amount of coolant/lubricant in the form of drops, producing a spray or mist in the cutting zone. Often, the amount of coolant (below 10 ml/min) is nearly 3 to 10 orders of magnitude lower than conventional flood cooling [18, 221]. Other advantages include reduced cost and tool wear, improved surface quality, a reduction in environmental and worker health hazards and nearly clean chips.

  Soo et al. [145] performed a series of micro-drilling experiments on Al 6061 with 200 μm carbide twist drills. Compressed air, pure MQL and nano-fluid MQL with paraffin and vegetable oils as base fluids. Nano-fluid MQL with nano-diamond particles exhibited a significant reduction in drilling torques and thrust forces. In addition, the quality and quantity of drilled holes was superior to those obtained when a pure MQL and compressed air was used. Zheng et al. [221] also indicate an improve in tool life and reduced material adhesion while micro-milling Ti-6Al-4V in contrast with dry cutting as seen in Figure 2.25. Air pressure and direction must be carefully selected as it shows an influence on burr formation.

  Atomization based cutting fluid (ACF), is an alternative proposed by Nath et al. [147] were droplets are produced by an ultrasonic atomizer and further pressurized through an air-CO_2 mixture. A better cooling and lubrication of cutting tool-chip interface was achieved while turning a titanium alloy Ti-6Al-4V, with a high chip evacuation at lower running cost and improved tool life up to 40-50% over flood cooling.

  Some authors have studied minimum quantity lubrication technique in combination with cooled air can improve cooling and lubricating performance during machining steel and difficult-to-machine materials [18]. MQL have a high potential in terms of improving overall process performance, but some issues still have to be studied regarding MQL supply (generator, coolant channels, control systems etc.), cutting tools and machine tool design.

- *Cryogenic cooling:* Cryogenic cooling uses liquid nitrogen (LN_2 at $-196°C$) or carbon

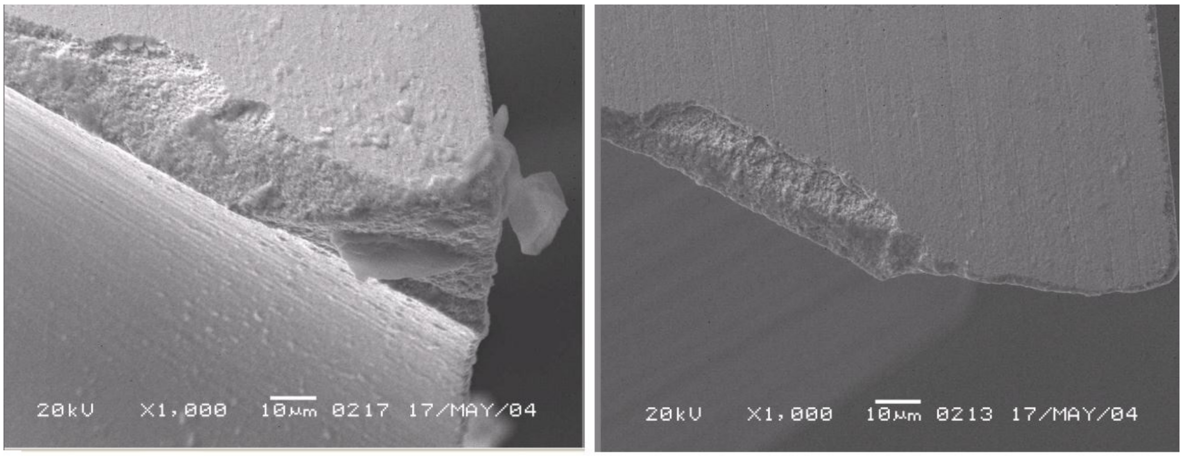

(a) (b)

Figure 2.25: Worn tools (same cutting conditions) [221]. (a) Dry machining; (b) MQL.

dioxide (CO_2 at $-78°C$) as support during machining through its application from the rake face or flank face of the cutting tool [94]. The use of liquid nitrogen also is an environmentally friendly alternative and non-toxic gas that contributes to process sustainability, while absorbing the generated heat and acting as a lubricant.

Micro-milling aided with cryogenic cooling has been applied successfully in soft polymer materials with low toughness, were material is changed from a rubbery state to a glassy state below the glass transition temperature. Several cutting tests were applied in Polydimethylsiloxane (PDMS) achieving better-shaped micro-grooves with a surface roughness up to 80 nm [90]. Friedrich [63] while micro-milling Polymethylmethacrylate (PMMA) below the glass transition temperature, as a result of the cryogenic cooling, the cutting force was held relatively constant. Also, the specific cutting energy increased linearly with a reduction in the temperature beside a rougher surface finish too. Extended life parameters were found while using a specially manufactured 22 μm diameter micro-tool with 70 nm edge radius. Ghosh et al. [67] applied cryogenic machining to avoid cracking and surface defects while micro-milling a soft hydrophobic intraocular lens (IOL) material (Figure 2.25).

Recent studies are focusing not only on the cryogenic effect on cutting forces and tool wear but also on surface integrity (roughness, microstructure, residual stresses, etc.) and proper parameters like number and positioning of nozzles, flow rates, etc. [18, 94].

- *Gaseous cooling:* Cooling systems based on gases are an alternative based on air, carbon dioxide, nitrogen, water vapor and others. Air is one of the most popular options mainly, due to its costs and low health risks and environmental impact. Although the air has a small cooling capacity, this property can be enhanced by its cooling, compression or liquefaction [18]. In cold compressed air systems, the required refrigeration capacity could be provided by various means such as liquid nitrogen, vapor-compression refrigeration, or through expansion by a vortex tube.

  The vortex tube should be remarked as an excellent alternative, as it offers an instant

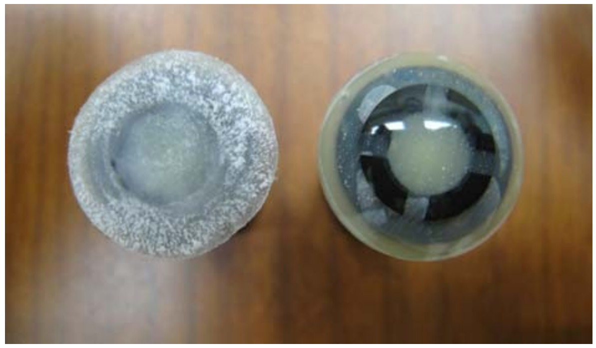

Figure 2.26: Comparison of IOL surfaces with compressed air (left) and cryogenic cooling (right) [67]

.

high-efficiency response at low-cost for cooling with no maintenance, no risk of explosion, no electricity and no additional parts. Its principle based on the Ranque-Hilsch effect and its applications have extended in the field of the machining processes.

Through the combination of cold compressed air with an environmentally friendly lubricant like vegetable oil, lignin containing fluids or liquid nitrogen could not only reduce the cutting forces and temperature but also make possible to apply high feed rates and cutting speeds [18].

2.3.5 Process parameters optimization

Micro-machining processes often use conservative depth of cuts, speeds and feed rates due to the fragility of the micro-tools. Market demands higher material removal rates as a productivity index while reducing operational costs (tool breakage, and quality). The most commonly used metrics to evaluate the performance of micro-milling processes can broadly be classified into two categories as either quality based or related economic criteria.

- *Cost:* Machining time and production costs are the main representatives of this category.
- *Quality:* This metrics are related to different factors which have a significant effect on the quality of the machined component. Some of them are tool wear, tool life, part accuracy, surface roughness, etc. and are depicted in Figure 2.27. Burr formation and other geometrically related features can be considered as included in part accuracy.

Weule et al. [205] studied micro-milling of steel with tungsten carbide tools and modified the process parameters for burr reduction (part accuracy) and tool life. In their research, the micro-cut material was Steel SAE H13 to produce a mold for a micro-car. The achievable surface roughness was 0.5 μm with a good machining time while compared to other processes like micro-EDM or laser ablation.

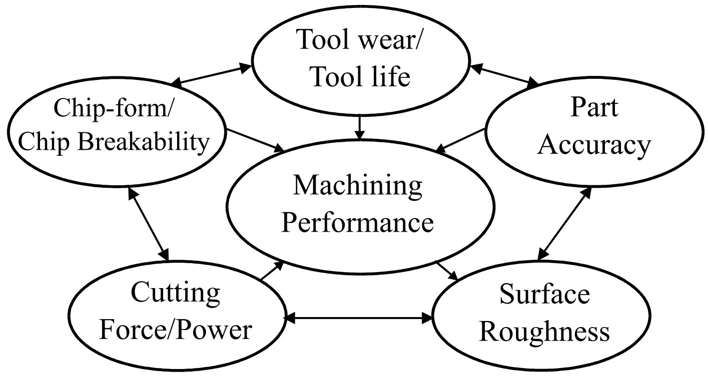

Figure 2.27: Representation of the factors influencing machining performance [23].

Dimov et al. [42] considered machining strategy to be of high importance in the micro-milling process optimization. In their case, machining strategy was chosen for an optimal surface finish which is often a critical factor when this technology is used to manufacture micro-tooling inserts. Besides, the avoidance of cutting tool breakages should be the primary consideration in selecting the most appropriate machining strategy because end-mills are extremely sensitive to the varying process conditions.

Kuram and Ozcelik [102] performed an optimization of machining parameters during micro-milling of Ti6Al4V titanium alloy and Inconel 718 materials through the application of Taguchi method. Their response variables were tool wear (flank wear), surface roughness and cutting forces. They found that depth of cut was the most important parameter influencing tool wear for Ti6Al4V titanium alloy and spindle speed in the case of Inconel 718 material while cutting with a two-flute flat end mill with a diameter of 800 μm. Figure 2.28 illustrates the main effects plot of signal to noise (S/N) ratios, where the optimal micro-milling parameters are highlighted in circles. Tool wear during micro-milling of Ti6Al4V titanium alloy decreased with an increment of spindle speed and, in general, increased with an increment of feed rate and depth of cut. For Inconel 718 material, tool wear increased with an increment of spindle speed and feed rate. The optimal set of parameters for each material and response combination could then be predicted through regression modeling. Jaffery et al. [78] also performed micro-milling tests of Ti6Al4V with similar results but also highlighting the differences between machining with an undeformed chip thickness below or above the tool edge radius.

Oosthuizen et al. [154] studied the effect of cutting parameters on surface quality to ensure that machined components are within the required surface quality tolerances. In their research, measurements of the surface roughness, micro-hardness, and the micro-structure of the workpiece while milling Ti6Al4V and tool wear analyses were performed. They observed an increase in hardness in subsequent layers due to internal work-hardening induced by the cyclic effects of the milling process. Also, higher feed rates promoted increments in surface roughness and higher tool wear on the rake and flank faces.

Process monitoring and optimization in high-speed micro-cutting applications are very

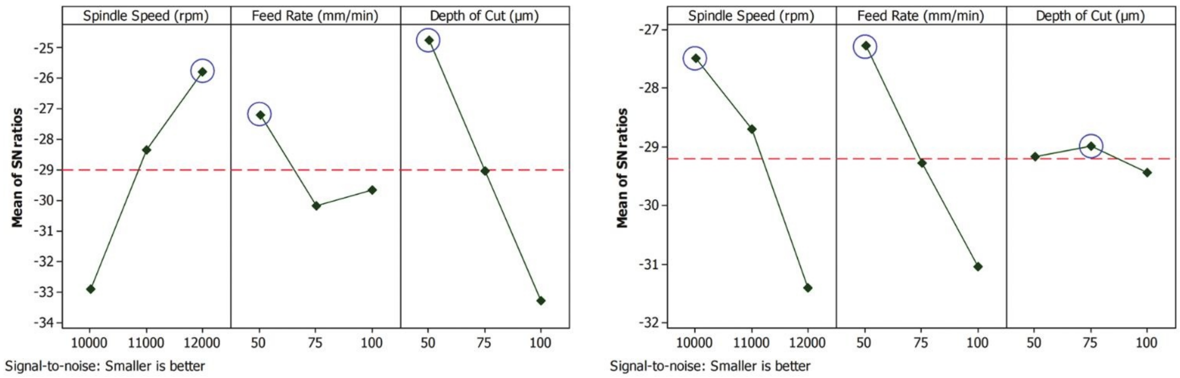

a) Ti-6Al-4V **b)** Inconel 718

Figure 2.28: Main effects plot of S/N ratios for tool wear during micro-milling [102].
(a) Ti6Al4V titanium alloy; (b) Inconel 718.

challenging with existing equipment and techniques. Several techniques have been adopted to approach an optimal set of parameters, but often one performance has to be sacrificed to attain another.

Chapter 3

Micro-milling modeling background

Contents

3.1 Introduction

New advances in machine tool and cutting tool technologies, along with advanced material development, all aimed at improved manufacturing productivity, product quality and cost reduction, require predictive performance models for use in process planning systems for machining processes [11]. To study machining is a quite complicated task where complex disciplines such as metallurgy, elasticity, plasticity, heat transfer, contact problems, fracture mechanics, and lubrication are involved [123]. The finite element method (FEM) is a numerical simulation technique that enables to predict different parameters which when used presents an advantage of decreasing the number of experimental tests. This technique allows eliminating prototypes or trials that would be required to analyze phenomena resultant of several manufacture processes and their respective parameters to chosen the better conditions [5, 38].

In machining processes FEM can be very advantageous, helping to define appropriate parameters that reduce the cutting forces, increase the tool life, improve the residual stresses and explain the complex micro-cutting mechanics. Different process performance metrics can be involved and evaluated through FEM, and often these parameters like forces, stresses, temperatures, etc. are related to industry-relevant outcomes like tool life, accuracy, burrs and others that focus into increased quality and productivity. To ease this relation, the combination with an empirical model can aid to a fast and direct estimation of aforementioned outcomes.

The aim of this chapter is to develop a framework to develop a hybrid numerical/empirical model of orthogonal micro-cutting considering tool geometry, material properties and critical factors defined in chapter 2 and needed to obtain great results of micro-milling processes simulations.

3.2 FEM Types

Predictive models resulting from simulations can be integrated into process planning systems to improve productivity and enhance product quality. Figure 3.1 illustrates the proposed flowchart for creating a model and processing different fundamental output variables and industry relevant characteristics. Several blocks of parameters need to be properly defined, beginning with identification of process, materials parameters and interactions. An hybrid numerical/empirical model is proposed, not only to validate the numerical results, but also to improve its capabilities and allowing to evaluate different industry relevant outcomes.

For FEM two basic models are in focus: orthogonal (two-force) models, and oblique (three-force) models. Most machining processes are oblique but the orthogonal model studies are easier to simulate and they can be useful and adequate for understanding the basic mechanics of machining processes [123]. This technique has been investigated and reported by various researchers, allowing to study the fundamental mechanisms of micro-scale cutting. In present work, the complex milling process is simplified to a 2-D orthogonal cut (as shown in Figure 3.2) based on the following machining assumptions and considerations:

- A low feed per tooth (while compared with the tool diameter) is often applied in micro-milling. In this study, for a end-mill with 1000 μm diameter, the feed is near 2 μm, indicating a relatively small deformation area (Figure 3.2)).

- The axial depth of cut of the micro-scale is very small where the helix angle of the tool may impose a little effect [104]. This depth of cut is represented by the thickness in the 2-D model.

- The force prediction and tool wear in 2-D is quick (lower computational load) and accurate while compared to 3-D simulations as experienced by other researchers [11, 192]. For temperature predictions, some adjustments need to be made due to the implications of concentrated parameters that may affect heat diffusion and dissipation effects.

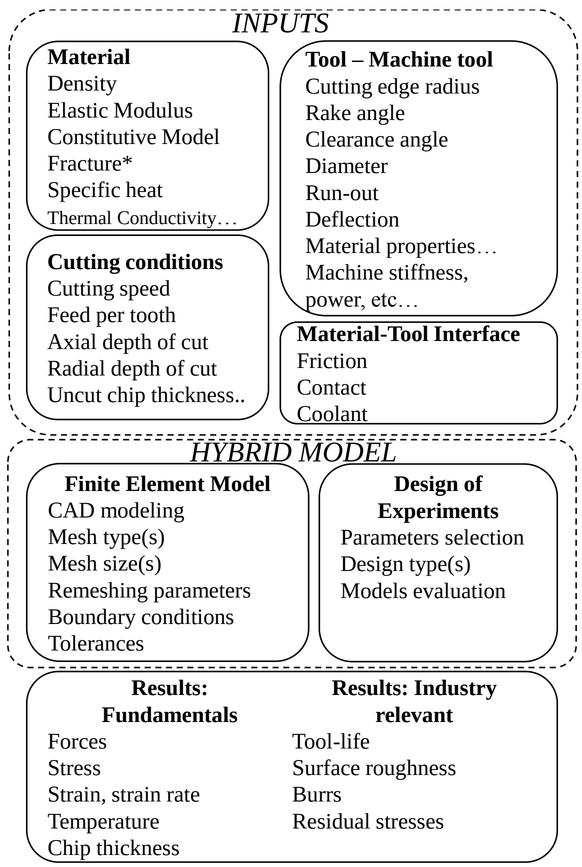

Figure 3.1: Proposed approach for micro-milling modeling.

It is known that the success and the reliability of modeling depends upon accurate properties and realistic machining conditions. Therefore, effects as undeformed chip thickness (related to run-out, deflection, machine stiffness, and others), constitutive models parameters and properties are carefully analyzed as they are basic requirements for the hybrid modeling approach.

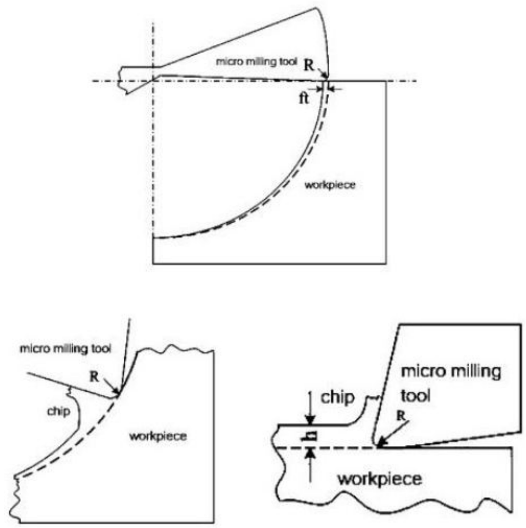

Figure 3.2: Simplifications for micro-milling process with orthogonal machining [104].

3.3 Micro-milling mechanics

3.3.1 Uncut chip thickness modeling

The overall material removal process in micro-milling when the edge radius is large relative to the feed rate is influenced by three types of material removal mechanisms during micro-machining [86] as discussed in chapter 2. These mechanisms are described as (Figure 3.3):

- Elastic deformation: When the uncut chip thickness is below the critical value h_m and only elastic deformation occurs in the workpiece. Then, the deformed material fully recovers to its original position, and as a result, no chip is formed (rubbing, plowing phenomenon).

- Elastic-plastic deformation: As the uncut chip thickness increases near h_m, an elastic-plastic deformation occurs in the workpiece where there is a constant percentage (p_e) of the material undergoing plastic deformation.

- Plastic deformation: Over h_m the workpiece material is removed by the cutter as a chip and the elastic recovery is very small ($p_e = 0$) and negligible (shearing-dominated zone).

These types of material removal mechanisms may occur in a single path of each flute as depicted in Figure 3.4. The region of elastic-plastic deformation is very small and can be ignored in the cutting force modeling. As these forces are calculated also depending on the undeformed chip thickness, the determination of the true trajectories of the cutting edges relative to the workpiece is essential.

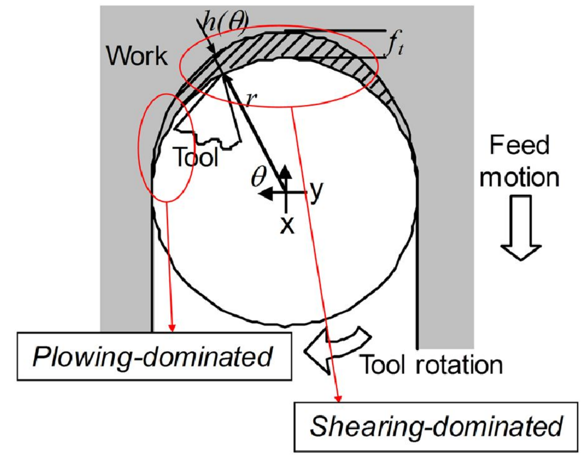

Figure 3.3: Switchover between cutting mechanisms during micro-milling [87].

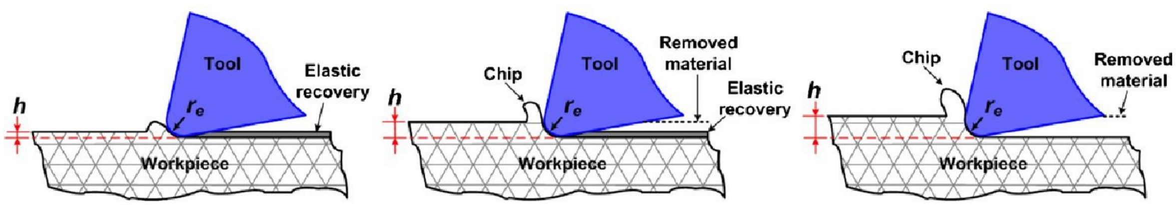

(a) $h < h_m$ (b) $h \cong h_m$ (c) $h > h_m$

Figure 3.4: Chip formation relative to the minimum chip thickness in micro-scale machining [7]

For above mentioned purpose, the earliest milling studies [131, 96, 8, 214] considered a circular tool path. This trajectory produces a sinusoidal variation in chip thickness and is given by:

$$\begin{aligned} h &= r + f_t \sin\theta - \sqrt{r^2 - f_t^2 \cos^2\theta} \\ h &= f_t \sin\theta \qquad\qquad \textit{when small } \tfrac{f_t}{r} \end{aligned} \tag{3.1}$$

where h represents nominal uncut chip thickness, for a position angle θ, r is the radius of the tool, and f_t is the feed per tooth. This approach provides the simplest approximation and avoids complex numerical calculations for cases where the feed per tooth is much smaller than the cutting tool diameter. However, the presence of run-out (or a cutter offset with respect to the center of rotation) and deflection, causes a deviation in tool tip trajectory and chip load to vary over the rotation of a multi-tooth cutter. This varying chip load will affect average forces, peak forces and the instantaneous force profile to different degrees depending on the cutting conditions, cut geometry and characteristics of the run-out. This will, of course, impact the problems of cutter breakage, cutter wear, the surface error generation mechanism and the dynamic behavior of the machine tool and cutting process. Thus, this conventional computation model of uncut chip thickness cannot precisely describe the actual chip formation of micro-end-milling [113].

Bao and Tansel [16] investigated the cutting force characteristics of micro-end-milling operations with tool run-out. They developed a new chip thickness model using a geometric approach that considers a trochoidal tool tip trajectory (Figure 3.5). Their proposed simplified model is given by:

$$h = f_t \sin\theta - \frac{z}{2\pi r} f_t^2 \sin\theta \cos\theta + \frac{f_t^2}{2r} \cos^2\theta \tag{3.2}$$

where h is the undeformed chip thickness, r is the radius of the tool, z is the number of cutting flutes, f_t is the feed per tooth and θ is the angular position of the tool. If the physical meaning of each term of the expression Eq.3.2 is evaluated, the first term is a major contributor to the chip thickness. In the conventional model (Eq.3.1), only this term was considered. The second term presents the difference between up and down-milling (the chip thickness of down-milling is always bigger than that of up-milling) and the third term is an additional chip thickness [16]. It must be noted that their model assumed that in milling, the feed per tooth to the tool radius ratio (f_t/r) is very high. But it cannot be generalized as it depends on the size of the product and the required machining parameters.

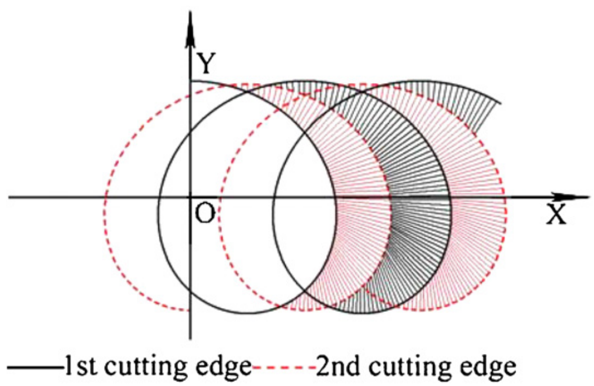

Figure 3.5: Graph of determined chip thickness by a conventional algorithm for a two-flute tool [113].

Li, Liu, and Li [114] developed a numerical method to evaluate undeformed chip thickness for engaged cutting tooth through finding the interception point of the path curve described by the proceeding tooth and the line of the current tool tip and tool axis. The closed form of his model is given as:

$$h \cong r \left[1 - \sqrt{1 - \frac{2 f_t \sin\theta}{r + \frac{z f_t}{2\pi} \cos\theta} - \frac{f_t^2 \cos(2\theta)}{\left(r + \frac{z f_t}{2\pi} \cos\theta\right)^2} + \frac{f_t^3 \sin\theta \cos^2\theta}{\left(r + \frac{z f_t}{2\pi} \cos\theta\right)^3}} \right] \tag{3.3}$$

Vogler, Kapoor, and DeVor [202] proposes an algorithm, consisting on the following steps:

1. Compute the rotation angle θ_{fi} of flute f_N during the ith tool pass as:

$$\theta_{fi} = \theta - \frac{2f_N\pi}{N} - \frac{\tan\beta}{r}z \tag{3.4}$$

   where β is the helix angle, and z is the coordinate of the point under consideration.

2. Evaluate the coordinates of the tool center (x_{ci}, y_{ci}) in the presence of runout

$$\begin{aligned} x_{ci} &= \tfrac{2f_t\theta}{2\pi} + \rho\sin(\theta-\alpha) \\ y_{ci} &= \rho\cos(\theta-\alpha) \end{aligned} \tag{3.5}$$

   where ρ is the magnitude of the parallel axis offset distance, and α is the locating angle of the offset axis.

3. Obtain the coordinates of the cutting edge (x_{fi}, y_{fi}) as:

$$\begin{aligned} x_{fi} &= x_c + r\sin\theta_{fi} \\ y_{fi} &= y_c + \rho\cos\theta_{fi} \end{aligned} \tag{3.6}$$

4. Beginning with the tool pass 0, the rotation angle θ_0 results in the cutting edge f_0 intersecting the line connecting the tool center and the cutting edge of the ith tool pass. The current angular location θ_{fi} is added to the workpiece surface, and the angular location for the previous tool pass θ_{f0} is removed from the workpiece surface. If the value of θ_{f0} does not lie on the surface for the zeroth tool pass, then the procedure is repeated for the next tool pass until either an intersection has been found or until all tool passes have been tried. The above coordinates are illustrated in Figure 3.6 for 1.5 revolutions with a two-fluted end-mill.

$$h = r - \sqrt{(x_{f0} - x_{ci})^2 + (y_{f0} - y_{ci})^2} \tag{3.7}$$

The model proposed by Jun et al. [86, 85] considers the elastic-plastic nature in the plowing process to study its effects on a cutting force model. A comprehensive chip thickness model was developed to determine the effects of the trochoidal toolpath, minimum chip thickness, elastic recovery and tool vibrations (or process faults). The micro-end-mill in presence of process faults is shown in Figure 3.7.

The $X-Y-Z$ frame is the reference plane and $\bar{X}-\bar{Y}-\bar{Z}$ axes with origin at O, define the rotating spindle frame. The tool also rotates about the z axis where $x-y-z$ axes define the shank frame. The $x_t - y_t - z_t$ axes define the tool frame in the presence of the faults at the tool (cutting edges). The process fault variables associated with misalignment at the spindle and manufacturing errors at the cutting edges are defined as the following: ε_s, shank parallel offset run-out; λ_s, shank parallel offset runout locating angle; α_s, spindle/shank tilt; ϕ_s, spindle/shank tilt locating angle; ε_t, tool parallel offset run-out; λ_t, tool parallel offset runout locating angle; α_t, tool tilt; ϕ_t, tool tilt locating angle.

The steps to determine the uncut chip thickness as proposed by Jun et al. [86, 85] are:

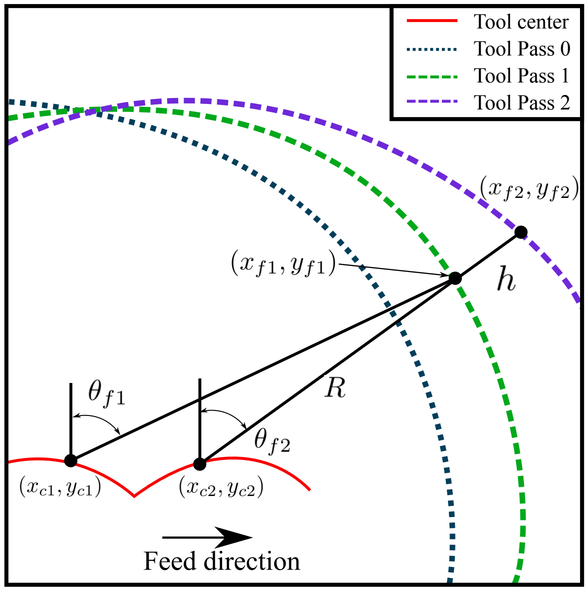

Figure 3.6: Illustration of chip thickness computation [202].

- Determine the net shank run-out r_s for the i_sth disk element and its locating angle ϕ_{Ls}, where the subscripts s and t are for the shank and the tool, respectively (Figure 3.7).

$$\begin{aligned} r_s(i_s)^2 &= \epsilon_s^2 + \tan^2\alpha_s Z_s(i_s)^2 + 2\epsilon_s \tan\alpha_s Z_s(i_s)\cos\phi_s \\ \phi_{Ls}(i_s, i_t) &= \begin{cases} \lambda_s(i_t) + \phi_s - \phi_{Rs}(i_s) & if \quad \phi_s < \pi \\ \lambda_s(i_t) + \phi_s + \phi_{Rs}(i_s) & otherwise \end{cases} \end{aligned} \tag{3.8}$$

where

$$\begin{aligned} \lambda_s(i_t) &= \lambda_s + (L_t - Z_t(i_t))\tfrac{\tan\beta}{R} \\ \phi_{Rs}(i_s) &= \tan^{-1}\left(\tfrac{\epsilon_s \sin\phi_s}{Z_s(i_s)\tan\alpha_s + \epsilon_s\cos\phi_s}\right) \end{aligned} \tag{3.9}$$

and β is the helix angle. Note that $\lambda_s(i_t)$ is respect to the cutting edge locations, then, $Z_t(i_t)$ is the distance to the i_tth element (Figure 3.8).

- Determine the net tool runout r_t for the i_tth disk element and its locating angle ϕ_{Lt} as follows:

$$\begin{aligned} r_t(i_t)^2 &= \epsilon_t^2 + \tan^2\alpha_t Z_t(i_t)^2 + 2\epsilon_t \tan\alpha_t Z_t(i_t)\cos\phi_t \\ \phi_{Lt}(i_t) &= \begin{cases} \lambda_t(i_t) + \phi_t - \phi_{Rt}(i_t) & if \quad \phi_t < \pi \\ \lambda_t(i_t) + \phi_t + \phi_{Rt}(i_t) & otherwise \end{cases} \end{aligned} \tag{3.10}$$

where

$$\begin{aligned} \lambda_t(i_t) &= \lambda_t + (L_t - Z_t(i_t))\tfrac{\tan\beta}{R} \\ \phi_{Rt}(i_t) &= \tan^{-1}\left(\tfrac{\epsilon_t \sin\phi_t}{Z_t(i_t)\tan\alpha_t + \epsilon_t\cos\phi_t}\right) \end{aligned} \tag{3.11}$$

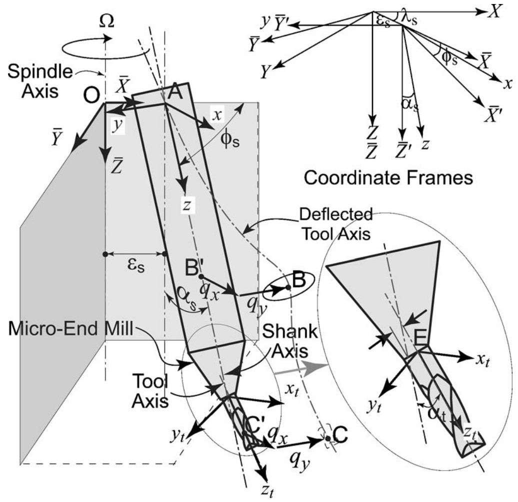

Figure 3.7: Coordinate frames for the micro-end-mill in the presence of process faults [86].

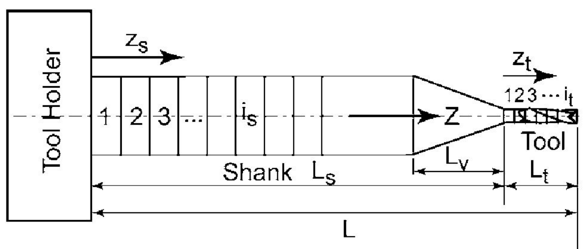

Figure 3.8: Discretization of the micro-tool [86].

- Evaluate the total net runout r and its locating angle ϕ_L from:

$$
\begin{aligned}
r(i_t)^2 = r_s(N_s+i_t)^2 + r_t(i_t)^2 + 2r_s(N_s+i_t)r_t(i_t)\cos(\phi_{Lt}(i_t) - \phi_{Ls}(N_s+i_t,i_t)) \\
\phi_L(i_t) = \begin{cases} \phi_{Ls}+\phi_R & if \quad \phi_{Ls} < \phi_{Lt}\, or\, \phi_{Ls} > \phi_{Lt}+\pi \\ \phi_{Ls}-\phi_R & otherwise \end{cases} \\
\phi_R = \cos^{-1}\left(\frac{r(i_t)^2 + r_s(N_s+i_t)^2 - r_t(i_t)^2}{2r_s(N_s+i_t)r(i_t)}\right)
\end{aligned}
\tag{3.12}
$$

where N_s is the number of elements on the shank.

- Calculate the radius at which each cutting edge rotates:

$$R_c(i_t,j) = \left[r(i_t)^2 + R^2 + 2r(i_t)R\cos(\phi_L(i_t) + (j-1)\theta_p)\right]^{1/2} \tag{3.13}$$

where R is the radius of the tool and θ_p is the pitch angle between flutes.

- Calculate the cutting edge locations from the trochoidal path trajectory:

$$
\begin{aligned}
x_{F_i^j}(i_t) &= R_c(i_t, j)\cos\psi + x_{C_i^j}(i_t) \\
y_{F_i^j}(i_t) &= R_c(i_t, j)\sin\psi + y_{C_i^j}(i_t)
\end{aligned}
\tag{3.14}
$$

where ψ is the rotation angle of the tool. $\left(x_{F_i^j}, y_{F_i^j}\right)$ represents the position of the cutting edge of the jth flute for the ith disk element, and $\left(x_{C_i^j}, y_{C_i^j}\right)$ represents the tool position as shown in Figure 3.9.

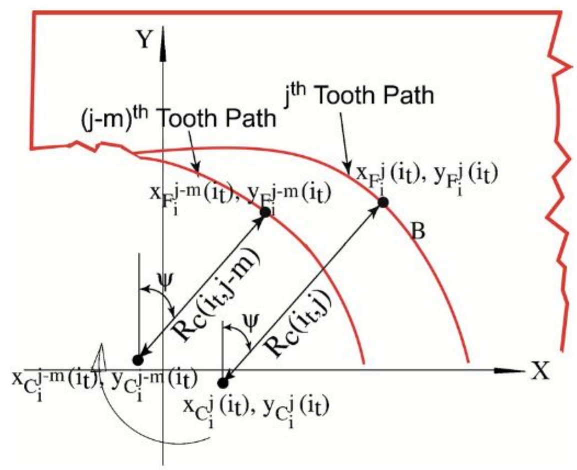

Figure 3.9: Positions for chip thickness calculation [86].

- Figure 3.10 shows the surface generation and chip thickness computation in the presence of elastic recovery, which is represented as the shaded region. Points C and F represent the tool center and cutting edge locations, respectively. The superscript denotes the tooth pass number, and the subscript represents the rotational angle. Point I is found at the intersection between the previously generated surface from the previous tooth pass and the line connecting C and F for the current tooth pass. Then, the chip thickness can be formulated as:

$$
h = max\left(0, \left\|C_i^j F_i^j\right\| - \left\|C_i^j I_i^{j-1}\right\|\right) \tag{3.15}
$$

Their model, also includes the effect of elastic recovery, by considering that the surface springs back by the amount of κh, where κ is the elastic recovery rate expressed as:

$$
\kappa = \begin{cases} 1.0 & when \quad h < h_e r \\ p_e & when \quad h_e r < h < h_m \\ 0 & when \quad h > h_m,\ or\, h = 0 \end{cases} \tag{3.16}
$$

Li et al. [113] proposed a model based on iterative process indicated in Figure 3.11. The steps required for this method are given as:

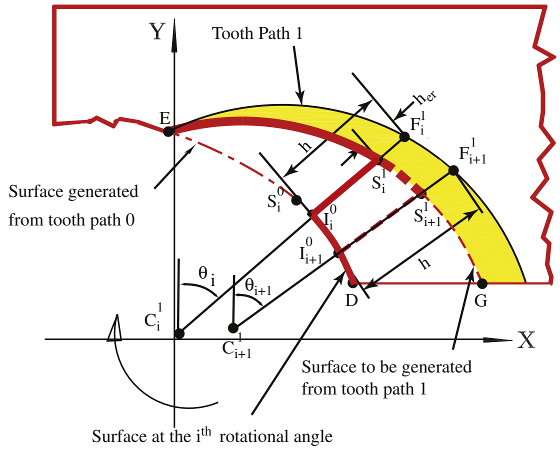

Figure 3.10: Chip thickness model considering elastic recovery [86].

1. The trajectory of the kth tool tip at time t can be described by:

$$\begin{aligned} x(t,k) &= \tfrac{ft}{60} + r\sin\left(\omega t - \tfrac{2\pi k}{K}\right) + r_o \sin\left(\omega t + \gamma\right) \\ y(t,k) &= r\cos\left(\omega t - \tfrac{2\pi k}{K}\right) + r_o \cos\left(\omega t + \gamma\right) \end{aligned} \tag{3.17}$$

   where f is the feed rate (mm/min), ω is the spindle speed (rad/s), r_o is the runout length (mm), γ the runout angle (rad) and r is the tool radius (mm).

2. Apply Newton-Raphson iterative method to solve time t_s in the following equation:

$$\begin{aligned} F(t_s) = r\tan\left(\omega t - \frac{2\pi k}{K}\right)\cos\left[\omega t_s - \frac{2\pi(k-1)}{K}\right] + r_o \tan\left(\omega t - \frac{2\pi k}{K}\right)\cos\left(\omega t_s + \gamma\right) \\ - r_o \tan\left(\omega t - \frac{2\pi k}{K}\right)\cos\left(\omega t_s + \gamma\right) - \frac{ft_s}{60} + \frac{ft}{60} - r\sin\left[\omega t_s - \frac{2\pi(k-1)}{K}\right] \\ - r_o \sin\left(\omega t_s + \gamma\right) + r_o \sin\left(\omega t + \gamma\right) = 0 \end{aligned} \tag{3.18}$$

   where a proper initial value can be defined based on the periodicity of chip formation:

$$t_{s_0} = t - \frac{2\pi}{\omega K} \tag{3.19}$$

   According to Newton-Raphson iterative method, for each loop, t_{s_i} can be updated according to value of $t_{s_{i+1}}$ which can be determined from the following equation:

$$t_{s_{i+1}} = t_{s_i} - \frac{F(t_{s_i})}{F'(t_{s_i})} \tag{3.20}$$

   where $i = 0, 1, 2, \ldots$. According to Li et al. [113], the value of t_s corresponding to any time t will converge only through less than five iterative loops even though ε is as small as 0.0001% of tool radius. $F'(t_{s_i})$ can be evaluated as the time derivative of the $F(t_{s_i})$

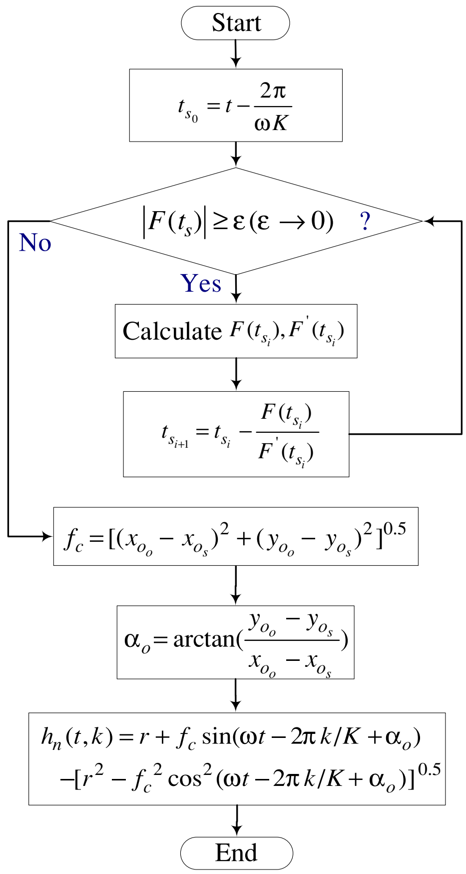

Figure 3.11: Procedure of the iterative algorithm for uncut chip thickness (h_n) [113].

function:

$$\begin{aligned} F'(t') = -\omega \Bigg[& r \tan\left(\omega t - \frac{2\pi k}{K}\right) \sin\left(\omega t' - \frac{2\pi(k-1)}{K}\right) \\ & + r_o \tan\left(\omega t - \frac{2\pi k}{K}\right) \sin\left(\omega t' + \gamma\right) + r \cos\left(\omega t' - \frac{2\pi(k-1)}{K}\right) \\ & + r_o \sin\left(\omega t' + \gamma\right) - f/60 \end{aligned} \quad (3.21)$$

3. Calculate the the distance between the two tool center points O and point O_0 which correspond to time t and time t respectively, namely f_c and evaluate the nominal uncut chip thickness (h_n):

$$f_c = \left[(x_{O_o} - x_{O_s})^2 + (y_{O_o} - y_{O_s})^2\right]^{1/2} \quad (3.22)$$

$$h_n(t,k) = r + f_c \sin\left(\omega t - \frac{2\pi k}{K} + \alpha_0\right) - \left[r^2 - f_c^2 \cos^2\left(\omega t - \frac{2\pi k}{K} + \alpha_0\right)\right]^{1/2} \quad (3.23)$$

where $\alpha_0 = \arctan\left(\frac{y_{O_o} - y_{O_s}}{x_{O_o} - x_{O_s}}\right)$

4. When the current engagement h_a is smaller than the minimum chip thickness, the workpiece elastically and plastically deforms under the action of cutting forces. In this scenario, the actual uncut chip thickness may be expressed as:

$$h_a\left(t + \frac{2\pi}{\omega K}, k+1\right) = h_a(t,k) + h_n\left(t + \frac{2\pi}{\omega K}, k+1\right) \tag{3.24}$$

If the current cut is larger than the minimum chip thickness, then material is assumed to be removed as a chip ($h_a \geq h_{min}$). Therefore, the actual uncut chip thickness can be determined by:

$$h_a\left(t + \frac{2\pi}{\omega K}, k+1\right) = h_n\left(t + \frac{2\pi}{\omega K}, k+1\right) \tag{3.25}$$

Bissacco, Hansen, and Slunsky [20] consider the corresponding edge segment cutting at any instant. This is done by means of a mathematical relationship dr(z) that expresses the radial offset of the flute j as a function of the axial position z. Thus, taking into account the surface generated by the previous tooth $j-1$, the instantaneous uncut chip thickness for flute j, at axial level z and angular position θ can be calculated by means of the following equations as shown in Figure 3.12, where r is the nominal end mill radius and f_z is the feed per tooth:

$$\begin{gathered} \gamma = \tfrac{\pi}{2} - \theta - \arctan\left(\tfrac{r\cos\theta}{f_t + r\sin\theta}\right) \\ h_j = f_t \sin\theta + dr_j - \tfrac{dr_{j-1}}{\cos\gamma} \end{gathered} \tag{3.26}$$

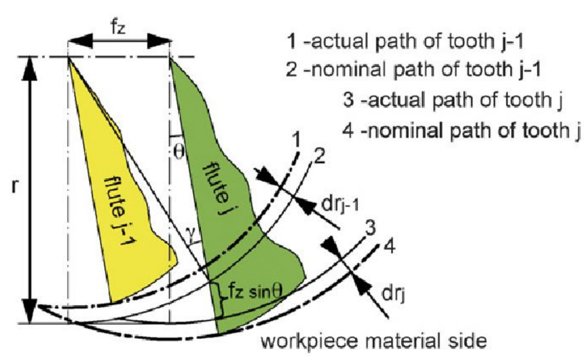

Figure 3.12: Effect of run out on chip thickness calculation in down milling mode [20]

Zhang, Yu, and Wang [217] proposed an instantaneous uncut chip thickness model that accounts for the cutting edge radius size effect, tool run-out, tool deflection and the exact trochoidal trajectory of tool flute. The variations of entry and exit angles of tool caused by tool run-out are also concerned in their model. The theoretical undeformed chip thickness is calculated as a function of the micro-end-mill center position for each z-axis (tool axis) disk element, which represents an elemental cutting edge segment. Also, four tool parameters are included: offset distance (ρ), direction angle of tool axial offset (α), tilt angle between tool axis and spindle axis (τ) and local tilt angle (ϕ). Their model can be applied based on the following steps:

1. Apply Newton-Raphson iterative method to solve time t' in the following equation:

$$
\begin{aligned}
F(t') = f_t t + (R(z) - R)\sin\left(\alpha_0 + \omega t - \frac{z\tan\lambda_s}{R} + \frac{2\pi j}{N_z}\right) + R\sin\psi(t) \\
- f_t t' - (R(z) - R)\sin\left(\alpha_0 + \omega t' - \frac{z\tan\lambda_s}{R} + \frac{2\pi(j-1)}{N_z}\right) - R\sin\psi(t') \\
- \tan\psi(t)\,(R(z) - R)\cos\left(\alpha_0 + \omega t - \frac{z\tan\lambda_s}{R} + \frac{2\pi j}{N_z}\right) - R\tan\psi(t)\cos\psi(t) \\
+ \tan\psi(t)\,(R(z) - R)\cos\left(\alpha_0 + \omega t' - \frac{z\tan\lambda_s}{R} + + \frac{2\pi(j-1)}{N_z}\right)
\end{aligned} \tag{3.27}
$$

where the radius of the tool (R), helix angle (λ_s), number of tooth (N_z), spindle speed in rad/s (ω), axial depth of cut (a_p), radial depth of cut (a_e), feed per tooth f_z, tool run-out offset ($R(z)$). An initial guess value can be taken as follows:

$$t'_o = t - \frac{2\pi}{\omega K} \tag{3.28}$$

Also, the tool run-out offset and tilt can be expressed as follows:

$$
\begin{aligned}
R(z) = \Bigg[\rho^2 + R^2 + (L-z)^2\sin\tau + 2R\rho\cos\left(-\alpha + \varphi + \frac{2j\pi}{N_z}\right) \\
+ 2(L-z)\sin\tau\left(\rho\cos\phi + R\cos\left(\phi - \alpha + \varphi + \frac{2j\pi}{N_z}\right)\right)
\end{aligned} \tag{3.29}
$$

where L is the tool overhang length after installation. The corresponding lag angle, $\varphi(z)$ at a specified axial depth z, can be expressed as:

$$\varphi(z) = \frac{z\tan\lambda_s}{r} \tag{3.30}$$

2. Evaluate the coordinates of point Q on the trajectory of the $(j-1)$th tooth:

$$
\begin{aligned}
x_Q = f_t t' + (R(z) - R)\sin\left(\alpha_0 + \omega t' - \tfrac{z\tan\lambda_s}{R} + \tfrac{2\pi(j-1)}{N_z}\right) + R\sin\psi(t') \\
y_Q = (R(z) - R)\cos\left(\alpha_0 + \omega t' - \tfrac{z\tan\lambda_s}{R} + + \tfrac{2\pi(j-1)}{N_z}\right) + R\cos\psi(t')
\end{aligned} \tag{3.31}
$$

Correspondingly, the coordinates of P on the trajectory of the jth tooth are:

$$
\begin{aligned}
x_P = f_t t + (R(z) - R)\sin\left(\alpha_0 + \omega t - \tfrac{z\tan\lambda_s}{R} + \tfrac{2\pi j}{N_z}\right) + R\sin\psi(t) \\
y_P = (R(z) - R)\cos\left(\alpha_0 + \omega t - \tfrac{z\tan\lambda_s}{R} + + \tfrac{2\pi j}{N_z}\right) + R\cos\psi(t)
\end{aligned} \tag{3.32}
$$

Then $\psi(t)$ is given by:

$$\tan \psi(t) = \frac{x_P - x_Q}{y_P - y_Q} \tag{3.33}$$

3. The theoretical instantaneous uncut chip thickness with tool run-out can be determined as follows:

$$h_c = \left[(x_P - x_Q)^2 + (y_P - y_Q)^2 \right]^{1/2} \tag{3.34}$$

For comparison purposes, Figure 3.13 illustrates the difference between models predictions for uncut chip thickness variation due to tool rotation and run-out. The cutting parameters are based on a two-fluted end-mill tool of 1000 μm diameter, rotating at 25.000 RPM with a feed of 3 $\mu m/tooth$ and a run-out of 0.5 μm with an angle of 45°. It can be noted the difference between the model proposed by Martellotti [131] and the one proposed by Li et al. [113], being the latest the one that includes the tool runout effects.

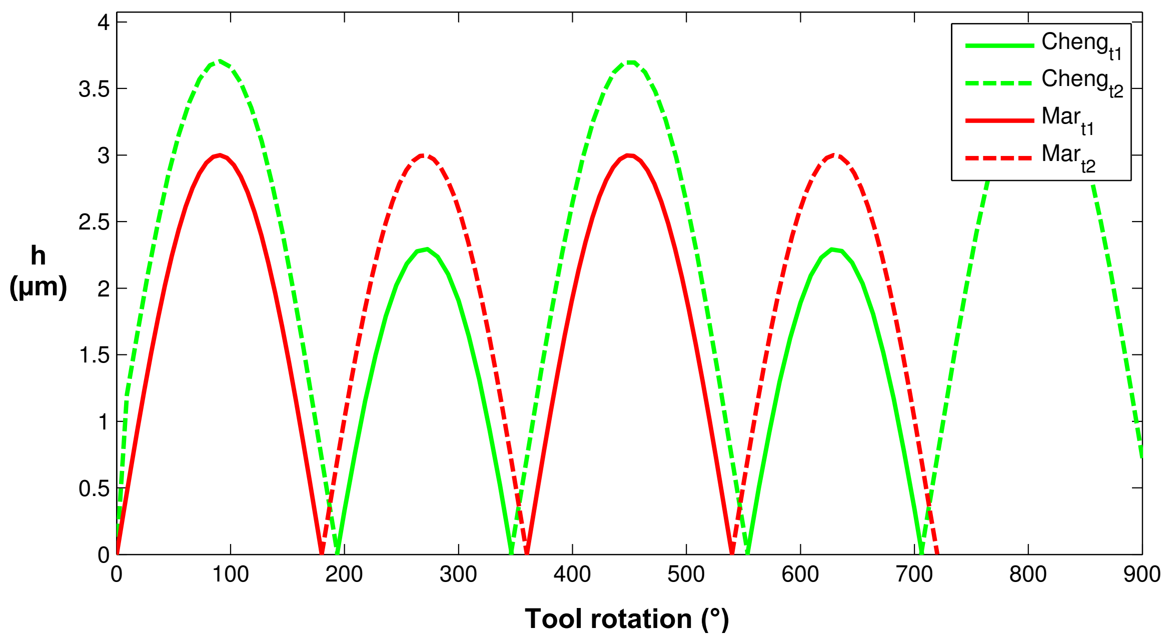

Figure 3.13: Uncut chip thickness models comparison.

3.3.2 Tool-workpiece dynamics

Due to their small diameter, micro-milling tools have much lower stiffness but experience much higher stress variation on the shaft while compared with conventional tools; this makes them more prone to tool wear and breakage [33].

Then, while fully considering the combination of the exact trochoidal trajectory of the tool tip, tool run-out and machining system dynamics, the milling process becomes highly intermittent, especially when the magnitude of the tool run-out and dynamic vibration is comparable to the feed rate. Cutting edges may not be in contact with the workpiece for some time during one tooth passing period. The chip generated by one cutting tooth is intermittent even in one tool edge passing period.

The tool and workpiece system are schematically represented in Figure 3.14, where the vibration of both components will change the real trajectory during machining. Hence the actual uncut chip thickness becomes very complicated when considering tool run-out, the dynamic performance of the cutting system and the transient separation of the tool-workpiece interface.

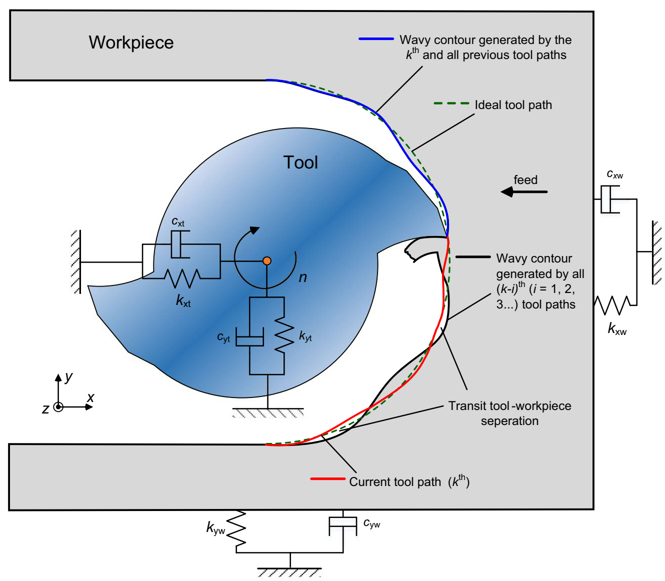

Figure 3.14: Schematic of micro-milling dynamic system [33].

To establish the dynamic model of the system, two interacting loops can be considered and simplified within two degrees of freedom in x (feed direction) and y (cross feed direction), respectively. Then, the equations of motion are given as follows:

$$\begin{gathered} m_{xt}\ddot{x}_t(t) + c_{xt}\dot{x}_t(t) + k_{xt}x_t(t) = F_x(t) \\ m_{yt}\ddot{y}_t(t) + c_{yt}\dot{y}_t(t) + k_{yt}y_t(t) = F_y(t) \\ m_{xw}\ddot{x}_w(t) + c_{xw}\dot{x}_w(t) + k_{xw}x_w(t) = -F_x(t) \\ m_{yw}\ddot{y}_w(t) + c_{yw}\dot{y}_w(t) + k_{yw}y_w(t) = -F_y(t) \end{gathered} \tag{3.35}$$

where m, c and k are the mass, damping, and stiffness of the cutter-machine (t) or the workpiece (w) in each direction. F represents the instantaneous cutting force, and $\ddot{x}$, $\dot{x}$ and x are the accelerations, velocities, and positions of the cutter (t) or the workpiece (w). This model can be transformed into the frequency domain by applying Laplace transform:

$$\begin{aligned} X_t(s) &= \left(m_{xt}s^2 + c_{xt}s + k_{xt}\right)^{-1} F_x(s) \\ Y_t(s) &= \left(m_{yt}s^2 + c_{yt}s + k_{yt}\right)^{-1} F_y(s) \\ X_w(s) &= -\left(m_{xw}s^2 + c_{xw}s + k_{xw}\right)^{-1} F_x(s) \\ Y_w(s) &= -\left(m_{yw}s^2 + c_{yw}s + k_{yw}\right)^{-1} F_y(s) \end{aligned} \tag{3.36}$$

Then, the relative dynamic displacements between the tool and the workpiece can be calculated from:

$$\Delta x = x_t - x_w \Delta y = y_t - y_w \tag{3.37}$$

After applying a proper parameter identification for the previous equation, and static cutting force predictions (with empirical, numerical or mechanistic models) the dynamic displacements can be calculated at each time increments. Through this methodology, the dynamic chip thickness and the real tool trajectory can be obtained, also allowing to simulate the topography of the machined surface [137].

Parameters, as mentioned above, must be found experimentally for accurate chatter prediction. Chatter unstable vibration is a result of a self-excitation mechanism in the generation of chip thickness during cutting operations. In the case of micro-milling, often a combination of Experimental Modal Analysis (EMA) and Receptance Coupling (RC) is employed to identify tool tip dynamics [1, 69, 27]. EMA is an experimental method to acquire dynamic parameters of mechanical systems. Usually, impact hammers are used to deliver initial exciting forces and measure the response through sensors. This type of testing cannot be applied to micro-milling due to the fragility of the tool; instead, RC is used to combine EMA results and finite element model of the micro-tool to obtain the dynamics of the tool. The RC technique allows separating the system into a lower substructure A containing the cutting portion (simulated by FE) and an upper part, substructure B (analyzed by EMA). The EMA is applied through the use of impact hammers and accelerometers on blank cylinders [69, 27] with reduced overhand (less than 15mm), then the joint of the substructures is assumed to be rigid, and the frequency response functions can be assembled based on the compatibility and equilibrium conditions. The FE analysis of the remaining tool can be modeled using Timoshenko beam theory, and by using the compatibility conditions of the joint, the tooltip dynamics is obtained with:

$$G_{11} = \frac{X_1}{F_1} = H_{11} - H_{12}\left(H_{22} + H_{33}\right)^{-1} H_{21} \tag{3.38}$$

where G and H denote the assembled and substructure dynamics respectively. X_1 and F_1 are the displacement and force applied at point 1. H_{33} is found directly through impact hammer tests at point 3, and the rests can be calculated from FEA. It is common to simplify the helix portion of a cutting tool to a cylinder of reduced diameter for FEA to reduce computational costs. For two-fluted helix tools, it has been found that the simplified equivalent diameter model that best matched the helix model results when the cylinder diameter is 68% of the cutter diameter [69].

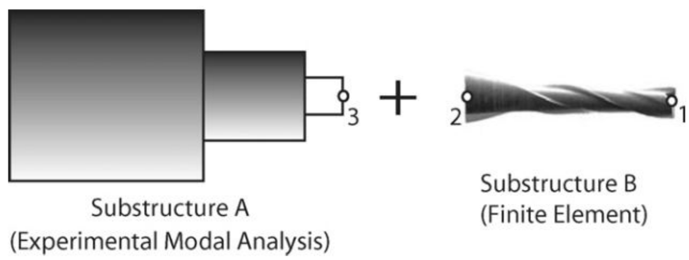

Figure 3.15: Receptance coupling modeling of micro-end-mill [128].

Different approaches have been used for tool tip dynamic studies. Vogler, DeVor, and Kapoor [200] analyzed the spectrum of the cutting force while micro-milling slots in single-phase ferrite and pearlite and multiphase ductile iron. Their results state the presence of high-frequency components in the ductile iron, mainly due to the multiphase micro-structure. Figure 3.16 illustrates frequency components around 15 kHz corresponding to a wavelength of 53.3 μm in the experimental data. This wavelength is close to the ferrite grain spacing of 50 μm used to generate a microstructure with near 70% ferrite by volume. The same technique was applied by Afazov et al. [1] who used the Fast Fourier Transform (FFT) to the measured cutting forces to recognize chatter if the FFT force magnitude is high at the tool natural frequency. Figure 3.17 illustrates their results while comparing to chatter stability lobes for micro-milling AISI4340 with TiN coated tools of 500 μm diameter and two flutes.

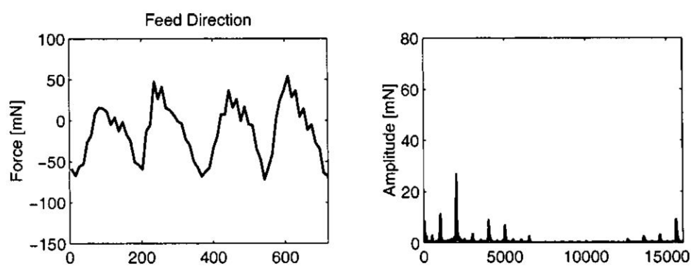

Figure 3.16: Cutting forces in the micro milling of ferritic ductile iron [200].

Malekian, Park, and Jun [127] developed chatter stability lobes of ploughing dominant full immersion micro-milling operations in Al6061 (Figure 3.18), indicating that to accurately capture the cutting forces, regenerative chatter-free machining conditions are imperative. Also, eliminating chatter becomes an integral part of optimizing machining operations to increase the tool life, and improve the machined surface quality [69].

3.4 Material and tool modeling

Material properties like flow stress used for metal cutting should be determined under conditions involving large strains, high strain rates and elevated temperatures [38]. The constitutive equations that describe the flow stress or instantaneous yield strength at which work material

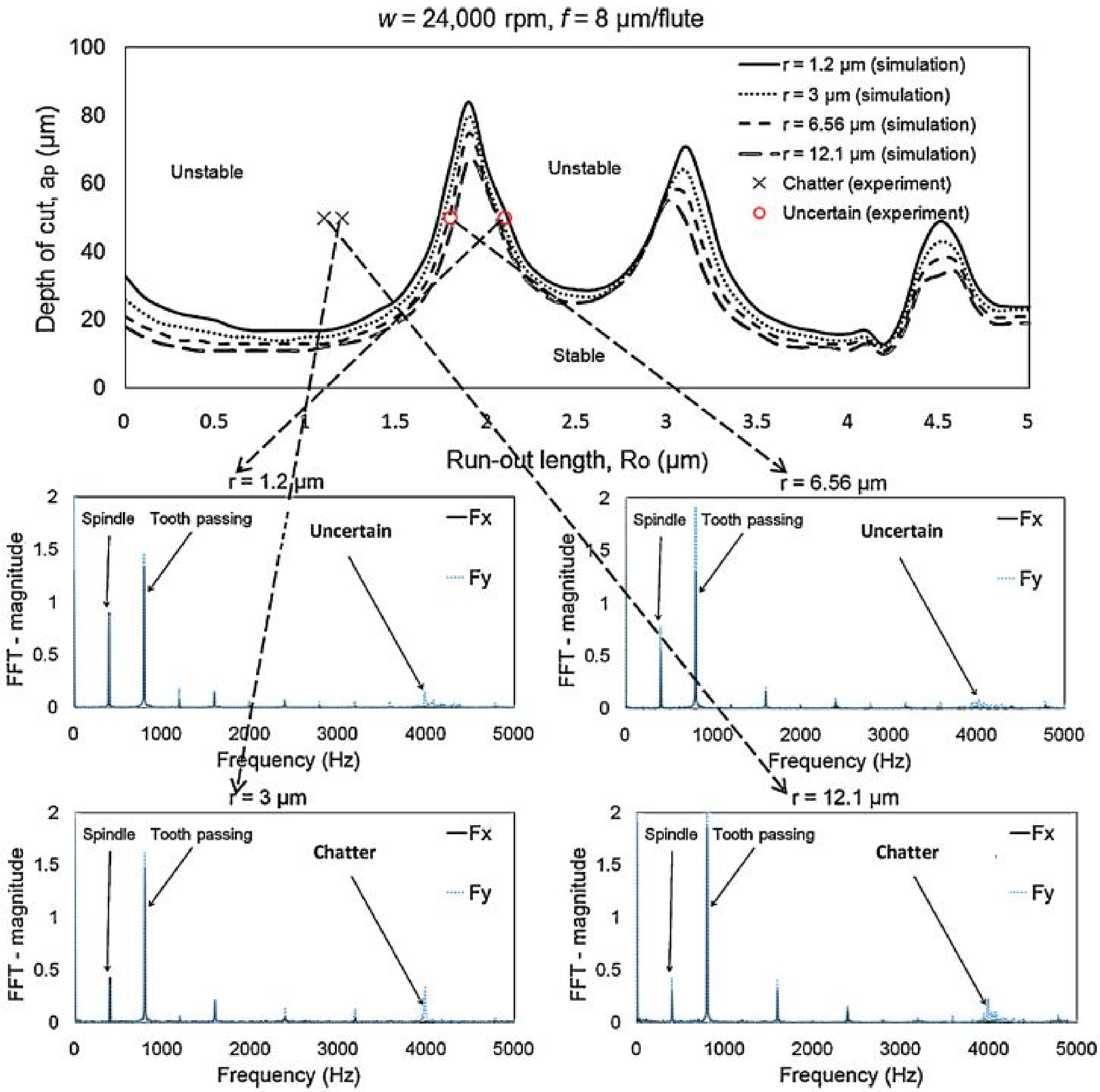

Figure 3.17: Experimental and modeled stable micro-milling AISI 4340 [1].

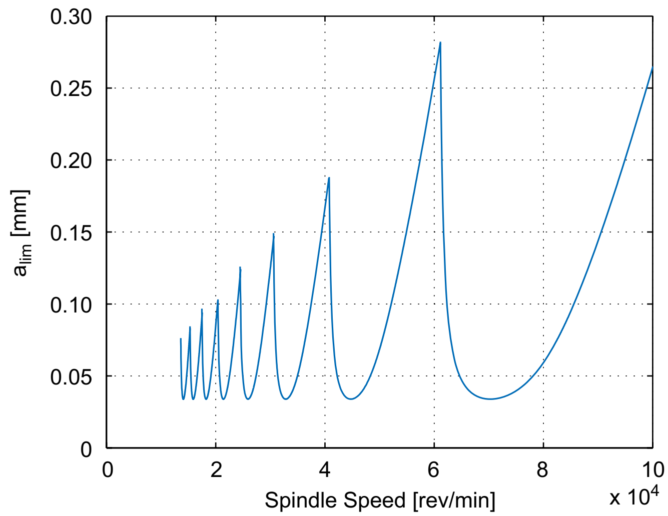

Figure 3.18: Regenerative chatter stability lobes for full immersion micro-milling of Al6061 [127].

starts to plastically deform or flow have been extensively studied. The main flow constitutive models used in FEM are summarized in Table 3.1, among which the Johnson-Cook (JC) and its modified variants is the overwhelming commonly used model in machining simulations [117].

The first model is based on tabular data to relate stress with plastic strain, strain rate and temperature. The model suggested by Oxley, is related manly for carbon steel with σ_1 for the material flow stress and n as the strain hardening exponent. Both are functions of temperature T which allows the combined effect of temperature and strain rate $\dot{\varepsilon}$. Several relationships have been developed since this model ranging from isotropic elastic models suitable for large-scale structural modeling, to crystal plasticity formulations designed to capture grain scale inelastic behavior. Therefore, a prior knowledge of the deformation process is required for an adequate selection of the required model.

3.4.1 Johnson-Cook Model

The JC model consists of three terms, where the first one being the elasto-plastic term to represent strain hardening, the second is viscosity, which demonstrates that material flow stress increases for high strain rates and the temperature softening term; it is a thermo-elasto-visco-plastic material constitutive model, described as:

$$\sigma = \underbrace{(A + B\varepsilon^n)}_{\text{Elasto-plastic}} \underbrace{\left(1 + C \ln \frac{\dot{\varepsilon}}{\dot{\varepsilon}_0}\right)}_{\text{Strain rate sensitivity}} \underbrace{\left[1 - \left(\frac{T - T_r}{T_m - T_r}\right)^m\right]}_{\text{Thermal softening}} \tag{3.39}$$

Model	Representations	Constants
Tabular format	$\sigma = f\left(\varepsilon, \dot{\varepsilon}, T\right)$	N/A
Oxley	$\sigma = \sigma_1 \left(\varepsilon\right)^n$ $T_{mod} = T\left[1 - 0.09\log(\dot{\varepsilon})\right]$	σ_1, n
Vinh	$\sigma = F\varepsilon^n \left(\frac{\dot{\varepsilon}}{\dot{\varepsilon_0}}\right)^m \exp\left(\frac{W}{T}\right)$	F, n, m, W
Johnson and Cook	$\sigma = \left(A + B\varepsilon^n\right)\left(1 + C\ln\frac{\dot{\varepsilon}}{\dot{\varepsilon_0}}\right)$ $\left[1 - \left(\frac{T-T_r}{T_m-T_r}\right)^m\right]$	A, B, C, m, n
Shikarashi and Usui	$\sigma = A\varepsilon^n\dot{\varepsilon}^m\left[-\lambda\left(T - T_0\right)\right]$	A, m, n, λ
Zerilli and Armstrong	$\sigma = C_0 + C_1 exp\left[-C_2T + C_3T\ln\dot{\varepsilon}\right]$ $+C_4\varepsilon^{1/2}exp\left[-C_5T + C_6T\ln\dot{\varepsilon}\right]$	$C_0, C_1, C_2,$ C_3, C_4, C_5

Table 3.1: Main flow stress constitutive models [173, 84, 34].

where A is the yield stress of the material under reference deformation conditions (MPa), B is a strain hardening constant (MPa), n is a strain hardening coefficient, C represents a strain rate strengthening, m is a thermal softening coefficient, and T, T_r, T_m indicate the deformation, room and melting temperatures respectively.

The Johnson-Cook constitutive law appears very interesting to be used in metal machining simulation, since it allows the coupling between different effects (hardening, strain hardening, and thermal softening) with a reduced number of coefficients. Characterization data are needed to determine its parameters. These data must be representative of the studied material response under machining loading conditions. Experimental data are generally obtained at high strain rates (until $10^3 s^{-1}$) and low strains (< 0.5) using the Split Hopkinson Pressure Bar (SHPB) method but not in the range observed in cutting regimes [24, 39]. Besides, a wide availability of JC parameters can be found in literature (often not from specialized laboratories), but also, a large variation of parameter sets determined for the same material which cannot be ignored since it strongly influences on prediction quality in terms of material flow description, chip morphology, cutting forces, and temperature distribution once they are not suitably selected [211]. Other tests used are torsion tests, compression ring tests and projectile impact tests [39].

The JC model sometimes is combined with strain softening where the flow stress decreases with plastic strain or with a damage model. In the latter case damage (as explained in next section), ω is used to compute effective stress by [117]:

$$\sigma_{real} = \frac{\sigma_{nom}}{1 - \omega} \tag{3.40}$$

It most be noted that strain and thermal softening effects often causes notorious mesh dependency. A modified equation was developed by Calamaz, Coupard, and Girot [25], where the magnitude of strain softening is controlled by parameter f:

$$\sigma = \left(A + B\left(\frac{1}{\dot{\varepsilon}}\right)^{f} \varepsilon^{n-0.12(\varepsilon\dot{\varepsilon})^{f}}\right)\left(1 + C\ln\frac{\dot{\varepsilon}}{\dot{\varepsilon_0}}\right)\left[1 - \left(\frac{T - T_r}{T_m - T_r}\right)^{m}\right] \tag{3.41}$$

In their work, they state that the JC flow stress should not be adopted for strains larger than 0.3 an strain rates larger than $1000s^{-1}$. Another model was introduced by Karpat [92] for the FEM simulation of machining titanium alloy with a hyperbolic tangent function. The interrelationships between strain and temperature, strain and strain rate, and flow softening at high strains are added.

$$\sigma = (E\varepsilon^{n})\left(FT^{2} + GT + H\right)\left(1 - \left[1 - \left(\frac{\ln\dot{\varepsilon_0}}{\ln\dot{\varepsilon}}\right)^{q}\right]\frac{1}{L\tanh(\varepsilon)}\right)$$
$$\left(M + (1-M)\left[\tanh\left(\frac{1}{(\varepsilon + p)^{r}}\right)\right]^{s}\right) \tag{3.42}$$

Sima and Özel [181] introduced a model with better control on the thermal softening. In this model, the flow softening is defined with a decreasing behaviour in flow stress with increasing strain beyond a critical strain value, below this value, the material still exhibits strain hardening. Their model is given as:

$$\sigma = \left(A + B\varepsilon^{n}\left(\frac{1}{\exp\varepsilon^{g}}\right)\right)\left(1 + C\ln\frac{\dot{\varepsilon}}{\dot{\varepsilon_0}}\right)\left[1 - \left(\frac{T - T_r}{T_m - T_r}\right)^{m}\right]$$
$$\left[D + (1-D)\left[\tanh\left(\frac{1}{(\varepsilon + p)^{r}}\right)\right]^{s}\right] \tag{3.43}$$

where

$D = 1 - \left(\frac{T}{T_m}\right)^{l}$ and $p = \left(\frac{T}{T_m}\right)^{h}$

Lai et al. [104] proposes a new constitutive model, considering that conventional Johnson-Cook flow stress (σ_{jc}) is non-dimensional and independent of the length scale, and hence not suitable for describing the significant size effect in micro-cutting. Their strain gradient plasticity model includes the effect of material strengthening behavior and the minimum chip thickness. Their model can be expressed explicitly as:

$$\sigma = \sigma_{jc}\sqrt{1 + \left(\frac{18\alpha^{2}G^{2}b}{\sigma_{jc}^{2}L}\right)^{\mu}} \tag{3.44}$$

where the strain gradient parameters are given by G as the shear modulus (MPa), b the Burgers vector (nm), μ as the total dislocation density. L is the shear zone length and is given by:

$$L = \begin{cases} \frac{h}{\sin(\phi)} & when \quad h > h_m \\ \frac{\arccos\left(\frac{R-h}{R}\right)\pi R}{180} & when \quad h < h_m \end{cases} \tag{3.45}$$

where ϕ is the shear angle and R the cutter edge radius.

Daoud, Chatelain, and Bouzid [37] investigated the effect of three different sets of JC constants obtained from machining tests for three rake angles ($0°, -8°$ and $+8°$), where the predicted cutting forces error due to wrong set of parameters can be up to 30%, chip thickness and tool chip contact length also illustrated the same trend. Similar results were noted by Ducobu and Filippi [47] by using twenty sets of JC parameters for Ti-6Al-4V, noting significant differences of parameters and resulting flow stresses available in literature as depicted in Figure 3.19. Information concerning the experimental conditions of the tests and detailed material characteristics is required for a proper selection. Also, it is recommended to perform preliminary metal cutting simulations and compare the predicted results with those measured [219]; as constants are determined through curve fitting, the parameters cannot be extrapolated beyond the available data [84].

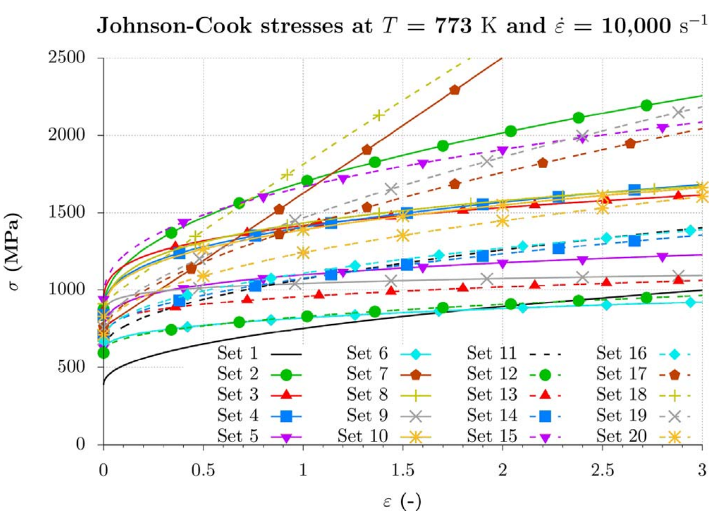

Figure 3.19: Stress-strain curves of twenty sets of JC parameters for Ti-6Al-4V [47].

3.4.2 Zerilli-Armstrong Model

An alternative constitutive model for metals is derived from dislocation mechanics theory with a crystal structure distinction by Zerilli and Armstrong. Their model was initially developed for relatively simple materials where the dislocation slip in several kind of crystal structures was considered. They distinguished two equations based on crystal structure of the material. One is for the body-centered cubic material (BCC) where temperature softening and strain rate hardening are higher with the increase of strain and another for face-centered cubic material (FCC) which exhibits dependencies of the strain hardening factor from the strain-rate hardening, thermal softening and the grain size.

Their model incorporates the thermal activation necessary in order for the overcoming obstacles for dislocation motion and dislocation interaction in materials (and the initial microstructure of the material) [84]. For machining, it must be modified for increased softening at large strains and high temperatures. Some studies have demonstrated its applications for analyzing the dynamic response of metals over a range of temperatures and strain rates with better or worse results compared to JC depending on mechanical characteristics [38, 136].

Identification of constitutive models parameters The parameters of the constitutive laws are obtained through testing material samples in experimental high speed equipment such as Taylor's impact tests or Hopkinson's compression and shear devices [11].

The Split Hopkinson Pressure Bar (SPHB), also referred to as Kolsky bar, is a technique where a short material is placed between two pressure bars. The specimen is loaded by a stress wave generated in one of the bars thanks to a pressure unit that generates a constant-amplitude pulse on a striker bar (Figure 3.20). Once the specimen is loaded, part of the loading wave propagates through to the other bar (known as transmitter bar) and part reflects back to the loading bar (incident bar). The load and deformation (until fracture) in the specimen are determined by monitoring the stress waves in the bars, which remain elastic during the test. Based on one-dimensional elastic wave propagation theory and on the records of the incident, reflected and transmitted pulses, the average compression strain, strain rate and stress at fixed temperature are obtained [110]. The technique was initially used for specimens loaded in compression, and has subsequently been modified for tension and torsion loadings allowing to generate strain rates on the order of 10^3 - $10^4 s^{-1}$ [186].

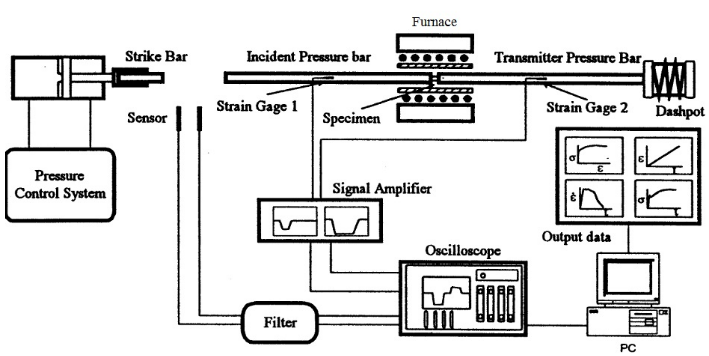

Figure 3.20: SPHB apparatus schematic [110].

Achieving higher strain rates ($10^6 - 10^8 s^{-1}$) than normally possible with a SHPB apparatus requires shock inducing impact tests. Even though flow stress curves cannot be extracted from these tests, constitutive models can be adjusted to match the shape of the deformed sample

[136]. A summary of the major testing regimes and the associated material test methods is shown in Figure 3.21.

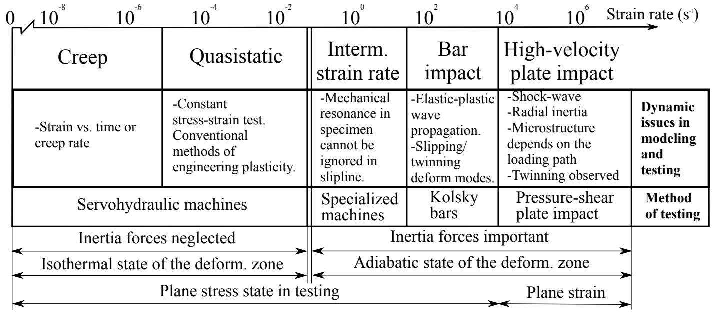

Figure 3.21: Techniques for different strain rate measurements [100].

3.4.3 Friction

Friction plays a significant effect on the simulated results such as cutting forces, temperature, chip geometry and tool wear in the machining simulation. In the micro-machining literature is possible to find a high range of friction coefficients and a variety of friction models for the tool-chip interface, but often the predictions are clearly found to be most accurate when utilizing friction models based on the measured normal and frictional stresses and when implemented as variable.

One of the most commonly used friction models is proposed by Zorev [223] and assumes that the interface area between chip and cutting tool can be divided into two regions (sticking and sliding regions)[173]. Near the tool tip, shear stresses are assumed to be equal to shear strength of the material being machined, whereas, in the sliding region, the frictional stress is proportional to the normal stress σ_n as shown in Figure 3.22.

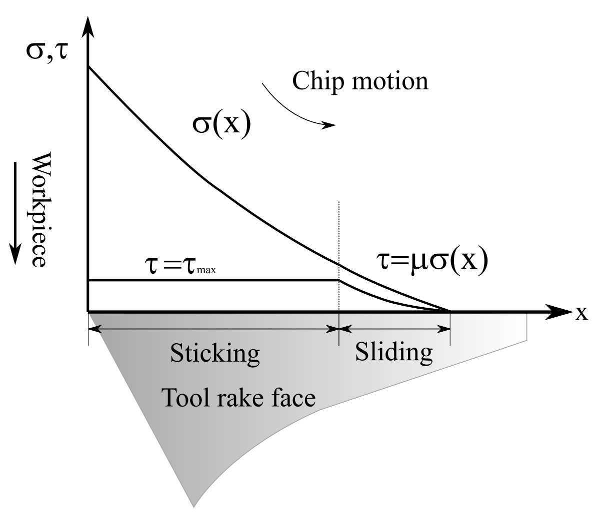

Figure 3.22: Distribution of normal and shear stress along the tool rake face.

Shear friction law Often applied in sticking region defined by the area close to the cutting edge where high normal stresses cause plastic deformation. Frictional stress τ cannot exceed the shear yield strength of the material, but at the same time being proportional to it.

$$\tau = m_f k = m_f \frac{\sigma_e}{\sqrt{3}} \tag{3.46}$$

where m_f is the shear friction factor, k is the shear yield strength and σ_e is the effective stress.

Coulomb friction law Considers low normal stresses and small plastic deformation in the sliding region. Also in this area, frictional stress can be assumed to be dependent of the normal stress and is given by:

$$\tau = \mu \sigma_n \tag{3.47}$$

where μ is the coefficient of friction and σ_n is the normal stress.

Several researchers have focused their work to develop more realistic models to incorporate the friction behaviour at the tool – chip interface to get reliable results from simulation. Son, Lim, and Ahn [183] verified the effects of friction coefficient on the minimum cutting thickness. For a fixed depth of cut, the ratio of normal to tangential force is proportional to friction coefficient. Also its effects on minimum cutting thickness h_{min} is seen in the following relation:

$$h_{min} = r\left(1 - \cos\left(\frac{\pi}{4} - \frac{\beta}{2}\right)\right) \tag{3.48}$$

where r is the tool edge radius and β is the friction angle between a tool and uncut workpiece under the tool. It is certain from previous equation that minimum cutting thickness is closely related to the friction coefficient and the tool edge radius.

Sartkulvanich, Altan, and Soehner [173] indicates that shear friction factor (m_f) and coefficient of friction (μ) have similar effects on cutting force, thrust force, chip geometry and interface temperature. An increasing value on those factors introduce an increase of contact length with it associated effects (higher cutting forces and temperatures).

Özel [157] investigates the effects of interfacial friction models on the accuracy of the predicted process variables in FEM simulations of chip formation in orthogonal cutting of low carbon steel. The most accurate predictions were found while utilizing friction models based on the measured normal and frictional stresses on the tool rake face. A variable shear friction model as shown in Figure 3.23 is recommended based on results of Dirikolu, Childs, and Maekawa [45]:

$$m_f = \frac{\tau}{k}\left[1 - \exp\left(-\left(\frac{\sigma_n}{\tau}\right)^n\right)\right]^{m/n} \tag{3.49}$$

where m is between 0 and 1, and n is a fixed parameter.

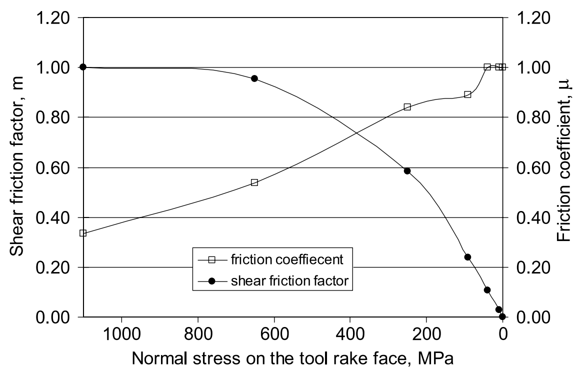

Figure 3.23: Variable shear friction and variable friction coefficient as functions of normal stress on the tool rake face [157].

Thepsonthi and Ozel [190] performed micro-milling of Ti-6Al-4V alloy with a thin layer of cBN, achieving better tool life and improved surface roughness due to a reduced sliding friction. Sliding friction contact ($\mu = 0.7$ for WC/Co and $\mu = 0.4$ for cBN coating) along the rake face had also a significant effect on temperature rise between different coatings for same cutting conditions.

3.4.4 Damage

In order to model the material machining process with accurate prediction of the chip morphology, different strategies can be used. Some researchers directly use ductile fracture models [155, 211], while others use frequent re-meshing with alternative (to JC) flow stress models to indirectly simulate separation [203, 181]. The JC fracture model is the most used model to analyze the damage in cutting [38], and according to it, the fracture strain ε_f is given by:

$$\varepsilon_f = (D_1 + D_2 \exp(D_3\sigma^*))\left(1 + D_4 \ln\frac{\dot{\varepsilon}}{\dot{\varepsilon}_0}\right)\left[1 - D_5\left(\frac{T - T_r}{T_m - T_r}\right)^m\right] \tag{3.50}$$

where D_1 is the initial fracture strain, D_2 is an exponential factor, D_3 is a triaxiality factor, D_4 a strain rate factor, and D_5 a temperature factor. Also, σ^* equals the ratio of the average of the three normal stresses (hydrostatic pressure) to the von Mises stress. This model is often suitable for high strain rate deformation, such as high speed machining [155].

The damage in a given finite element is initiated when a scalar damage parameter ω

exceeds 1. This parameter is based on a cumulative law defined as:

$$\omega = \sum \frac{\Delta\varepsilon}{\varepsilon_f} \tag{3.51}$$

where $\Delta\varepsilon$ is the accumulated increment of equivalent plastic strain during each integration step. Due to the use of progressive damage, damage initiation is followed by damage evolution criterion which governs the propagation of damage until an ultimate failure happens. Figure 3.24 illustrates the response of a ductile metal under uniaxial stress-strain where the response is initially linear elastic (O-A), followed by plastic yielding with strain hardening (A-B). The effect of the damage becomes sensitive at point B, leading to a progressive decrease in the hardening modulus. Then point D corresponds to maximum stress, point E indicates observed fracture and point F the final fracture. The deformation between B-F is localized in a neck region of the specimen [220].

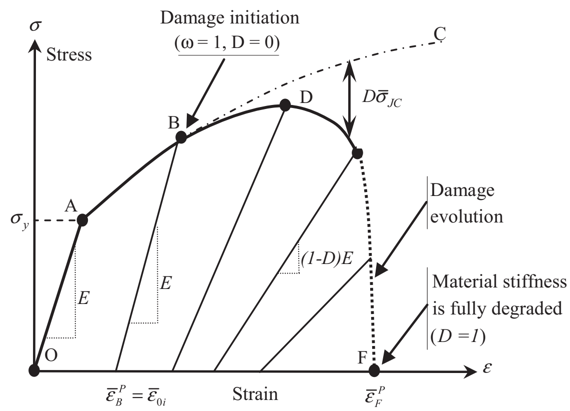

Figure 3.24: Uniaxial stress-strain curve with damage evolution [220].

As shown before, the material failure process can be divided into two sections: the first section undergoes softening of material yield stress until initial damage occurs (point B); the second section concerns the degradation of elasticity until the final fracture occurs (point F).

The model given by JC fracture defines the damage initiation; however, the law for damage evolution is also required. The fracture energy model proposed by Hillerborg et al., mitigates the mesh dependency and assumes to open a unit area of crack and defines fracture energy G_f as a material parameter. This governs the softening of material according to a stress-displacement response after damage initiation rather than a stress-strain response [155].

$$G_f = \int_{\varepsilon_o}^{\varepsilon_f} L\sigma_y d\varepsilon = \int_0^{u_f} \sigma_y du \tag{3.52}$$

where, u is the equivalent plastic displacement given as the fracture work conjugate of the yield stress after the initialization of damage. Before damage initiation $u = 0$; then after damage initiation $u = L\varepsilon$. L is the known characteristic length of an element in the simulation. The damage variable (D) increases according to the following equation until reaches the value of 1, where the equivalent plastic strain indicates failure and the concerned element is removed from the computation (often its set at 0.99 to ease the element deletion).

$$D = \frac{L\varepsilon}{u_f} \tag{3.53}$$

The fracture energy, can be determined as:

$$G_f = K_t^2 \left(\frac{1 - \upsilon^2}{E} \right) \tag{3.54}$$

where K_t is the fracture toughness and υ is the Poisson ratio.

Other used criteria include the Latham–Cockroft damage [36], where the critical damage value is considered as a material constant even though it is affected by the process conditions.

$$C = \int_0^{\varepsilon_f} \frac{\sigma_{max}}{\sigma_h} d\varepsilon \tag{3.55}$$

where σ_{max} and σ_h represent the maximum and effective stresses respectively, ε_f is the limit fracture strain, and C is the material constant in the fracture criterion which is given by uniaxial tensile test. This criterion implies that ductile fracture is dependent both on shear and on tensile stresses.

Some researchers have achieved better results with this damage model while studying chip morphology and segmentation when machining Ti-6Al-4V [76, 25].

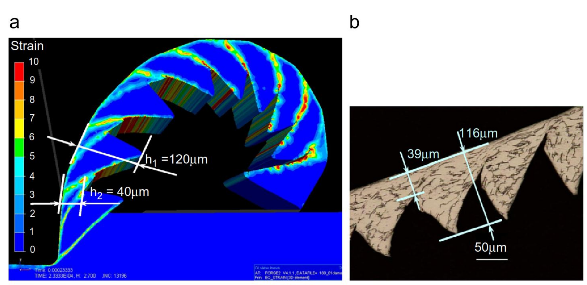

Figure 3.25: Predicted (a) and experimental (b) chips with Latham-Cockroft model [25].

3.5 Meshing

The definition of meshing requires great caution, because of the element type and element size interference in the results and also due to computational effort [38]. There are two primary mathematical formulations of continuum-based FEM: Eulerian and Lagrangian [11].

3.5.1 Lagrangian and Eulerian formulation

In the Eulerian representation, the grid is spatially fixed, with the material flowing through the meshed control volume. These models are free from element distortion problems as their shapes do not alter throughout the course of the simulation (hence no re-meshing is necessary), but they require knowing or assuming the initial shape of chip and contact conditions [184]. This formulation also assume a viscoplastic material model with no elastic properties included, therefore, residual stress analysis on the workpiece surface cannot be performed. It is widely agreed to be better suited for fluid mechanics problems rather than for machining.

In Lagrangian analysis, the computational grid deforms in time with the material during cutting [138]. For metal cutting simulations this formulation is preferable due to the more convenient modeling of the evolution of the chip from the incipient stage to steady where changes are developed through the course of the analysis as a function of the physical deformation process, cutting parameters and properties. The main disadvantage of this formulation is that the elements experience severe distortion and material non-linearities are introduced in the FE equations, increasing the computational load. This often requires the application of a re-meshing technique to achieve an adequate accuracy without stopping due to the high level of distortion [84]. This procedure has been the topic of several papers, and generally, there is not a universal criterion.

The latest development in the Lagrangian formulation, an updated Lagrangian analysis, has overcome the disadvantage of a chip separation criterion by applying continuous re-meshing and adaptive meshing, dealing at the same time with the mesh distortion but adding considerable calculation time [39].

Finally, it's worth to mention that both formulations may be able to implement implicit or explicit time integration techniques (conditionally stable, for nonlinear problems).

3.5.2 Arbitrary Lagrangian-Eulerian (ALE)

Due to the limitations and disadvantages of purely Lagrangian and purely Eulerian descriptions, a technique has been developed that exceeds both to a certain extent by combining the best features of each approach. Such a technique is known as the Arbitrary Lagrangian-Eulerian (ALE) description, where the mesh does not remain fixed in space neither moves attached to material points. In this case, the grid points have their own governing equations of motion [138]. This extended freedom allows handling greater distortions of the continuum with better resolution than that offered by a purely Eulerian approach.

A significant number of researchers have studied the problem of micro-cutting through orthogonal models with continuous chips using the ALE procedure [138, 2, 81, 83, 155]. Mainly, two approaches can be made for orthogonal cutting as follows [10]:

- A model with Eulerian and Lagrangian boundaries, with the Eulerian boundaries from the inflow, chip-flow and outflow ends and with Lagrangian boundaries at the top and bottom surfaces of the workpiece as shown in Figure 3.26a. This FEM model requires a pre-defined chip geometry and is more suited for steady state problems [45]. The chip surfaces are defined with Lagrangian boundary conditions, and the chip upper surface is defined with Eulerian boundary conditions. Therefore, the chip flow is bound at a vertical position. This technique can avoid the distortion in the region surrounding the tool tip and be making possible to simulate a long machined surface to obtain, for example, stabilized residual stresses [138].

- A scheme with pure Lagrangian boundaries is designed, and kinematic penalty contact conditions between the tool and the workpiece are defined as Figure 3.26b. This model allows simulating transient chip formation from the incipient to steady state. The explicit dynamic procedure performs a large number of small time increments. The use of adaptive meshing with fine-tuned parameters is required to simulate plastic flow over the tool round edge properly. Because of the relative displacement between the mesh and the material, an ALE model with pure Lagrangian boundaries does not lead to a chip with a geometry close to the experimental one when segmented (or saw-toothed) chip is observed [50].

3.5.3 Coupled Eulerian-Lagrangian (CEL)

A Coupled Eulerian-Lagrangian model is composed of an Eulerian mesh representing the volume in which the Eulerian material flows and interacts with Lagrangian parts. These models avoid the need of workpiece remeshing or even element deletion to make possible the chip to be generated [169]. In this case, attention must be paid to the Eulerian mesh definition: the covered volume should be large enough to prevent the Eulerian material to flow out of it and be lost for the simulations [50].

Zhang, Outeiro, and Mabrouki [219] investigated the effect of three numerical formulations (LAG, ALE, and CEL) on chip thickness, cutting force and temperatures (Figure 3.27). They found that the differences between the LAG and ALE/CEL models are since the damage model, which is used to produce chip formation and chip segmentation, is only supported in the LAG model. The LAG model also suffers from two main drawbacks, which are the high mesh distortion and the material loss induced by the sacrificial layer. These problems are minimized or avoided in the ALE and CEL models.

Ducobu, Rivière-Lorphèvre, and Filippi [50] also achieved excellent results through the application CEL formulation with good chip morphology prediction and forces calculation. The absence of element deformation in the workpiece (thanks to the Eulerian formulation) give significant advantages with promising improved computation times while compared to ALE models, thus allowing to keep the stable time increment constant.

Saez-De-Buruaga et al. [169] applied the same technique as [50] to evaluate fundamental variables as cutting and feed forces, tool temperature, chip thickness and chip-tool contact

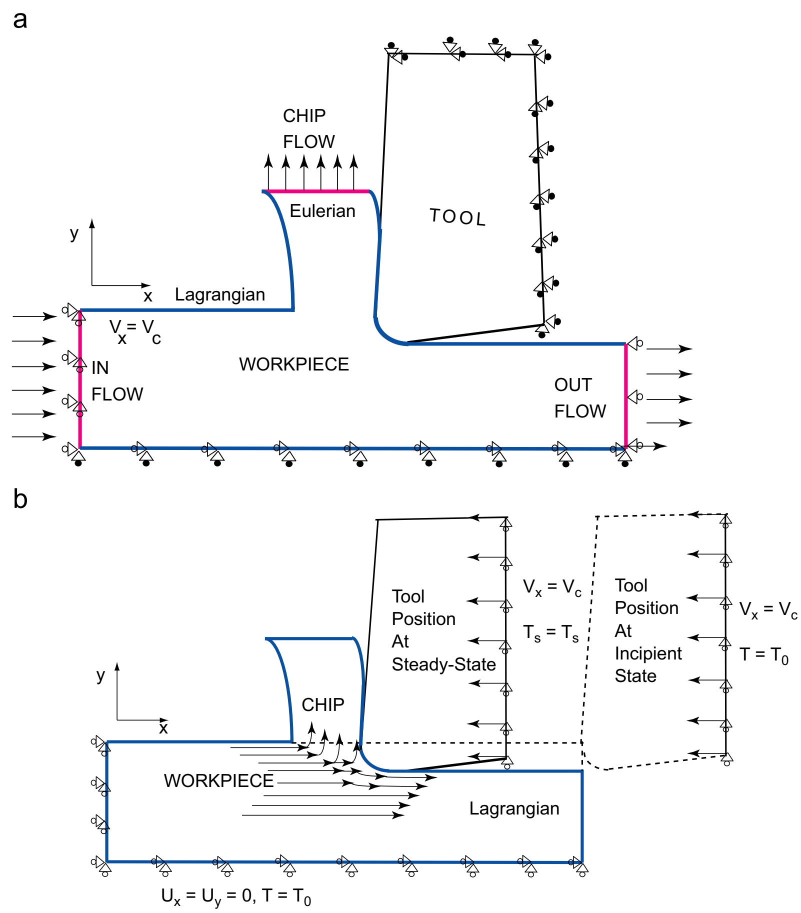

Figure 3.26: ALE formulation with different boundary conditions [10].
(a) Eulerian and Lagrangian boundary conditions, and (b) pure Lagrangian boundary conditions.

length. Their results indicate a good correlation between predicted and experimental forces and temperatures. Chip thickness and tool-chip contact length seemed to be very sensitive to friction behavior and material strain hardening. Finally, a reasonable prediction on tool wear rate was found.

3.5.4 Adaptivity and remeshing

Mesh adaptivity is divided into three different types of categories, to create a new spatial discrimination and improved mesh quality: h-adaptivity, p-adaptivity and r-adaptivity. The h-adaptivity consists in changing the size h of the finite elements, then the new mesh has different number of elements and the connectivity of the nodes is changed. In p-adaptivity the degree of the interpolating polynomials is changed. Finally, r-adaptivity is based on the relocation of the nodes without altering the topology.

During machining, large deformations are very common, so mesh elements size must be

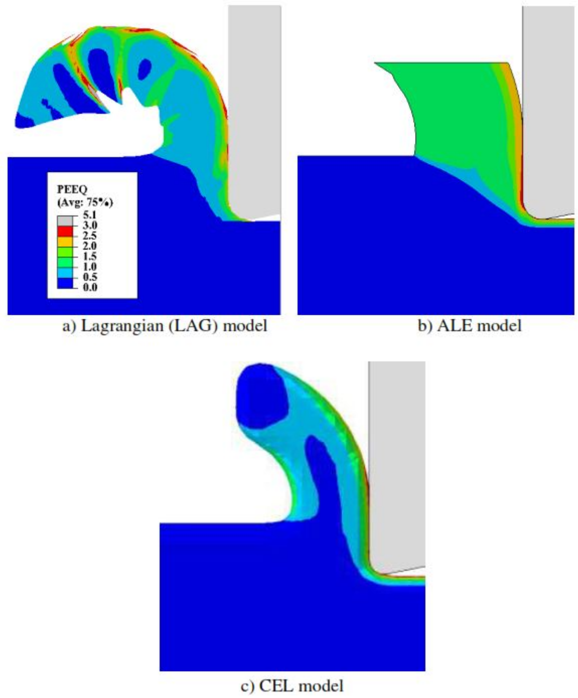

Figure 3.27: Equivalent plastic strain distribution for different formulations [219].

properly selected. Two constraints can be retained for the evaluation of h: First, the size should be relative large (to save computing time), second the result should be similar or close to experimental values (in terms of cutting force and chip morphology). Also, r-adaptivity meshing nodes are moved to more favorable positions to improve mesh distortion. In addition, solution dependent meshing is supplied to concentrate mesh towards the developing boundary concave, e.g., chip separation area in the vicinity of the cutting edge, and produce local mesh refinement in this area [170]. During mentioned adaptive meshing (often given by a combination of h- and r-adaptivity), a smooth computational mesh within ALE domain is first regenerated and subsequently, solution variables like energy, density and others are mapped from the previous distorted mesh to the new mesh [10].

3.6 FEM software

Recently, there are many commercial FE codes that are capable of modeling the machining process (ABAQUS, ANSYS, Deform, LS -DYNA, AdvantEdge, Comsol, etc). A comparison between different software capabilities oriented to the requirements for simulation of cutting processes is shown in Figure 3.28. Most of available software packages offer a user friendly interface with capability of defining user parameters and libraries. These features allow a relatively simple setup of complex 3-D models and make it feasible for application by industry [184]. The present contribution exploits the capabilities of ABAQUS to simulate orthogonal cutting case of commercially pure Titanium.

This software provides a gentle graphic user interface (GUI) and is flexible to establish user-defined subroutines. ABAQUS allows ALE, CEL and Lagrangian analysis as well as implicit and explicit integration schemes. Simultaneously, it is possible to simulate diversified problems like stress/displacement, frequency analysis and others.

Criteria \ Programm	ABAQUS	ANSYS/ LS-DYNA	AdvantEdge	DEFORM	COMSOL
Creation of geometries	Creation of geometries and import of CAD data	Import of CAD data	Creation of simple geometries and import of CAD data	Creation of simple geometries and import of CAD data	Creation of simple geometries and import of CAD data
Material catalogue	No, has to be defined	Yes, expandable	Yes, wide	Yes, new catalogue importable	yes
Element type	Every type	Every type	tetrahedron, rectangle	tetrahedron, rectangle	Every type
Time integration	Implicit / Explicit	Implicit / Explicit	Explicit	Implicit	Implicit
Remeshing routine	none	none	yes	yes	yes
use	general	general	cuttingprocess	Deforming process	general
Influence on simulation computation	High, by Python	Possible, by Fortran	no	High, by Fortran	High, by Matlab
parallelisation	possible	possible	possible	possible	possible
Usage at the WZL	Eigenfrequency analysis, elast. Tool behavior, elasto-plastic component behavior	no	no	Cutting simulation	Thermo-elastic deformation

Figure 3.28: FE software comparison [97].

The general steps for designing and analyzing a cutting process in FEM are:

- CAD modeling of tool and work geometries.
- Defining proper mesh type(s) and size(s) and re-meshing parameters if needed.
- Apply material properties and boundary conditions with interactions.
- Define tolerances and run simulations.
- Post-process simulation results.

To speed up calculations without compromising the accuracy of simulation results, it is necessary to take appropriate simplifications or assumptions on tool and workpiece models as well as object types. In general, 3-D analysis can be more accurate but time-consuming than the 2-D study, but as mentioned, there are factors like constitutive model selection, friction behavior, uncut chip thickness model and others that can contribute to a higher source of error.

3.6.1 Mass scaling

The conditional stability is the only concern about explicit integration, requiring a very small time step. This time is in the order of the time required by a stress wave to cross the smallest element in the model, typically around 10^{-9} to 10^{-10}s, leading to a large calculation time.

The time efficiency of this phase can be improved with the use of mass scaling as has been reported in literature [138]. This is known as the Courant–Friedrichs–Lewy condition, which is given as:

$$\Delta t \leq f\left(\frac{h}{c}\right) \tag{3.56}$$

where Δt is the stable time step, h the smallest element dimension in the model, $c = \sqrt{E/\rho}$ is the acoustic wave speed based on Young's modulus (E) and density (ρ), f is a scale/safety factor to improve stability (typically 0.9). This method can be implemented in different ways:

- Full mass scaling in which the mass of every element is scaled, where it needs to be considered that increasing the mass of large elements could influence the results of the model due to an increase of inertial effects.
- Adaptive mass scaling where it only increases the mass of the elements whose time incrementation is less than a set value. It is common to check after simulation that the mass scaling does not significantly affect the results through a comparison between the kinetic energy and the internal energy of the system. This ratio is often chosen below $5 - 10\%$ [51].

Ducobu, Rivière-Lorphèvre, and Filippi [51] achieved a reduction of almost 71% of CPU computing time with mass scaling enabled with the same chip morphology while simulating orthogonal micro-cutting of Ti-6Al-4V. No significant effects on other model results were observed.

3.7 Design of Experiments (DOE)

Design of Experiments (DOE) is a systematic approach to determine the influence of controlling factors on the process outputs, allowing to understand the cause and effect relationship of a certain process (Figure 3.29). Physical micro-milling experiments are often conducted in order to collect all necessary data or output responses produced from manipulation of different relevant input variables. To guarantee that an experiment is conducted effectively, statistical experimental design is generally recommended where appropriate data can be recorded and statistically analyzed for valid conclusions to be drawn [143].

Several design models for DOE like factorial design, central composite design, Taguchi and respose surface can be applied for solving complex and multifactor engineering problems. During the application of mentioned designs, Analysis of variance (ANOVA) tool is frequently applied to detect any differences in the average performance of groups of factors tested. It is a powerful statistically based objective decision tool for researchers. In addition to ANOVA, other approaches such as observation, ranking, column effects and plotting methods can also be considered to support and enhance the analysis of data. Finally, after applying optimization schemes according to the user needs, a confirmation test is often recommended to verify the experimental results as shown in Figure 3.29.

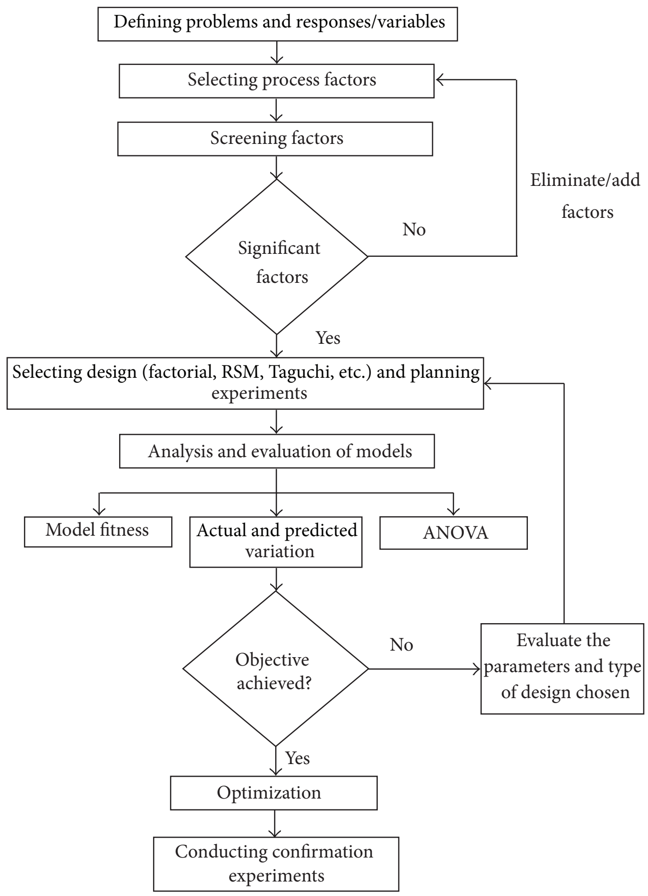

Figure 3.29: Flowchart for optimization [12].

3.7.1 Factorial Design

Full factorial experimental designs are not easy to use because they need a large number of tests, specially in the case of machining if the number of parameters increases. This makes this kind of design generally feasible when only a few factors and levels are to be investigated, otherwise this approach can lead to an excessive number of trials: n^k where n is the number of levels and k the number of factors. The advantage of this type of design is that all possible combinations of the levels of the factors are investigated, allowing to achieve a better estimate of the interactions and yielding conclusions that are valid over a range of experimental conditions [143].

In order to reduce the number of experimental runs, fractional factorial was introduced, in which a fraction of total number of trials is used. The number is determined by n^{k-p}, reducing to $1/n^p$ of the full factorial design for same number of factors and levels. The major use of fractional factorials is in screening experiments where many factors are considered and the objective is to identify those factors (if any) have large effects.

3.7.2 Central Composite Design (CCD)

Central Composite Design (CCD) is a factorial or fractional factorial design with center and star points that can be adjusted to a greater extend on the region of operability and to influence the variance distribution of such region. CCD is one of the most popular classes of designs to develop first and second order models with an excellent efficiency [143].

A CCD has three groups of design points:

- Two-level factorial or fractional factorial n_f design points (2^k), consisting of possible combinations of ± 1 levels of factor.
- $2k$ axial/star n_a points fixed axially at a distance α from the center to generate quadratic terms. These points are shown in Figure 3.30 as unfilled circles.
- Center points n_0 which represent replicate terms. They also provide a good and independent estimate of the experimental error. Generally, three to five center runs are recommended [143].

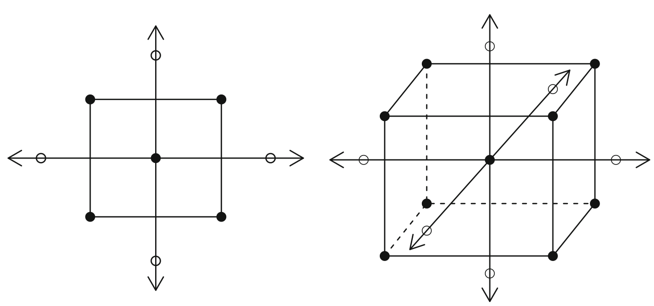

(a) 2 factors **(b)** 3 factors

Figure 3.30: Central Composite Designs [40].

Considering these points, the number of experiments by CCD will be:

$$N = k^2 + 2k + n \tag{3.57}$$

where N is the total number of experiments, k is the number of factors studied, and n is the number of replicates. In CCD, a parameter known as α is important to calculate as it could determine the location of axial points in experimental domain and the rotatability of the design. A rotatable design achieves a constant variance of predicted response (or an equal precision of estimation in all directions). A popular recommendation for α is given in [40] as:

$$\alpha = (n_f/r)^{\frac{1}{4}} \tag{3.58}$$

where n_f indicates the number of factorial points and r the number or repetitions. In a spherical CCD, all the factorial and axial design points lie on the surface of a sphere, where α is given by:

$$\alpha = \sqrt{k} \tag{3.59}$$

Spherical CCD are rotatable, offer an effective model based parameter estimation [212], but require five levels of design factors.

In many scenarios, a cubic region of interest is desired, which is often called Central Composite Face-centered design (CCF), in which $\alpha = 1$ is desirable because it ensures the position of axial point within factorial portion region. CCF only needs 3 parameter levels, they do not require many center points as spherical CCD, but are not rotatable designs.

Box-Behnken Designs Box-Behnken designs are three level designs for fitting response surfaces. They are formed by combining 2^k fractional factorials with incomplete block designs in a particular manner. The resulting designs are usually very efficient in terms of the number of required runs, and they are either rotatable or nearly rotatable. Box-Behnken is a spherical design with all points lying on a sphere of radius $\sqrt{2}$, requiring only three levels per factor thereby requiring fewer treatments combinations than a CCD. Also, as shown in Figure 3.31 the Box-Behnken design does not contain any points at the vertices of the cubic region which may be prohibitively expensive or impossible to test because of physical process constraints [143]. This also makes a response surface inaccurate near the vertices because they lie relatively far from the samples [40].

3.7.3 Taguchi Method

Taguchi method is a robust statistical tool that allows the independent evaluation of the responses with minimum number of experiments. The desirable effect for the output characteristic is called as "signal", and "noise" means the undesirable effect for the output characteristic. It employs orthogonal arrays for experimental design and signal-to-noise (S/N) ratio instead of responses itself to determine the optimum settings of control factors and thus neglects the variations caused by uncontrollable factors. With this method, utilizing full fractional designs (orthogonal arrays), experimental results can be analyzed through S/N ratio and ANOVA with simultaneously evaluating the significance of the factors in terms of their contribution to the response values.

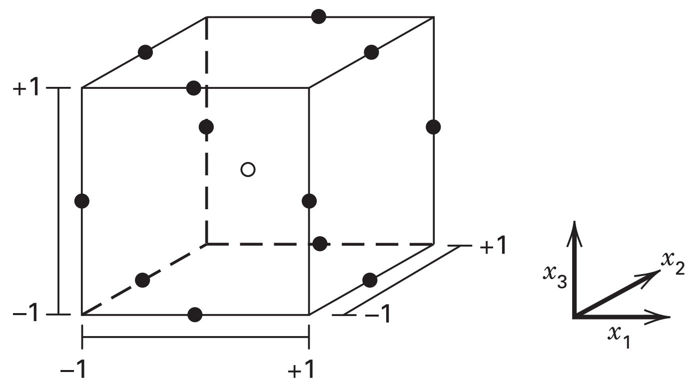

Figure 3.31: A Box-Behnken design for three factors [143].

In Taguchi method, the "signal" implies the mean value while "noise" shows the standard deviation term. Then, a lower variability in the process is ensured through maximizing the S/N ratio [12]. However, depending on the type of response desired, S/N ratio is classified into three categories:

- Smaller is better: When the response variable is to be minimized.

$$S/N = -10 \log \left[\frac{1}{n} \left(\sum_{k=1}^{n} y_i^2 \right) \right] \tag{3.60}$$

- Larger is better: When the response variable is to be maximized.

$$S/N = -10 \log \left[\frac{1}{n} \left(\sum_{k=1}^{n} \frac{1}{y_i^2} \right) \right] \tag{3.61}$$

- Nominal is better: When a target value is sought for the response variable.

$$S/N = -10 \log \left[\frac{1}{n} \left(\sum_{k=1}^{n} \frac{\mu^2}{\sigma^2} \right) \right] \tag{3.62}$$

where $\mu = \sum_{k=1}^{n} y_i$; $\sigma^2 = \frac{\sum_{k=1}^{n}(y_i-\mu)^2}{n-1}$. Also, y_i represents the response variables and n indicates the number of experiments.

Taguchi method has been applied by Kuram and Ozcelik [102] to minimize the tool wear during the micro-milling of Ti-6Al-4V alloy, where spindle speed of 12,000 RPM, feed rate of 50 mm/min and depth of cut of 50 μm is required. For this material, tool wear decreases with an increment of spindle speed and, in general, increased with an increment of feed rate and depth of cut. For Inconel 718, the combination given by 10,000 RPM, feed rate of 50 mm/min and depth of cut of 75 μm reduces the tool wear to minimum [102]. Also, Bandapalli et al.

[13] applied this design with similar results for Titanium alloy (grade 2), with the interaction effects of S/N ratios is illustrated in Figure 3.32, where the optimal micro-milling parameters for lower cutting forces are given by high spindle speeds, low depth of cut and low feed rates.

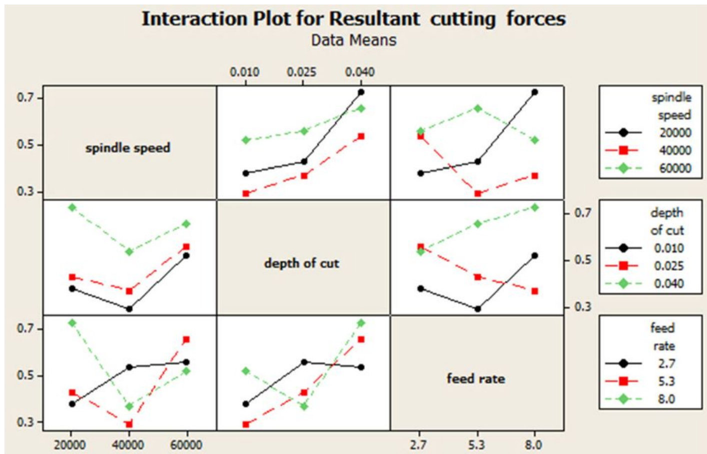

Figure 3.32: Interaction plot of resultant cutting forces [13].

3.7.4 Response Surface Methodology (RSM)

Response Surface Methodology is a wide-spread Design of Experiments technique for determining the relationship between various factors and corresponding output responses within the desired criteria. This method allows to determine and represent the cause and effect relationship between the responses and input control variables, being useful for process developing, improving and optimizing [143, 144].

The first step in RSM is to find the suitable approximation for the true functional relationship between the response (y) and the set of independent variables (x). The proposed mathematical model between the n-independent parameters and the dependent variable is presented in the following form where the multi-variable function f could represent a linear or non-linear function with constant coefficients and ε is a residual error.

$$y = f(x_1, ..., x_n) + \varepsilon \tag{3.63}$$

Often a first-order model is called a main effect model, because it includes only the main effect of the variables. If there is an interaction between these variables, the interaction terms can be easily added introducing a curvature into the response function. The second-order models are widely used because they are very flexible and are able to capture strong curvature in responses. An estimation of the regression coefficients can be done easily by the method of least squares with the aid of different statistical simulation software available.

Many studies have employed DOE and RSM to study and analyze micro-milling process [168, 32, 53, 212, 102]. Primary machining variables such as cutting speed, feed per tooth and axial depth of cut, cutting strategy, lubricant/coolant application and type, which are easily controllable, are frequently considered in building the models as influencing processing parameters. Tool wear, tool life, acoustic emissions, surface roughness and burr formation are among the studied responses.

Thepsonthi and Özel [191] applied a Taguchi orthogonal array with three factors (spindle speed, feed and axial depth of cut) and three levels to analyze their effect on top burr and surface roughness. The surface and contour plots for top burr response are depicted in Figure 3.33 and allow to visualize the behavior of the response variable throughout the design space.

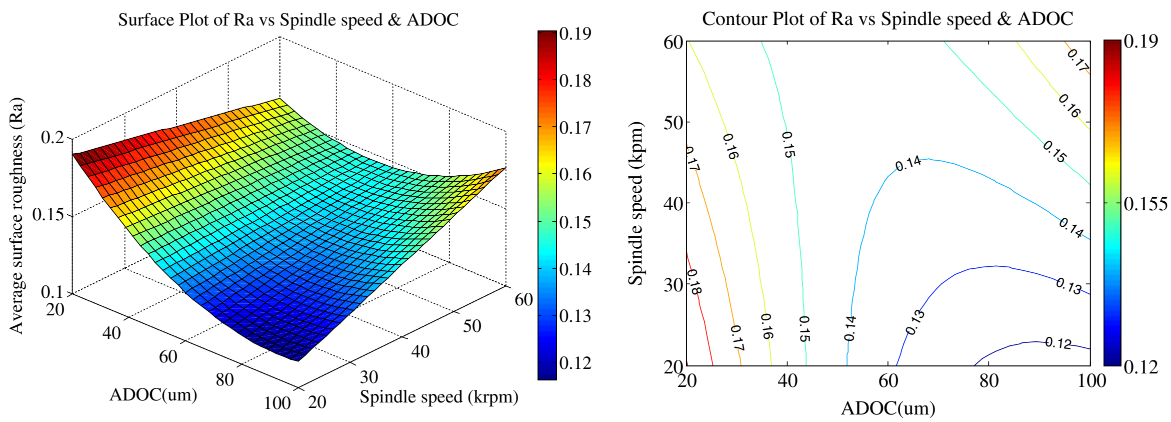

Figure 3.33: Surface and contour plots of top burr width while micro-milling Ti-6Al-4V [191].

Chapter 4

Model simulation and validation

Contents

4.1 Material

Titanium and its alloys are commonly used for several micro-feature based applications in aerospace industry, chemical industry, medical field and others, based on its excellent properties such as high specific strength, improved physical and mechanical properties, corrosion resistance, and high biocompatibility [160, 162]. It is also used increasingly or being considered for employment in other industrial and commercial applications, such as petroleum refining, chemical processing, surgical implantation, pollution control, nuclear waste storage, food processing, electrochemical and marine applications [55]. Despite being abundant on the earth crust (is the 4th most abundant metal, after aluminum, iron, and magnesium) it is expensive while compared to many metals because of the complexity of the extraction process, the difficulty of melting and problems during fabrication and machining [55].

According the microstructure of pure titanium, it is known that it undergoes an allotropic behavior with a reversible crystal structure transformation from the low-temperature alpha (α) hexagonal closed-packed (HCP), arrangement to beta (β), body-centered cubic (BCC), crystallographic structure when the temperature is increased above $882°C$ [55]. By adding different alloying materials to titanium, the crystal structure transition temperature can be changed. Alpha-stabilizing materials, such as aluminum (Al) and oxygen (O), raise the transition temperature, while beta-stabilizing materials, such as vanadium (V) and tungsten (W), lower it [150]. Ti-alloys have different mechanical, physical, thermal, chemical, electrical and optical properties for various grades obtained by the addition of alloying elements [14]. Two different types of titanium: the commercially pure titanium (Ti-CP grade 2) and alloy Ti-6Al-4V (grade 5) are the most commonly used alloys and account for over 60% of the total compounds production [150, 78].

Titanium also brings some machining challenges due to a relatively low elastic module, high toughness, low thermal conductivity and chemical reactivity at high temperatures contribute to accelerated tool wear and uneven micro-burr formation [55, 154]. Challenges as mentioned above, often are coupled with some factors like size effect, plowing, vibration, deflection, workpiece microstructure and other issues that may become significant while scaling the conventional milling process. As a result, to obtain the desired performance in micro-milling can be harder than in macro (or conventional) milling [26, 34, 66].

Some of the main influencing parameters when machining Ti alloys are [84]:

- It is necessary to keep the *cutting speed* low to minimize the temperature rise and consequently reduce the influence of heat on the tool tip and edge.

- The *feed rate* should be kept high while taking into consideration that a work-hardened layer is formed after each cut and the consecutive cut needs to be larger than the thickness of this layer.

- Often a generous amount of *cutting fluid* or a proper cooling strategy should be applied to reduce *temperatures* as well as to clear the work area of chips and reduce cutting forces.

- The *sharpness* of the tools used in machining is going to affect the surface finish and if not adequate can cause tearing as well as deflection of the tool and workpiece. Chatter must be avoided especially for finish machining where the low modulus of elasticity increases the spring-back effect, also higher *cutting forces* and its chemical reactiveness tends to fasten tool wear [55].

Residuals	N	H	O	C	Ti
0.40	0.03	0.015	0.25	0.08	Bal

Bal: Balance (weight).

Table 4.1: Chemical composition of CP-Ti (max wt.%) [193].

4.1.1 Commercially pure titanium

The material used in this chapter for cutting tests was a grade 2, commercially pure titanium (CP-Ti) in the form of sheets of 5mm thickness complying with the specification of ASTM B265 [187] with a chemical composition similar to shown in Table 4.1. Figure 4.1 illustrates the microstructure of the material of the sheets, where an ASTM grain size number of 6.4 is found [139] corresponding to an average grain diameter of 39.8 μm similar to results shown in [194, 215]. At service temperature, it consists of 100% HCP α-phase (thereby also known as α-Titanium). As a single-phase material, its properties are controlled by chemistry (iron and interstitial impurity elements) and grain size.

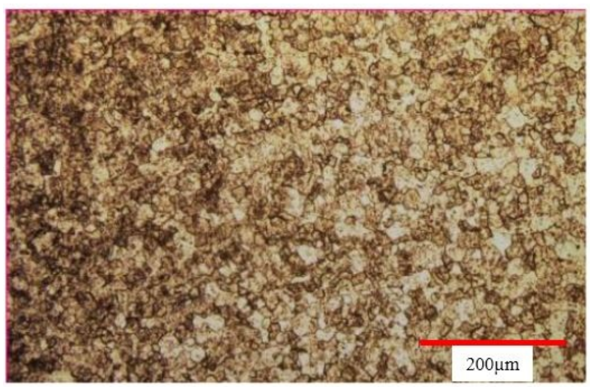

Figure 4.1: Microstructure of CP-Ti sheet (100X)[139].

The mechanical properties of CP-Ti grade 2 in comparison with other alloys and metals are summarized in Table 4.2. It is important to note that titanium alloys exhibit a relatively constant modulus, but their yield strength can change with a gain up to 180% [134]. Due to its low thermal conductivity, it's common to apply wet conditions for machining, but green (dry) machining is gaining the attention of researchers due to environmental, health and costs concerns [55, 14, 78, 28].

Grade 2 is widely used because it combines excellent formability and moderate strength with superior corrosion resistance. This combination of properties makes CP titanium Grade 2 a candidate for a large variety of chemical, marine, aerospace and medical applications [89]. Fixed-bed reactors (Figure 4.2), dentistry devices (such as implants, crowns, bridges, and prosthesis), artificial joints, other biocompatible components and shell components are application examples of this materials. Other alloys like Ti-6Al-4V ($\alpha - \beta$ alloy) are usually more commercialized, accounting for 45% to 60% of the total practical usage of titanium and

Property	Cp-Ti Grade 2	Ti-10V-2Fe-3Al (β alloy)[d]	Ti-6Al-4V ($\alpha - \beta$ alloy)[d]	AL7075-T6[d]	Inconel 718[d]
Density, ρ (kg/m^3)	4510[a]	4650	4420[d]	2810	8220
Poisson's ratio, υ	0.32[b]	-	0.33[e]	-	-
Hardness (HRC)	10-13 (eq.)[c]	-	30-41[d]	aprox 7 (eq.)	38-44
Young's modulus, E (GPa)	105-120[a]	110	113.8[d]	71.7	200
Shear modulus, G (GPa)	44[b]	-	42.8[e]	-	-
Ultimate tensile strength, (MPa)	485[a]	970	950[e]	572	1350
Yield strength, (MPa)	345[a]	900	880[e]	503	1170
Thermal conductivity, (W/mK)	21.79[a]	7.8	6.7[e]	130	11.4

References: a. [193]. b. [44]. c. [139]. d. [78]. e. [219].

Table 4.2: Mechanical properties of selected materials.

are especially suitable for aerospace as well as for biomedical applications [78].

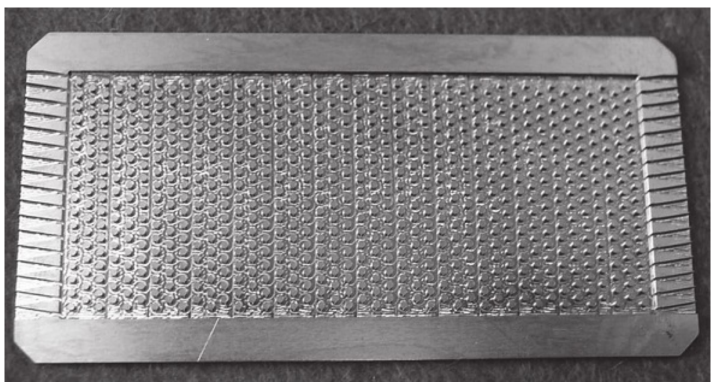

Figure 4.2: Pin array of a fixed-bed reactor machined in CP-Ti grade 2 [89].

4.1.2 Constitutive modeling

An accurate evaluation of the flow behavior at a wide variety of experimental conditions is a time-consuming and complex work based on significant variations of this parameter with conditions regarding temperature, strain, strain rate and others. For this material, flow stress increases with the increase of strain rate and a decrease of the deformation temperature (a typical characteristic of dynamic recrystallization softening), also its complex deformation behavior includes often a twinning effect (strain hardening) that is affected by material microstructure [194, 207].

Different flow stresses approaches through phenomenological and physically-based models of the CP-Ti have been studied. Table 4.3 summarizes some constitutive modeling studies for adequately describing the relationship between stress and strain for CP-Ti. For the current study, results from Nemat-Nasser, Guo, and Cheng [148] research are used to fit a rate-dependent (phenomenological) Johnson-Cook model to describe the material behavior under machining conditions. Johnson-Cook model allows a numerically robust and simple form with few parameters that can be easily integrated into different FEM packages. The results from reference mentioned above were selected based on the broad range of strain rates and temperatures at static and dynamic tests.

Flow stress model calibration Figure 4.3 illustrates the true stress-strain curves of CP-Ti for indicated strain rates and temperatures used for constitutive model fitting. The material used for different tests was a 99.99% CP-Ti in the form of a 6.35 mm diameter extruded rod. The material was annealed, and a metallographic examination revealed an average grain size of 40 μm [148] which is consistent with material considered in the current study (Figure 4.1).

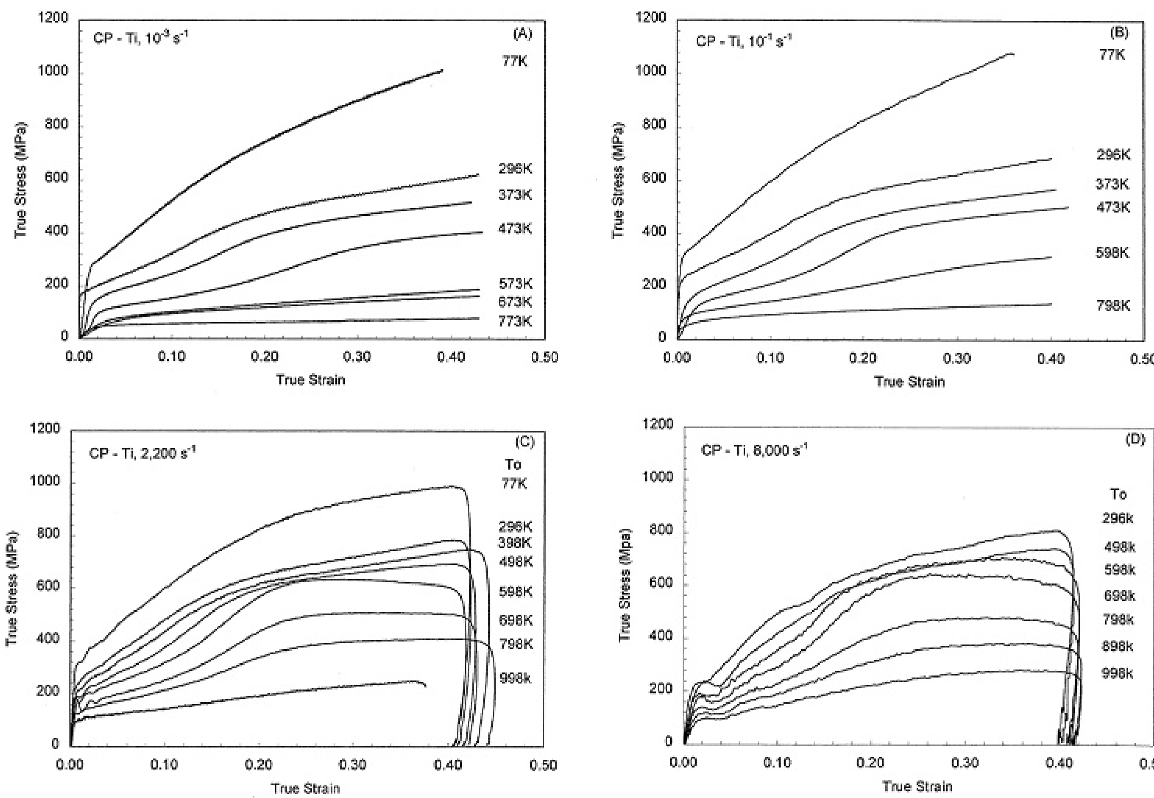

Figure 4.3: True stress-strain curves for CP-Ti grade 2 [148].

The first step in calibrating the JC model to the materials test data is to set the strain hardening parameters (A, B, n) since they are considered independent with respect to strain rate and temperature. A temperature of $25°C(298K)$ and a strain rate of $10^{-3}s^{-1}$ was selected as a reference for strain hardening parameters. Then a model was fitted to the test data through the least square method. The mean square error was calculated using the following equation:

$$MSE = \frac{1}{n}\sum_{i=1}^{n}(\sigma - \sigma_{pred}) \tag{4.1}$$

where σ represents the true experimental stress and σ_{pred} is the predicted stress. For the strain rate sensitivity parameter, the yield stress values are drawn as a function of the

Author (year)	**Constitutive/ Fracture Model**	**Remarks**
Sheikh-Ahmad and Bailey (1995) [177]	Johnson-Cook / NA	Adiabatic torsion test were conducted with temperatures from ambient to 750°C and strain rates from 0.19 to 122s^{-1}.
Nemat-Nasser, Guo, and Cheng (1999) [148]	Physically based / NA	Performs static and dynamic tests with strains over 40% with temperature range of 77-1000K and strain rates 10^{-3} – $8000s^{-1}$ on extruded rod. Model predictions are good only for some temperature values.
Li, Xu, and Bassim (2004) [115]	Zerilli-Armstrong based model / NA	Applied SHPB test at different strain rates from $2600s^{-1}$ to $3000s^{-1}$ in α-titanium with higher impurities.
Tsao et al. (2012) [194]	Power law / NA	Develops flow stress formula for strain rates from 8.3×10^{-4} to 0.05 and temperatures from 623K to 773K (warm sheets) with a fairly good fit with experimental values.
Magargee, Morestin, and Cao (2013) [124]	Modified Hollomon & Johnson Cook Models / NA	Conducted uniaxial tension tests on CP-Ti subjected to electrically assisted deformation at constant strain rate of $0.002s^{-1}$.
Ding and Shin (2014) [44]	Dislocation density-based model / NA	Develops dislocation density-based models calibrated with data from [177]. Performs orthogonal simulations with grain refinement effects on deformation and temperatures.
Won et al. (2014) [207]	Physically based model / NA	Analyzes three grades of pure Ti with different interstitial solutes at low strain rates 2×10^{-4} and temperature ranges 135-393K the model exhibits good prediction capability.
Zhai et al. (2016) [215]	Physically based model / Ductile Damage	Analyzes CP-Ti fracture initiation and propagation with a modified and calibrated GTN model considering material anisotropy, void volume damage and shear damage being consistent with different experimental tests.

NA: Not available.

Table 4.3: Different of constitutive modeling studies for CP-Ti.

strain rate as shown in Figure 4.4. Finally, the temperature softening coefficient is calculated by considering the flow stress curves at different temperatures and applying the least square method. Hence, the flow stress relation based on JC formulation is given as:

$$\sigma(MPa) = \underbrace{\left(173 + 860.6\varepsilon^{0.7493}\right)}_{\text{Elasto-plastic}} \underbrace{\left(1 + 0.01624 \ln \frac{\dot{\varepsilon}}{0.001}\right)}_{\text{Strain rate sensitivity}} \underbrace{\left[1 - \left(\frac{T - 296K}{1941K - 296K}\right)^{1.499}\right]}_{\text{Thermal softening}} \quad (4.2)$$

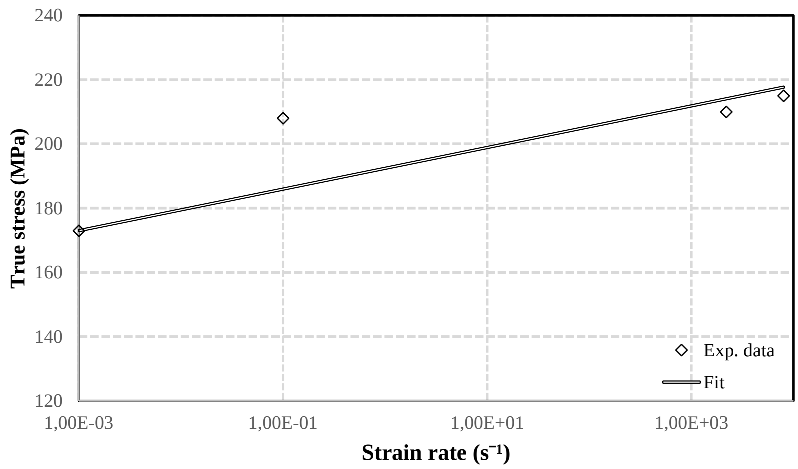

Figure 4.4: Plastic stress vs strain rate for CP-Ti grade 2.

4.1.3 Fracture model

The damage model developed by Johnson-Cook is also used in conjunction with their flow stress model. As mentioned in previous sections, this model used as a damage initiation criterion, is suitable for considering the influence of strain rate and temperature effects on material failure and has been applied successfully for micro-cutting force and chip formation by many researchers [219, 155, 211, 162]. The current study, considers the experimental results from Zhai et al. [215] studies, to fit three of the original JC model parameters:

$$\varepsilon_f = (D_1 + D_2 \exp(D_3 \sigma^*)) \quad (4.3)$$

where D_1 is the initial fracture strain, D_2 is an exponential factor, D_3 is a triaxiality factor. Strain rate and temperature constants (D_4, D_5) are not included due to the lack of experimentation for fracture at different strain rates and temperatures. In many metal cutting models, the fracture is ignored, because it is easier to model chip formation using non-physical criterion such as the remeshing procedure, but inducing unrealistic material behavior [219].

The further implementation of damage evolution (or propagation) criterion allows avoiding mesh dependency problems since the material follows a stress-displacement relation rather than a stress-strain relation [48, 211]. Considering the fracture energy (G_f)criterion, as soon as the specified value of G_f is reached in a finite element, it is deleted, and all its stress components are zero, generating a crack in the workpiece, making it possible for a chip formation. The value of G_f can be determined by the corresponding fracture toughness K_f according to:

$$G_f = \frac{1-\upsilon^2}{E}K_f^2 = \frac{1-0.32^2}{105GPa} \times \left(66\frac{MPa}{m^{1/2}}\right)^2 = 0.564\frac{N}{mm} \tag{4.4}$$

Fracture model fitting The model proposed by Zhai et al. [215] is a modified Gurson-type for porous material which accounts for the plastic anisotropy and tension-compression asymmetry exhibited by CP-Ti. This model exhibits a proper fitting for different quasi-static test configurations as shown in Figure 4.5.

In their research, the tensile specimens in the rolling (RD) and transverse (TD) were extracted at 0° and 90° respectively from the rolling direction of a hot-rolled 12.7mm CP-Ti sheet (from Timet manufacturer). The specimen geometry followed the ASTM E-8 standard (subsize specimens). For the smooth round specimens, the length of the gauge section is 36 mm, and the diameter is 8.89 mm. Three notched specimens namely B, D and E were prepared with notch radius of 1.524, 0.762 and 3.81 mm, respectively with a minimum diameter of 4.57mm [215].

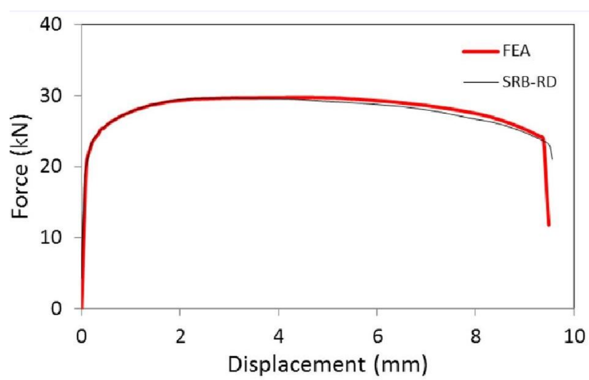

Figure 4.5: Numerical predictions and experimental data for tension specimen [215].

The surrogate-based algorithm is applied for an efficient approach towards the approximation to the coefficients D_1, D_2 and D_3 of the JC model that predict similar results as the available GTN model. To apply this technique, the following steps are taken [165]:

- Select the initial sampling points with a DoE technique.
- Perform the FE simulation at the selected points.

- Fit the surrogate model.
- Optimize the model and find the new set od samples.
- Iterate steps 2-4 to reach desired convergence.

A set of simulations were conducted according to a design of experiments shown in Table 4.4, were the displacement at fracture d_f was recorded and calculated the mean square error for each test. The displacement at failure is $9.5mm$ [215]. Different constant sets yielded various results as shown in Figure 4.6 where some cases exhibited a premature fracture while compared to results from Figure 4.5. The nearest approximation is given by set 7, where $D_1 = 0.1$, $D_2 = 0.1$ and $D_3 = 1.0$.

	Coded			**Real**				
Run	**A**	**B**	**C**	D_1	D_2	D_3	d_f (mm)	MSE (mm^2)
1	-1	-1	-1	-0.3	0.1	0.0	0.649	78.342
2	-1	0	0	-0.3	0.3	0.5	0.012	90.014
3	-1	1	1	-0.3	0.5	1.0	0.598	79.240
4	0	-1	0	-0.1	0.1	0.5	0.009	90.080
5	0	0	1	-0.1	0.3	1.0	4.994	20.304
6	0	1	-1	-0.1	0.5	0.0	24.384	221.518
7	1	-1	1	0.1	0.1	1.0	11.809	5.330
8	1	0	-1	0.1	0.3	0.0	24.384	221.525
9	1	1	0	0.1	0.5	0.5	33.195	561.464

Table 4.4: Smooth round tensile test runs results.

Figure 4.7 shows the contour plots of stress for the smooth round tensile specimen immediately after fracture with the aforementioned parameters.

The material failure model in the cutting simulation allow to increase the accuracy and validity of the results by including the effects of material damage and element deletion in the FE model.

4.2 Tool

The micro-end-mills used in this study were two fluted AlTiN coated tungsten carbide (WC) with 1000 μm diameter (reference 1610-0197L059), a cutting length of 3 mm and a helix angle of 30° (Table 4.5). Table 4.6 shows the material compatibility of tools as mentioned above and Table 4.7 illustrates the recommended milling speeds and feeds by the tool's manufacturer.

In the current study, higher cutting speeds and feeds while compared to manufacturer recommendations were selected (see experimentation section), as the parameters mentioned

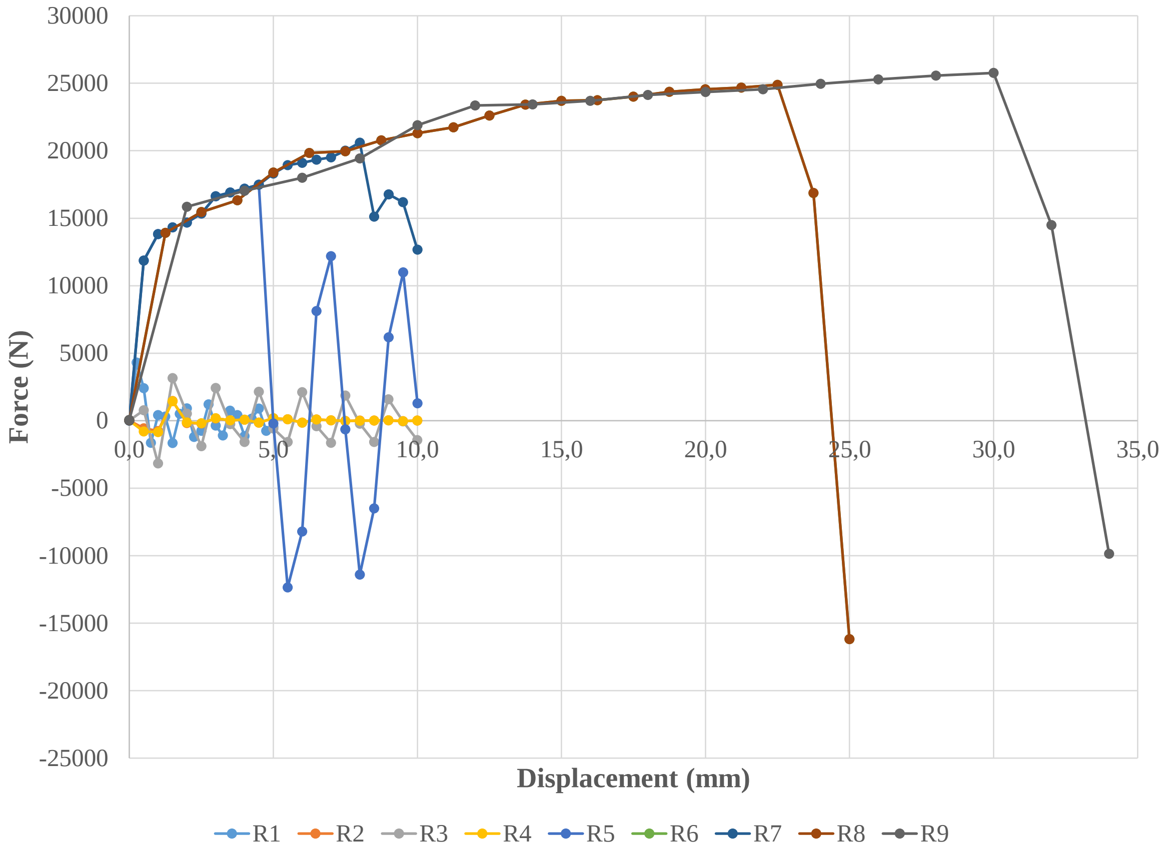

Figure 4.6: Force-displacement comparison for several run tests.

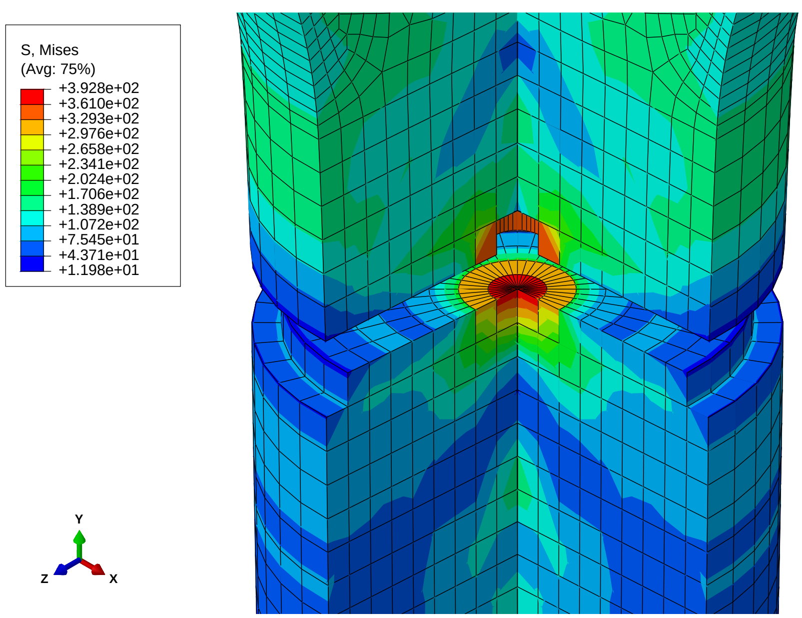

Figure 4.7: Contour plots for stress (in MPa) on fractured specimen at run 7 conditions.

in Table 4.7 cover a wide range of Titanium alloys. Also, through the selection of more aggressive parameters, higher cutting forces and increased tool wear should be expected at reduced cutting lengths/times.

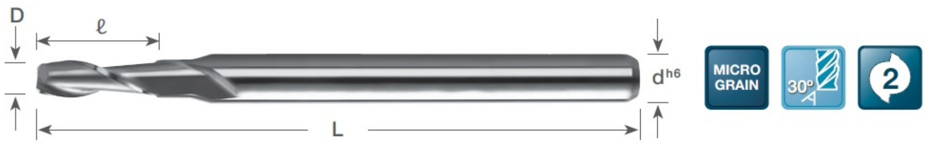

STANDARD Length (Metric Sizes)

Dimensions (mm)				Uncoated		AlTiN Coating	
D $^{+0.00mm}_{-0.02mm}$	d^{h6}	ℓ	L	Part Number	Stock	Part Number	Stock
1.00	3	3.00	38	1610-0394.118	●	1610-0394L118	■

Table 4.5: End mill dimensions [103].

SERIES 1610 **WORKPIECE MATERIAL**														
Coating	P Steel ~30HRC	P Steel 30~40HRC	H Hardened Steel ~55HRC	H Hardened Steel ~68HRC	M Stainless Steel	K Cast Iron	N Aluminum	N Graphite	N Copper Alloy	N CFRP	N Plastic	N Thermoset Plastic	N High Density Plastic	S Nickel / Cobalt	S Titanium Alloy
AlTiN	★	★	★	☆	☆	☆								☆	☆
Uncoated							☆	☆	★	☆	★	★	☆		☆

★ : Priority ☆ : Applicable Materials

Table 4.6: End mill workpiece material compatibility [103].

Material	Property	Vc : m/min Uncoated	Vc : m/min AlTiN	Feed : (mm/t)	Ø0.2	Ø0.5	Ø0.8	Ø1.0	Ø1.5	Ø2.0	Ø3.0
P Steel ~30HRC	<500 MPa	60	80	Slotting ap = 1.0 ae = 1.0	0.001	0.001	0.002	0.002	0.003	0.004	0.006
				Finishing ap = 1.0 ae = 0.3	0.001	0.001	0.001	0.001	0.001	0.001	0.001
	<800 MPa	60	80	Slotting ap = 1.0 ae = 1.0	0.001	0.001	0.002	0.002	0.003	0.004	0.006
				Finishing ap = 1.0 ae = 0.3	0.001	0.001	0.001	0.001	0.001	0.001	0.001
S Titanium Alloy	-	-	25	Slotting ap = 1.0 ae = 1.0	0.001	0.001	0.002	0.002	0.003	0.004	0.006
				Finishing ap = 1.0 ae = 0.3	0.001	0.001	0.001	0.001	0.001	0.001	0.001
K Cast Iron	-	60	80	Slotting ap = 1.0 ae = 1.0	0.001	0.001	0.002	0.002	0.003	0.004	0.006
				Finishing ap = 1.0 ae = 0.3	0.001	0.001	0.001	0.001	0.001	0.001	0.001

Table 4.7: Manufacturer recommended cutting speeds & feeds [103].

Tool deflection effects due to cutting forces, imperfections in spindle-holder assembly, and manufacturing accuracies are not considered in current approach for predicted forces. To incorporate the shear deformation and rotary inertia effects, some authors consider the tool as a Timoshenko beam element to describe the beam deflections [60, 129]. Also, the coating of a thin layer of AlTiN which may result in increased tool life and improved surface roughness is not considered. Higher cutting forces may be expected (while compared to uncoated tools) in some cases, based on a higher tool edge radius but lower friction effects and cutting temperatures [190] may allow for successful dry cutting.

4.3 FEM

A 2-D finite element model under plane strain deformation was used based on ABAQUS/Explicit platform. Explicit, dynamic and adiabatic analysis is applied since the work material is subjected to deformations in a short period of time with large plastic strains during micro-cutting.

Some important assumptions are made to reduce complexity in FE model:

- The tool is modeled as a rigid body (no coating effects or machine dynamics are included).
- The tool orientation and velocity are held constant (and normal to the cutting edge).
- The workpiece material is homogeneous and isotropic. Micro-cracks and micro-structural effects of material on properties are neglected.
- Heat transfer between tool and workpiece and cooling are neglected. No thermal effects on parameters are included. A constant friction interaction is considered.
- Plain strain assumption for 2-D elements is applied.

Figure 4.8 shows a schematic representation of the constructed model with the geometries of the cutting tool and the workpiece. The parameterized model can consider geometrical variations in tool rake angle (α), clearance angle (γ) and tool edge radius (r_e); also, workpiece dimensions as length (w_l) and height (w_h) can be adjusted for different uncut chip thicknesses (h). The tool edge radius (r_e) is approximated to 7.5 μm according to measurements from optical microscopy. The rake angle (α) and clearance angle (γ) are 12° and 20° respectively.

4.3.1 Meshing

The workpiece is partitioned into three sections as shown in Figure 4.8. An Arbitrary Lagrangian-Eulerian (ALE) formulation is applied in the model to the workpiece-tool interaction zone (marked as I), to increase the elements freedom and to allow to handle greater distortions of the continuum with good resolution. This formulation also allows reduced force oscillations in results [2, 81]. The Lagrangian regions (marked as II and III) are those that won't be exposed to severe element distortion and are constrained to move in X and Y directions.

A 4-node bilinear plane strain, quadrilateral, with reduced integration and automatic hourglass control CPE4R element type was applied to the workpiece. More than 13,000

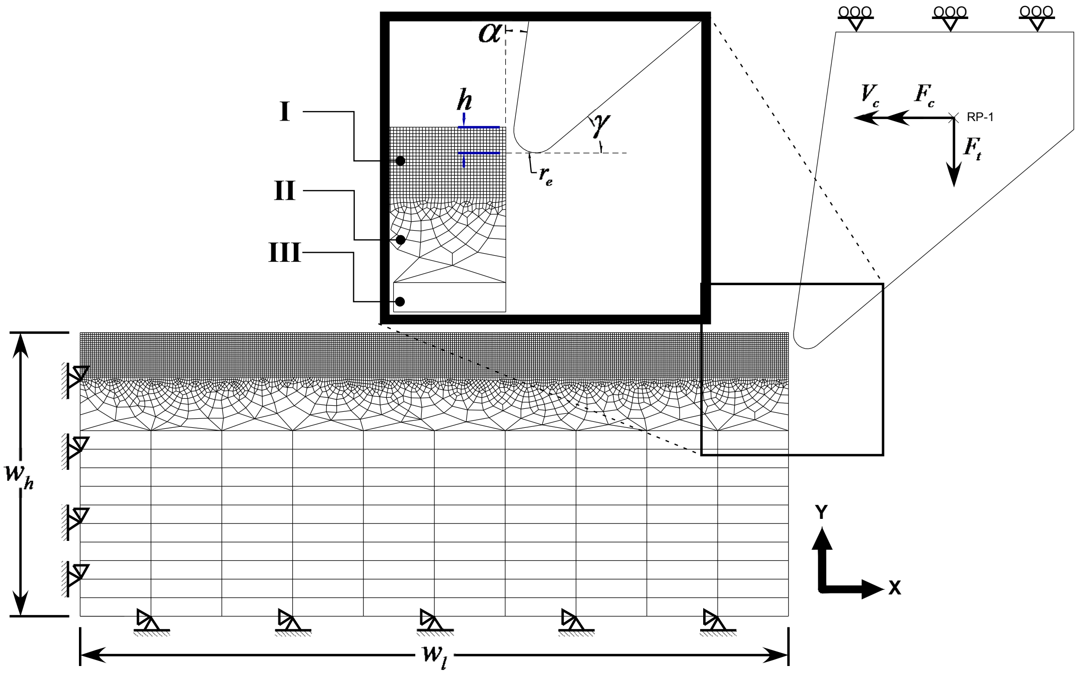

Figure 4.8: Orthogonal model geometry and boundary conditions.

elements with an approximate size of 0.75 μm were used in the zone I to achieve a good precision and to reduce computational load after a mesh dependency test.

Mass scaling The computational cost was further reduced through the application of mass scaling. A semi-automatic mass scaling was implemented with negligible effects on the results by comparison on the resultant forces and ensuring a good ratio between kinetic energy and internal energy of the system (often below 5–10%) [51].

4.3.2 Boundary conditions and interactions

The workpiece is fixed in its bottom and left sides, while the proper cutting speed (V_c) is applied to the rigid tool which is constrained to move in other directions. The tool is modeled as an isothermal rigid body represented by the reference point (RP) to apply the velocity constraint and gather the forces in cutting (F_c) and tangential (F_t) directions.

Friction modeling Despite the availability of many friction models in the literature [173, 136] from simple to more complex, the prediction of material contact phenomenon during machining is not yet understood entirely, since it is substantially dependent on multiple variables. In the current scenario, the FE model includes the effect of tool-workpiece contact with frictional interaction modeled with the Coulomb friction model. This model is commonly used and allows a simple implementation of friction effects. Current research includes the effect of finite sliding, where previous studies consider a value of 0.17 [21], 0.2 [219], 0.5 [162], 0.7 [31, 190, 158] to 0.85 [181] for Ti-6Al-4V. In current study, the friction coefficient was set to 0.7 as it was applied more frequently through explored literature.

4.3.3 Cutting forces prediction

Micro-orthogonal cutting simulations were performed at different uncut chip thicknesses (up to 15 μm) and cutting speeds (up to 942 mm/s, which correspond to 18000 RPM for 1 mm diameter end-mill) for CP-Ti. Figure 4.9 illustrates the evolution of cutting forces with respect to time. It can be noted that at a certain time (near 42 μs) the cutting force in tangential (or thrust) direction experiences a sudden drop, indicating that chips start to form. This is explained as an equilibrium between the upward flow of material and downward flow along the cutting edge of the tool. When stable cutting conditions are reached, then both forces remain relatively constant. The steady state values are recorded and averaged for different conditions and are summarized in Figure 4.10 where the effect of cutting speed on the force prediction can be neglected, due to low variations in the given test range (628 to 942 mm/s). Also, the forces in the cutting direction (F_c) are higher at increased uncut chip thicknesses while compared to forces in the tangential direction (F_t). This indicates that cutting forces in feed direction will be dominant at high feed rates and tangential (or thrust) forces will be more noticeable at low feed rates (at small uncut chip thicknesses) due to the size effect.

As shown in the Figure 4.10, a logarithmic relationship between the uncut chip thickness and the cutting forces can be established as:

$$\begin{bmatrix} F_c \\ F_t \end{bmatrix} = \begin{bmatrix} 7768 \log h + 16692 \\ 2564 \log h + 8363 \end{bmatrix} \tag{4.5}$$

were R^2 and adjusted R^2 values which were found to be 95.7% and 95.3% respectively for the forces in the cutting direction, and 99.4% and 99.2% respectively for the forces in the tangential direction.

The micro-milling cutting forces in the X and Y directions can be evaluated through a coordinate transformation (Figure 4.11) given by:

$$\begin{bmatrix} F_x \\ F_y \end{bmatrix} = \begin{bmatrix} -\cos\theta & -\sin\theta \\ -\sin\theta & \cos\theta \end{bmatrix} \begin{bmatrix} F_c \\ F_t \end{bmatrix} \tag{4.6}$$

where θ is the angle of rotation, and F_x and F_y represent the forces per unit length (N/m). Hence, to evaluate the total cutting forces, the uncut chip thickness (h) algorithm proposed by Li et al. [113] described in the previous chapter (section 3.3.1) need to be implemented with given cutting parameters to obtain forces per unit length which must be multiplied by the axial depth of cut.

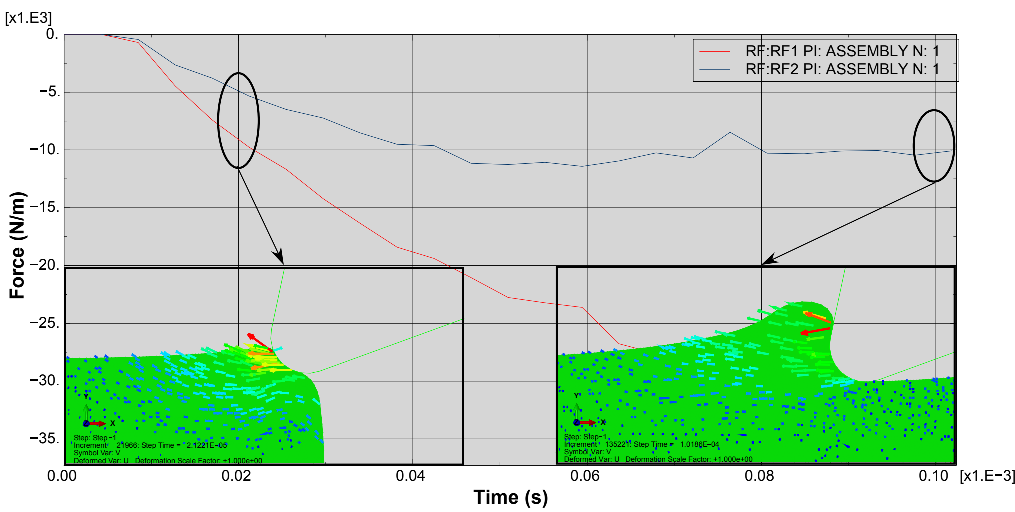

Cutting speed: 942 mm/s (18000 RPM), uncut chip thickness: 3 μm.

Figure 4.9: Cutting ($R1$=F_c) and tangential ($R2$=F_t) forces evolution.

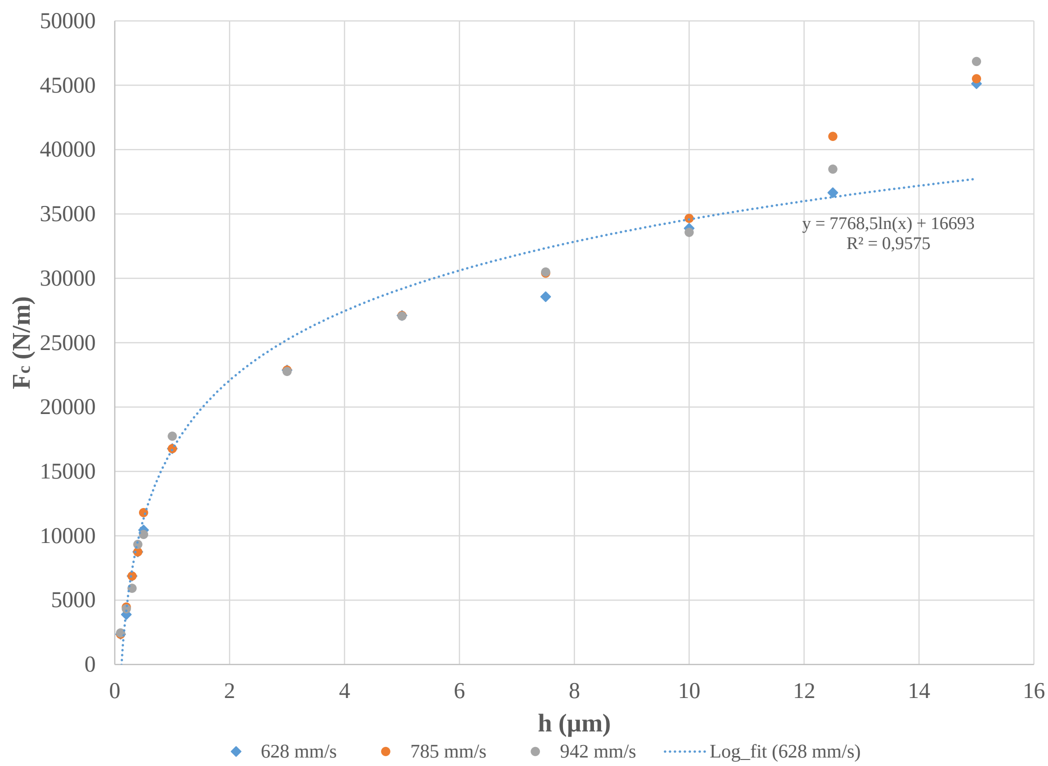

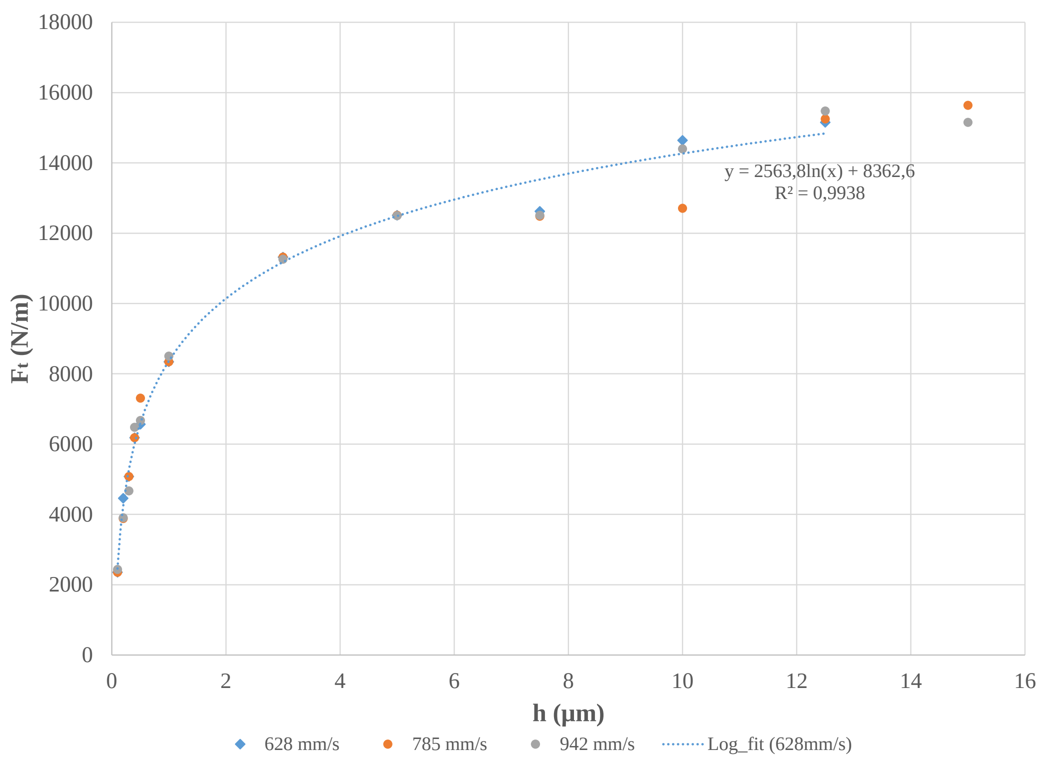

Figure 4.10: Cutting forces in the cutting (F_c) and tangential (F_t) directions.

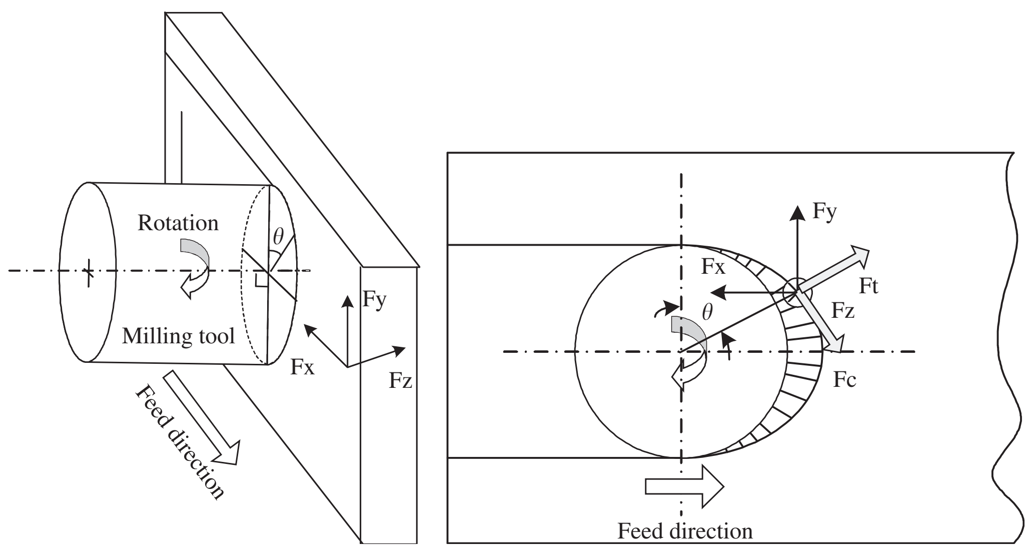

Figure 4.11: Micro-milling forces decomposition [104].

4.4 Experimentation

A high-speed spindle NSK HES510 was attached to a Deckel Maho DMC1035V CNC milling machine (Figure 4.7). The run-out of the spindle is certificated to be below 3 μm according to NSK inspection standards. The workpiece material was CP-Ti grade 2 in the form of sheets of 5mm thickness. Two fluted AlTiN coated tungsten carbide (WC) tools with 1000 μm diameter (reference 1610-0197L059), a cutting length of 3mm and a helix angle of 30° were used. All tools were replaced for each set of cutting parameters and were installed with an overhang of 13mm to reduce the effects of variations of initial tool wear and deflection on results.

The cutting strategy consisted in full-immersion slot micro-end-milling of 1000 μm straight grooves (channels) with different parameters. A total of 20 grooves were made for each cutting test conditions, considering a total cutting length of 780mm approximately. All experiments were performed under dry machining conditions.

Cutting forces measurements were made with a Kistler 9257BA 3-component dynamometer that incorporates built-in 3-channel charge amplifier which converts the charge signals into voltage signals. NI PXI4472B 8-channel Dynamic Signal Acquisition (DSA) module was installed on a NI PXI1042 chassis for data sampling and processing. The cutting forces were sampled at a minimum of 20kHz and maximum of 30kHz to guarantee a minimum of 100 samples per tool's revolutions (near 3.6°/sample).

The zero-point in the Z direction was found by moving the tool until an acoustic emission (AE) signal was detected, which were processed at higher sampling rates (70kHz).

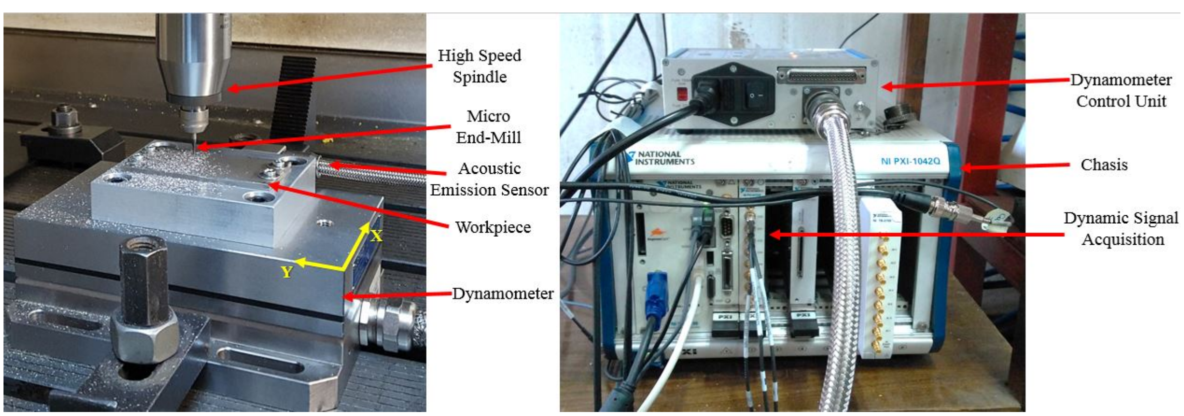

Figure 4.12: Setup for (a) milling machine and (b) data sampling-processing.

4.4.1 Experimental design

The micro-milling experimental runs were specified through Taguchi experimental design method to investigate the effect of three factors (spindle speed, feed and axial depth of cut) on the cutting forces and to validate the predictions through FEM simulations. Three levels

Levels	Low	Center	High
Coding	-1	0	+1
Spindle Speed ($kRPM$)	12	15	18
Feed ($\frac{\mu m}{tooth}$)	1.4	2.0	2.6
Depth of cut (μm)	200	400	600

Table 4.8: Independent variables levels and coding.

	Coded			**Real**				
Run	**A**	**B**	**C**	**Spindle Speed** ($kRPM$)	**Feed** ($\frac{\mu m}{tooth}$)	**Depth of cut** (μm)	**Cut speed** ($\frac{m}{min}$)	**Feed rate** ($\frac{mm}{min}$)
1	-1	-1	-1	12	1.4	200	37.7	34
2	-1	0	0	12	2.0	400	37.7	48
3	-1	1	1	12	2.6	600	37.7	62
4	0	-1	0	15	1.4	400	47.1	42
5	0	0	1	15	2.0	600	47.1	60
6	0	1	-1	15	2.6	200	47.1	78
7	1	-1	1	18	1.4	600	56.5	50
8	1	0	-1	18	2.0	200	56.5	72
9	1	1	0	18	2.6	400	56.5	94

Table 4.9: Taguchi L_9 (3^3) orthogonal array.

for each independent variable were considered as shown in Table 4.8. A change of 20% in spindle speed, 30% in feed and 50% in depth of cut between central and lower/upper values are applied to explore a wide range of cutting conditions.

The previously mentioned conditions were more demanding concerning cutting speeds and feeds than the manufacturer recommendations (depicted in Table 4.7) for given tool-workpiece set. The final set of experimental runs for given cutting conditions is summarized in Table 4.9.

4.4.2 Results

Figures 4.13 & 4.14 illustrate a sample of cutting force signals for X (feed) and Y (transverse to feed) directions while milling the first slot of each test condition. It can be noticed that there is some noise level in the force component in the feed direction (F_x), especially in the cases of run 6 and run 8. This noise can be related to the machine-assembly rigidity and the tool run-out. While observing the graphs of the experimental cutting forces, it can be verified the effect of a small tool run-out and tool wear, as the difference between force peaks during the cutting of each flute can be noted.

To analyze the cutting force signals, the data from 4 seconds was chosen (from 800 to 1200 revolutions according to spindle speed) and different parameters like RMS, negative and positive peak values. Table 4.10 summarizes the measured cutting forces during each test

			1	2	3	4	5	6	7	8	9
Run			1	2	3	4	5	6	7	8	9
Spindle Speed ($kRPM$)			12	12	12	15	15	15	18	18	18
Feed ($\frac{\mu m}{tooth}$)			1.4	2	2.6	1.4	2	2.6	1.4	2	2.6
Feed rate (mm/min)			34	48	62	42	60	78	50	72	94
Depth of cut (μm)			200	400	600	400	600	200	600	200	400
Slot 1	$\boldsymbol{F_x}$	*Mean (DC)*	0.545	1.016	2.220	4.219	3.325	1.262	2.580	1.955	2.525
		Negative peak	0.254	0.568	1.013	3.166	2.096	0.122	1.739	1.310	1.793
		Peak to peak	0.673	0.997	2.292	2.234	2.400	2.424	1.999	1.273	1.566
		Positive peak	0.927	1.565	3.306	5.400	4.497	2.546	3.738	2.583	3.359
		RMS	0.567	1.044	2.295	4.249	3.355	1.300	2.609	1.964	2.546
	$\boldsymbol{F_y}$	*Mean (DC)*	0.501	0.994	3.011	2.799	2.546	0.995	2.157	1.077	2.548
		Negative peak	0.186	0.528	1.346	1.737	1.110	0.508	0.984	0.669	1.658
		Peak to peak	0.735	1.113	3.129	2.331	2.571	1.103	2.274	0.860	1.553
		Positive peak	0.920	1.641	4.475	4.068	3.681	1.611	3.258	1.529	3.211
		RMS	0.532	1.032	3.098	2.864	2.594	1.031	2.207	1.100	2.574
	$\boldsymbol{F_r}$	*RMS*	0.777	1.468	3.855	5.124	4.241	1.659	3.417	2.251	3.620
Slot 20	$\boldsymbol{F_x}$	*Mean (DC)*	2.513	3.555	4.388	5.072	4.972	2.485	5.046	1.765	3.356
		Negative peak	2.067	2.219	2.082	3.565	3.581	0.387	3.559	1.339	2.396
		Peak to peak	1.008	2.931	3.767	3.099	2.596	4.201	3.022	1.062	2.113
		Positive peak	3.075	5.150	5.848	6.665	6.178	4.588	6.581	2.401	4.509
		RMS	2.524	3.611	4.449	5.117	5.006	2.539	5.070	1.774	3.378
	$\boldsymbol{F_y}$	*Mean (DC)*	2.492	2.643	3.445	4.558	3.705	1.231	2.835	1.275	2.867
		Negative peak	2.048	0.946	1.255	2.753	1.776	0.631	1.238	0.816	1.597
		Peak to peak	1.072	3.421	4.385	3.983	3.478	1.371	3.271	1.005	2.176
		Positive peak	3.120	4.367	5.641	6.737	5.254	2.002	4.510	1.821	3.774
		RMS	2.507	2.773	3.581	4.636	3.781	1.286	2.905	1.297	2.904
	$\boldsymbol{F_r}$	*RMS*	3.558	4.552	5.711	6.905	6.274	2.846	5.843	2.198	4.454

Forces in Newtons.
F_x: Force in X direction. F_y: Force in Y direction. $F_r = \sqrt{F_x^2 + F_y^2}$: Resultant cutting force.

Table 4.10: Characteristics and evolution of cutting forces for each cutting condition.

and at different stages: slot 1, corresponding to new tools with cut length near to 39mm, and slot 20 with a cut length near 780mm. The effect of cutting conditions and cut length/time on measured forces is noticeable. In some cases, a change over 70% between final and initial resultant forces can be observed as depicted in Figure 4.15.

Figure 4.16 shows the initial average and peak-to-peak resultant force for each test. Conditions in runs 4, 5, 7 and 9 exhibit a lower peak-to-peak average resultant force while compared to initial resultant force itself. This suggests that those cutting parameters may generate a steadier cutting force.

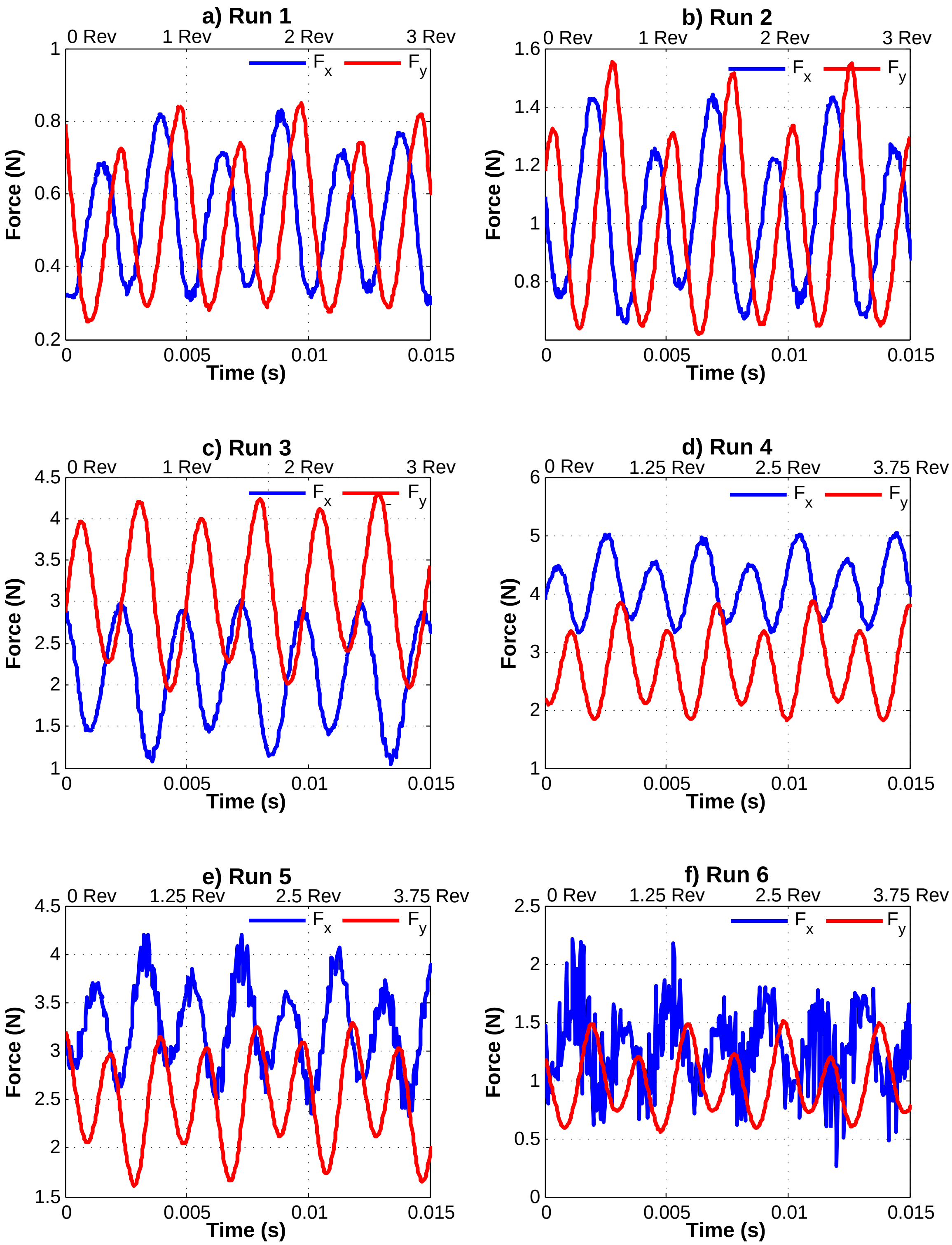

Figure 4.13: Experimental cutting forces for each cutting condition (Run 1 to 6).

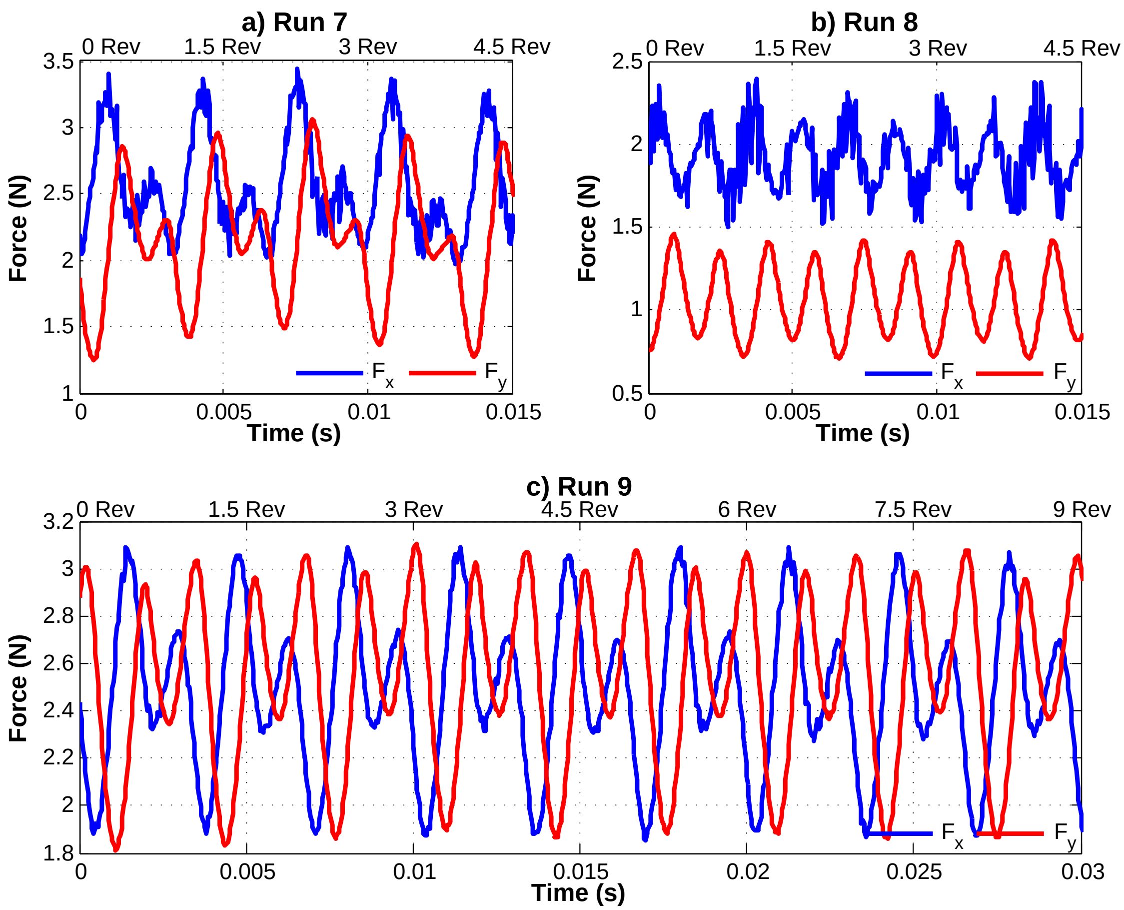

Figure 4.14: Experimental cutting forces for each cutting condition (Run 7 to 9).

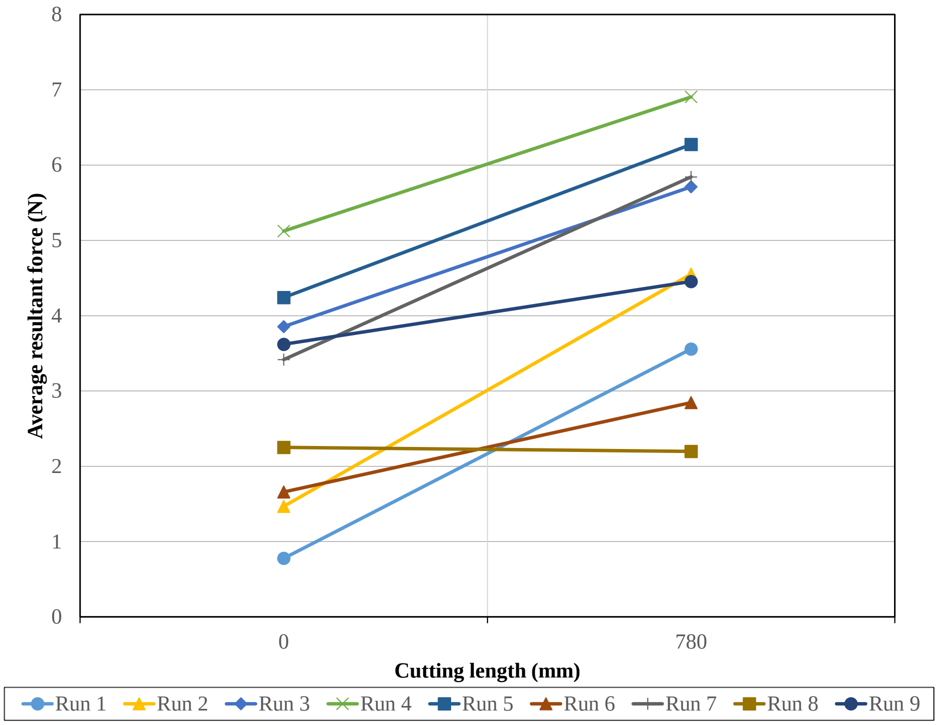

Figure 4.15: Average resultant milling forces evolution.

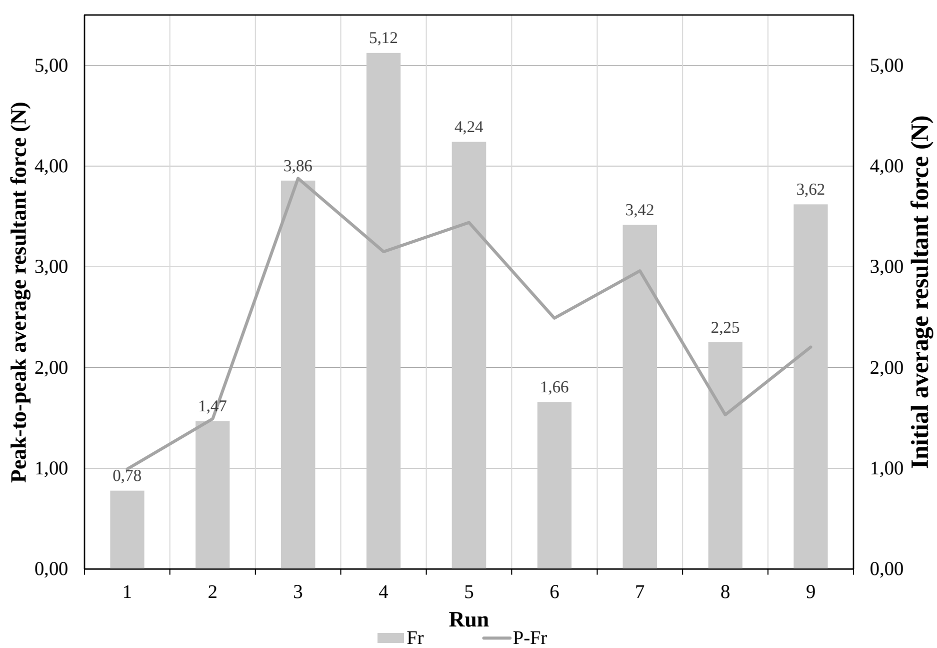

Figure 4.16: Initial average and peak-to-peak resultant forces.

4.4.3 Modeling

ANOVA The analysis of variance allows studying the relative significance of the cutting conditions on the resultant forces for a given regression model. Table 4.11 illustrates the ANOVA for a linear model to estimate initial resultant forces based on spindle speed (A), feed (B) and axial depth of cut (C). It is important to note that a y^{-1} (inverse) transform was applied to the response to improve model fitting. The model adequacy is shown through R^2 and adjusted R^2 values which were found to be 73.1% and 56.9% respectively, indicating a good fit with real data. Predicted R^2 was estimated as 0% indicating an overfitted model to given data. In the current case, the model fits the original data (with its noise) but is less capable of providing valid predictions for new observations.

According to ANOVA results, the values of Prob$>F$ inferior to 0.05 indicate a significant predictor (at 95% confidence level). In the current case, the axial depth of cut (C) is a statistically significant model term.

Residuals are described by a normal distribution as shown in the normal probability plot Figure 4.17a. The assumption of parameters independence is also satisfied as residuals do not exhibit any explicit pattern or trend (Figures 4.17b and c). Finally, the plot shown in Figure 4.17d indicates an adequate precision between predicted and actual response values as proved by a good set R^2 parameters. These plots do not suggest any problem with model assumptions.

To study the behavior of the response and to find a suitable approximation of its true form, a first order polynomial is fitted for F_r. The coefficients shown in Table 4.12 were calculated using least-squares fit. It is important to note that this model only includes main effects. Then the resultant force, in terms of real variables can be predicted as:

$$F_r^{-1} = 2.3559 - 0.06747A - 0.17678B - 0.00129C \tag{4.7}$$

Figure 4.18 illustrates different contour plots of mentioned regression model for resultant

Source	**SS**	**DOF**	**MS**	F Value	Prob$>F^*$
A	0.3223	2	0.1612	2.20	0.3126
B	0.0695	2	0.0348	0.47	0.6783
C	0.4355	2	0.2178	2.97	0.2518
Error	0.1466	2	0.0733		
Total	0.9739	8			

SS: Sum of Squares, DOF: Degree Of Freedom, MS: Mean Square.
$R^2 = 73.1\%$; Adjusted $R^2 = 56.9\%$, Predicted $R^2 = 0\%$.
$*$ Value of F variable at 95% confidence level.

Table 4.11: ANOVA for main effects.

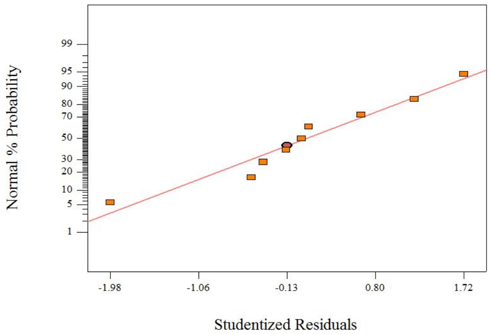

(a) Normal probability.

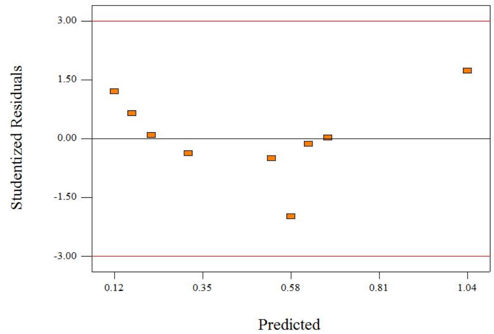

(b) Residuals vs Predicted.

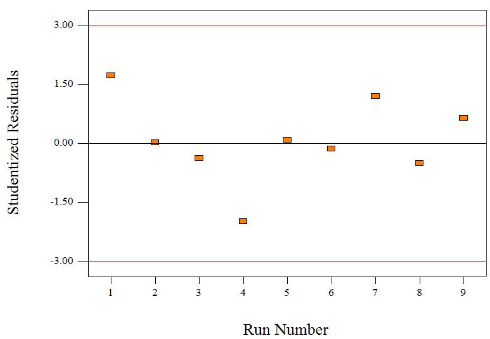

(c) Residuals vs Run Number.

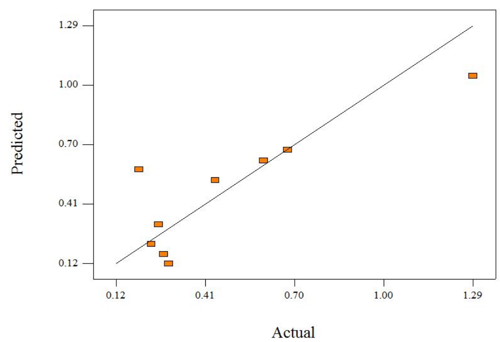

(d) Predicted vs actual.

Figure 4.17: Micro-cutting simulations.

Source	F_r^{-1}	
	Coded	**Real**
Intercept	0.47494	2.3559
A	-0.20241	-0.06747
B	-0.10607	-0.17678
C	-0.25769	-0.00129

Model: $y = Intercept + A + B + C$.

Table 4.12: Regression model coefficients.

force (value inside parentheses) in coded and real variables. In the design space, it can be noted that contour lines are parallel, indicating an increase in cutting force towards higher depth of cut and feeds (and material removal rates) as expected. As shown in Figure 4.19, the forces are more sensitive to axial depth of cut, followed by feed.

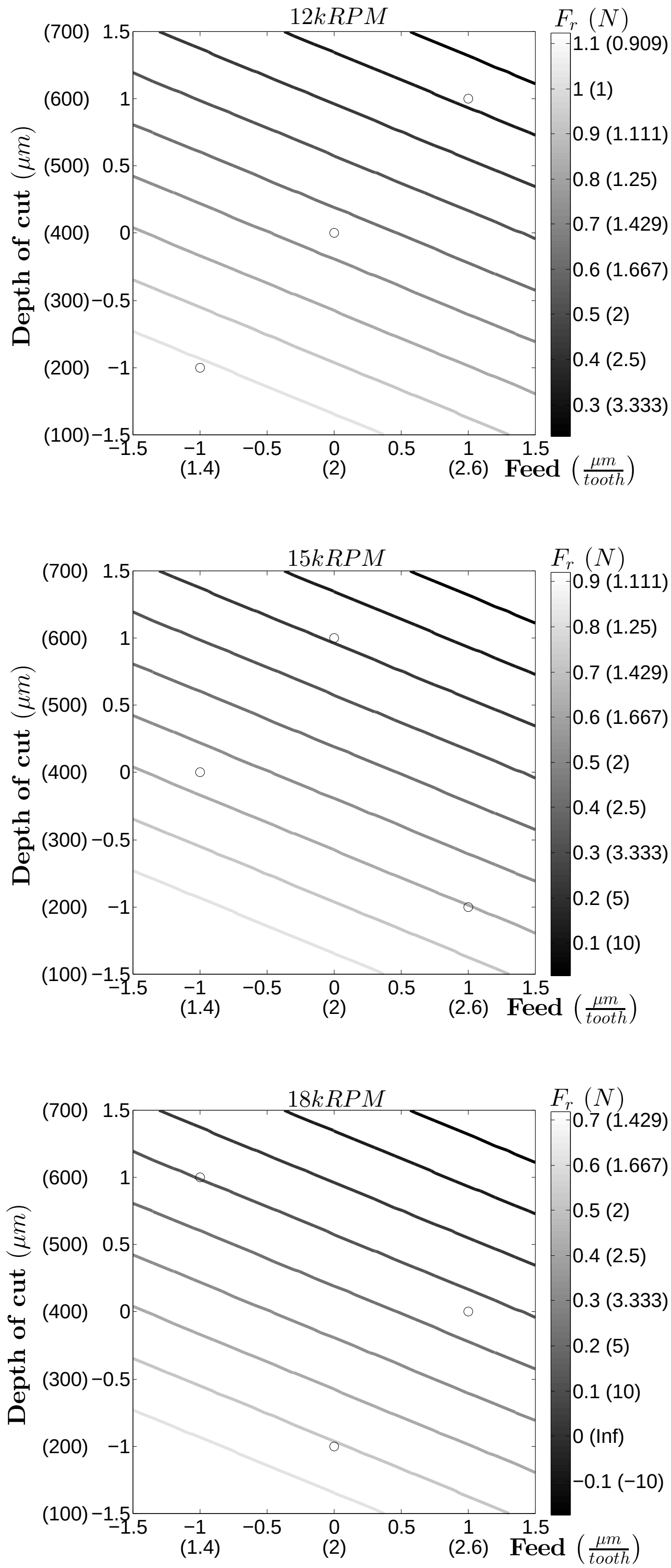

Experimental data points are represented by ∘.

Figure 4.18: Contour plots for resultant force at different spindle (cutting) speeds.

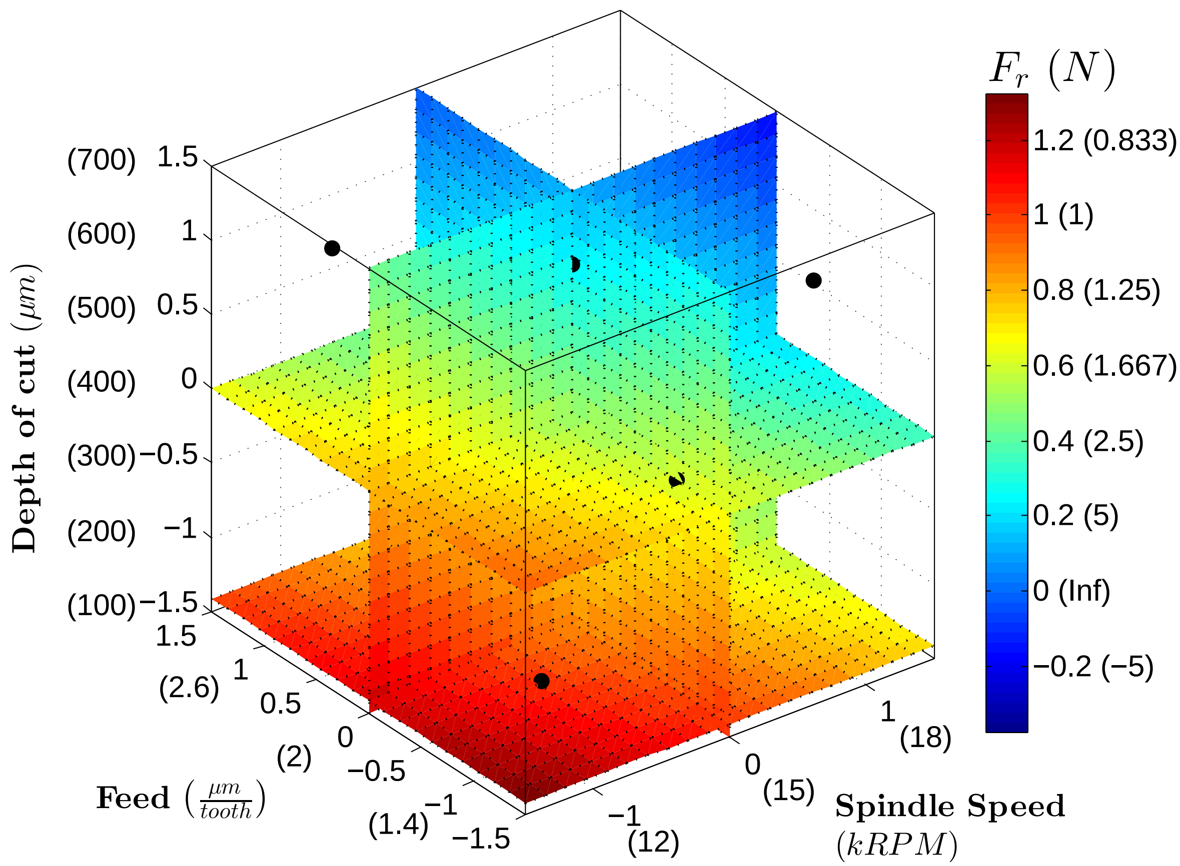

Experimental data points are represented by •.

Figure 4.19: Iso-force planes.

4.4.4 Process stability

The measured cutting force signals are used to properly identify vibrations by applying the Fast Fourier Transformations (FFT). In such cases, chatter can be identified when the FFT force magnitude at the tool natural frequency is relatively high [1]. As shown in Figures 4.21, 4.22 and 4.23 the spindle rotational speeds (200, 250 and 300 Hz) and the tooth passing frequencies (400, 500 and 600 Hz) are always below the natural frequency of the force measurement system with embedded quartz force sensor (2000 Hz). This ensures a precise measurement compliant with the dynamometer sensitivity.

In both feed and traverse direction forces, the tooth passing frequency is dominant for runs 1,2,3,4,5,6 and 8. For runs 7 and 9 the higher peak at the frequency of the spindle speed indicates that the spindle and tool run-out combination plays an essential role in micro-milling. Also, it can be noted that in some cases, the end mill tooth passing frequency plays a more dominant role in the y direction rather than in the x (feed) direction, e. g. in run 3 which is consistent with findings shown in Figure 4.13.

The workpiece-table natural frequency was also analyzed considering the existing bolted joint. The workpiece dimensions of 39 mm width, 80 mm height, 5 mm thickness with 4 holes of 3.175mm diameter for M3 bolts. Dynamometer base plate is modeled as a rigid surface, and boundary conditions are applied according to the existing conditions with general contact. The eigenvalues are extracted (with the Lanczos algorithm) to calculate the natural frequencies and the corresponding mode shapes, considering initial preload and a linear perturbation procedure performed with Abaqus software. After conducting the modal analysis, the natural frequency at the first shape is found to be at 5916 Hz (shown in Figure 4.20) followed by a second shape at 7802 Hz. Both conditions are far from existing cutting and measuring capabilities.

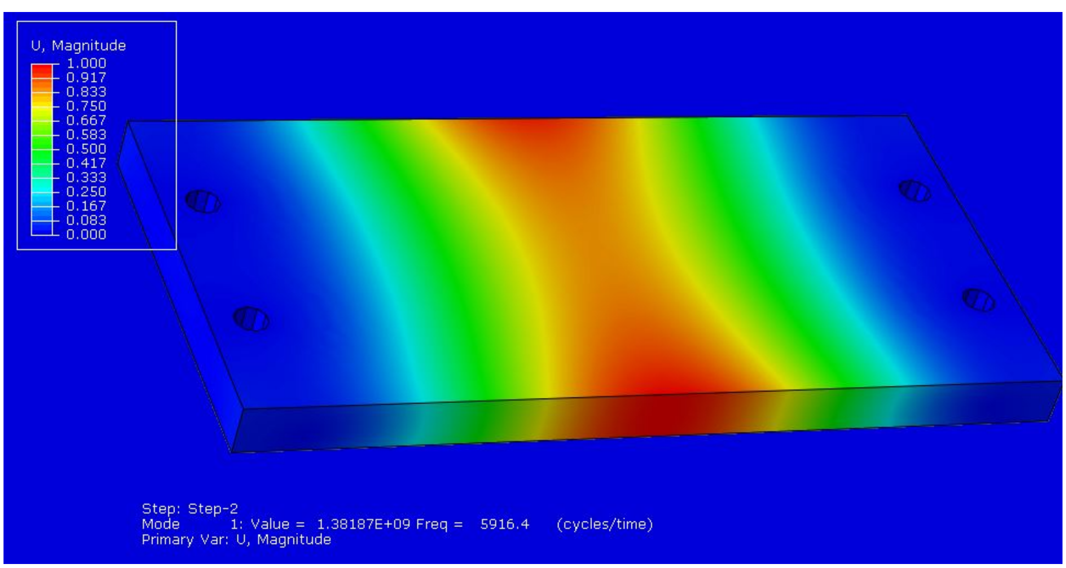

Figure 4.20: Workpiece first shape mode natural frequency.

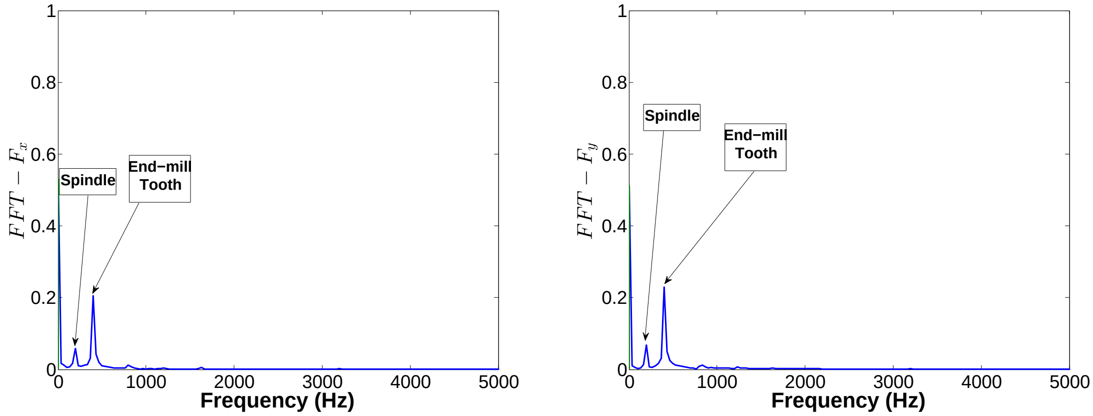

$\omega = 12kRPM$; $V_c = 37.7m/min$; $f_z = 1.4\frac{\mu m}{tooth}$; $a_p = 200\mu m$.

a) Run 1 frequency spectrum.

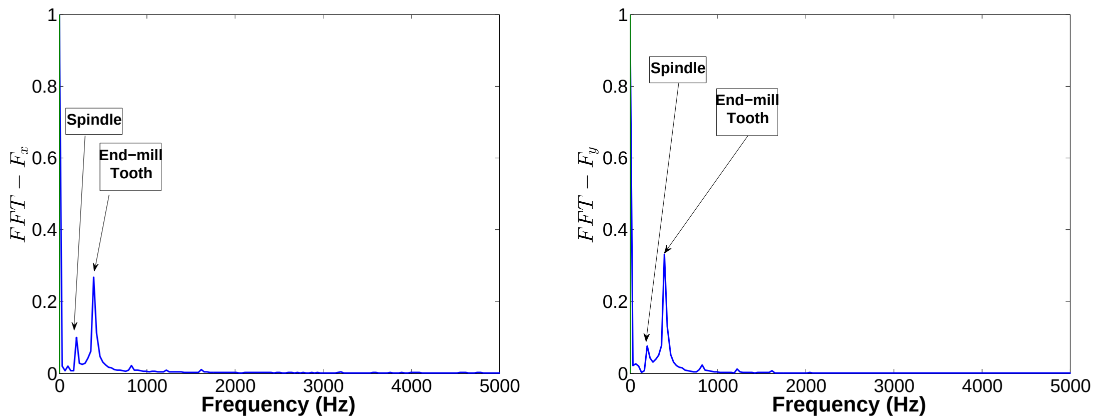

$\omega = 12kRPM$; $V_c = 37.7m/min$; $f_z = 2.0\frac{\mu m}{tooth}$; $a_p = 400\mu m$.

b) Run 2 frequency spectrum.

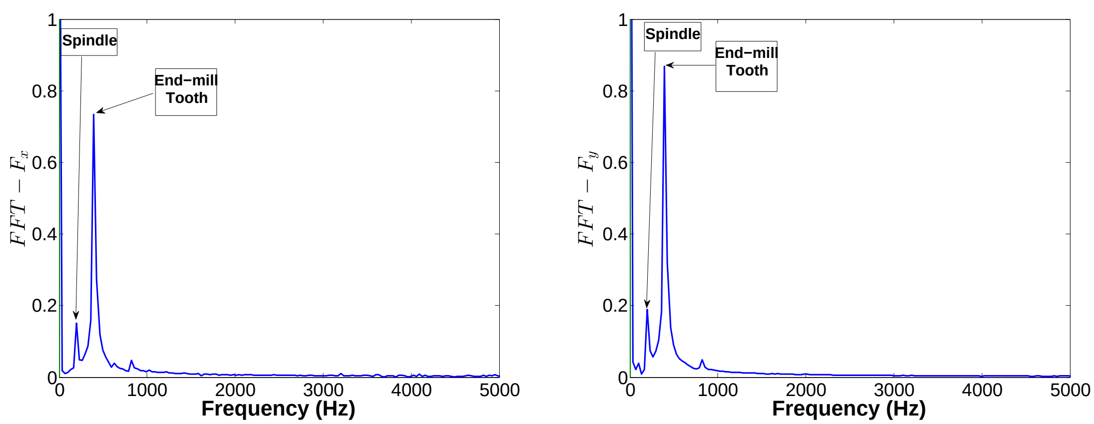

$\omega = 12kRPM$; $V_c = 37.7m/min$; $f_z = 2.6\frac{\mu m}{tooth}$; $a_p = 600\mu m$.

c) Run 3 frequency spectrum.

Figure 4.21: FFT of the cutting forces signal (Run 1 to 3).

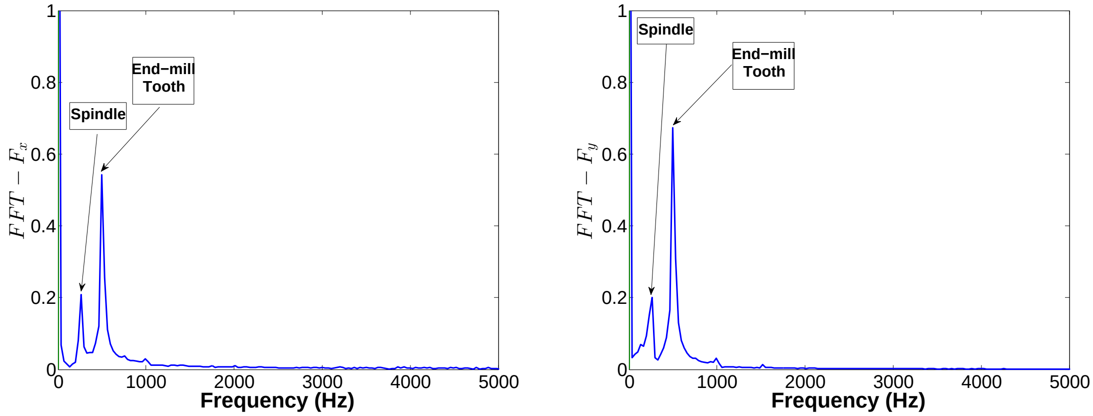

$\omega = 15kRPM$; $V_c = 47.1m/min$; $f_z = 1.4\frac{\mu m}{tooth}$; $a_p = 400\mu m$.

a) Run 4 frequency spectrum.

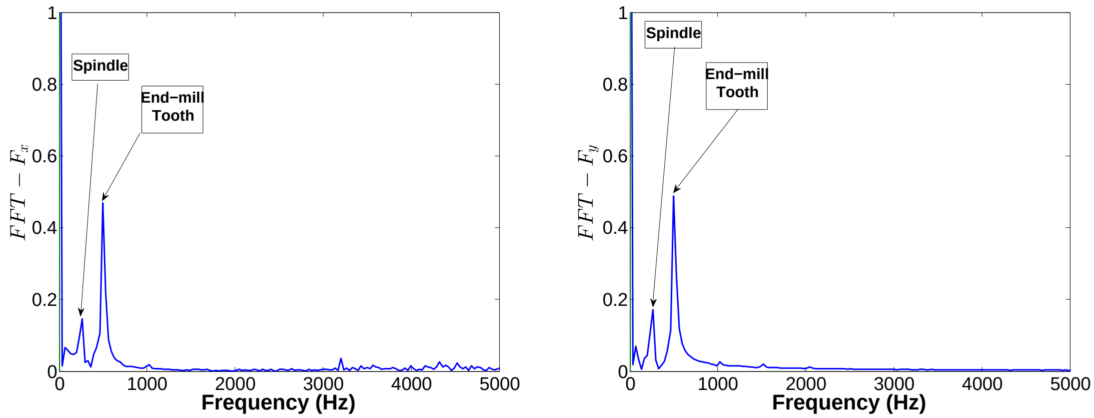

$\omega = 15kRPM$; $V_c = 47.1m/min$; $f_z = 2.0\frac{\mu m}{tooth}$; $a_p = 600\mu m$.

b) Run 5 frequency spectrum.

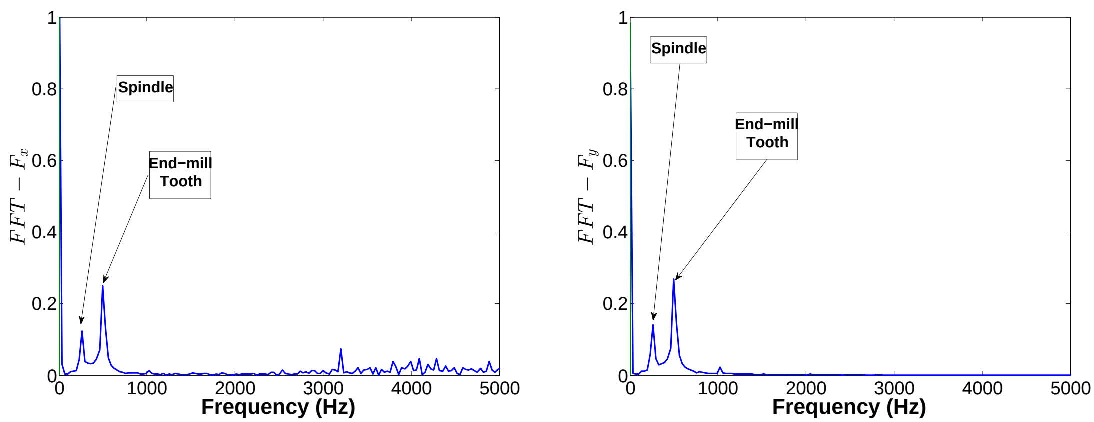

$\omega = 15kRPM$; $V_c = 47.1m/min$; $f_z = 2.6\frac{\mu m}{tooth}$; $a_p = 200\mu m$.

c) Run 6 frequency spectrum.

Figure 4.22: FFT of the cutting forces signal (Run 4 to 6).

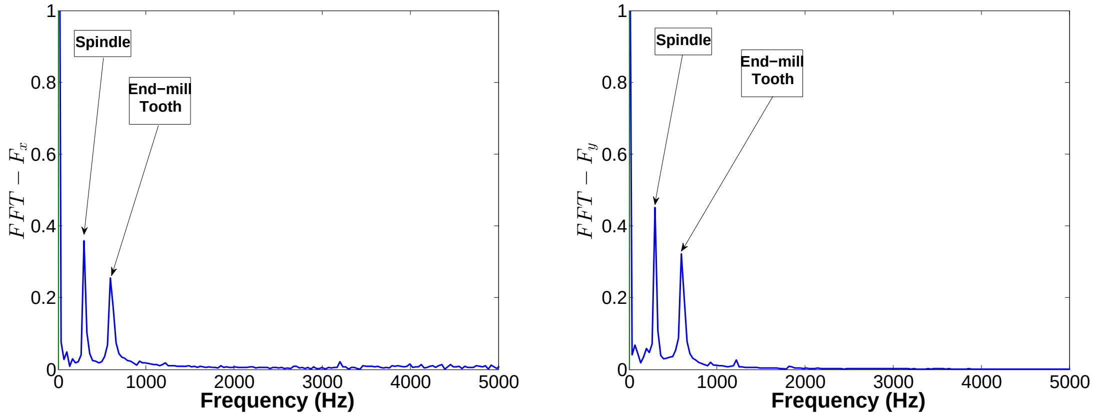

$\omega = 18kRPM$; $V_c = 56.5m/min$; $f_z = 1.4\frac{\mu m}{tooth}$; $a_p = 600\mu m$.

a) Run 7 frequency spectrum.

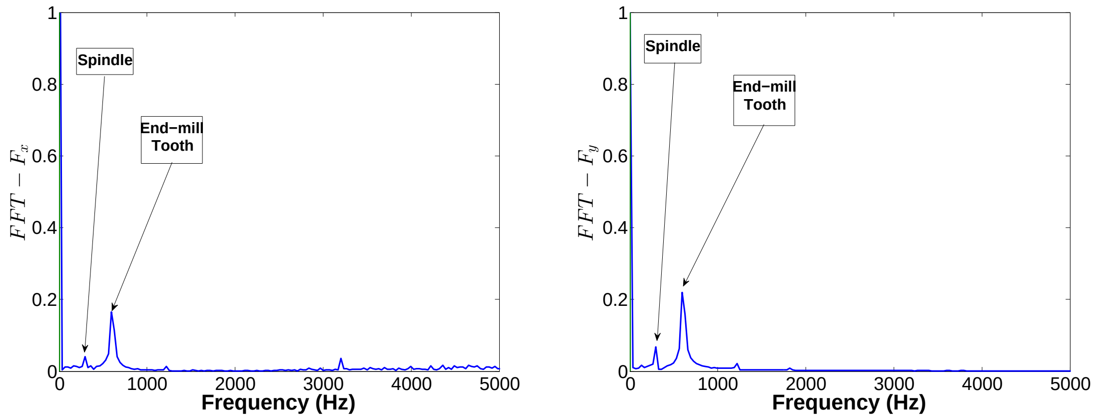

$\omega = 18kRPM$; $V_c = 56.5m/min$; $f_z = 2.0\frac{\mu m}{tooth}$; $a_p = 200\mu m$.

b) Run 8 frequency spectrum.

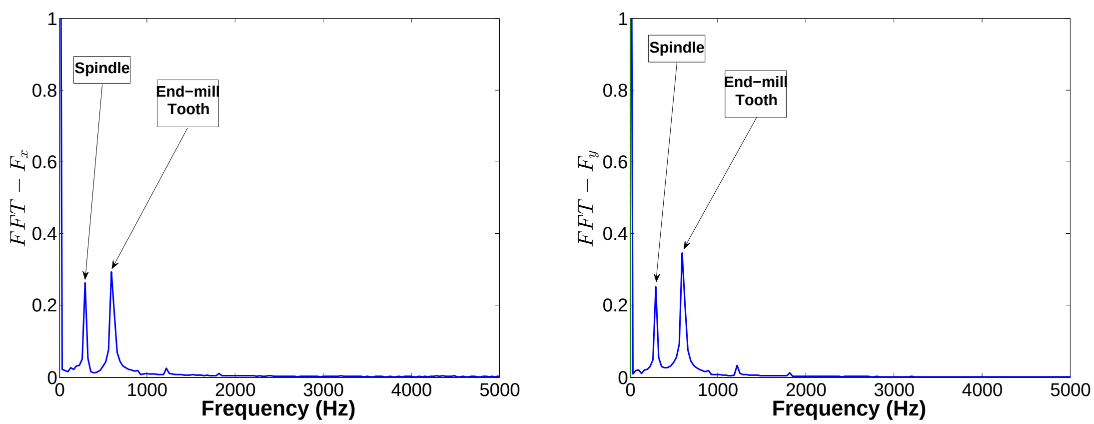

$\omega = 18kRPM$; $V_c = 56.5m/min$; $f_z = 2.6\frac{\mu m}{tooth}$; $a_p = 400\mu m$.

c) Run 9 frequency spectrum.

Figure 4.23: FFT of the cutting forces signal (Run 7 to 9).

The Finite Element method was also applied to predict the natural frequencies and mode shapes of the tool. A 3-D model of the tool according to dimensions shown in Table 4.5 was developed, where a cylinder approximated the cutting flutes with a diameter equal to 68% [69]. The density, elastic modulus and Poisson ratio of the material are 14450 kg/m^3, 580 GPa, 0.28 respectively [85, 69]. The tool is modeled as a cantilever beam constrained at the shank end without rotational motion. Tetrahedral elements were used with a smaller element size at tapper and flute sections. To ensure the accuracy, a convergence study was also performed with an increased number of elements with a tolerance of 5% between consecutive simulations.

The first and third frequencies (2908 and 29183 Hz) are due to rotation (around X-Z axis) about fixed base and torsion around Y axis. Differences between real and FE predictions may arise mainly due to a different boundary condition at the clamping region of the tool and geometry simplifications. The first mode and natural frequency could be considered as shown in Figure 4.24 at 17180 Hz which is consistent with findings of Filiz and Ozdoganlar which predicts a value over 14 kHz for current tip diameter [61]. Therefore, for the current study, the simulated environment provides a more critical dynamic scenario than the one imposed by real cutting conditions where the spindle and tooth passing frequencies are far below the tool natural frequency.

For an accurate prediction of the tool dynamics, often a combination of Experimental Modal Analysis (EMA) and Receptance Coupling (RC) is used. This strategy estimates the dynamics of the spindle/machine structure directly using EMA through impact hammer testing, and this result is mathematically combined (through compatibility and equilibrium conditions) with the dynamics of the tool structure which is found through finite element analysis [69].

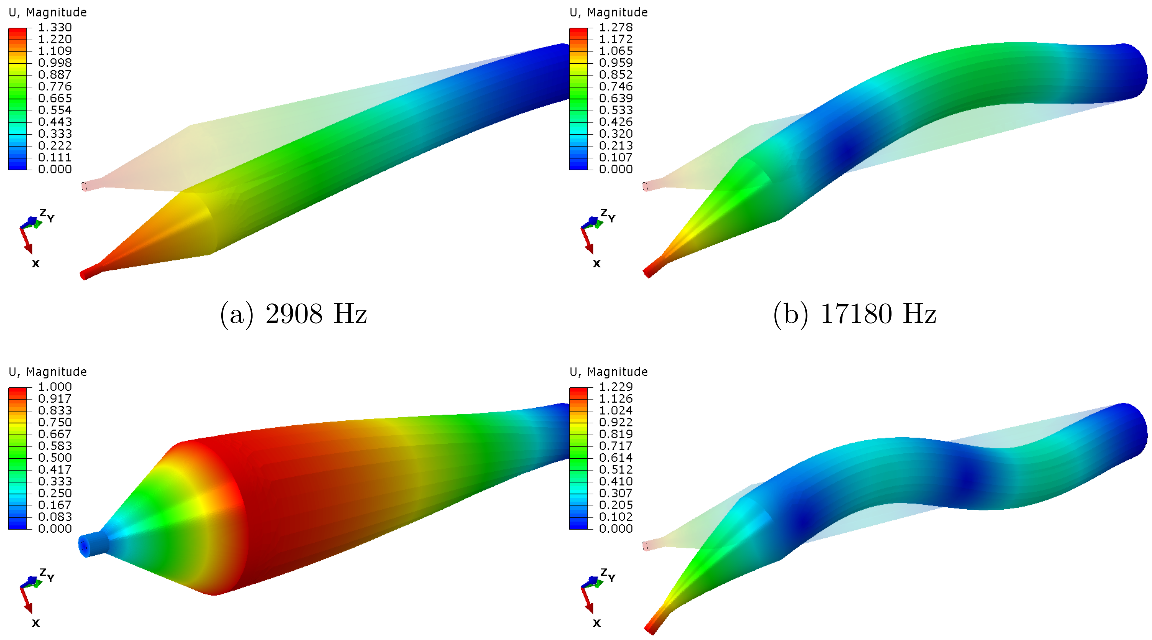

(a) 2908 Hz (b) 17180 Hz

(c) 29183 Hz (d) 44677 Hz

Figure 4.24: Mode shapes and natural frequencies of the tool.

4.5 Numerical-Experimental comparison

The predicted (F_{pred}) resultant forces were calculated according to forces in cutting (F_c) and tangential (F_t) directions, and axial depth of cut a_p. Also, the real (F_{real}) resultant forces were calculated considering measurements in X (F_x) and Y (F_y) directions as follows:

$$\begin{gathered} F_{pred} = \left(\sqrt{F_c^2 + F_t^2}\right) a_p \\ F_{real} = \sqrt{F_x^2 + F_y^2} \end{gathered} \tag{4.8}$$

The micro-milling cutting conditions described in experimentation section were considered, and the iterative algorithm proposed by Li et al. [113] for uncut chip thickness described in Figure 3.11 was applied to include the effects of runout. In the current case, a runout length $r_o = 0.15$ μm and runout angle ($\gamma = 45°$) was applied to include a small runout effect (based on maximum measurement of the spindle manufacturer to be below of $3\mu m$). The predicted and measured (real) average cutting forces are shown in Table 4.13, and some conditions are shown in Figure 3.11. It can be observed that the predicted forces with the empirical model (linear model, equation 4.7) allow an average error of 40% along all the measured conditions with high variability (over 48%). Considering the numerical FE model, errors above 100% can be noted for almost all cases.

Run	Spindle Speed ($kRPM$)	Feed ($\frac{\mu m}{tooth}$)	Depth of cut (μm)	F_{real} (N)	FE model F_{pred} (N)	FE model Error (%)	Empirical model F_{pred} (N)	Empirical model Error (%)
1	12	1.4	200	0.767	2.442	218%	0.961	25%
2	12	2.0	400	1.468	7.598	418%	1.478	1%
3	12	2.6	600	3.850	12.628	228%	3.199	17%
4	15	1.4	400	5.026	6.587	31%	1.723	66%
5	15	2.0	600	4.127	11.487	178%	4.623	12%
6	15	2.6	200	1.624	4.233	161%	1.597	2%
7	18	1.4	600	3.332	9.921	198%	8.337	150%
8	18	2.0	200	2.241	3.839	71%	1.887	16%
9	18	2.6	400	3.571	8.478	137%	6.031	69%

Table 4.13: Models comparison and validation.

The main error sources may arise from:

- *In numerical (FE) calculations:* The precision of numerical results can be greatly affected by tolerance identification of entry parameters (more than 20, as shown in Table 4.14) including differences on material properties, cutting conditions, tool - machine tool characteristics, and material-tool interface (summarized in Figure 3.1). In the current study, material properties were adapted from existing literature studies with CP-Ti with similar microstructure, thereby inducing deviations between simulation applied conditions and real parameters. Different researchers have analyzed the effect of variations in workpiece material and contact parameters into the cutting forces such as:
  - Sensibility analysis by other researchers [9, 149, 37, 47] indicate that only due to a wrong set of parameters of a JC constitutive model can lead to an error up to 30% in predicted forces.
  - Cutting conditions accuracies and interaction parameters such as the friction model applied can also have a significant influence in predicting chip geometry, forces, stresses and temperatures during machining [173, 157, 10, 117].

  The tool parameters such as the rake and clearance angles, cutting edge radius coupled with process conditions like cutting speed, feed, depth of cut, and uncut chip thickness variations relative to real parameters are also a significant source of error. According to Miranda et al. [140], micro-tools may have substantial geometrical variations in cutting edge radius and rake angle, therefore promoting differences of measured forces only due to a different tool (in this research, nine new tools were used for each set of cutting conditions).

  Finally, the numerical formulations developed for uncut chip thickness model, and the orthogonal FE model itself may become a relevant source of deviation against experimental results.

Property		Parameters	Test/measurement method
Workpiece and Tool material input parameters	Density	ρ	Combined mass and volume (lengths) measurement
	Poisson's ratio	v	Tensile test
	Young's modulus	E	Idem
	Constitutive model	A, B, n, m, C	SHPB, Shock inducing impact tests
	Fracture model	D_1, D_2, D_3, D_4, D_5	Uniaxial tensile and compressive tests
	Temperature	T	IR Thermography
	Thermal conductivity	λ	Guarded hot plate, laser flash difussivity
	Specific heat	C_p	Conventional calorimetry, pulse methods
	Inelastic heat fraction	β	Thermomechanical experiments with IR thermal measurements
Contact	Friction coefficient	μ	Cutting force measurements (turning or milling), conventional or special tribometer
	Heat partition coefficient	α	Idem
Tool - Machine tool	Cutting speed	V_c	Machine tool settings, adapted sensors, indirect methods
	Feed per tooth	f	
	Axial depth of cut	a_p	
	Radial depth of cut	a_e	
	Tool cutting edge radius	r_e	Optical microscopy, Scanning Electron Microscopy (offline methods)
	Tool rake angle	α	
	Tool clearance angle	γ	
	Tool diameter	ϕ	
	Tool runout	ρ, α	Laser sensors, capacitive sensors
	Tool deflection	τ, ψ	

Table 4.14: Physical parameters of workpiece and cutting tool for simulation studies.

- *In experimental procedures:* Different source of errors can evolve from measurement estimations and uncertainties of parameters. Real cutting conditions such as depth of cut, feed rate, and spindle speed precise settings, and machine stiffness are another notable source of errors at this micro-scale.

4.5.1 Sensitivity analysis

As previously mentioned, there are several simulation entry parameters like material constants, contact behavior parameters, simulation settings and others that have a remarkable influence in numerical cutting forces results. It is important to mention that is very complex to identify the parameters used in the simulation at conditions similar to the micro-machining conditions concerning strains, strain rates, and temperatures, therefore often material behavior is extrapolated for most studies [9].

In this section, a sensitivity analysis was performed to examine the influence of a specific parameter on the cutting forces. The effect of different friction coefficients at the tool-chip interface was considered by only changing this parameter, that according to literature could vary from 0.17 to 0.85 (indicated in section 4.3.2 FE boundary conditions and interactions). All other settings remained the same, obtaining the results shown in Figure 4.25 were a significant change in F_c can be noted and a negligible change in F_t. Then a friction coefficient of 0.2, the cutting forces can be established as (with $R^2 = 94\%$):

$$\begin{bmatrix} F_c \\ F_t \end{bmatrix} = \begin{bmatrix} 5039 \log h + 9163 \\ 2564 \log h + 8363 \end{bmatrix} \tag{4.9}$$

Table 4.15 compares the prediction of FE models with variations in friction coefficient. It can be seen that the overall error for all test runs, dropped below 89% only due to a change in friction coefficient consistent with available literature used range.

					$\mu = 0.7$		$\mu = 0.2$	
Run	**Spindle Speed** $(kRPM)$	**Feed** $(\frac{\mu m}{tooth})$	**Depth of cut** (μm)	F_{real} (N)	F_{pred} (N)	**Error** (%)	F_{pred} (N)	**Error** (%)
1	12	1.4	200	0.767	2.44	218%	1.612	110%
2	12	2.0	400	1.468	7.598	418%	5.002	241%
3	12	2.6	600	3.850	12.628	228%	8.302	116%
4	15	1.4	400	5.026	6.587	31%	4.342	14%
5	15	2.0	600	4.127	11.487	178%	7.558	83%
6	15	2.6	200	1.624	4.233	161%	2.783	71%
7	18	1.4	600	3.332	9.921	198%	6.538	96%
8	18	2.0	200	2.241	3.839	71%	2.524	13%
9	18	2.6	400	3.571	8.478	137%	5.574	56%

Table 4.15: FE models prediction comparison and validation.

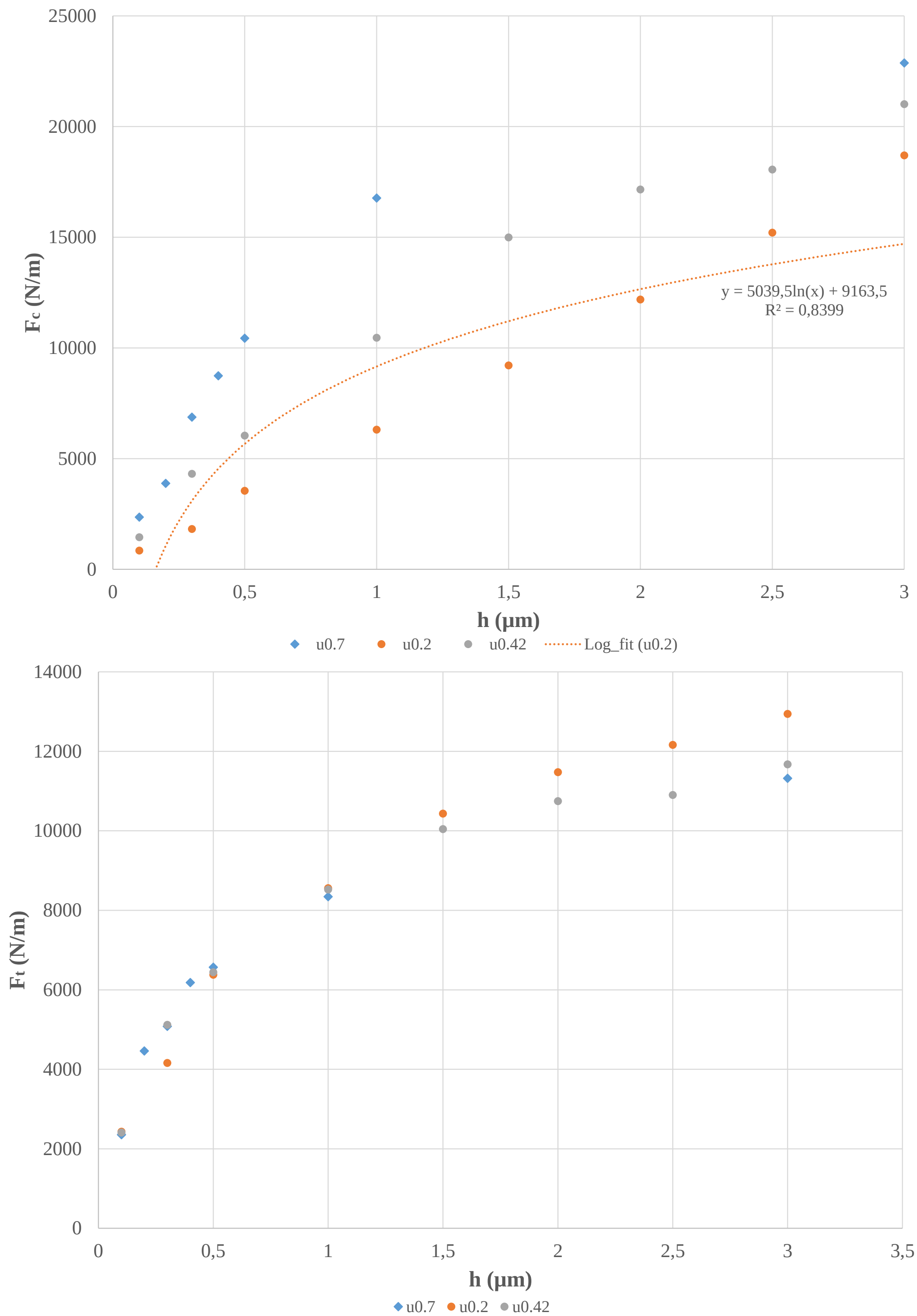

Figure 4.25: Cutting forces in the cutting (F_c) and tangential (F_t) directions (μ variations).

4.6 Discussion

A numerical model to predict forces during micro-milling has been successfully developed. This model includes the determination of the undeformed chip thickness, considering the runout, feeds, number of flutes, tool diameter, and spindle angular velocity, for the prediction of accurate trajectories of the cutting edges relative to the workpiece. This calculation of undeformed chip thickness is then coupled to a developed FE model to predict the forces in the cutting and tangential directions. The material parameters were calibrated with existent literature data (from similar conditions CP-Ti) to include the behavior at different strains, strain rates, temperature and damage criterion. The FE model allowed to create a non-linear equation to predict the relation between forces and uncut chip thickness.

An experimental approach is developed based on a reduced number of experimental tests through Taguchi experimental design method to measure cutting forces at different cutting conditions. Statistical techniques are applied to fit a linear regression model for the resultant cutting force.

The proposed hybrid approach allows acquiring an *a priori knowledge* related to cutting forces, stresses, strain and strain rates that can be used to correctly set and conduct reduced experimental tests for validation and measure industry relevant parameters such as tool-life, surface roughness, burrs and others. After experimentation, empirical or mechanistic force models can be developed, or numerical parameters (such as JC coefficients or friction models) can be adjusted to fit the real data.

CHAPTER 5

Tool wear

Contents

5.1 Introduction

Several critical issues are associated with micro-milling operations that arise from the miniaturization of components, tools and mechanics effects. Miniature tools are more likely to experience relatively large vibrations and forces due to size, reduced stiffness and the size effect [128]. These factors bring several challenges to achieve the desired performance in terms of an efficient tool life while micro-milling. Tool life is closely related to machining quality, stability and efficiency, which highlights tool life evaluation, in particular, for many difficult-to-cut materials resulting in fast tool wear [80].

Wear criteria are usually used in assessing tool life. Different criterion based on cutting time required for a given limit for flank wear, tool edge radius or tool diameter are often applied. In conventional machining ISO 8688-2 specifies recommended procedures for tool-life testing and flank wear limits in end milling; however, there is no general definition of tool wear level in micro-machining. Often, previously mentioned measurable factors are all related to the cutter geometry and can be monitored for gaining a better understanding of the micro-cutting mechanisms and progression of the tool wear [53].

5.2 Tool wear in CP-Ti micro-milling

5.2.1 Methodology

The following phases were followed to improve CP-Ti micro-milling performance in terms of reduced tool wear:

- Experimentation: Experiments considering variations in spindle speed, feed and axial depth of cut were done. Their effect on process outputs was collected for proper analysis. The application of Taguchi orthogonal arrays was vital to explore a good experimental design space with efficient use of time and resources.
- Modeling: Through the application of statistical methods, the collected data is studied, and predictive models are developed.
- Optimization: Optimal regions are found through the study of defined performance indices.

To investigate tool wear during CP-Ti micro-milling, an experimental setup was implemented as shown in Figure 5.1. Milling equipment consisted in a high-speed spindle NSK HES510 attached to a Deckel Maho DMC1035V CNC milling machine. A certified tool run-out is guaranteed to be below $3\mu m$ according to NSK inspection standards. Tool condition was monitored on-line with a Dino-Lite Edge Digital Microscope AM4815ZTL positioned inside the working area (without removing the tool from the spindle). Images were scaled with a calibration ruler with 10 μm divisions.

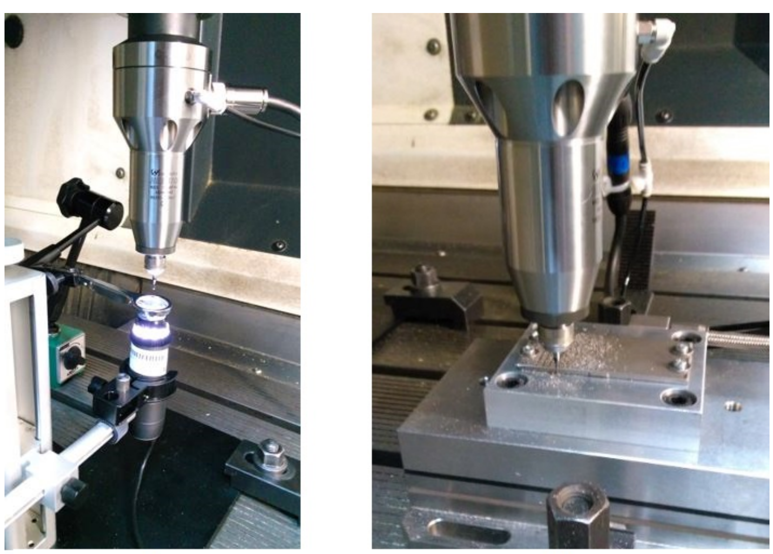

a) b)

Figure 5.1: Setup for (a) microscope and (b) workpiece machining.

	Coded			Real				
Run	**A**	**B**	**C**	**Spindle Speed** ($kRPM$)	**Feed** ($\frac{\mu m}{tooth}$)	**Depth of cut** (μm)	**Cut speed** ($\frac{m}{min}$)	**Feed rate** ($\frac{mm}{min}$)
1	-1	-1	-1	12	1.4	200	37.7	34
2	-1	0	0	12	2.0	400	37.7	48
3	-1	1	1	12	2.6	600	37.7	62
4	0	-1	0	15	1.4	400	47.1	42
5	0	0	1	15	2.0	600	47.1	60
6	0	1	-1	15	2.6	200	47.1	78
7	1	-1	1	18	1.4	600	56.5	50
8	1	0	-1	18	2.0	200	56.5	72
9	1	1	0	18	2.6	400	56.5	94

Table 5.1: Taguchi L_9 (3^3) orthogonal array.

The workpiece material was CP-Ti grade 2 in the form of sheets of 5mm thickness. Two fluted AlTiN coated tungsten carbide (WC) tools with 1000 μm diameter (reference 1610-0197L059), a cutting length of 3 mm and a helix angle of 30° were used. All tools were replaced for each set of cutting parameters and were installed with an overhang of 13 mm to reduce the effects of variations of initial tool wear and deflection on results.

The cutting strategy consisted in full-immersion slot micro-end-milling of 1000 μm straight grooves (channels) with different parameters. A total of 20 grooves were made for each cutting test conditions, considering a total cutting length of 780 mm approximately. All experiments were performed under dry machining conditions.

Experiments were performed as based on the design shown in Table 5.1 considering variations in spindle speed (A), feed (B) and axial depth of cut (C). Taguchi orthogonal array allowed to evaluate the three parameters at three different levels. The levels were chosen to develop more aggressive conditions than the ones recommended by tool's manufacturer (therefore expecting greater tool wear rates).

Tool geometry In this research flat end micro-mills are considered. Their geometrical features are adopted from the macro-milling tool as a scaled down version. A schematic illustration of typical two-fluted micro-mill is given in Figure 5.2. The typical geometry of the commercial tool includes three main parts, namely the shank, the neck and the cutting part. The shank connects the cutting tool to the tool holder. The cutting part contains the cutting edges. Finally, the neck part allows connecting the cutting part with the shank part [39].

The cutting edge radius is the most influential factor on the tool performance with significant effects on cutting forces, tool stresses and temperatures, chip formation and surface quality. Current manufacturing technology cannot fabricate a micro-tool with perfectly sharp edges. Often, current tools have an edge radius ranging from 1 to 5 μm; also a significant variation in tool diameter, up to 10% can be expected. Based on this observations, it is imperative the inspection of tools before machining to minimize errors and maintain consistent results.

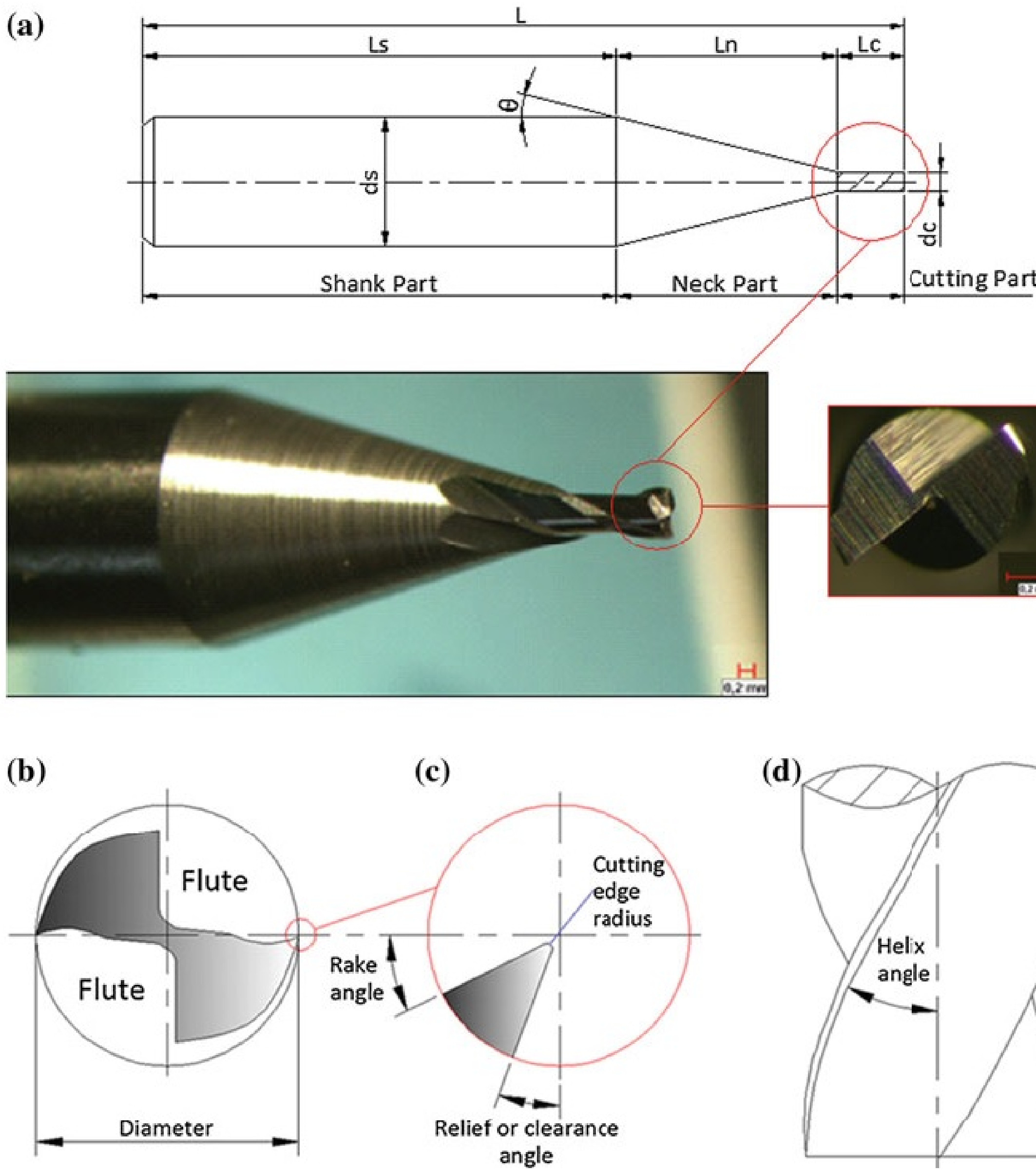

Figure 5.2: Two-flute end mill cutter (a) geometry; (b) cross section; (c) cutting edge; (d) side view [39].

Figure 5.3 shows the geometry and morphology of a new and worn tool. Variations in cutting edge (rounded) geometry can be noted due to wear consequently affecting the accuracy and roughness of the produced component. Some wear modes may exist like coating delamination, abrasive wear, and workpiece material deposition. In the current study, a direct measurement of tool condition was made during machining tests. Images for different geometrical parameters were taken, as shown in Figure 5.4. A flank wear zone (V_{Bj}) and edge rounding (r_{ej}) can be identified for each cutting edge (j).

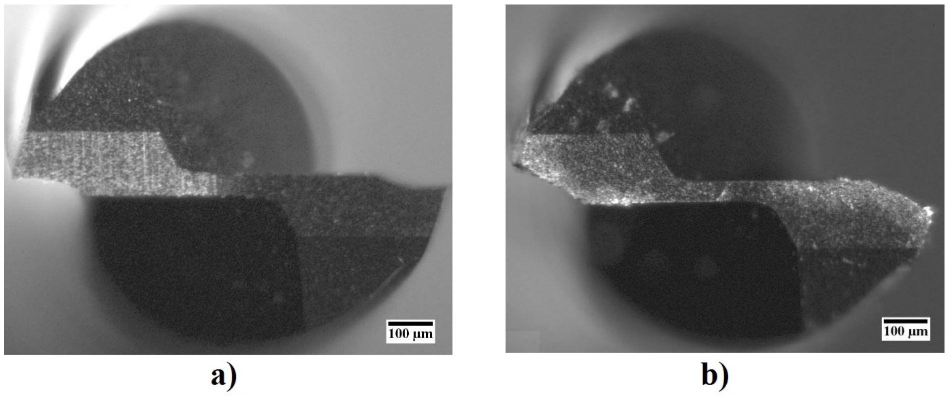

Figure 5.3: Comparison of (a) new and (b) worn tool.

For all the experimental conditions given in Table 5.1, both parameters are measured at the beginning of the experiment (initial condition, cut length = 0 μm) and at the end of each test (final condition, cut length = 780 μm) as depicted in Figure 5.5. The average values of each geometrical parameter are evaluated as follows to compare a given tool wear state:

$$\begin{aligned} V_{Bai} &= \left(V_{B1} + V_{B2}\right)/2 \\ r_{ea} &= \left(r_{e1} + r_{e2}\right)/2 \end{aligned} \tag{5.1}$$

To eliminate the influence of the initial tool flank wear and edge rounding, the measurements are normalized relative to unused values for each tool (new tools). Then, the following equation allows to calculate the corresponding increase in each geometrical parameter:

$$\begin{aligned} V_{Bi} &= \frac{V_{Baf} - V_{Bai}}{V_{Bai}} \times 100 \\ r_{ei} &= \frac{r_{eaf} - r_{eai}}{r_{eai}} \times 100 \end{aligned} \tag{5.2}$$

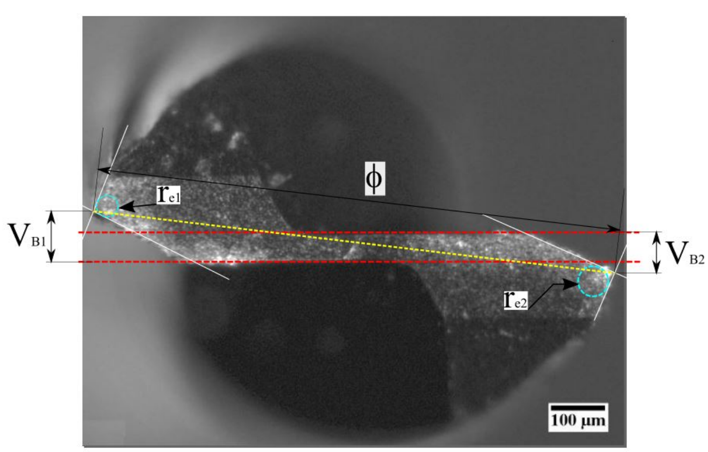

Figure 5.4: Tool wear geometrical measurements.

5.2.2 Results

Figure 5.5 displays the initial and final states of used tools for each cutting tests according to the randomized experimental design illustrated in Table 5.1. The tool wear geometrical measurements are summarized in Table 5.2. As it can be noted, initial measurements indicate variations on geometrical parameters for different tools revealing an average $V_{Bai} = 43.8$ μm and $r_{eai} = 18.1$ μm with a standard deviation up to 30% for both dimensions. These dimensions are near the resolution of the calibration ruler (with 10 μm divisions) used to scale the images taken with the digital microscope, therefore including a high measurement uncertainty which will be discussed in further sections. The variability in the initial condition dimensions can be associated with multiple factors related to the tools manufacturing processes which often involve abrasive grinding and coating operations that due to nature and scale involved, can lead to significant difficulties in achieving or maintaining geometrical accuracy, tolerances, and integrity. No flaws or defects like chipped/broken cutting edges or significant marks were found on used tools.

Figure 5.6 reveals the evolution of the average flank wear and edge rounding through cutting length/time. As expected, both wear parameters trend to increase with the total cutting time or material removed. Relative dimensional changes seem to be more noticeable on tools exposed to some set of parameters like run 4, as evidenced in Figure 5.7.

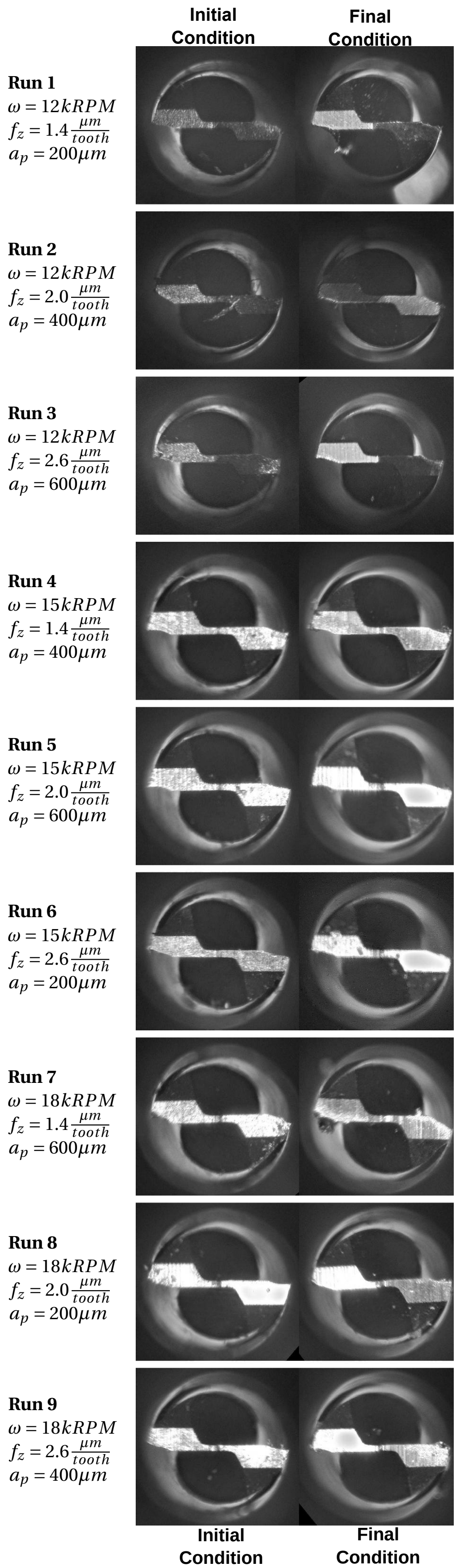

Figure 5.5: Tool initial and final conditions.

	Initial condition					
Run	V_{B1}	r_{e1}	V_{B2}	r_{e2}	V_{Bai}	r_{eai}
1	43.7	20.4	53.2	20.4	48.4	20.4
2	79.3	33.4	35.6	19.4	57.5	26.4
3	55.1	26.6	40.6	18.1	47.8	22.3
4	27.2	16.0	33.4	14.6	30.3	15.3
5	25.3	16.9	35.9	11.1	30.6	14.0
6	46.1	16.4	27.1	22.3	36.6	19.4
7	80.3	15.1	57.5	20.5	68.9	17.8
8	49.9	13.2	22.7	6.8	36.3	10.0
9	47.0	21.6	27.0	12.9	37.0	17.2

			Final condition					
Run	V_{B1}	r_{e1}	V_{B2}	r_{e2}	V_{Baf}	r_{eaf}	V_{Bi}	r_{ei}
1	44.6	24.5	57.7	25.9	51.2	25.2	6%	23%
2	61.6	61.6	78.9	47.4	70.3	54.5	22%	106%
3	62.8	33.0	42.5	20.2	52.7	26.6	10%	19%
4	58.0	35.9	72.6	22.3	65.3	29.1	115%	90%
5	30.8	22.5	42.0	11.8	36.4	17.2	19%	22%
6	49.1	23.7	35.2	29.2	42.1	26.4	15%	37%
7	87.0	21.8	62.6	27.3	74.8	24.6	9%	38%
8	39.9	21.1	49.5	11.0	44.7	16.0	23%	61%
9	49.7	28.1	44.9	13.9	47.3	21.0	28%	22%

Table 5.2: Tool wear measurements (μm).

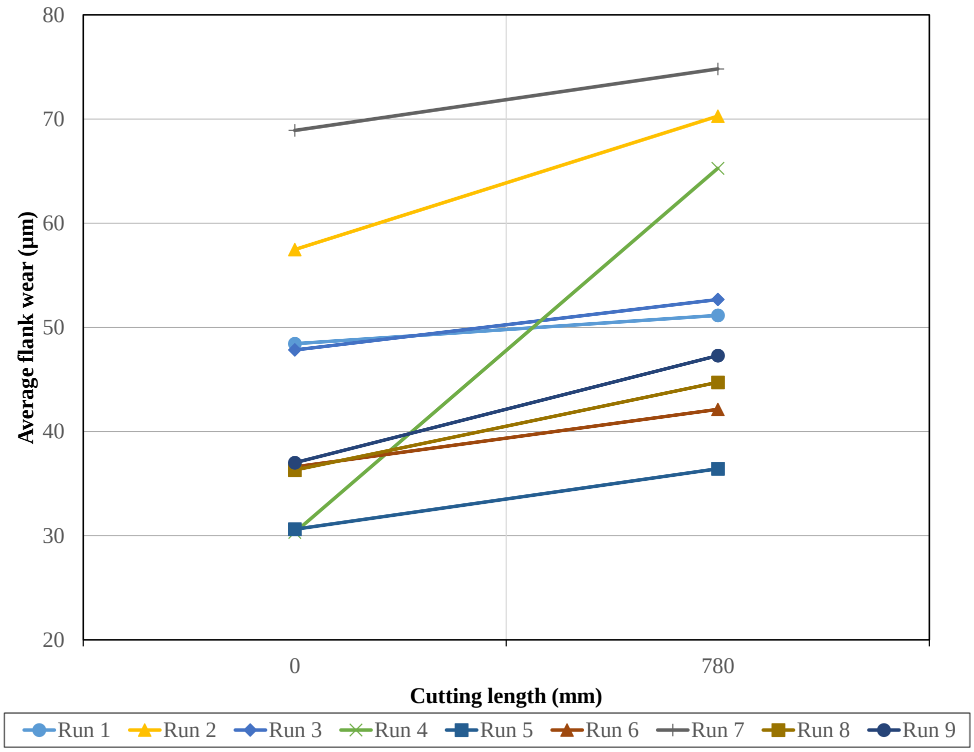

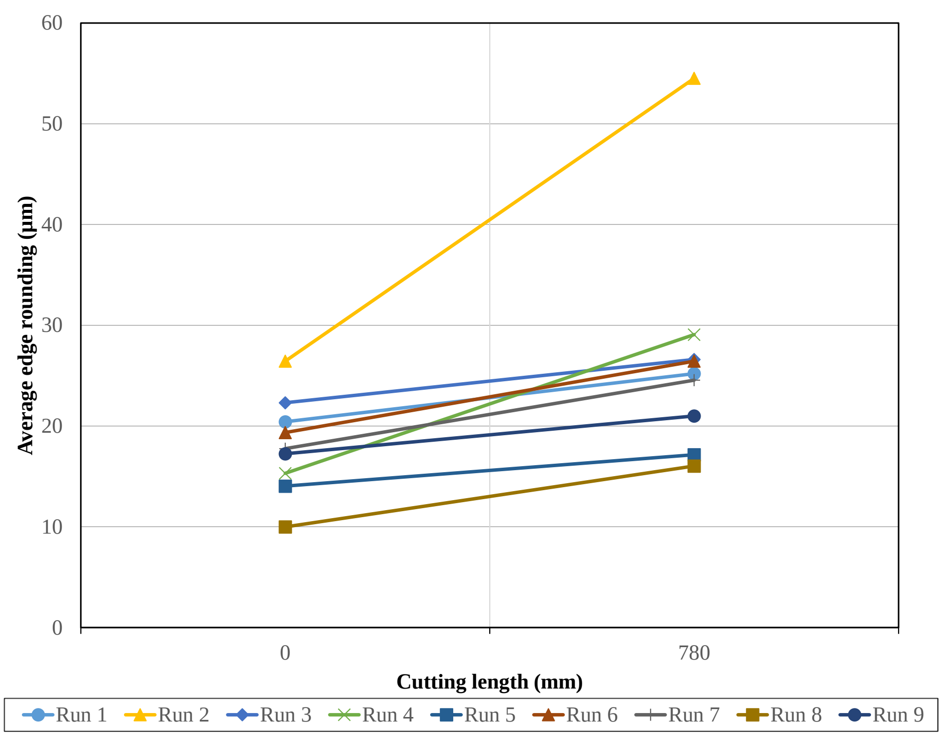

Figure 5.6: Tool wear evolution measurements.

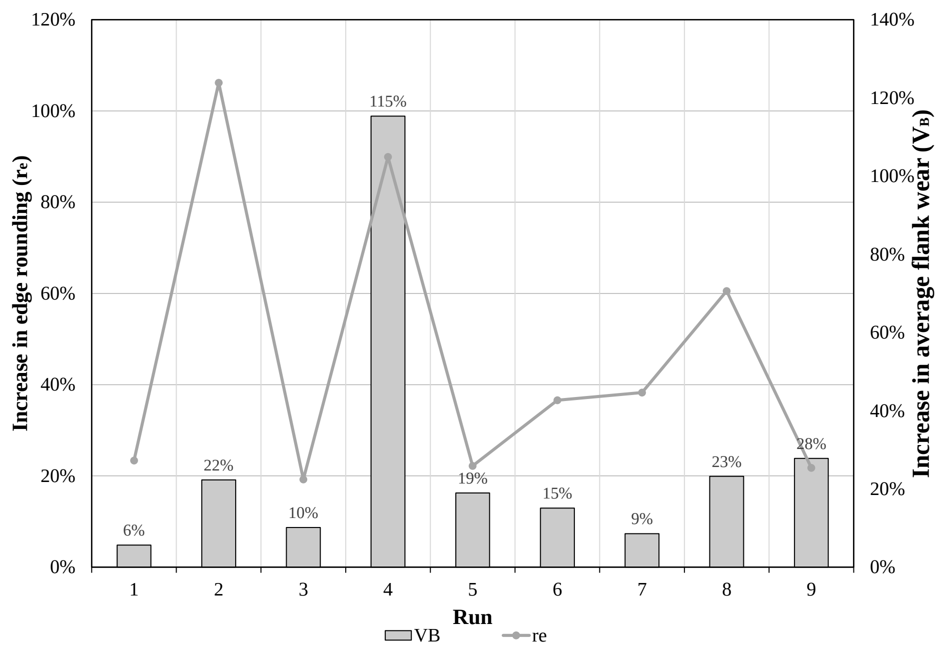

Figure 5.7: Relative increase in average flank wear and edge rounding.

5.2.3 Modeling and Simulation

Through the application of the procedure shown in the previous chapter, micro-orthogonal cutting simulations were conducted at different uncut chip thicknesses (up to 15 μm) and tool edge radius (up to 12 μm) at a constant speed of 628 mm/s for CP-Ti. This group of simulations is summarized in Figure 5.8, showing the predicted forces at tool edge radius of 3, 7.5 and 12 μm corresponding to a $\pm 60\%$ change in the used parameter for simulations in the previous chapter. A reduction/increase of $20 - 30\%$ in resultant cutting force can be appreciated if the tool edge radius reduces to 3 μm or increases to 12 μm, respectively.

From Figure 5.8 can be seen that by increasing the tool edge radius, the forces in the cutting (F_c) and tangential (F_t) directions increase, mainly since the contact length is increased creating more friction. Also, F_t exhibits a higher change in magnitude due to r_e than F_c, indicating an increased influence of wear on the forces in the tangential direction rather than in the cutting direction.

5.2.4 Discussion

Full immersion dry micro-milling of 1000 μm straight slots were made in CP-Ti grade 2 according to cutting parameters shown in Table 5.1.

During phases of the study, the following interpretations can be made:

- *Experimentation*: Figure 5.7 compares the flank wear length and tool edge rounding percentual increase of the micro-milling experiments. For flank wear increment, it can be seen that conditions of runs 1, 7 and 3 yielded more favorable results while compared to other cases. Considering tool edge radius growth, the conditions given in experimental runs 1, 3, 5 exhibited better results.

  The rough and uneven initial geometrical conditions in cutting tools, lead to variations in cutting forces, tool wear and surface quality that may be considered. As cutting time increased, it can be noted that both flutes tend to develop similar wear states. For some cases some built-up edge (BUE) can be seen, indicating weld-on states of chips on tool edge which may break-off during cutting, affecting tool wear (and coating delamination). This formation was also noted by other researchers while cutting titanium alloys [150, 192, 101]. Such BUE increases effective cutting edge radius, generates more burrs, work-hardens the machined sub-surface and deteriorates the surface quality [19].

  The poor thermal conductivity of titanium (while compared to other metals such as steel or aluminum), implies that heat generated by the cutting process cannot be easily dissipated [71], therefore concentrating heat in the cutting edge promoting increased wear.

- *Simulation*: The results summarized in Figure 5.8 indicate the evident effect of tool edge radius wear on the cutting forces. Is important to note that measurement uncertainties

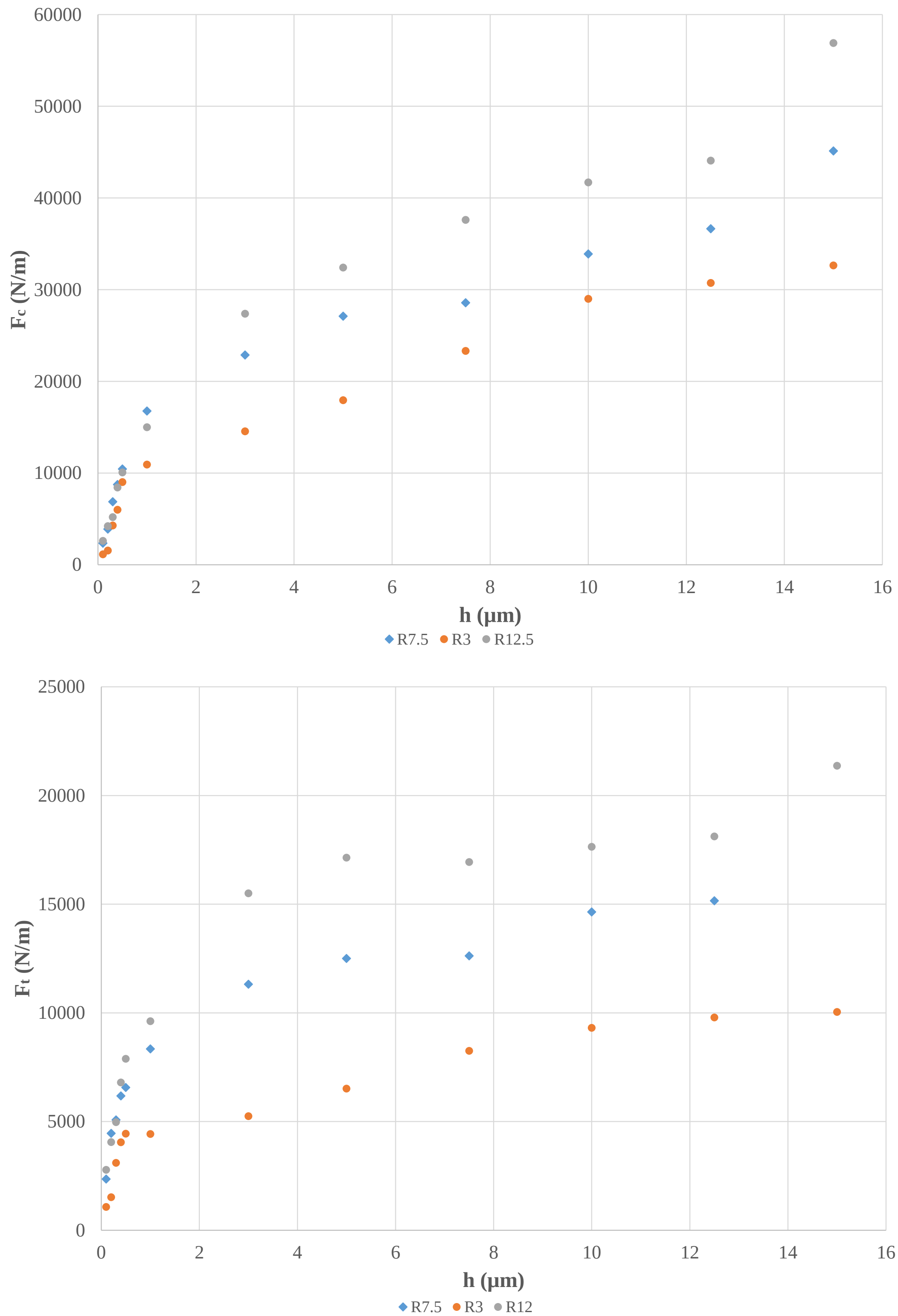

Figure 5.8: Cutting forces in the cutting (F_c) and tangential (F_t) directions at 628 mm/s.

can lead to high prediction errors due to the high sensitivity of the cutting forces. But, the predictions can be applied to estimate a limit for tool edge radius based material, cutting parameters and machine-tool characteristics.

Chapter 6

Burr formation and control

Contents

6.1 Introduction

Reducing burr formation in machining operations is of vital importance as they can decrease the functionality of components and can cause injuries. Burrs are unavoidable and often lead to the application of additional processes which may require in some cases over 35% of the time needed to machine a part [199].

In micro-machining, many studies have shown that burr formation can be minimized to an acceptable level through the modification machining processes [107, 62, 112, 191, 208]. Different parameters like material properties, cutter geometry, tool wear and cutting parameters may have a significant influence on burr formation and surface quality. In this chapter, a method for burr reduction in micro-milling is presented and applied for CP-Ti.

6.2 Burr formation and control in CP-Ti micro-milling

6.2.1 Methodology

The following phases were followed to achieve an improved surface quality in terms of burr formation while micro-milling CP-Ti:

- Experimentation: Experiments considering variations in spindle speed, feed and axial depth of cut were done. Their effect on process outputs was collected for proper analysis. The application of Taguchi orthogonal arrays was vital to explore a good experimental design space with efficient use of time and resources.
- Modeling: Through the application of statistical methods, the collected data is studied, and predictive models are developed.
- Optimization: Optimal regions are found through the study of defined performance indices.

To investigate burr formation during CP-Ti micro-milling, an experimental setup was implemented as shown in Figure 6.1. Milling equipment consisted in a high-speed spindle NSK HES510 attached to a Deckel Maho DMC1035V CNC milling machine. A certified tool run-out is guaranteed to be below $3\mu m$ according to NSK inspection standards.

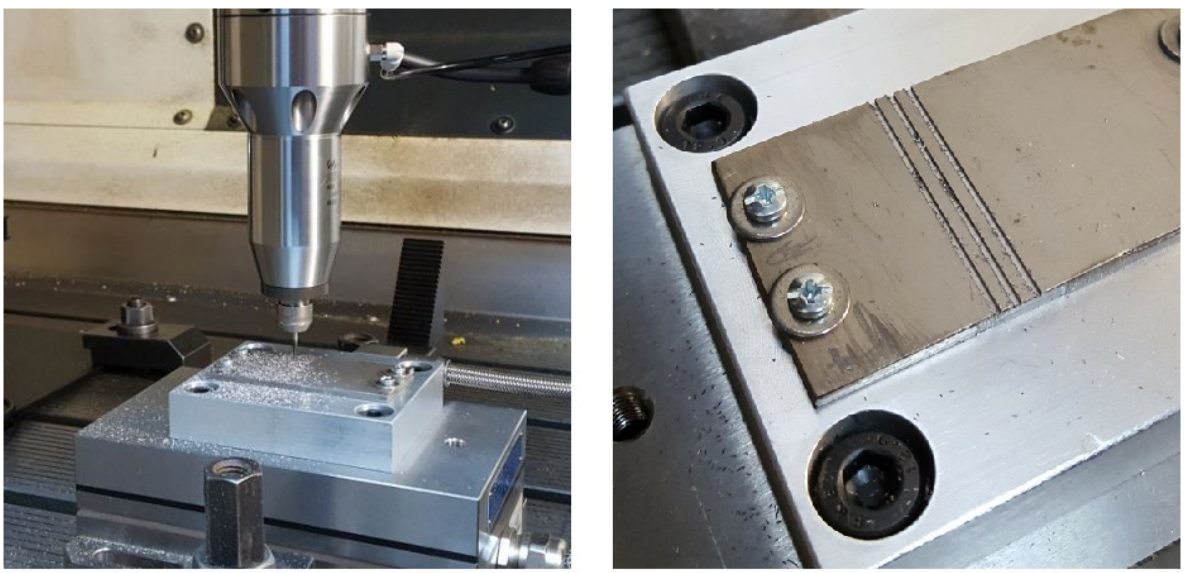

a) **b)**

Figure 6.1: Experiment setup (a) Machine setup; (b) machined workpiece.

The workpiece material was CP-Ti grade 2 in the form of sheets of 5mm thickness. Before each test, material surface flatness was verified to be lower than $50\mu m$ with a dial gage indicator as depicted in Figure 6.2. Two fluted AlTiN coated tungsten carbide (WC) tools with 1000 μm diameter (reference 1610-0197L059), a cutting length of 3 mm and a helix angle of 30° were used. All tools were replaced for each set of cutting parameters and were installed with an overhang of 13 mm to reduce the effects of variations of initial tool wear and deflection on results.

The cutting strategy consisted in full-immersion slot micro-end-milling of 1000 μm straight grooves (channels) with different parameters. A total of 20 grooves were made for each cutting

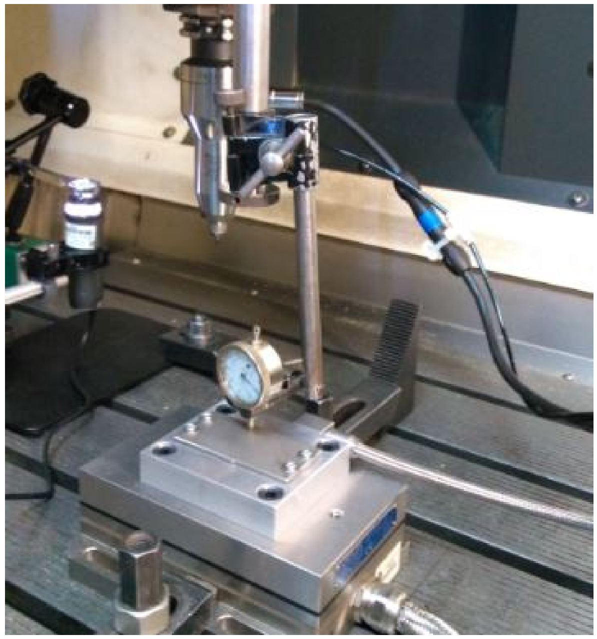

Figure 6.2: Surface flatness measurement.

test conditions, considering a total cutting length of 780 mm approximately. All experiments were performed under dry machining conditions.

Experiments were performed as based on the design shown in Table 6.1 considering variations in spindle speed (A), feed (B) and axial depth of cut (C). Taguchi orthogonal array allowed to evaluate the three parameters at three different levels. Figure 6.3 shows the machined workpieces were it can be noted that conditions of run 3, 5 and 7 indicate chip was clogging in slots which will be discussed later in this section. No deburring or surface finishing techniques were applied.

A Dino-Lite Edge Digital Microscope AM4815ZTL was used at a magnification of 145×

	Coded			**Real**				
Run	**A**	**B**	**C**	**Spindle Speed** ($kRPM$)	**Feed** ($\frac{\mu m}{tooth}$)	**Depth of cut** (μm)	**Cut speed** ($\frac{m}{min}$)	**Feed rate** ($\frac{mm}{min}$)
1	-1	-1	-1	12	1.4	200	37.7	34
2	-1	0	0	12	2.0	400	37.7	48
3	-1	1	1	12	2.6	600	37.7	62
4	0	-1	0	15	1.4	400	47.1	42
5	0	0	1	15	2.0	600	47.1	60
6	0	1	-1	15	2.6	200	47.1	78
7	1	-1	1	18	1.4	600	56.5	50
8	1	0	-1	18	2.0	200	56.5	72
9	1	1	0	18	2.6	400	56.5	94

Table 6.1: Taguchi L_9 (3^3) orthogonal array.

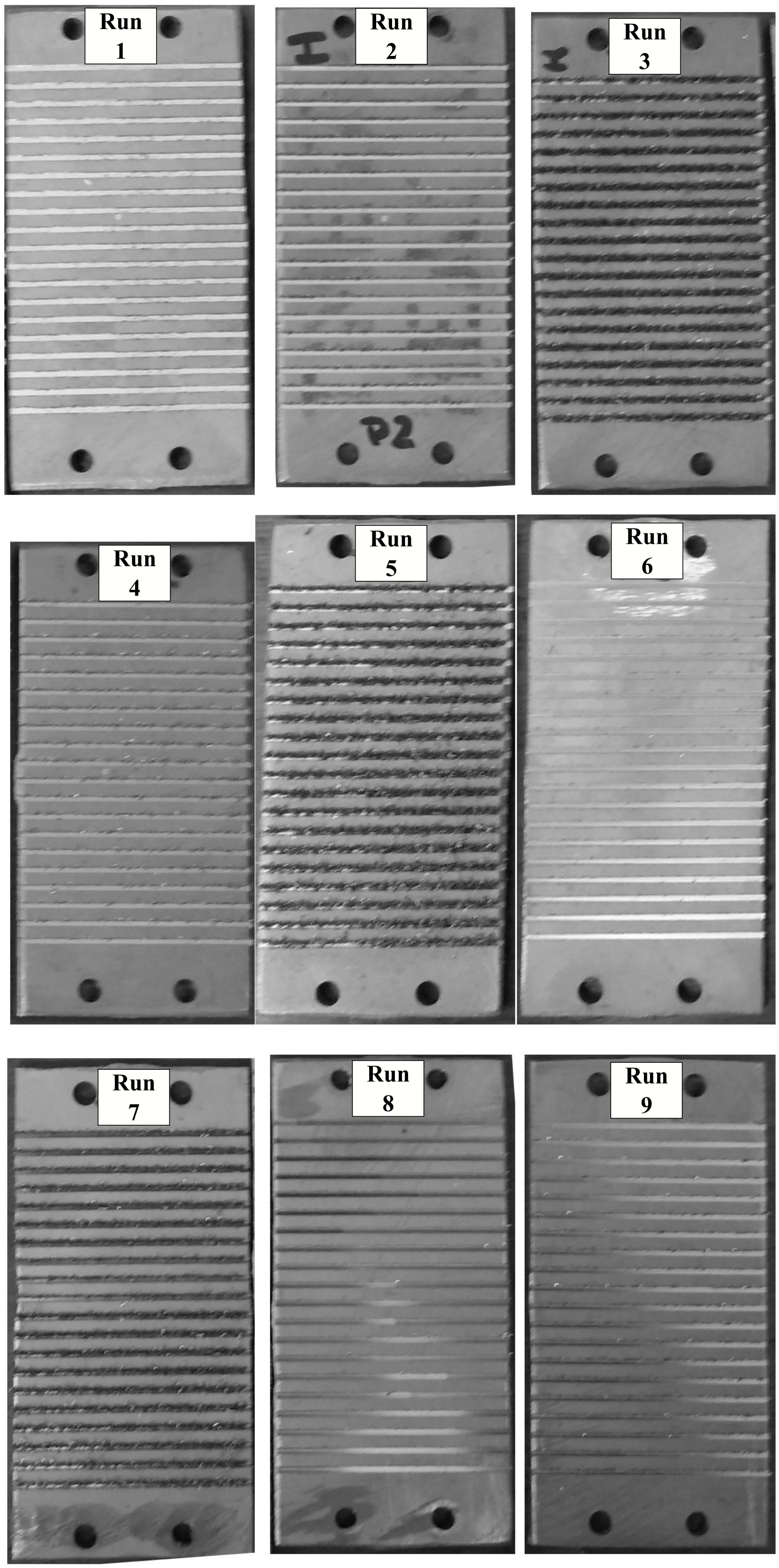

Figure 6.3: Machined workpieces.

to measure and analyze the micro-channels.

Quantitative characterization of burr formation Classical burr measurement methods as described in chapter 2 were not applied. Instead, to quantitatively measure a degree of top burr formation and clogged chip area in micro-channels, burr index was measured as an indicator of burr size. Burr index allows considering variations in burr height levels on each slot, where the top burr height being defined as the perpendicular distance from the channel wall to the end of the burr (h_0) according to ISO 13715. Then, the burr index is defined as follows:

$$BI_i = \frac{A_{bc}}{A_s} \times 100\% \tag{6.1}$$

were BI_i is the burr index for slot i, A_{bc} indicates the combined burr-clogged chip area and A_s indicates the reference slot area (1000 μm × 1750 μm for current case). Figure 6.4 illustrates a sample image from Run 8 specimen at the slot 9. Through image processing software ImageJ, the burr-chip area for up and down milling conditions can be measured for all specimen slots, as the burr area inscribed within a square of 1750 μm (Figure 6.4b) allowing a consistent, repeatable method for each condition. Also, through the application of full-immersion slot micro-milling, different approaches were applied; one side wall was machined with up (conventional) milling while the other was machined with down (climb) milling.

Conventional (up) milling is characterized by the workpiece moving directly against the cutting teeth of the end-mill at the point of contact, such that the tool adds resistance to the workpiece motion [70]. In contrast, climb (down) milling represents as if the end-mill was reducing resistance to the workpiece motion and chip thickness decreases from maximum to zero and no sliding, and rubbing phenomenon occurs.

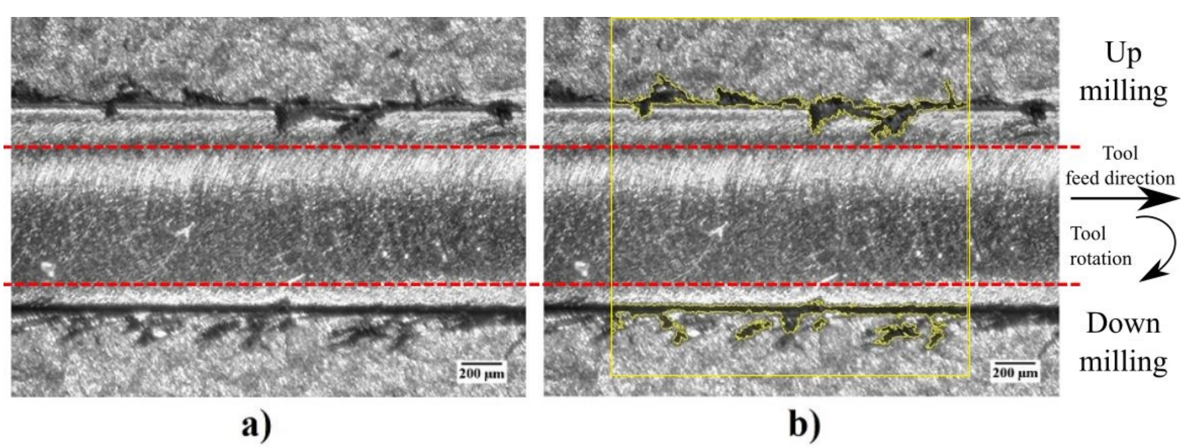

Figure 6.4: Burr and clogged chip area measurement (a) Sample image (Run 8, Slot 20); (b) Selected area (yellow).

Images for area measurements were taken from different locations where burr height was uniform. The difference in up and down milling burr is noticeable and leads to separate analysis as will be shown in modeling section. The equivalent area is also calculated considering burr and clogged chip as a criterion for quality and further processes requirements (like deburring or additional finishing passes). This equivalent area can be stated as:

$$EA_{bc} = A_{bc.av}\left(1 - \frac{A_{bc.sd}}{A_{bc.av}}\right) \tag{6.2}$$

Such equivalence takes into account the average value (av) and standard deviation (sd) through measured slots, thus penalizing conditions with severe variations on chip-burr area due to process variability and tool wear among others.

6.2.2 Results

Figure 6.6 shows the different channels obtained after machining according to cutting conditions described in the randomized experimental design illustrated in Table 6.1. The measured areas and indices for each cutting condition are shown in Table 6.2. As stated previously, conditions of run 3, 5 and 7 indicate chip was clogging in grooves (Figure 6.5). These are also known as rollover burrs which are developed when the material tears in front of the tool and gets deposited on either side of the channel [133]. This effect was also noted by Ervine, O'Donnell, and Walsh [54] while micro-milling polymers due to a greater material adhesion at insufficient feed per tooth and high cutting speeds leading to an unsuccessful evacuation of debris from the cutting zone.

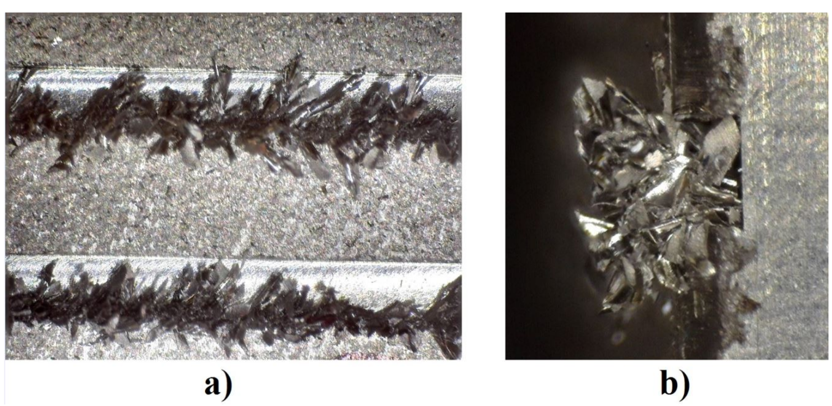

Figure 6.5: Clogged chip in Run 3 (a) Top view; (b) Side view.

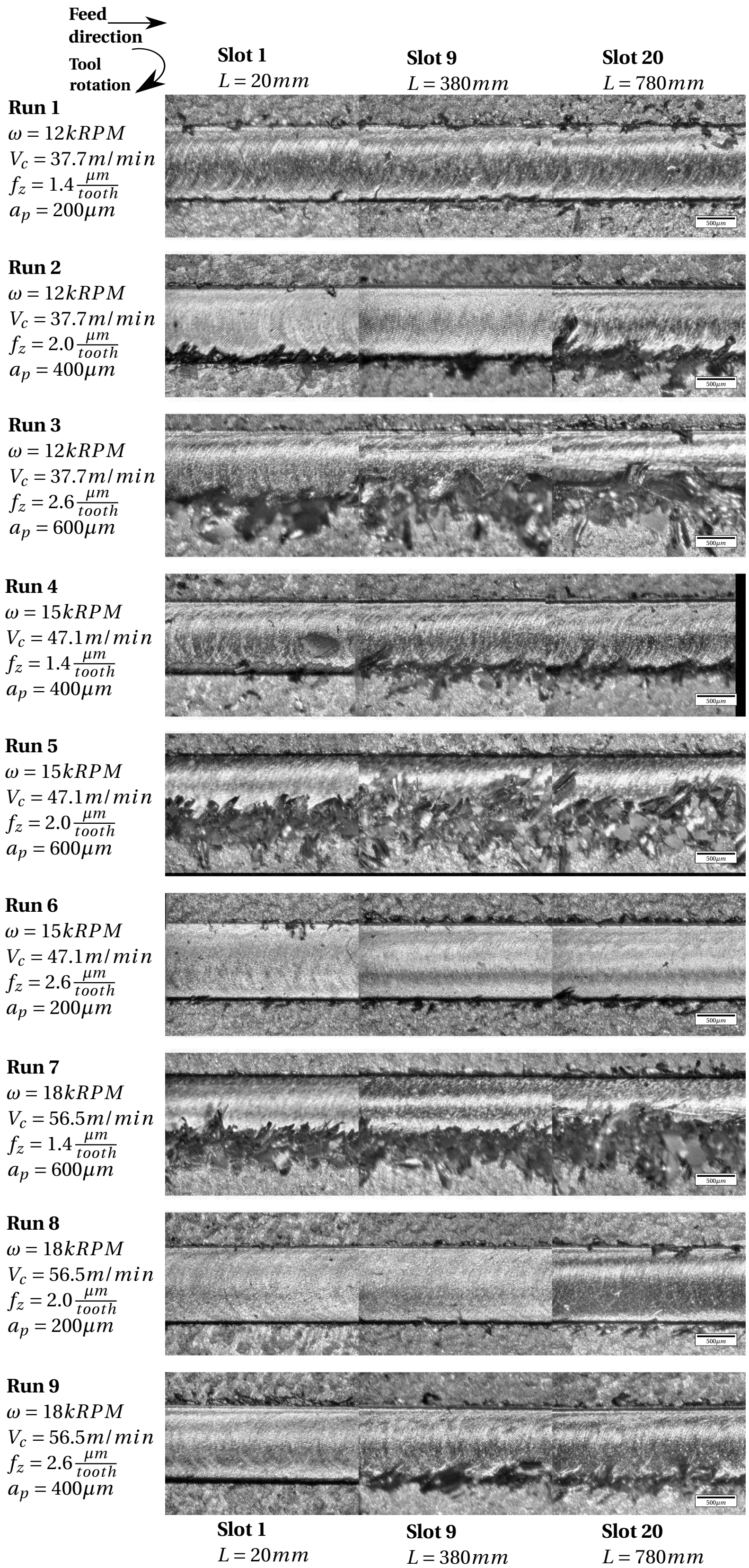

Figure 6.6: Cutting conditions and machined slots.

Run	Slot 1		Slot 9		Slot 20	
	Up milling	**Down milling**	**Up milling**	**Down milling**	**Up milling**	**Down milling**
1	52,907	66,424	94,179	95,910	100,116	128,040
2	66,050	339,338	56,821	230,961	130,228	516,186
3	41,748	592,982	80,821	699,598	155,706	754,275
4	79,659	78,294	62,335	316,509	78,439	235,298
5	143,687	956,612	131,026	1,268,420	137,546	1,156,299
6	74,773	128,653	97,908	111,868	106,412	199,089
7	89,934	603,805	82,374	605,507	131,852	1,044,621
8	48,390	78,444	63,843	85,599	103,680	106,597
9	132,815	91,091	137,337	209,329	95,735	166,750

Run	Total area				Average	
	Up milling	**Down milling**	**Total**	**Up/Down**	**Up milling**	**Down milling**
1	247,202	290,374	537,576	85%	82,401	96,791
2	253,099	1,086,485	1,339,584	23%	84,366	362,162
3	278,275	2,046,855	2,325,130	14%	92,758	682,285
4	220,433	630,101	850,534	35%	73,478	210,034
5	412,259	3,381,331	3,793,590	12%	137,420	1,127,110
6	279,093	439,610	718,703	63%	93,031	146,537
7	304,160	2,253,933	2,558,093	13%	101,387	751,311
8	215,913	270,640	486,553	80%	71,971	90,213
9	365,887	467,170	833,057	78%	121,962	155,723

Run	Standard Deviation		Equivalent area			Burr index		
	Up milling	**Down milling**	**Up milling**	**Down milling**	**Total**	**Up milling**	**Down milling**	**Total**
1	25,714	30,817	56,686	65,974	122,660	3.2%	3.8%	7.0%
2	39,985	143,976	44,382	218,186	262,568	2.5%	12.5%	15.0%
3	57,909	82,028	34,849	600,257	635,106	2.0%	34.3%	36.3%
4	9,669	121,100	63,809	88,933	152,742	3.6%	5.1%	8.7%
5	6,331	157,940	131,088	969,170	1,100,259	7.5%	55.4%	62.9%
6	16,374	46,279	76,657	100,258	176,915	4.4%	5.7%	10.1%
7	26,653	254,015	74,734	497,296	572,029	4.3%	28.4%	32.7%
8	28,527	14,633	43,444	75,581	119,025	2.5%	4.3%	6.8%
9	22,826	59,885	99,137	95,838	194,975	5.7%	5.5%	11.1%

Table 6.2: Burr and clogged chip area $(\mu m)^2$.

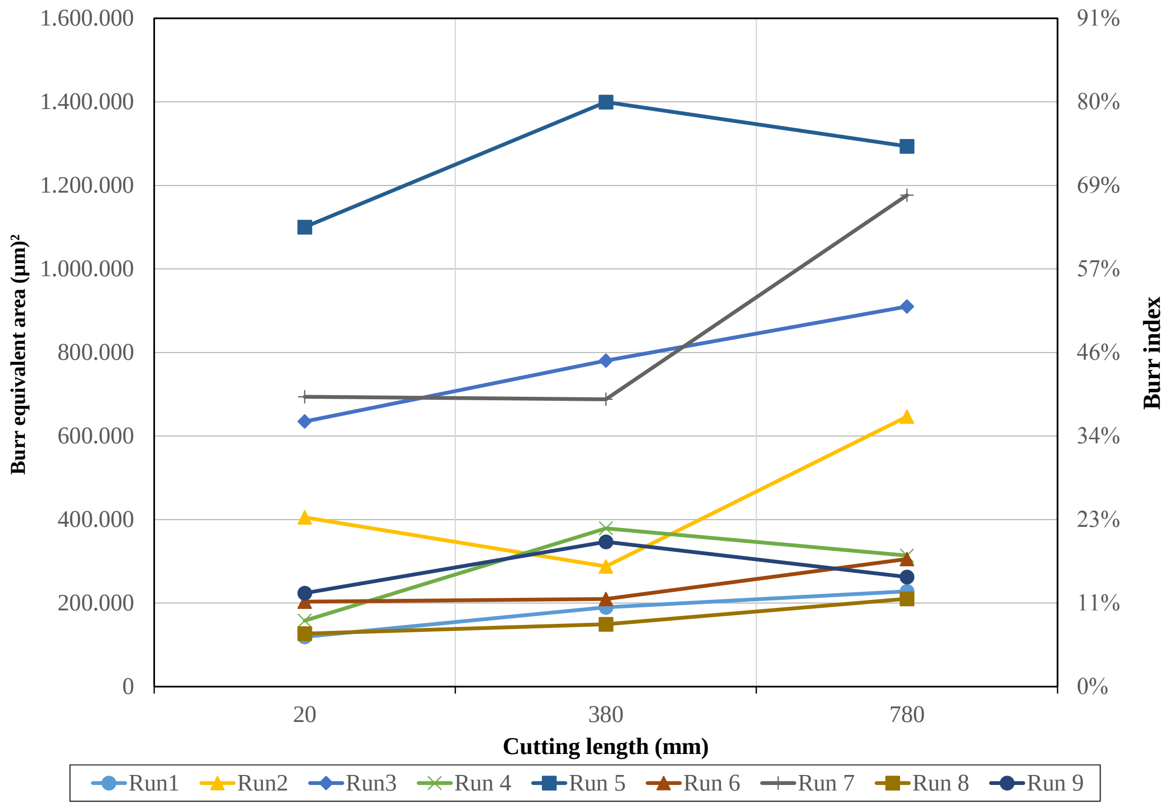

Figure 6.7: Trend showning burr size variation through slots micro-milling.

6.2.3 Modeling

ANOVA The analysis of variance of the experimental data allows studying the relative significance of the parameters on the output response for a given regression model. Table 6.3 illustrates the ANOVA for a linear model to estimate total burr equivalent area based on spindle speed (A), feed (B) and axial depth of cut (C). It is important to note that a $\log_{10}$ transform was applied to response variable, due to a high ratio of maximum to minimum response (near 9.3). The model adequacy is shown through R^2 and adjusted R^2 values which were found to be 84.2% and 74.6% respectively, indicating a good fit with real data. Predicted R^2 was estimated as 59% ensuring a basic prediction capability.

According to ANOVA results, the values of Prob$>F$ inferior to 0.05 are available on significant predictors (at 95% confidence level). In the current case, the axial depth of cut (C) is a statistically significant model term. This can be quickly noted in machined workpieces where chip clogging was found in grooves (run 3, 5 and 7).

Previous observations are described by a normal distribution as shown in the normal probability plot Figure 6.8a. The assumption of parameters independence is also satisfied as residuals don't exhibit any specific pattern or trend (Figures 6.8b and c). Finally, the plot shown in Figure 6.8d indicates an adequate precision between predicted and actual response

Source	SS	DOF	MS	F Value	Prob> F*
A	0.02047	2	0.01024	0.71	0.5843
B	0.04345	2	0.02173	1.51	0.3984
C	0.88281	2	0.4414	30.67	0.0316
Error	0.02878	2	0.01439		
Total	0.97551	8			

SS: Sum of Squares, DOF: Degree Of Freedom, MS: Mean Square.
$R^2 = 84.2\%$; Adjusted $R^2 = 74.6\%$, Predicted $R^2 = 59\%$.
$*$ Value of F variable at 95% confidence level.

Table 6.3: ANOVA for main effects.

values as proved by a good set R^2 parameters. These plots do not suggest any problem with model assumptions.

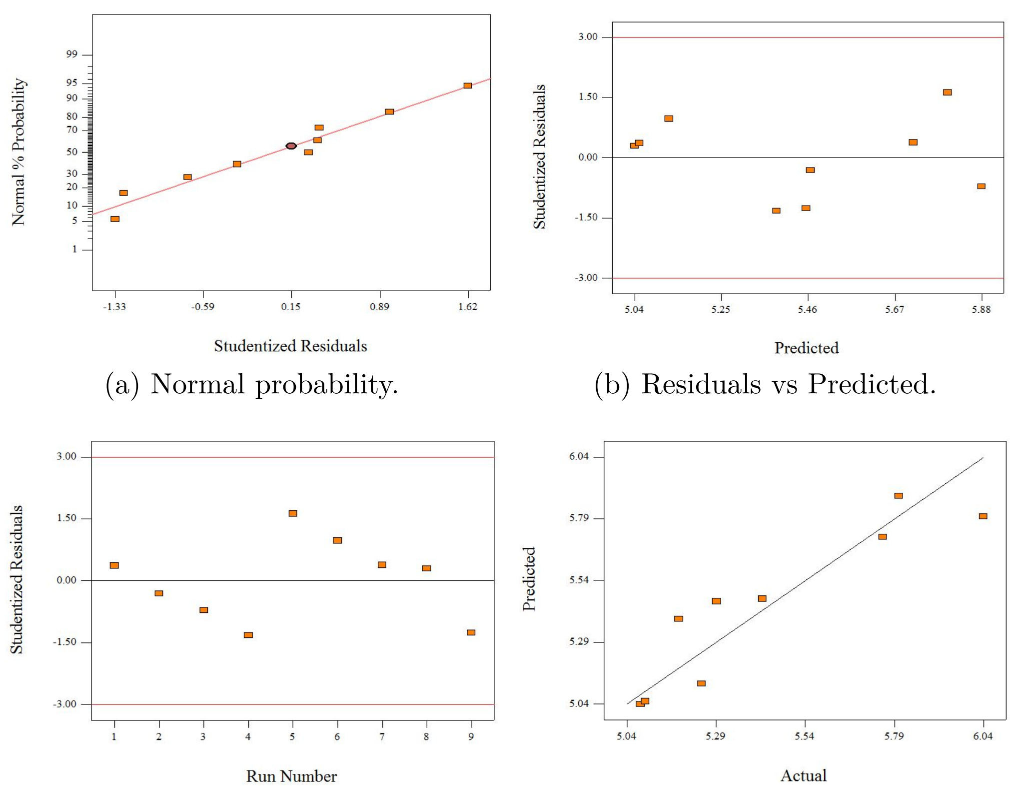

(a) Normal probability.

(b) Residuals vs Predicted.

(c) Residuals vs Run Number.

(d) Predicted vs actual.

Figure 6.8: Micro-cutting simulations.

To study the behavior of the response and to find a suitable approximation of its correct form, a first order polynomial is fitted for the equivalent area and burr index. The same model used in ANOVA was applied to find the coefficients shown in Table 6.4 using least-squares fit. It is important to note that this model only includes main effects. Then, the effective area

Source	$\log_{10} EA$		$\log_{10} BI$	
	Coded	**Real**	**Coded**	**Real**
Intercept	5.4341	4.6882	1.1907	0.4451
A	-0.031293	-0.01043	-0.0315	-0.0105
B	0.0517	0.0863	0.0517	0.0862
C	0.3649	0.0018	0.3652	0.0018

Model: $y = Intercept + A + B + C$.

Table 6.4: Regression model coefficients.

and burr index can be evaluated in terms of real variables as:

$$\begin{aligned} \log_{10} EA &= 4.6882 - 0.01043A + 0.0863B + 0.0018C \\ \log_{10} BI &= 0.4451 - 0.0105A + 0.0862B + 0.0018C \end{aligned} \tag{6.3}$$

Figure 6.9 illustrates different contour plots of the regression model for the equivalent area with variables in coded and real values. For experimentation range, contour lines are almost horizontal, indicating a more significant contribution of the axial depth of cut to the burr formation as determined by ANOVA. Low influence of feed can also be noticed (a reduced contribution) indicating an increase of burr formation at higher feeds with higher removal rates for an experimental set of parameters.

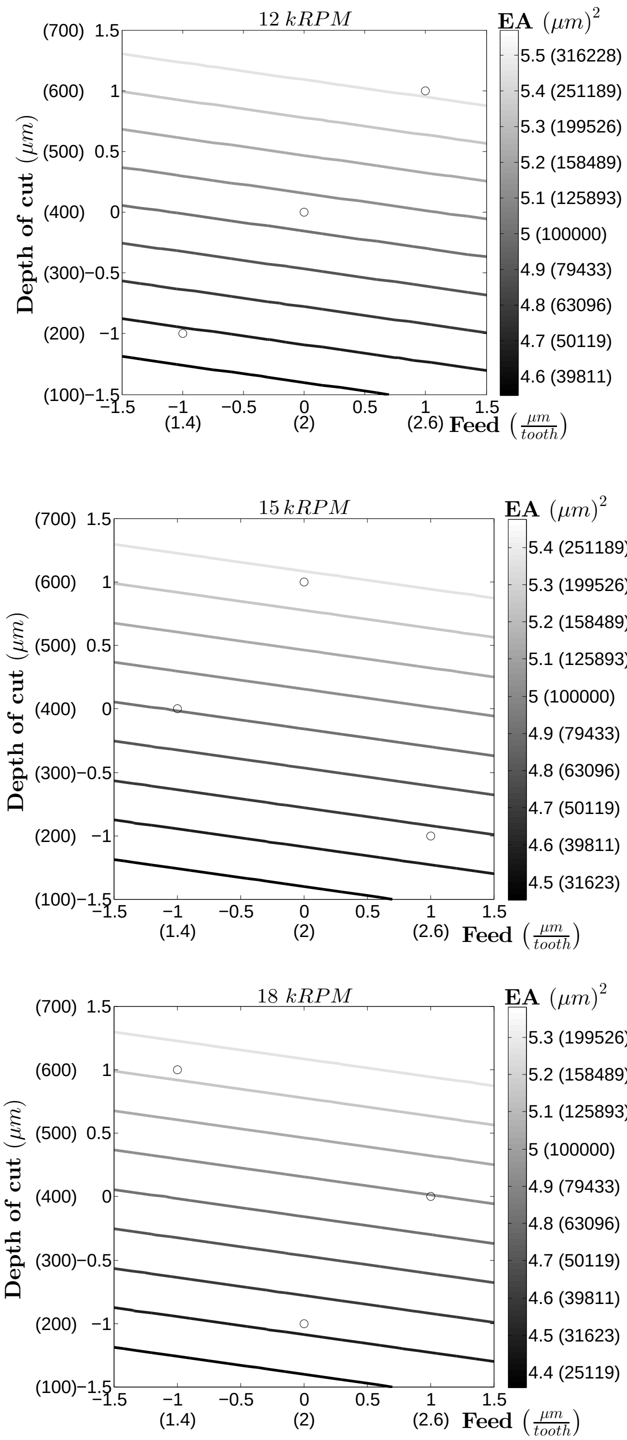

Experimental data points are represented by ○.

Figure 6.9: Contour plots for burr equivalent area at different spindle (cutting) speeds.

6.2.4 Optimization

Taguchi method is a robust statistical tool that allows the independent evaluation of the responses with a reduced number of experiments. Its applications lead to an optimum level of input parameters according to the desired response. In micro-milling, the aim is to reduce as possible the burr formation. This is achieved through a smaller signal-to-noise (S/N) ratio of equivalent area. The S/N ratios are computed for each cutting conditions and are shown in Table 6.4.

	Coded			Real				
Run	**A**	**B**	**C**	**Spindle Speed** ($kRPM$)	**Feed** ($\frac{\mu m}{tooth}$)	**Depth of cut** (μm)	**EA** $(\mu m)^2$	**EA S/N** (dB)
1	-1	-1	-1	12	1.4	200	122,660	-101.774
2	-1	0	0	12	2.0	400	262,568	-108.384
3	-1	1	1	12	2.6	600	635,106	-116.056
4	0	-1	0	15	1.4	400	152,742	-103.679
5	0	0	1	15	2.0	600	1,100,259	-120.829
6	0	1	-1	15	2.6	200	176,915	-104.955
7	1	-1	1	18	1.4	600	572,029	-115.148
8	1	0	-1	18	2.0	200	119,025	-101.512
9	1	1	0	18	2.6	400	194,975	-105.799

Table 6.5: Experimental signal-to-noise ($\log_{10} EA$).

The main effects plot of S/N ratios are illustrated in Figure 6.10, and the optimal set of cutting parameters are highlighted in red dots. The smallest S/N ratio means the optimal level. Therefore, to minimize the burr formation during full-immersion micro-milling of slots in CP-Ti grade 2, spindle speed of 18,000 RPM, feed 1.4 $\frac{\mu m}{tooth}$ and depth of cut of 200 μm were selected. From the given regression models, the predicted equivalent area and burr index can be evaluated as follows:

$$\log_{10} EA = 4.6882 - 0.01043(18) + 0.0863(1.4) + 0.0018(200) = 4.9861 \rightarrow EA = 96857(\mu m)^2$$
$$BI = 5.5\% \tag{6.4}$$

Confirmation run After the analysis of experimental data and optimization of parameters, a confirmation experiment was made to evaluate the predicted results. The same measurement procedure was applied in this sample shown in Figure 6.11a. The results indicate an up milling area of 85,605 $(\mu m)^2$ and a down milling area of 79,927 $(\mu m)^2$ for a real equivalent area of 165,532 $(\mu m)^2$ were the error is up to +41% while compared with predicted value from linear model. This error level is compliant with the R values of the current model and process

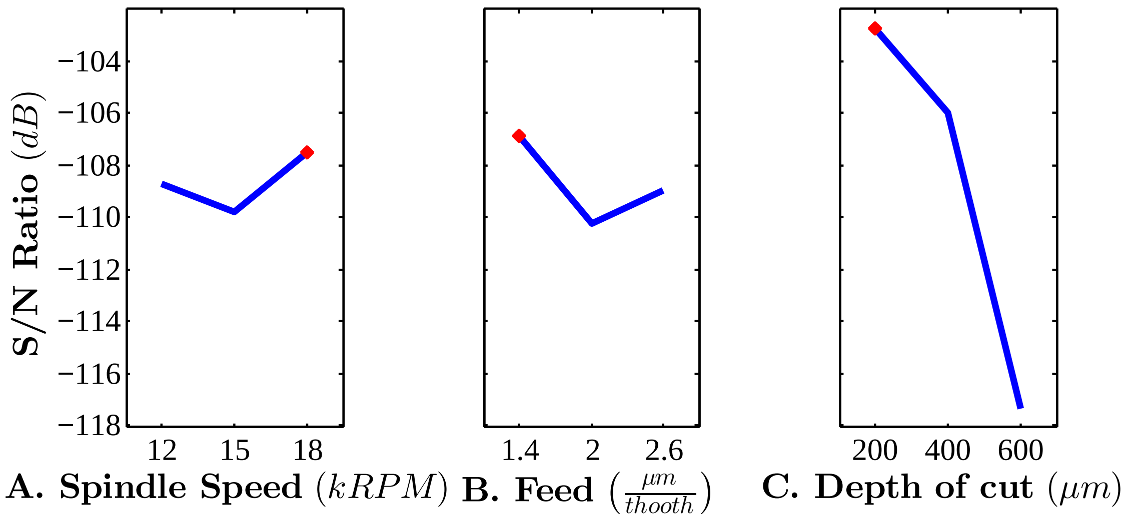

Figure 6.10: Main effects plot of S/N ratios for equivalent area.

variability. Hence, for reduced error, higher order predictors with multiple replicates could be applied (with increasing experimental costs/resources).

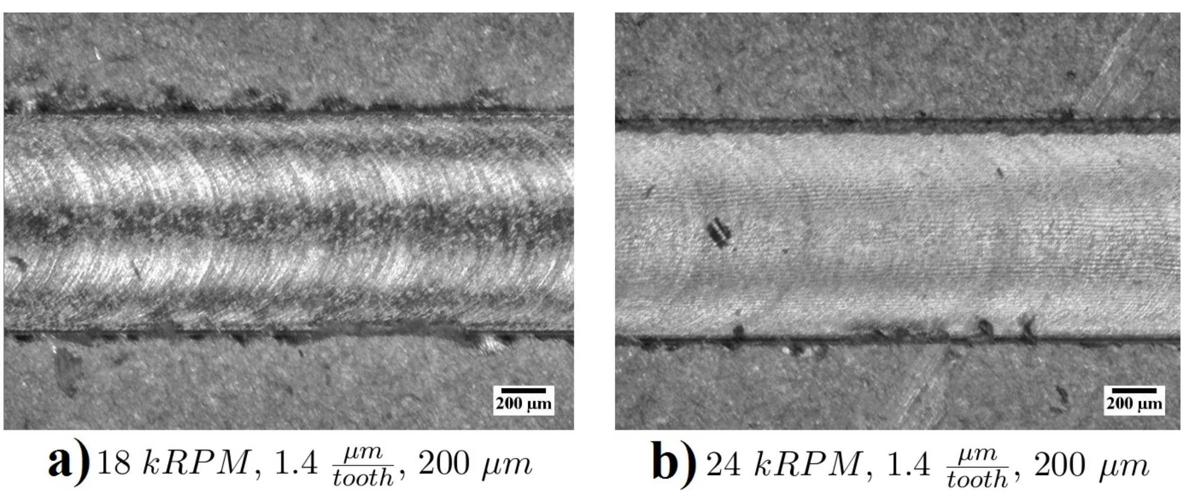

Figure 6.11: Confirmation runs.

An additional test was done at a spindle speed of 24,000 RPM, feed 1.4 $\frac{\mu m}{tooth}$ and depth of cut of 200 μm to evaluate the effect of higher cutting speeds (Figure 6.11b). The regression model predicts an equivalent area of $83,858(\mu m)^2$ and a burr index of 4.8%. The real equivalent area was found to be $108,516(\mu m)^2$; there the predicted error is calculated as +23%, therefore, demonstrating its prediction capabilities beyond the design area.

6.2.5 Discussion

Full immersion dry micro-milling of 1000 μm straight slots were made in CP-Ti grade 2 according to cutting parameters shown in Table 6.1. Different top burr shapes were obtained thanks to a various set of cutting parameters (speeds, feeds and depths of cut); also, the combination of tool rotation and tool feed directions provided both milling types (conventional and climb milling). During phases of the study, the following interpretations can be made:

- *Experimentation*: Down (climb) milling side in general, exhibits larger top burr than the up milling side (Figure 6.6). For these cases, the large tool edge radius-to-chip load ratio causes rubbing and compression (due to size effect) instead of cutting and generates more burrs [119]. The larger size of top burr in down milling mode was also confirmed by other researchers [189, 62, 19, 171, 208]. Some of them also reported better side wall surface finish with down milling than with up milling [171].

  Non-uniform burrs and chip clogging in grooves was found for some conditions (run 3,5 and 7). This indicates that the material tears in front of the tool and get deposited on either side of the channel [133]. Some researchers suggest that an increase of feed per tooth and lower cutting speeds can aid for a successful evacuation of debris [54].

  Figure 6.7 depicts the burr formation trend where variations in burr equivalent area and index indicate a clear tendency to increase burr size against cutting time and the length of cut.

- *Modeling*: Table 6.3 presents an ANOVA for main effects, where the axial depth of cut seems to have a higher impact on total burr area and burr index. This is consistent with visual evidence from machined grooves where higher depths of cut (over 600 μm) indicated superior top burr sizes and chip clogging while compared with the lowest setting on the depth of cut.

  Linear models on transformed response exhibited an adequate model fit with basic prediction capability, achieving a R^2, adjusted R^2 and predicted R^2 values of 84.2%, 74.6% and 59% respectively. The regression model coefficients for real and coded variables were obtained through least squares method and are summarized in Table 6.4 to allow further response analysis.

  Using the developed linear model, different contour plots shown in the Figure 6.9 exhibit the higher effect of depth of cut on burr formation with a direct relationship. Also, the intensity of burr formation increases with feed, which is also consistent with existing literature [78].

- *Optimization*: Main effects plot (Figure 6.10) confirm the dominance of axial depth of cut over the equivalent area. The Taguchi method allowed a fast and practical approach to an optimum set of parameters identified in main effects plot of equivalent area.

  The experimental confirmation runs were done at the optimal parameter setting with an acceptable consistency with model predictions (Figure 6.11). An additional test was done outside of experimentation area exhibiting a good model prediction capability and burr reduction. These results ensure that the developed mathematical model could be employed for an adequate prediction of burr size in the micro-milling of CP-Ti grade 2.

6.2.6 Conclusions

The effect of different dry micro-milling cutting parameters as spindle speed, feed and axial depth of cut on the burr formation of CP-Ti grade 2 was analyzed, and optimization has been performed with the aid of design of experiment techniques (Taguchi method). The application of Taguchi method allowed a cost-effective investigation of parameters (without concerning any interaction or second-order effects) over the desired process response.

As noted during experimentation, the excessive and nonuniform burrs pose a challenging task to remove them after micro-milling. Some experimental conditions induced chip clogging in machined slots that further required additional processes to remove. For this reason, results considered top burrs and clogged chip areas for comparison, as both conditions yielded undesirable characteristics. An extra milling process with opposite feed direction and small width are suggested on the down milling side to remove the large top burr and clogged chips.

The top burrs in micro-milling are relatively large (mostly for down milling side) for some cases and seem to be influenced by tool wear rate (with increased induced size effect), as the general trend indicates an increase of burr size with the cutting time or length.

The results showed that the top burr size in micro-milling of CP-Ti grade 2 could be controlled or kept within acceptable levels through proper setting of cutting parameters according to developed models.

Chapter 7

Process parameter optimization

Contents

7.1 Introduction

Micro and miniature components with tightly specified dimensions and accuracies exhibit an increased demand during last decades and have led to the development of micro and nano-technology [34, 164]. Micro-milling among the micro-machining processes has the potential to be one of the most cost-effective and efficient material removal processes due to ease of use and accessibility of the tools, allowing to produce complex two-dimensional and three-dimensional shapes in a great variety of engineering materials.

Titanium and its alloys are commonly used for several micro-feature based applications in aerospace industry, chemical industry, medical field and others, based on its excellent properties such as high specific strength, excellent physical and mechanical properties, corrosion resistance, and high biocompatibility [140, 160]. Some machining challenges arise, due to a relatively low elastic module, high toughness, low thermal conductivity and chemical reactivity at high temperatures contribute to accelerated tool wear and uneven micro-burr formation [154]. The current study aims at optimizing the performance of the commercially pure Titanium (ASTM SB 265 GR2) micro-milling through the application of numerical and experimental techniques. Different responses like cutting forces, tool wear, burr formation and material removal rate are considered as affected by different process parameters as spindle speeds (or cutting speeds), feeds and axial depth of cut. The grey relational analysis was applied to normalize the responses and measure the degree of approximation among the experimental tests to the desired performance, allowing a fast and straightforward approach (while compared to other optimization techniques) [166] to the solution of the multi-objective optimization problem.

7.2 Methodology

The following phases were followed to improve CP-Ti micro-milling performance concerning reduced forces, reduced tool wear, reduced burr formation and increased material removal rate while micro-milling CP-Ti:

- Experimentation: Experiments considering variations in spindle speed, feed and axial depth of cut were done. Their effect on process outputs was collected for proper analysis. The application of Taguchi orthogonal arrays was vital to explore a good experimental design space with an efficient use of time and resources.

- Modeling: Through the application of statistical methods, the collected data is studied, and predictive models are developed.

- Optimization: Optimal regions are found through the study of defined performance indices.

A high-speed spindle NSK HES510 was attached to a Deckel Maho DMC1035V CNC milling machine. The tool run-out is certificated to be below $3\mu m$ according to NSK inspection standards. The workpiece material was CP-Ti grade 2 in the form of sheets of 5mm thickness. Two fluted AlTiN coated tungsten carbide (WC) tools with 1000 μm diameter (reference 1610-0197L059), a cutting length of $3mm$ and a helix angle of 30° were used. All used tools were replaced for each set of cutting parameters and were installed with an overhang of $13mm$ to reduce the effects of variations of initial tool wear and deflection on results.

The cutting strategy consisted in full-immersion slot micro-end-milling of 1000 μm straight grooves (channels) with different parameters. A total of 20 grooves were made for each cutting test conditions, considering a total cutting length of $780mm$ approximately. All experiments were performed under dry machining conditions, and different parameters were measured as follows:

- *Cutting forces* measurements were made with a Kistler 9257BA 3-component dynamometer. NI PXI4472B 8-channel Dynamic Signal Acquisition (DSA) module was installed on a NI PXI1042 chassis for data sampling and processing. The cutting forces were sampled at a minimum of 20kHz and maximum of 30kHz to guarantee a minimum of 100 samples per tool's revolutions (near 3.6°/sample). The resultant force (RMS) was calculated during a cutting length of 39mm.

- *Tool wear* condition was monitored on-line with a Dino-Lite Edge Digital Microscope AM4815ZTL positioned inside the working area (without removing the tool from the spindle). Images were scaled with a calibration ruler with 10 μm divisions. The percentual increase in tool edge rounding was recorded for each test as a performance index after a total cutting length of 780 mm.

- *Burr formation* equivalent area in $(\mu m)^2$ was measured for each cutting condition considering burr and clogged chip as a criterion for quality and further processes requirements (like deburring or additional finishing passes). This area is an index that considers the evolution of burr formation through different cutting lengths and its inscribed within a square of 1750 μm.

- *Material removal rate (MRR):* The material removal rate is calculated using the general formula for milling operations:

$$MRR = f_r \times w \times a_z \tag{7.1}$$

  where f_r is the feed rate, w is the cut width or working engagement (tool diameter in the current case), and a_z is the cutting depth. The previous formula assumes constant cutting parameters and negligible effects of vibrations, run out, etc.

The zero-point in the Z direction was found by moving the tool until an acoustic emission (AE) signal was detected, which were processed at higher sampling rates (70kHz).

7.3 Results

Experiments were performed as based on the design shown in Table 7.1 considering variations in spindle speed (A), feed (B) and axial depth of cut (C). Table 7.1 illustrates the Taguchi orthogonal array used to evaluate the three parameters at three different levels and the experimental results obtained.

Run	**Spindle Speed** $(kRPM)$	**Feed** $(\frac{\mu m}{tooth})$	**Depth of cut** (μm)	**Cutting force** (N)	**Tool wear** (%)	**Burr area** $(\mu m)^2$	**MRR** (mm^3/min)
1	12	1.4	200	0.777	23%	122,660	7
2	12	2.0	400	1.468	106%	262,568	19
3	12	2.6	600	3.855	19%	635,106	37
4	15	1.4	400	5.124	90%	152,742	17
5	15	2.0	600	4.241	22%	1,100,259	36
6	15	2.6	200	1.659	37%	176,915	16
7	18	1.4	600	3.417	38%	572,029	30
8	18	2.0	200	2.251	61%	119,025	14
9	18	2.6	400	3.620	22%	194,975	37

Table 7.1: Experimental results.

7.3.1 Optimization

The relationship between cutting conditions and performance related parameters, can be non-linear and often involve multiple objectives (i.e., in the current study) that may be conflicting with each other. In this study, for the multi-objective optimization, the grey relational analysis is performed to reduce the optimization problem into a single-objective (named the grey relational grade). This method offers many advantages over classical methods based on iterative search and allows to consider the process variation due to its statistical nature. This optimization technique is applied for modern machining processes [166] through the evaluation of grey coefficients and relational degree. For this technique, the data must be normalized (in a range between 0 to 1) according to one of the following criterions:

- Smaller is better: When the kth response variable is to be minimized. Applied to cutting forces, tool wear and burr formation for better performance.

$$x_i^*(k) = \frac{\max\left(x_i^0(k)\right) - x_i^0(k)}{\max\left(x_i^0(k)\right) - \min\left(x_i^0(k)\right)} \tag{7.2}$$

- Larger is better: When the kth response variable is to be maximized. Applied to MRR, as higher values indicate better performance.

$$x_i^*(k) = \frac{x_i^0(k) - \min\left(x_i^0(k)\right)}{\max\left(x_i^0(k)\right) - \min\left(x_i^0(k)\right)} \tag{7.3}$$

Then, the grey relational coefficients are calculated as $(\xi_i(k))$:

$$\xi_i(k) = \frac{\mathit{\Delta}_{min} + \psi\mathit{\Delta}_{max}}{\mathit{\Delta}_{0i}(k) + \psi\mathit{\Delta}_{max}} \tag{7.4}$$

where $\mathit{\Delta}_{0i}(k)$ is the deviation of reference (0) and comparability (i) sequence given by:

$$\mathit{\Delta}_{0i}(k) = \|x_0^*(k) - x_i^*(k)\| \tag{7.5}$$

Also, $\mathit{\Delta}_{min}$ and $\mathit{\Delta}_{max}$ represent the smallest and largest value of $\mathit{\Delta}_{0i}$ respectively. ψ is the distinguishing coefficient ($0 \leq \psi \leq 1$) often considered as 0.5. Finally, the grey relational grade is obtained as a weighted sum of the grey coefficients, defined as follows:

$$\alpha_i = \sum_{k=1}^{n} \beta_k \xi_i(k) \tag{7.6}$$

where β_k coefficients are the relative weights of each response, compliant with: $\sum_{k=1}^{n} \beta_k = 1$. After conducting the normalization, and evaluating each grey relational coefficient, the grey relational grades for each set of cutting conditions are summarized in Table 7.2 considering equal relative weights for each response.

Since the grey relational grades represent the level of correlation between the reference and the comparability sequences, the larger grey relational grade means the comparability sequence is exhibiting a stronger correlation with the reference sequence (indicating a condition nearer to ideal). Based on this study, the cutting conditions in experimental runs 1 and 9 exhibits the highest grey relational grade as shown in Figure 7.1, therefore achieving optimal micro-milling conditions for minimum cutting force, tool wear and burr formation and maximum material removal rate, while compared to the other experiments. The best combination values for maximizing the multiple responses during full-immersion micro-milling of slots in CP-Ti grade 2 are spindle speed of 18,000 RPM, feed 2.6 $\frac{\mu m}{tooth}$ and depth of cut of 400 μm.

Run	Spindle Speed ($kRPM$)	Feed ($\frac{\mu m}{tooth}$)	Depth of cut (μm)	Normalized responses			
				Cutting force	**Tool wear**	**Burr area**	**MRR**
1	12	1.4	200	1.000	0.952	0.996	0.000
2	12	2.0	400	0.841	0.000	0.854	0.406
3	12	2.6	600	0.292	1.000	0.474	1.000
4	15	1.4	400	0.000	0.187	0.966	0.328
5	15	2.0	600	0.203	0.966	0.000	0.953
6	15	2.6	200	0.797	0.800	0.941	0.289
7	18	1.4	600	0.393	0.781	0.538	0.766
8	18	2.0	200	0.661	0.525	1.000	0.250
9	18	2.6	400	0.346	0.971	0.923	1.000

Run	Grey coefficients				Grade	Rank
	Cutting force	**Tool wear**	**Burr area**	**MRR**		
1	1.000	0.913	0.993	0.333	0.810	2
2	0.759	0.333	0.774	0.457	0.581	8
3	0.414	1.000	0.487	1.000	0.725	3
4	0.333	0.381	0.936	0.427	0.519	9
5	0.386	0.937	0.333	0.914	0.642	5
6	0.711	0.715	0.894	0.413	0.683	4
7	0.452	0.696	0.520	0.681	0.587	7
8	0.596	0.513	1.000	0.400	0.627	6
9	0.433	0.945	0.866	1.000	0.811	1

Table 7.2: Grey relational analysis.

Performing the grey relational analysis with the FE model-predicted forces shown in Table 4.15 for $\mu = 0.2$ the grey coefficients and grades (with same responses weights) are determined and summarized in Table 7.3 where it can be noted that there is no significant difference between approaches. Figure 7.1 shows that the grey relational grade follows the same trend and similar values after using FE predictions. This indicates that FE predictions have the potential to be used as an approach to optimum conditions that consider the cutting force response without performing physical measurements.

Different weights can be imposed to responses, according to desired performance. For example, a case with $\beta_1 = 30\%$ (force), $\beta_2 = 10\%$ (tool wear), $\beta_3 = 50\%$ (burr formation), $\beta_4 = 10\%$ (MRR) can be analyzed to explore cutting parameters that promote reduced burr formation (quality) and cutting forces, over tool wear and MRR (productivity). By performing the same procedure, the grey relational grades can be calculated as shown in Table 7.4. In such case, the optimal settings are given by a spindle speed of 12,000 RPM, feed 1.4 $\frac{\mu m}{tooth}$ and depth of cut of 200 μm.

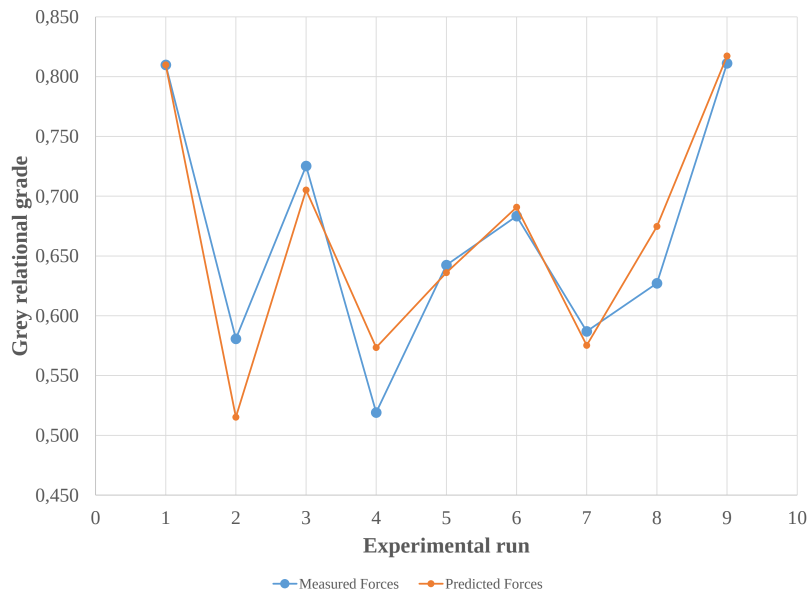

Figure 7.1: Grey relational grade.

	Grey coefficients					
Run	**Cutting force**	**Tool wear**	**Burr area**	**MRR**	**Grade**	**Rank**
1	1.000	0.913	0.993	0.333	0.810	2
2	0.497	0.333	0.774	0.457	0.515	9
3	0.333	1.000	0.487	1.000	0.705	3
4	0.551	0.381	0.936	0.427	0.573	8
5	0.360	0.937	0.333	0.914	0.636	6
6	0.741	0.715	0.894	0.413	0.691	4
7	0.404	0.696	0.520	0.681	0.575	7
8	0.786	0.513	1.000	0.400	0.675	5
9	0.458	0.945	0.866	1.000	0.817	1

Table 7.3: Grey relational analysis (with FE predicted forces).

The ANOVA of grey relational grade can be done for main effects as shown in Table 7.5. The depth of cut (C) exerts the higher influence over the expected performance as shown by its contribution of 84%. Other parameters as spindle speed (A) and feed (B) don't have a significant effect on the objective.

Run	Spindle Speed $(kRPM)$	Feed $(\frac{\mu m}{tooth})$	Depth of cut (μm)	Grey relational Grade	Rank
1	12	1.4	200	0.921	1
2	12	2.0	400	0.694	5
3	12	2.6	600	0.568	7
4	15	1.4	400	0.649	6
5	15	2.0	600	0.467	9
6	15	2.6	200	0.773	2
7	18	1.4	600	0.533	8
8	18	2.0	200	0.770	3
9	18	2.6	400	0.757	4

$\beta_1 = 30\%$ (force), $\beta_2 = 10\%$ (tool wear), $\beta_3 = 50\%$ (burr formation), $\beta_4 = 10\%$ (MRR)

Table 7.4: Grey relational analysis.

Source	**SS**	**DOF**	**MS**	F Value	Prob$>F$*	Contribution
A	0.0144	2	0.00722	2.77	0.265	9%
B	0.0064	2	0.00320	1.23	0.448	4%
C	0.1354	2	0.06769	26.01	0.037	84%
Error	0.0052	2	0.0026			
Total	0.16142	8				

SS: Sum of Squares, DOF: Degree Of Freedom, MS: Mean Square.
$*$ Value of F variable at 95% confidence level.

Table 7.5: ANOVA for main effects of grey relational grade (multiple responses).

7.4 Proposed optimization methodology

As stated previously, this research work aims to an optimal process parameter selection for micro-milling process specifically applied to CP-Ti. However, the same techniques applied in this study can be extrapolated to other processes with orthogonal cutting approximation like turning, planning or broaching following a general procedure as shown in Figure 7.2 composed of the following steps:

- *Step 1:* Define the process variables and responses to be considered according to current needs and available resources.
- *Step 2:* Develop or investigate a knowledge database with appropriate data about the associated parameters and their effect on process responses. This may include previous empirical or analytical knowledge about the process, history or past experiences (from researchers, manufacturers, etc.) to support parameters design space. For example, material properties such as density, elastic modulus, constitutive and fracture models parameters, thermal properties and others may be required and

may also require additional testing for accurate measurement at desired conditions.

– *Step 3:* Develop and evaluate numerical models with formulation (FEM, SPH, MS) depending on available resources, skills, and required responses. Fundamental parameters such as forces, stresses, strains, strain rates, temperatures and chip formation can be explored at this phase. Perform adjustments in process variable ranges to explore in further stages according to results.

– *Step 4:* Perform experimental tests with recommended ranges from previous stages applying systematical DOE techniques adjusted to requirements. Fractional factorial or Taguchi orthogonal designs, for example, may allow low-cost screening and evaluation of responses. Central composite design (CCD), D-optimal, and Box-Behnken designs can also be for process optimization allowing to create a response surface, but also limited considering available time and resources. Industry relevant parameters such as tool life, surface roughness, and burrs can be measured in this step as required.

– *Step 5:* Apply optimization strategies (Neural Networks, Fuzzy Logic, Taguchi or others) to obtain an optimal set of process variables that achieve the expected performance at established responses.

– *Step 6:* Perform confirmation tests to verify the experimental results quality and consistency with numerical and experimental models predictions.

– *Step 7:* As adjustments may arise from any of the previous steps, is always necessary to provide feedback to improve the obtained results, modifying the number of process variables, their limits, measured responses, etc.

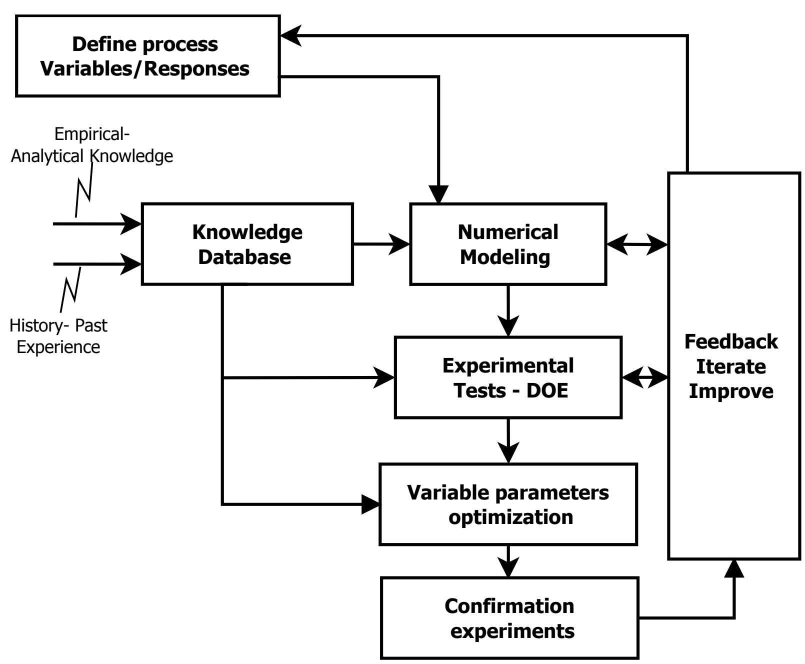

Figure 7.2: Flowchart for cutting parameters optimization.

7.5 Conclusions

The effect of different dry micro-milling cutting parameters as spindle speed, feed and axial depth of cut on cutting forces, tool wear, burr formation and MRR of CP-Ti grade 2 was analyzed, and a multi-objective optimization has been performed with the aid of design of experiment techniques (Taguchi method) and grey relational analysis. From the results, the following conclusion can be drawn:

- The overall optimum cutting conditions through grey relational analysis (with similar relevant responses) during full-immersion micro-milling of slots in CP-Ti grade 2 are spindle speed of 18,000 RPM, feed 2.6 $\frac{\mu m}{tooth}$ and depth of cut of 400 μm.
- Different set of optimum conditions can be found considering other relative weights. For example, a case with $\beta_1 = 30\%$ (force), $\beta_2 = 10\%$ (tool wear), $\beta_3 = 50\%$ (burr formation), $\beta_4 = 10\%$ (MRR) guide to an optimum composed of a spindle speed of 12,000 RPM, feed 1.4 $\frac{\mu m}{tooth}$ and depth of cut of 200 μm. In this case, according to ANOVA of grey relational grade, the axial depth of cut is the most significant controlling factor for the process responses.
- Performing the grey relational analysis with the FE model-predicted forces could lead to similar results and trends obtained from experimental force measurements. FE predictions have the potential to be used as an approach to optimum conditions that consider the cutting force as a response, therefore reducing costs and resources associated with experimentation.
- The application of Taguchi method allowed a cost-effective investigation of the influence of parameters over the desired responses. Similar experimentation with higher degree predictors would require 18+ experiments for a CCD or 27 experiments for a full factorial design, thereby using reduced time/resources for faster analysis.
- The proposed methodology for multi-objective optimization of machining parameters can be extrapolated to optimize other processes, materials, and responses successfully.

Appendix A

Equipment

Some of the used equipment during experimentation is summarized as follows:

Feature	Description	Application
Milling machine	• KERN Evo Ultra Precision Machining Center with automatic tool change • Deckel Maho DMC1035V (Equipped with NSK HES510 spindle)	Cutting tests
Tools	• Kyocera 1610-0079.024 (diam. 200 μm) • Kyocera 1610-0197L059 (diam. 500 μm) • Kyocera 1610-0394L118 (diam. 1 μm)	Cutting tests
Workpiece materials	• Timet 50A - Commercially pure titanium (ASTM Grade 2) • Contamac Filcon II Silicone Hydrogel (Biopolymer)	Cutting tests
Small distances measurement	• Mitutoyo dial indicator - resolution 1 μm	Part set-up
Acoustic emissions	• Kistler 8152C	
Dynamometer & Charge Amplifier	• Kistler 9257BA	Force measurement
Data Acquisition System	• NI PXI1042 (chasis) • NI PXI44728 (8-channel DSA module)	Data Acquisition
Digital Microscope	• Dino-Lite Edge Digital Microscope AM4815ZTL	Tool dimensions (wear) Burr dimensions (burr formation)
Optical Microscope	• TESA-VISIO 200 GL Optical Microscope	
SEM	• JEOL JSM-5600	Tool dimensions (wear)
Workshop tools	• Vertical milling machine, drill press, precision saw, etc.	Workpiece preparation

Technical Data
KERN Evo

Axes:	
Travel X/Y/Z	300/280/250 mm (11.81/11.02/9.84")
Clamping area max.	350 x 230 mm (13.78 x 9.06")
Drives	digital (AC Servo)
Workpiece weight max. (3-axis)	50 kg
Feed rate	0.01-16,000 mm/min (0.00039-629.92 "/min)
Acceleration	8 m/s² (314.96 "/s²)
Precision according to VDI/DGQ 3441:	
Resolution	0.1 µm (0.0000039")
Positioning scatter P_S	±0.5 µm (0.0000196")
Positioning tolerance P	±1.0 µm (0.0000393")
Precision on the workpiece (3-axis)	±2.0 µm (0.0000787")
Choice of spindles:	up to 50,000; 80,000; 90,000;160,000 rpm etc.
Taper	HSK 25 (using spindles up to 50,000 rpm max.)
Tool changer capacity	32 tools, optionally 63 or 95 tools
Tool diameter max.	50 mm
Tool changing time	approx. 3 s
Chip to chip	approx. 5 s
4th / 5th axis:	
Rotational	360° continuous
Swivelling	-10° up to +100°
Precision	≤ 5"
Feed rate	C/B 7000 / 3000 °/min
Automation:	
Automatic workpiece changing system	24, 36, 60 and more positions
Kern Evo:	
Space requirements min.	2.80 x 2.50 x 2.20 m (110.24 x 98.43 x 86.61")
Weight	approx. 3,000 kg
Controller	Heidenhain

Subject to technical changes

Machine design with polymer concrete

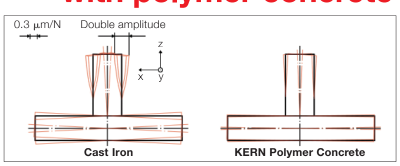

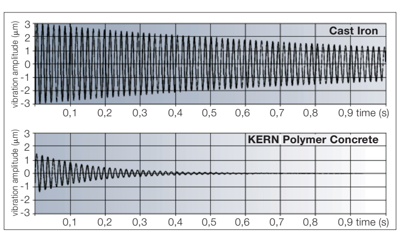

Maximum rigidity – static and dynamic
Cross-sections with exceptionally big dimensions are used on the KERN machines, thanks to the 1.8 tonnes polymer concrete construction on a 2.5 m² footprint. The static and dynamic rigidity inherent in our polymer concrete machine frame is much higher than the limits of a cast iron structure.

Vibration absorption 10 times better
The vibration dampening characteristics of the monobloc frame are of paramount importance to balance the high dynamic forces exerted by our digital direct feed drives. Polymer concrete monobloc absorbs up to 10 times more vibrations than cast iron, resulting in longer tool life of up to 30 % and superior surface quality with Ra ≤ 0.1 µm.

Low sensitivity to temperature fluctuations
The polymer concrete monobloc frame of KERN machines is known to have a 50 % lower heat conductibility than that of a steel or cast iron design. Polymer concrete does not react to short temperature fluctuations. The very low thermal conductivity minimises any deformation due to temperature variations. This in turn increases the workpiece accuracy.

KERN Micro- und Feinwerktechnik GmbH & Co. KG
Olympiastr. 2, 82438 Eschenlohe, Germany
Phone: +49 (0)8824 9101 0, Fax: +49 (0)8824 9101 124
Email: mtsales@kern-microtechnic.com
Internet: http://www.kern-microtechnic.com

01/2008e

Vertical processing center

DECKEL MAHO DMC 1035 V

The vertical processing centers DECKEL MAHO DMC 1035 V are designed for various machine operations of average details, performed with high cutting speed and feed. DMC 1035 V offer opportunities for full 3-axis milling.

OPTIMAL DESIGN:
- minimal heat distortion;
- absence of vibration in the working process;
- high and stable geometric accuracy;

TECHNICAL SPECIFICATIONS		
Stroke	X (mm)	**1035**
	Y (mm)	**560**
	Z (mm)	**510**
Dimensions of the table	mm	**1200 x 560**
Maximum weight per a detail	kg	**1000**
Rapid stroke	m/min	**25**
Spindle speed	rpm	**20-8000**
Cone of the spindle		**ISO 40 / SK 40**
CNC control type		**3D-Control SIEMENS 810D**
Automatic tool storage	number of slots	**20**
Machine equipment		AC – main engine 13/9 kW
		Tool tightening DIN 69872
		Standard cooling system 22l/min, 3.7 bar, 170l vessel
		OMP40-2 edge finder with optical receiver
		OTS device for instrument measurement
		OMI-2T optical receiver
		Manual control panel

ULTRA-PRECISION HIGH-SPEED MILLING SPINDLE

HES510 *Electric System*

The Ultra-Precision, High-Speed HES510 spindles allow you to use your existing equipment for a much larger variety of operations. Conventional milling machines and machining centers can now do high-speed machining, small diameter drilling and milling with extremely good surface finishes with the HES510. **Max. Output 340W**

HES510 Features

● 5,000-50,000 min^{-1}(rpm)

● Maximum Output 340W

The HES510 motor is a brushless DC motor that utilizes hall elements and rare-earth magnets to realize max. output 340W in a very compact size.

● Ceramic Bearings

The spindle uses a double pair of ceramic bearings in the front and in the rear. This arrangement maximizes both radial and axial rigidity to insure extremely high-precision cutting.
The motor also uses ceramic bearings to maximize life expectancy.

● Smooth Rotation

The absence of a commutator and the use of a photo coupler sending a feedback signal of 48 pulses per revolution result in very smooth rotation with low vibration throughout the speed range.

● One-Piece motor and spindle construction

The motor and spindle are built as a single unit minimizing size and weight and allowing usage on a very wide variety or machines.

● Emergency Connector

The system incorporates an emergency, breakaway connector to help prevent system damage in case the machine's main spindle is rotated accidentally.

● Excellent Durability by air-cooling system

Air-cooling motor uses a small volume of air (1.0 CFM) to prevent heat buildup and allow long, continuous operation.

● Best for small diameter drilling and milling

Less than ø0.08" (ø2 mm) small diameter drilling and milling with extremely good surface finishes, using a high-speed brushless motor.

● Cooling Air

Clean dry air is required to cool the motor and protect the spindle from contaminants. Please use a filter and regulator.
(Proper air pressure 28-42PSI) (Use Air Line Kit AL-C1204)

● Large Variety of Tapers Available

BT, NT, CAT, IT, ST32, R8 and HSK A tapers are available.

● Protection Circuit

The control unit is compact and lightweight. It features a protection circuit to stop the motor automatically in case of overload ensuring safe and smooth operation.

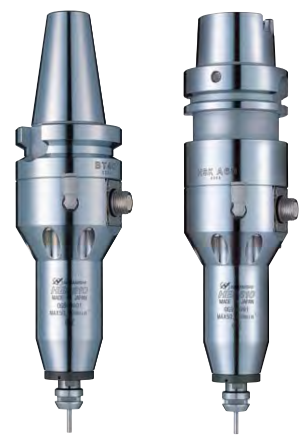

HES510 Specifications

- Speed ········ 5,000-50,000 min^{-1}(rpm)
- Max. Output Power ········ 340W
- Spindle Accuracy ········ Within 1 µm
- Standard Size Collet (CHK-3.175) ········ ø1/8"

< Optional >

- Air Line Kit (AL-C1204) ········ For Control Unit NE211
- Collet (CHK-▯▯) ········ ø0.5 mm-ø6.35 mm (See Page 6-p3 for details)
- Motor Cord (EMCD-810-▯▯) ········ Length 13 ft (9248) / 19 ft (9249) / 26 ft (9250) Provided with Air Cooling Hose ø4 mm

Note : Motor Cord is sold separately.

Torque & Output Power Characteristic of HES510

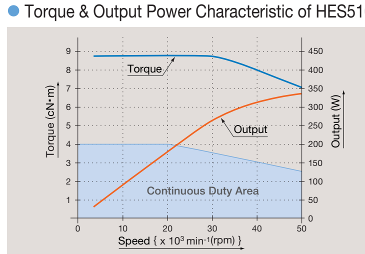

HES510 Connection Drawing

The HES510 motor and spindle require dry, clean, regulated air.
Please refer to the drawing to the right for proper components.
Air Line Kit AL-C1204 supplies clean dry air to the control unit through the filter and the regulator.

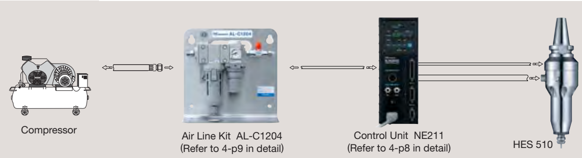

1 EmaxEVO ESPERT ROTUS IMPULSE PRESTO II SHEENUS neo SONIC CUTTER 2 iSpeed3 E2530 / E2550 E3000 E4000 3 MA MS 4 HES510 HES810 HTS HPS Xpeed 5 AIR LINE KIT 6 PARTS 7 TECHNICAL DATA 8 APPLICATION EXAMPLES INDEX

2 FLUTE

STANDARD LENGTH SQUARE END MILLS
GENERAL PURPOSE MACHINING

0.10mm - 6.00mm DIAMETER
Mirror Surface Finishes
Sub Micron Grain Carbide

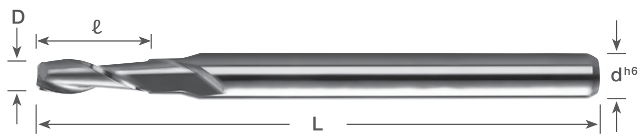

Symbol Descriptions ➜ ***Page 7***

STANDARD Length (Metric Sizes)

Dimensions (mm)				Uncoated		AlTiN Coating	
D $^{+0.00mm}_{-0.02mm}$	d^{h6}	ℓ	L	Part Number	Stock	Part Number	Stock
0.10	3	0.30	38	1610-0039.012	●	1610-0039L012	■
0.15	3	0.45	38	1610-0059.018	●	1610-0059L018	■
0.20	3	0.60	38	1610-0079.024	●	1610-0079L024	■
0.25	3	0.75	38	1610-0098.029	●	1610-0098L029	■
0.30	3	0.90	38	1610-0118.035	●	1610-0118L035	■
0.35	3	1.05	38	1610-0138.041	●	1610-0138L041	■
0.40	3	1.20	38	1610-0157.047	●	1610-0157L047	■
0.45	3	1.35	38	1610-0177.053	●	1610-0177L053	■
0.50	3	1.50	38	1610-0197.059	●	1610-0197L059	■
0.60	3	1.80	38	1610-0236.071	●	1610-0236L071	■
0.70	3	2.10	38	1610-0276.083	●	1610-0276L083	■
0.80	3	2.40	38	1610-0315.095	●	1610-0315L095	■
0.90	3	2.70	38	1610-0354.106	●	1610-0354L106	■
1.00	3	3.00	38	1610-0394.118	●	1610-0394L118	■
1.10	3	3.30	38	1610-0433.130	●	1610-0433L130	■
1.20	3	3.60	38	1610-0472.142	●	1610-0472L142	■
1.30	3	3.90	38	1610-0512.154	●	1610-0512L154	■
1.40	3	4.20	38	1610-0551.165	●	1610-0551L165	■
1.50	3	4.50	38	1610-0591.177	●	1610-0591L177	■
1.60	3	4.80	38	1610-0630.189	●	1610-0630L189	■
1.70	3	5.10	38	1610-0669.201	●	1610-0669L201	■
1.80	3	5.40	38	1610-0709.213	●	1610-0709L213	■
1.90	3	5.70	38	1610-0748.224	●	1610-0748L224	■
2.00	3	6.00	38	1610-0787.236	●	1610-0787L236	■
2.50	3	7.50	38	1610-0984.295	●	1610-0984L295	■
2.80	3	9.00	38	1610-1102.354	●	1610-1102L354	■
3.00	3	9.00	38	1610-1181.354	●	1610-1181L354	■
3.50	4	10.50	50	1610-1378.413	●	1610-1378L413	■
3.80	5	12.00	50	1610-1496.473	●	1610-1496L473	■
4.00	5	12.00	50	1610-1575.473	●	1610-1575L473	■
4.50	5	13.50	50	1610-1772.532	●	1610-1772L532	■
4.80	5	15.00	50	1610-1890.590	●	1610-1890L590	■
5.00	5	15.00	50	1610-1968.590	●	1610-1968L590	■
5.50	6	16.50	50	1610-2165.650	●	1610-2165L650	■
5.80	6	18.00	50	1610-2283.709	●	1610-2283L709	■
6.00	6	18.00	50	1610-2362.709	●	1610-2362L709	■

SERIES 1610 **WORKPIECE MATERIAL**

Coating	P Steel ~30HRC	P Steel 30~40HRC	H Hardened Steel ~55HRC	H Hardened Steel ~68HRC	M Stainless Steel	K Cast Iron	N Aluminum	N Graphite	N Copper Alloy	N CFRP	N Plastic	N Thermoset Plastic	N High Density Plastic	S Nickel / Cobalt	S Titanium Alloy
AlTiN	★	★	★	☆	☆	☆								☆	☆
Uncoated							☆	☆	★	☆	★	★	☆		☆

★ : Priority ☆ : Applicable Materials

Symbol Descriptions ➜ ***Page 7***

U.S. Stock Standard : ●
NOT STOCKED - Call for Delivery : ■
Coming Soon : ▲

measure. analyze. innovate.

Description

The dynamometer consists of four 3-component force sensors fitted under high preload between a base plate and a cover plate. The force components are measured practically without displacement.

Application

- General 3-component force measurement (dynamic and quasistatic)
- Cutting force measurements for optimization of the manufacturing process (temporary measurement)
- Cutting force measurements (turning, milling, grinding) for training purposes

Technical Data

Dynamometer Type 9257BA

Range 1	F_x, F_y	kN	–0,5 … 0,5
	F_z	kN	–1 … 1
Range 2	F_x, F_y	kN	–1 … 1
	F_z	kN	–2 … 2
Range 3	F_x, F_y	kN	–2 … 2
	F_z	kN	–5 … 5
Range 4	F_x, F_y	kN	–5 … 5 [1]
F_z for F_x and F_y ≤0,5 F_z	F_z	kN	–5 … 10 [2]
Overload	F_x, F_y, F_z	kN	–7,5/7,5
F_z for F_x and F_y ≤0,5 F_z	F_z	kN	–7,5/15
Threshold		N	<0,01
Sensitivity	F_x, F_y	mV/N	10,0
Range 1	F_z	mV/N	5,00
Linearity, all ranges		% FSO	≤±1
Hysteresis, all ranges		% FSO	≤0,5
Cross talk		%	≤±3
Rigidity	c_x, c_y	kN/µm	>1
	c_z	kN/µm	>2
Natural frequency	f_n (x,y)	kHz	≈2,0
(mounted on flanges)	f_n (z)	kHz	≈3,5
Operating temperature range		°C	0 … 60
Drift (charge amplifier)	F_x, F_y	N/s	≤±0,005
at 25 °C	F_z	N/s	≤±0,01
Ground isolation		MΩ	>100
Connecting cable (integral)	l	m	5
Degree of protection			IP 67
Weight		kg	7,4

Control Unit Type 5233A1

Number of channels		3
Number of ranges per channel		4
Output signal	V	±5
Cut-off frequency of the built-in filter	Hz	200
Output connector	3xBNC neg. 37 pin D-Sub	
Operating temperature range	°C	0 … 60
Power supply	V/AC	230/115
(switchable)	%	+15/-22
Power consumption	VA	<23
Dimensions	mm	170x126x55
Weight	kg	1,52

[1] Application of force inside and max. 25 mm above top plate area.

[2] Range for turning, application of force at point A.

000-150e-06.03 (DB06.9257BAe)

Appendix B

Publications

Published

– *Burr formation and control for polymers micro-milling: A case study with vortex tube cooling.* Dyna. DOI: `https://doi.org/10.15446/dyna.v84n203.66095`.

– *Tool edge radius wear and material removal rate performance charts for Titanium micro-milling.* Journal of Precision Engineering and Manufacturing. DOI: `10.1007/s12541-018-0009-z`.

– *Avances recientes en sistemas de lubricación/refrigeración en procesos de mecanizado*, Lecturer, XVII Congreso Chileno de Ingeniería Mecánica, Santiago, Chile. Link: `http://cocim2017.usach.cl/`.

Submitted

– *A bibliometric analysis of micro-milling related research current trends, present application, and future prospects.* Scientometrics.

A comprehensive bibliometric analysis was used to trace global trends focused in micro-milling related research from 2001 to 2016, based on SCIE. Document types, categories, languages, authors, institutions, journals, countries and other aspects were analyzed to a gain a current view of the mainstream research on micro-milling all over the world (see next page).

Under preparation

– *FEM prediction and validation of micro-milling forces.* International Journal of Advanced Manufacturing Technology.

Noname manuscript No.
(will be inserted by the editor)

Bibliometric analysis of micro-milling research: current trends, present application, and future prospects

David Serje · Jovanny Pacheco · Eduardo Diez

Received: date / Accepted: date

Abstract Micro-milling through mechanical chip removal process has attracted much attention among researchers due to its flexibility and productivity that allow an extensive application for manufacturing several types of micro-components for the modern day world. Its potential is continuously growing as the market demands continuous innovation in the manufacturing of high precision products with progressively smaller dimensions. Its global research and available literature increased very fast in recent years. In this case study, a comprehensive bibliometric analysis was used to trace global trends focused in micro-milling related research from 2001 to 2016, based on Science Citation Index Expanded. Initially retrieved data indicated over 4,000 records that were analyzed and selected considering the different meanings of the term "micro-milling". The most representative journals this field are *International Journal of Advanced Manufacturing Technology* and *International Journal of Machine Tools & Manufacture*, with a high publication rate coming from China, United States, and South Korea. Results provide a current view of the mainstream research on micro-milling all over the world.

Keywords Micro-milling · Research trend · Bibliometric · Review · Micro-machining

David Serje
Department of Mechanical Engineering, Universidad del Norte, Barranquilla, Colombia.
E-mail: serjed@uninorte.edu.co

Jovanny Pacheco
Department of Mechanical Engineering, Universidad del Norte, Barranquilla, Colombia.
E-mail: jpacheco@uninorte.edu.co

Eduardo Diez
Department of Mechanical Engineering, Universidad de La Frontera, Temuco, Chile.
E-mail: eduardo.diez@ufrontera.cl

B.1 Tool edge radius wear and material removal rate performance charts for Titanium micro-milling

Abstract *Micro-machining applications have been extended from electronics to micro-scale medical implants and devices. Micro-milling among the micro-machining processes, has the potential to be the most cost effective and efficient material removal process due to ease of use and accessibility of the tools. Complex challenges are faced due to size effect, vibrations, and other uncontrollable factors coupled with a material like Titanium used in several aerospace and medical applications which is also a representative as difficult to machine material. This study analyzes tool edge wear on micro-end-milling of commercially pure Titanium (ASTM SB 265 GR2) applying design of experiment aided with response surface methodologies to find a proper set of cutting parameters. The results show that it is possible to achieve reduced tool wear while material removal rate is balanced simultaneously. Performance charts are developed to assist in appropriate selection of cutting parameters in Titanium micro-milling.*

Keywords Micro-milling; Titanium; Optimization; Tool edge; Tool wear.

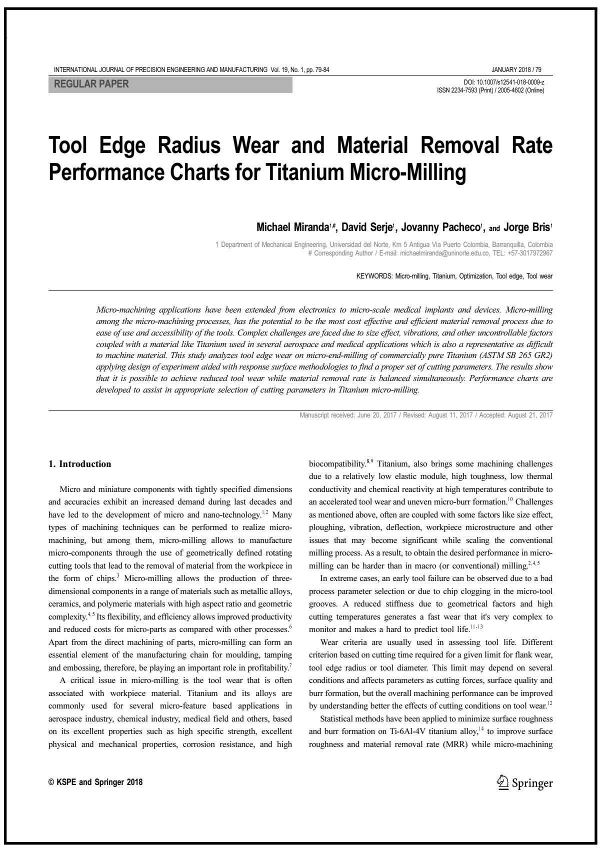

INTERNATIONAL JOURNAL OF PRECISION ENGINEERING AND MANUFACTURING Vol. 19, No. 1, pp. 79-84 JANUARY 2018 / 79
REGULAR PAPER
DOI: 10.1007/s12541-018-0009-z
ISSN 2234-7593 (Print) / 2005-4602 (Online)

Tool Edge Radius Wear and Material Removal Rate Performance Charts for Titanium Micro-Milling

Michael Miranda[1,#], David Serje[1], Jovanny Pacheco[1], and Jorge Bris[1]
1 Department of Mechanical Engineering, Universidad del Norte, Km 5 Antigua Via Puerto Colombia, Barranquilla, Colombia
Corresponding Author / E-mail: michaelmiranda@uninorte.edu.co, TEL: +57-3017972967

KEYWORDS: Micro-milling, Titanium, Optimization, Tool edge, Tool wear

Micro-machining applications have been extended from electronics to micro-scale medical implants and devices. Micro-milling among the micro-machining processes, has the potential to be the most cost effective and efficient material removal process due to ease of use and accessibility of the tools. Complex challenges are faced due to size effect, vibrations, and other uncontrollable factors coupled with a material like Titanium used in several aerospace and medical applications which is also a representative as difficult to machine material. This study analyzes tool edge wear on micro-end-milling of commercially pure Titanium (ASTM SB 265 GR2) applying design of experiment aided with response surface methodologies to find a proper set of cutting parameters. The results show that it is possible to achieve reduced tool wear while material removal rate is balanced simultaneously. Performance charts are developed to assist in appropriate selection of cutting parameters in Titanium micro-milling.

Manuscript received: June 20, 2017 / Revised: August 11, 2017 / Accepted: August 21, 2017

1. Introduction

Micro and miniature components with tightly specified dimensions and accuracies exhibit an increased demand during last decades and have led to the development of micro and nano-technology.[1,2] Many types of machining techniques can be performed to realize micro-machining, but among them, micro-milling allows to manufacture micro-components through the use of geometrically defined rotating cutting tools that lead to the removal of material from the workpiece in the form of chips.[3] Micro-milling allows the production of three-dimensional components in a range of materials such as metallic alloys, ceramics, and polymeric materials with high aspect ratio and geometric complexity.[4,5] Its flexibility, and efficiency allows improved productivity and reduced costs for micro-parts as compared with other processes.[6] Apart from the direct machining of parts, micro-milling can form an essential element of the manufacturing chain for moulding, tamping and embossing, therefore, be playing an important role in profitability.[7]

A critical issue in micro-milling is the tool wear that is often associated with workpiece material. Titanium and its alloys are commonly used for several micro-feature based applications in aerospace industry, chemical industry, medical field and others, based on its excellent properties such as high specific strength, excellent physical and mechanical properties, corrosion resistance, and high biocompatibility.[8,9] Titanium, also brings some machining challenges due to a relatively low elastic module, high toughness, low thermal conductivity and chemical reactivity at high temperatures contribute to an accelerated tool wear and uneven micro-burr formation.[10] Challenges as mentioned above, often are coupled with some factors like size effect, ploughing, vibration, deflection, workpiece microstructure and other issues that may become significant while scaling the conventional milling process. As a result, to obtain the desired performance in micro-milling can be harder than in macro (or conventional) milling.[2,4,5]

In extreme cases, an early tool failure can be observed due to a bad process parameter selection or due to chip clogging in the micro-tool grooves. A reduced stiffness due to geometrical factors and high cutting temperatures generates a fast wear that it's very complex to monitor and makes a hard to predict tool life.[11-13]

Wear criteria are usually used in assessing tool life. Different criterion based on cutting time required for a given limit for flank wear, tool edge radius or tool diameter. This limit may depend on several conditions and affects parameters as cutting forces, surface quality and burr formation, but the overall machining performance can be improved by understanding better the effects of cutting conditions on tool wear.[12]

Statistical methods have been applied to minimize surface roughness and burr formation on Ti-6Al-4V titanium alloy,[14] to improve surface roughness and material removal rate (MRR) while micro-machining

Springer

Figure B.1: Article: Tool edge radius wear in micro-milling [140].

B.2 Recent advances in cooling/lubrication for machining processes

The role of machining working fluids in burr reduction and control is based on reducing friction and heat dissipation in the tool-workpiece interface, also promoting lower tool wear rates. Current section explores different cooling/lubrication strategies currently available and develops a comprehensive analysis considering technical, economic and environmental concerns.

XVII CONGRESO CHILENO DE INGENIERÍA MECÁNICA | COCIM 2017
UNIVERSIDAD DE SANTIAGO DE CHILE
22 AL 24 DE NOVIEMBRE, 2017, SANTIAGO, CHILE

AVANCES RECIENTES EN SISTEMAS DE LUBRICACIÓN/REFRIGERACIÓN EN PROCESOS DE MECANIZADO

D. Serje[a,*], J. Pacheco[a], E. Diez[b]
[a] Departamento de Ingeniería Mecánica, Universidad del Norte, Km. 5 Vía Puerto Colombia, Barranquilla, Colombia
[b] Departamento de Ingeniería Mecánica, Universidad de La Frontera, Avenida Francisco Salazar 01145, Casilla 54-D, Temuco, Chile
*E-mail Autor: serjed@uninorte.edu.co

Resumen

Los procesos de manufactura por remoción de material, enfrentan una demanda creciente de productos cada vez a menor costo y mayor calidad. Ante los rápidos cambios en el mercado, las empresas de manufactura deben identificar continuamente mejoras en los procesos productivos e identificar oportunidades de reducción de costos mientras se apliquen procesos ambientalmente amigables que garanticen los niveles de acabado y precisión dimensional esperados. El uso de fluidos de corte en las operaciones de corte impacta directamente en el desempeño del proceso, en el ambiente y los costos de producción, alcanzando desde un 17% hasta un 30% de los costos totales del componente fabricado. La eliminación o una reducción significativa en el uso de lubricantes/refrigerantes ha promovido el desarrollo de nuevas formulaciones y técnicas como maquinado en seco, lubricación mínima (MQL), criogenia, refrigeración gaseosa y lubricación por sólidos entre otros. En este estudio, se desarrolla un análisis detallado de diferentes técnicas de refrigeración/lubricación y alternativas disponibles bajo consideraciones técnicas, económicas y ambientales.

Keywords: Mecanizado, Lubricación, Refrigeración, Impacto ambiental, MQL, Maquinado en seco.

1. Introducción

Durante el mecanizado se utilizan habitualmente una variedad de fluidos de corte para retirar calor, lubricar la zona de corte, remover virutas, incrementar la vida de la herramienta, mejorar el acabado superficial, reducir la formación de rebabas y adhesión de material en la herramienta [28]. También pueden llegar a limitar la difusión química entre el material de la herramienta y la pieza de trabajo y ayudan a proteger la superficie recién maquinada de la corrosión [2]. Su uso, tiene asociadas una serie de desventajas como su costo, su impacto ambiental y el riesgo para la salud de los trabajadores involucrados en su manipulación [6]. Para el año 2012, se estimó que en la Unión Europea se gastan alrededor de 320.000 Tm/año [16] y tan sólo en Estados Unidos se tiene un total de 7.5 billones de litros de fluidos de corte en el 2002 [1] y de estas cantidades, se pierde hasta un 30% debido a la evaporización, pérdida en los circuitos o virutas entre otros [3]. En el campo de la salud, el Instituto Nacional para la Seguridad y Salud Ocupacional (NIOSH) estima que anualmente cerca de 1.2 millones de trabajadores que se encuentran potencialmente expuestos a fluidos de corte en contacto directo con la piel o a través del sistema respiratorio, pudiendo llegar a presentar complicaciones de salud como la dermatitis y enfermedades respiratorias debido a los niveles de exposición [20]. Su impacto en los costos de producción, alcanza desde un 17% hasta un 30% (para materiales de difícil maquinabilidad) de los costos totales del componente fabricado [13]. La disposición final de los fluidos de corte puede representar hasta cuatro veces los costos de adquisición debido a que en su mayoría no son biodegradables y requieren de un tratamiento costoso [7].

Muchas instituciones (empresas, universidades y centros de investigación) han enfocado sus esfuerzos para desarrollar nuevas estrategias y tecnologías para encontrar métodos alternativos más económicos y ambientalmente amigables sin afectar la calidad y productividad. Algunas de las principales alternativas desarrolladas a la actualidad son maquinado en seco, lubricación mínima (MQL), criogenia y refrigeración gaseosa entre otros (véase Figura 1).

El maquinado en seco y los sistemas de lubricación mínima han sido evaluados ampliamente y gozan de buena aceptación gracias a ser técnicas ambientalmente amigables, pero algunas operaciones de corte aún requieren el uso de corte y es allí donde las otras técnicas han empezado a incursionar. El presente trabajo detalla cada una de estas alternativas bajo un análisis comparativo que permita discernir las virtudes y limitantes de cada una.

2. Fluidos de corte y técnicas alternativas

2.1. Mecanizado en seco (dry machining)

El mecanizado sin el uso de ningún fluido de corte, también conocido como mecanizado en seco, es muy popular entre los investigadores recientemente [7,23,26,29]. Este método se constituye en una alternativa económica y ambientalmente amigable (ver Figura 2), pero requiere de la implementación de algunos cambios para

Figure B.2: Conference: Recent advances in cooling/lubrication for machining processes [176].

B.3 Biopolymer burr formation and control

The results of this section can be found in (Figure B.3):

ARTICLE: Burr formation and control for polymers micro-milling: A case study with vortex tube cooling.

Abstract *Micro-machining of different polymer based components often require high precision and excellent surface quality at high production rates with low costs. Micro-milling is a cost-efficient micro-machining process capable of generating complex shapes in a wide range of materials. Challenges based on size effect, burr formation and adequate chip removal must be faced and are addressed in this research. Material removal mechanisms, as well as its impact on burr formation and control are reviewed, followed by a case study through the application of gaseous cooling based on vortex tubes. Different vortex generator configurations were tested, proving to be fast response an economically-friendly alternative for burr reduction while micro-milling biopolymers. Configurations, as mentioned above, were used for biopolymer micro-milling towards burr measurement after each test; achieving as a result, a burr reduction while cooling temperature decreases.*

Keywords Micro-milling; Burr; Polymer machining; Vortex cooling.

UNIVERSIDAD NACIONAL DE COLOMBIA
SEDE MEDELLÍN
FACULTAD DE MINAS

DYNA
http://dyna.medellin.unal.edu.co/

Burr formation and control for polymers micro-milling: A case study with vortex tube cooling

Michael Miranda-Giraldo, David Serje-Martínez, Jovanny Pacheco-Bolívar & Jorge Bris-Cabrera

Universidad del Norte, Barranquilla-Colombia.
michaelmiranda@uninorte.edu.co, serjed@uninorte.edu.co, jpacheco@uninorte.edu.co, jbrix@uninorte.edu.co

Received: July 4th, 2017. Received in revised form: August 1rd, 2017. Accepted: October 9th, 2017.

Abstract
Micro-machining of different polymer based components often require high precision and excellent surface quality at high production rates with low costs. Micro-milling is a cost-efficient micro-machining process capable of generating complex shapes in a wide range of materials. Challenges based on size effect, burr formation and adequate chip removal must be faced and are addressed in this research. Material removal mechanisms, as well as its impact on burr formation and control are reviewed, followed by a case study through the application of gaseous cooling based on vortex tubes. Different vortex generator configurations were tested, proving to be fast response an economically-friendly alternative for burr reduction while micro-milling biopolymers. Configurations, as mentioned above, were used for biopolymer micro-milling towards burr measurement after each test; achieving as a result, a burr reduction while cooling temperature decreases.

Keywords: Micro-milling; Burr; Polymer machining; Vortex cooling.

Formación de rebabas y su control para el micro-fresado de polímeros: Un caso de estudio con refrigeración por tubo vortex

Resumen
El micro-maquinado de diferentes componentes basados en polímeros a menudo requiere de gran precisión y un excelente acabado superficial a unas tasas elevadas de producción con un bajo costo. El micro-fresado es un proceso costo-efectivo de micro-maquinado capaz de generar formas complejas en una amplia variedad de materiales. Retos basados en el efecto tamaño, formación de rebabas y una adecuada remoción de la viruta deben ser enfrentados y son tratados en la presente investigación. Los mecanismos de remoción de material, al igual que su impacto en la formación de rebabas y su control, son revisados, acompañados de un caso de estudio a través de la aplicación de refrigeración gaseosa basada en tubos vortex. Diferentes configuraciones de generadores de vortex son probados, demostrando ser una alternativa de respuesta rápida, económica y amigable para la reducción de rebabas mientras se micro-fresan biopolímeros. Dichas configuraciones se utilizaron en el micro-mecanizado de un polímero bio-compatible, midiendo el tamaño de rebaba que se genera en cada prueba, dando como resultado la disminución de estas a media que baja la temperatura de refrigeración.

Palabras clave: Micro-fresado; Rebaba; Maquinado de polímeros; Refrigeración con tubo vortex.

1. Introduction

The growing biomedical industry demands continuous innovation in the manufacturing of high precision products with progressively smaller dimensions, thereby increasing the requirements of quality, materials, speeds and costs for current fabrication techniques [1]. Micro-manufacturing is the process of fabrication used for these micro parts and products, or for creating micro-features using scaled down manufacturing processes [2,3]. Among the different existing techniques, micro-machining stands out, referring to it as the removal of material by cutting, polishing, etching, thermal elimination process, and others [4]. The micro-milling is one of the most widely used techniques of micro-fabrication due

How to cite: Miranda-Giraldo, M., Serje-Martínez, D., Pacheco-Bolívar, J. and Bris-Cabrera, J., Burr formation and control for polymers micro-milling: A case study with vortex tube cooling DYNA, 84(203), pp. 150-159, December, 2017.

Revista DYNA, 84(203), pp. 150-159, December, 2017, ISSN 0012-7353
DOI: http://dx.doi.org/10.15446/dyna.v84n203.66095

Figure B.3: Article: Burr formation and control for polymers micro-milling [141].

Bibliography

[1] S. M. Afazov et al. "Effects of micro-milling conditions on the cutting forces and process stability". In: *Journal of Materials Processing Technology* 213.5 (2013), pp. 671–684.

[2] S.M. Afazov, S.M. Ratchev, and J. Segal. "Modelling and simulation of micro-milling cutting forces". In: *Journal of Materials Processing Technology* 210.15 (2010), pp. 2154 –2162.

[3] L. Alting et al. "Micro Engineering". In: *CIRP Annals - Manufacturing Technology* 52.2 (2003), pp. 635 –657.

[4] M.F. Aly et al. "Prediction of cutting forces in the micro-machining of silicon using a "hybrid molecular dynamic-finite element analysis" force model". In: *International Journal of Machine Tools and Manufacture* 46.14 (2006), pp. 1727 –1739.

[5] Ravi Shankar Anand and Karali Patra. "Modeling and Simulation of Mechanical Micro-Machining—A Review". In: *Machining Science and Technology* 18.3 (2014), pp. 323–347.

[6] M. Annoni et al. "Microcutting Force Prediction by Means of a Slip-line Field Force Model". In: *Procedia CIRP* 8 (2013), pp. 558 –563.

[7] A. Aramcharoen and P.T. Mativenga. "Size effect and tool geometry in micromilling of tool steel". In: *Precision Engineering* 33.4 (2009), pp. 402 –407.

[8] E.J.A. Armarego and R.C. Whitfield. "Computer Based Modelling of Popular Machining Operations for Force and Power Prediction". In: *CIRP Annals - Manufacturing Technology* 34.1 (1985), pp. 65 –69.

[9] P. J. Arrazola. "Material Flow Stress Sensitivity Analysis in Numerical Cutting Modeling". In: *AIP Conference Proceedings*. Vol. 712. AIP, 2004, pp. 1408–1413.

[10] Pedro J. Arrazola and Tuğrul Özel. "Investigations on the effects of friction modeling in finite element simulation of machining". In: *International Journal of Mechanical Sciences* 52.1 (2010), pp. 31–42.

[11] P.J. Arrazola et al. "Recent advances in modelling of metal machining processes". In: *CIRP Annals - Manufacturing Technology* 62.2 (2013), pp. 695 –718.

[12] Anam Asghar, Abdul Aziz Abdul Raman, and Wan Mohd Ashri Wan Daud. "A Comparison of Central Composite Design and Taguchi Method for Optimizing Fenton Process". In: *The Scientific World Journal* 2014 (2014), p. 14.

[13] C. Bandapalli et al. "Experimental investigation of machinability parameters in high-speed micro-end milling of titanium (grade-2)". In: *International Journal of Advanced Manufacturing Technology* 85.9-12 (2016), pp. 2139–2153.

[14] Chakradhar Bandapalli. "High Speed Machining of Ti-alloys- A critical Review". In: *Proceedings of the 1st International and 16th National Conference on Machines and Mechanisms* Cm (2013), pp. 324–331.

[15] W.Y. Bao and I.N. Tansel. “Modeling micro-end-milling operations. Part I: analytical cutting force model”. In: *International Journal of Machine Tools and Manufacture* 40.15 (2000), pp. 2155 –2173.

[16] W.Y. Bao and I.N. Tansel. “Modeling micro-end-milling operations. Part II: tool run-out”. In: *International Journal of Machine Tools and Manufacture* 40.15 (2000), pp. 2175 –2192.

[17] W.Y Bao and I.N Tansel. “Modeling micro-end-milling operations. Part III: influence of tool wear”. In: *International Journal of Machine Tools and Manufacture* 40.15 (2000), pp. 2193 –2211.

[18] E. Benedicto, D. Carou, and E.M. Rubio. “Technical, Economic and Environmental Review of the Lubrication/Cooling Systems Used in Machining Processes”. In: *Procedia Engineering* 184 (2017), pp. 99–116.

[19] D. Berestovskyi, W. N. P. Hung, and P. Lomeli. “Surface Finish of Ball-End Milled Microchannels”. In: *Journal of Micro and Nano-Manufacturing* 2.4 (Sept. 2014), pp. 041005–041005–10.

[20] G. Bissacco, H.N. Hansen, and J. Slunsky. “Modelling the cutting edge radius size effect for force prediction in micro milling”. In: *{CIRP} Annals - Manufacturing Technology* 57.1 (2008), pp. 113 –116.

[21] Benjámin Borsos et al. “Two-Dimensional Finite Element Analysis of Turning Processes”. In: *Periodica Polytechnica Mechanical Engineering* 61.1 (2017), pp. 44–54.

[22] Erhan Budak et al. “Thermo-mechanical modeling of the third deformation zone in machining for prediction of cutting forces”. In: *CIRP Annals - Manufacturing Technology* 65.1 (2016), pp. 121–124.

[23] G. Byrne, D. Dornfeld, and B. Denkena. “Advancing Cutting Technology”. In: *CIRP Annals - Manufacturing Technology* 52.2 (2003), pp. 483 –507.

[24] M. Calamaz et al. “Toward a better understanding of tool wear effect through a comparison between experiments and {SPH} numerical modelling of machining hard materials”. In: *International Journal of Refractory Metals and Hard Materials* 27.3 (2009), pp. 595 –604.

[25] Madalina Calamaz, Dominique Coupard, and Franck Girot. “A new material model for 2D numerical simulation of serrated chip formation when machining titanium alloy Ti-6Al-4V”. In: *International Journal of Machine Tools and Manufacture* 48.3-4 (2008), pp. 275–288.

[26] M.A. Camara et al. “State of the Art on Micromilling of Materials, a Review”. In: *Journal of Materials Science & Technology* 28.8 (2012), pp. 673 –685.

[27] Ziyang Cao and Hua Li. “Investigation of machining stability in micro milling considering the parameter uncertainty”. In: *Advances in Mechanical Engineering* 7.3 (2015), p. 168781401557598.

[28] D. Carou et al. “Latest advances in the micro-milling of titanium alloys: a review”. In: *Procedia Manufacturing* 13 (2017), pp. 275–282.

[29] Cesar Carriazo et al. “El desarrollo de implantes oftalmológicos en Colombia”. In: *Available from: http://www.propiedadpublica.com.co/el-desarrollo-de-implantes-oftalmologicos-en-colombia/* (2010).

[30] J. Chae, S.S. Park, and T. Freiheit. “Investigation of micro-cutting operations”. In: *International Journal of Machine Tools and Manufacture* 46.3–4 (2006), pp. 313 –332.

[31] M. J. Chen et al. “Research on the modeling of burr formation process in micro-ball end milling operation on Ti-6Al-4V”. In: *International Journal of Advanced Manufacturing Technology* 62.9-12 (2012), pp. 901–912.

[32] Pin Chuan Chen et al. “Optimization of micromilling microchannels on a polycarbonate substrate”. In: *International Journal of Precision Engineering and Manufacturing* 15.1 (2014), pp. 149–154.

[33] Wanqun Chen et al. “An improved cutting force model for micro milling considering machining dynamics”. In: *International Journal of Advanced Manufacturing Technology* (2017), pp. 1–12.

[34] K. Cheng and D. Huo. *Micro-Cutting: Fundamentals and Applications*. John Wiley & Sons, 2013.

[35] Gwo-Lianq Chern. “Experimental observation and analysis of burr formation mechanisms in face milling of aluminum alloys”. In: *International Journal of Machine Tools and Manufacture* 46.12-13 (2006), pp. 1517–1525.

[36] M.G. Cockcroft and D.J. Latham. “Ductility and the workability of metals”. In: *Journal of the Institute of Metals* 96.1 (1968), pp. 33–39.

[37] Monzer Daoud, Jean-François Chatelain, and Hakim Bouzid. “On the Effect of Johnson Cook Material Constants to Simulate Al2024-T3 Machining Using Finite Element Modeling”. In: *Volume 2A: Advanced Manufacturing*. ASME, 2014, V02AT02A044.

[38] J Paulo Davim. *Modern Manufacturing Engineering*. 1st ed. Springer, 2015.

[39] J Paulo Davim. *Modern Manufacturing Engineering: Research, Development and Education*. 1st ed. Springer, 2014.

[40] Angela Dean, Daniel Voss, and Danel Draguljić. *Design and Analysis of Experiments*. Springer, 2017.

[41] Yole Développement. “Status of the MEMS industry 2016”. In: *Available from: http://www.i-micronews.com/* (2016).

[42] S Dimov et al. “Micromilling strategies: Optimization issues”. In: *Proceedings of the Institution of Mechanical Engineers, Part B: Journal of Engineering Manufacture* 218.7 (2004), pp. 731–736.

[43] S.S. Dimov et al. “A roadmapping study in Multi-Material Micro Manufacture”. In: *4M 2006 - Second International Conference on Multi-Material Micro Manufacture*. Ed. by Wolfgang Menz, Stefan Dimov, and Bertrand Fillon. Oxford: Elsevier, 2006, pp. xi –xxv.

[44] Hongtao Ding and Yung C. Shin. “Dislocation Density-Based Grain Refinement Modeling of Orthogonal Cutting of Titanium”. In: *Journal of Manufacturing Science and Engineering* 136.4 (2014), pp. 041003–041003–11.

[45] M.H Dirikolu, T.H.C Childs, and K Maekawa. “Finite element simulation of chip flow in metal machining”. In: *International Journal of Mechanical Sciences* 43.11 (2001), pp. 2699 –2713.

[46] D. Dornfeld, S. Min, and Y. Takeuchi. “Recent Advances in Mechanical Micromachining”. In: *CIRP Annals - Manufacturing Technology* 55.2 (2006), pp. 745 –768.

[47] F Ducobu and E Filippi. “On the importance of the choice of the parameters of the Johnson-Cook constitutive model and their influence on the results of a Ti6Al4V orthogonal cutting model”. In: *International Journal of Mechanical Sciences* 122.January (2017), pp. 143–155.

[48] F Ducobu, E Filippi, and E Rivì. “Chip Formation in Micro-milling”. In: *Proceedings of the 8th National Congress on Theoretical and Applied Mechanics*. 2009, pp. 333–339.

[49] F.; Ducobu, E.; Filippi, and E. Rivière-Lorphèvre. “Chip formation and minimum chip thickness in micro-milling”. In: *Proceedings of the 12th CIRP Conference on Modeling of Machining Operations* 1 (2009), pp. 339–346.

[50] F. Ducobu, E. Rivière-Lorphèvre, and E. Filippi. “Application of the Coupled Eulerian-Lagrangian (CEL) method to the modeling of orthogonal cutting”. In: *European Journal of Mechanics, A/Solids* 59 (2016), pp. 58–66.

[51] F. Ducobu, E. Rivière-Lorphèvre, and E. Filippi. “On the introduction of adaptive mass scaling in a finite element model of Ti6Al4V orthogonal cutting”. In: *Simulation Modelling Practice and Theory* 53 (2015), pp. 1–14.

[52] Kornel F Ehmann et al. *International Assessment of Research and Development in Micromanufacturing*. Tech. rep. World Technology Evaluation Center Inc., Baltimore, MA., 2005.

[53] Abdelrahman Elkaseer et al. “Tool Wear in Micro-Endmilling: Material Microstructure Effects, Modeling, and Experimental Validation”. In: *Journal of Micro and Nano-Manufacturing* 2.4 (Aug. 2014), pp. 044502–044502–10.

[54] Paul Ervine, Garret E. O’Donnell, and Barry Walsh. “Fundamental Investigations Into Burr Formation and Damage Mechanisms in the Micro-Milling of a Biomedical Grade Polymer”. In: *Machining Science and Technology* 19.1 (2015), pp. 112–133.

[55] E.O. Ezugwu and Z.M. Wang. “Titanium alloys and their machinability—a review”. In: *Journal of Materials Processing Technology* 68.3 (1997), pp. 262–274. arXiv: `arXiv:1011.1669v3`.

[56] F Z Fang et al. “Tool geometry study in micromachining”. In: *Journal of Micromechanics and Microengineering* 13.5 (2003), pp. 726–731.

[57] N. Fang. “Slip-line modeling of machining with a rounded-edge tool - Part I: New model and theory”. In: *Journal of the Mechanics and Physics of Solids* 51.4 (2003), pp. 715–742.

[58] N Fang. “Slip-line modeling of machining with a rounded-edge tool—Part II: analysis of the size effect and the shear strain-rate”. In: *Journal of the Mechanics and Physics of Solids* 51.4 (2003), pp. 743–762.

[59] Fanuc. “Fanuc Robonano”. In: *Available from: http:/fanuc.co.jp/* (2017).

[60] Sinan Filiz and O. Burak Ozdoganlar. “Microendmill Dynamics Including the Actual Fluted Geometry and Setup Errors–Part I: Model Development and Numerical Solution”. In: *Journal of Manufacturing Science and Engineering* 130.3 (June 2008), pp. 031119–031119–10.

[61] Sinan Filiz and O. Burak Ozdoganlar. “Microendmill Dynamics Including the Actual Fluted Geometry and Setup Errors–Part II: Model Validation and Application”. In: *Journal of Manufacturing Science and Engineering* 130.3 (June 2008), pp. 031120–031120–13.

[62] Sinan Filiz et al. “An experimental investigation of micro-machinability of copper 101 using tungsten carbide micro-endmills”. In: *International Journal of Machine Tools and Manufacture* 47.7–8 (2007), pp. 1088 –1100.

[63] C. R. Friedrich. “Near-Cryogenic Machining of Polymethyl Methacrylate for Micromilling Tool Development”. In: *Materials and Manufacturing Processes* 15.5 (2000), pp. 667–678.

[64] G. Fromentin et al. “Development of a precision machine to perform and study orthogonal micro-cutting”. In: *Production Engineering* 10.2 (2016), pp. 217–226.

[65] Dimitri Germain et al. “From large-scale to micromachining: A review of force prediction models”. In: *Journal of Manufacturing Processes* 15.3 (2013), pp. 389 –401.

[66] Lorelei Gherman et al. “Manufacturing Technology: Micro-machining”. In: *Micro-Manufacturing Technologies and Their Applications: A Theoretical and Practical Guide*. Ed. by Irene Fassi and David Shipley. Cham: Springer International Publishing, 2017, pp. 97–127.

[67] Ranajit Ghosh et al. “Cryogenic Machining of Polymeric Biomaterials: An Intraocular Lens Case Study”. In: *Medical Device Materials IV: Proceedings of the Materials and Processes for Medical Devices Conference 2007*. February 2015. 2007, pp. 54–64.

[68] Saurav Goel et al. “Diamond machining of silicon: A review of advances in molecular dynamics simulation”. In: *International Journal of Machine Tools and Manufacture* 88 (2015), pp. 131 –164.

[69] E. Graham et al. “Robust prediction of chatter stability in micro milling comparing edge theorem and LMI”. In: *CIRP Journal of Manufacturing Science and Technology* 7.1 (2014), pp. 29–39.

[70] David J. Guckenberger et al. “Micromilling: a method for ultra-rapid prototyping of plastic microfluidic devices”. In: *Lab Chip* 15 (11 2015), pp. 2364–2378.

[71] Antoni Wagner Thomas Georgiadis Anthimos Guimarães Romário A Barceló. “Tool wear monitoring and prediction in micro milling process for medical applications. Experimental analysis and characterization of tool wear for titanium materials”. In: *KES Transactions on SDM I - Sustainable Design and Manufacturing 2014* 7.2 (2014), pp. 606 –617.

[72] Xiaoguang Guo et al. “Modelling the effects of tool edge radius on micro machining based on smooth particle hydrodynamics simulation method”. In: *International Journal of Machining and Machinability of Materials* 16.3-4 (2014), pp. 303–317.

[73] M. Hashimura, J. Hassamontr, and D. A. Dornfeld. “Effect of in-plane exit angle and rake angles on burr height and thickness in face milling operation”. In: *Journal of Manufacturing Science and Engineering* 121.1 (1999), p. 13.

[74] S. Hashmi. *Comprehensive Materials Processing.* Elsevier Science, 2014.

[75] Ali Hosseini and Hossam A. Kishawy. “Cutting Tool Materials and Tool Wear”. In: *Machining of Titanium Alloys.* Ed. by J. Paulo Davim. Berlin, Heidelberg: Springer Berlin Heidelberg, 2014, pp. 31–56.

[76] Jiang Hua and Rajiv Shivpuri. “Prediction of chip morphology and segmentation during the machining of titanium alloys”. In: *Journal of Materials Processing Technology* 150.1-2 (2004), pp. 124–133.

[77] M J Jackson et al. “Manufacture of diamond-coated cutting tools for micromachining applications”. In: *Proceedings of the Institution of Mechanical Engineers Part L-Journal of Materials Design and Applications* 217.L1 (2003), pp. 77–83.

[78] Syed H Imran Jaffery et al. “Statistical analysis of process parameters in micromachining of Ti-6Al-4V alloy”. In: *Proceedings of the Institution of Mechanical Engineers, Part B: Journal of Engineering Manufacture* 230.6 (2016), pp. 1017–1034.

[79] VK Jain et al. “Micromanufacturing: A review—Part I”. In: *Proceedings of the Institution of Mechanical Engineers, Part B: Journal of Engineering Manufacture* 228.9 (2014), pp. 973–994.

[80] Wei Ji et al. “A Novel Approach of Tool Wear Evaluation”. In: *Journal of Manufacturing Science and Engineering* 139.9 (2017), p. 091015.

[81] Xiaoliang Jin and Yusuf Altintas. “Prediction of micro-milling forces with finite element method”. In: *Journal of Materials Processing Technology* 212.3 (2012). Micro-Manufacturing Processes, pp. 542 –552.

[82] Xiaoliang Jin and Yusuf Altintas. “Slip-line field model of micro-cutting process with round tool edge effect”. In: *Journal of Materials Processing Technology* 211.3 (2011), pp. 339 –355.

[83] Xiubing Jing et al. “Modelling the cutting forces in micro-end-milling using a hybrid approach”. In: *The International Journal of Advanced Manufacturing Technology* 73.9 (2014), pp. 1647–1656.

[84] Mark J. Jackson Jonathan Morrell. *Machining with Nanomaterials*. Springer, 2009.

[85] Martin B. Jun, Richard E. DeVor, and Shiv G. Kapoor. “Investigation of the Dynamics of Microend Milling–Part II: Model Validation and Interpretation”. In: *Journal of Manufacturing Science and Engineering* 128.4 (Mar. 2006), pp. 901–912.

[86] Martin B. Jun et al. “Investigation of the Dynamics of Microend Milling–Part I: Model Development”. In: *Journal of Manufacturing Science and Engineering* 128.4 (Jan. 2006), pp. 893–900.

[87] Martin B. G. Jun et al. “A New Mechanistic Approach for Micro End Milling Force Modeling”. In: *Journal of Manufacturing Science and Engineering* 134.1 (2012), pp. 011006–1, 011006–9.

[88] Noor M. M. Rahman M. M. Harun W. S. W. & Haron C. H. C. Kadirgama K. “Finite Element Analysis and Statistical Method to Determine Temperature Distribution on Cutting Tool in End-Milling”. In: *European Journal of Scientific Research* 30.3 (2009), pp. 451–463.

[89] Mojtaba Kahrizi, ed. *Micromachining Techniques for Fabrication of Micro and Nano Structures*. InTech, 2012.

[90] Yasuhiro Kakinuma, Nobuhito Yasuda, and Tojiro Aoyama. “Micromachining of Soft Polymer Material applying Cryogenic Cooling”. In: *Journal of Advanced Mechanical Design, Systems, and Manufacturing* 2.4 (2008), pp. 560–569.

[91] Ik Soo Kang, Jeong Suk Kim, and Yong Wie Seo. “Cutting force model considering tool edge geometry for micro end milling process”. In: *Journal of Mechanical Science and Technology* 22.2 (2008), p. 293.

[92] Y. Karpat. “A modified material model for the finite element simulation of machining titanium alloy Ti-6Al-4V”. In: *Machining Science and Technology* 14.3 (2010), pp. 390–410.

[93] Yiğit Karpat and Tuğrul Özel. “Predictive Analytical and Thermal Modeling of Orthogonal Cutting Process–Part II: Effect of Tool Flank Wear on Tool Forces, Stresses, and Temperature Distributions”. In: *Journal of Manufacturing Science and Engineering* 128.2 (Sept. 2005), pp. 445–453.

[94] Yusuf Kaynak, Tao Lu, and I. S. Jawahir. “Cryogenic Machining-Induced Surface Integrity: A Review and Comparison with Dry, MQL, and Flood-Cooled Machining”. In: *Machining Science and Technology* 18.2 (2014), pp. 149–198.

[95] Kern. “Kern Evo”. In: *Available from: http://www.kern-microtechnik.com/* (2017).

[96] W.A. Kline and R.E. DeVor. “The effect of runout on cutting geometry and forces in end milling”. In: *International Journal of Machine Tool Design and Research* 23.2 (1983), pp. 123 –140.

[97] F. Klocke. *Finite element simulation of cutting processes*. WZL/Fraunhofer IPT. 2017.

[98] Muammer Koc and Tugrul Ozel. *Micro-Manufacturing: Design and Manufacturing of Micro-Products*. John Wiley & Sons, 2011.

[99] Kugler. "Kugler Micromaster 5X". In: *Available from: https://www.kugler-precision.com/* (2017).

[100] H Kuhn and D Medlin. "ASM Handbook, vol. 8". In: *Mechanical Testing and Evaluation, ASM International, OH* 717 (2000).

[101] Emel Kuram and Babur Ozcelik. "Effects of tool paths and machining parameters on the performance in micro-milling of Ti6Al4V titanium with high-speed spindle attachment". In: *International Journal of Advanced Manufacturing Technology* 84.1-4 (2016), pp. 691–703.

[102] Emel Kuram and Babur Ozcelik. "Optimization of machining parameters during micro-milling of Ti6Al4V titanium alloy and Inconel 718 materials using Taguchi method". In: *Proceedings of the Institution of Mechanical Engineers, Part B: Journal of Engineering Manufacture* 231.2 (2015), pp. 228–242.

[103] Kyocera. *2018 Global Product Catalog*. 2018.

[104] Xinmin Lai et al. "Modelling and analysis of micro scale milling considering size effect, micro cutter edge radius and minimum chip thickness". In: *International Journal of Machine Tools and Manufacture* 48.1 (2008), pp. 1 –14.

[105] D. E. Lee et al. "Precision manufacturing process monitoring with acoustic emission". In: *International Journal of Machine Tools and Manufacture* 46.2 (2006), pp. 176–188.

[106] Han Ul Lee, Dong Woo Cho, and Kornel F. Ehmann. "A mechanistic model of cutting forces in micro-end-milling with cutting-condition-independent cutting force coefficients". In: *Journal of Manufacturing Science and Engineering, Transactions of the ASME* 130.3 (June 2008), pp. 311021–311029.

[107] Kiha Lee and David A. Dornfeld. "Micro-burr formation and minimization through process control". In: *Precision Engineering* 29.2 (2005), pp. 246 –252.

[108] Kiha Lee, Boris Stirn, and David A. Dornfeld. "Burr Formation in Micro-machining Aluminum, 6061-T6". In: *Initiatives of Precision Engineering at the Beginning of a Millennium: 10th International Conference on Precision Engineering (ICPE) July 18–20, 2001, Yokohama, Japan*. Ed. by Ichiro Inasaki. Boston, MA: Springer US, 2002, pp. 47–51.

[109] Ming-Hsing Lee, Ming-Chyuan Lu, and Jhy-Cherng Tsai. *Development of Sound Based Tool Wear Monitoring System in Micro-Milling*. 2010.

[110] Woei-Shyan Lee and Chi-Feng Lin. "High-temperature deformation behaviour of Ti6Al4V alloy evaluated by high strain-rate compression tests". In: *Journal of Materials Processing Technology* 75.1-3 (1998), pp. 127–136.

[111] Ravi Lekkala et al. "Characterization and modeling of burr formation in micro-end milling". In: *Precision Engineering* 35.4 (2011), pp. 625 –637.

[112] J. Leopold and R. Wohlgemuth. "Modeling and Simulation of Burr Formation: State-of-the-Art and Future Trends". In: *Burrs - Analysis, Control and Removal: Proceedings of the CIRP International Conference on Burrs, 2nd-3rd April, 2009, University of Kaiserslautern, Germany.* Ed. by Jan C. Aurich and David Dornfeld. Berlin, Heidelberg: Springer Berlin Heidelberg, 2010, pp. 79–86.

[113] Chengfeng Li et al. "Modeling of three-dimensional cutting forces in micro-end-milling". In: *Journal of Micromechanics and Microengineering* 17.4 (2007), p. 671.

[114] H. Z. Li, K. Liu, and X. P. Li. "A new method for determining the undeformed chip thickness in milling". In: *Journal of Materials Processing Technology* 113.1-3 (2001), pp. 378–384.

[115] Qiang Li, Y. B. Xu, and M. N. Bassim. "Dynamic mechanical behavior of pure titanium". In: *Journal of Materials Processing Technology* 155-156.1-3 (2004), pp. 1889–1892.

[116] J. Limido et al. "Metal cutting modelling SPH approach". In: *International Journal of Machining and Machinability of Materials* 9.3-4 (2011), pp. 177–196.

[117] Lars Erik Lindgren et al. "Towards predictive simulations of machining". In: *Comptes Rendus - Mecanique* 344.4-5 (2016), pp. 284–295.

[118] Jian Liu, Juan Li, and Chengying Xu. "Cutting Force Prediction on Micromilling Magnesium Metal Matrix Composites With Nanoreinforcements". In: *Journal of Micro and Nano-Manufacturing* 1.1 (Mar. 2013), pp. 011010–011010–10.

[119] X. Liu et al. "The Mechanics of Machining at the Microscale: Assessment of the Current State of the Science". In: *Journal of Manufacturing Science and Engineering* 126.4 (Feb. 2005), pp. 666–678.

[120] Ming-Chyuan Lu and Bing-Syun Wan. "Study of high-frequency sound signals for tool wear monitoring in micromilling". In: *The International Journal of Advanced Manufacturing Technology* 66.9 (2013), pp. 1785–1792.

[121] Xiaohong Lu et al. "A modified analytical cutting force prediction model under the tool flank wear effect in micro-milling nickel-based superalloy". In: *The International Journal of Advanced Manufacturing Technology* 91.9 (2017), pp. 3709–3716.

[122] NP L'vov. "Determining the minimum possible chip thickness". In: *Machines & Tooling* 4 (1969), pp. 40–45.

[123] Jaroslav Mackerle. "Finite-element analysis and simulation of machining: a bibliography (1976–1996)". In: *Journal of Materials Processing Technology* 86.1–3 (1999), pp. 17 –44.

[124] James Magargee, Fabrice Morestin, and Jian Cao. "Characterization of Flow Stress for Commercially Pure Titanium Subjected to Electrically Assisted Deformation". In: *Journal of Engineering Materials and Technology* 135.4 (June 2013), pp. 041003–041003–10.

[125] Makino. "Makino Hyper2J". In: *Available from: https://www.makino.com/* (2017).

[126] M. Malekian et al. “Modeling of minimum uncut chip thickness in micro machining of aluminum”. In: *Journal of Materials Processing Technology* 212.3 (2012). Micro-Manufacturing Processes, pp. 553 –559.

[127] Mohammad Malekian, Simon S. Park, and Martin B.G. Jun. “Modeling of dynamic micro-milling cutting forces”. In: *International Journal of Machine Tools and Manufacture* 49.7–8 (2009), pp. 586 –598.

[128] Mohammad Malekian, Simon S. Park, and Martin B.G. Jun. “Tool wear monitoring of micro-milling operations”. In: *Journal of Materials Processing Technology* 209.10 (2009), pp. 4903–4914.

[129] Ali Mamedov, S.Ehsan Layegh K., and Ismail Lazoglu. “Machining Forces and Tool Deflections in Micro Milling”. In: *Procedia CIRP* 8 (2013), pp. 147 –151.

[130] Soumen Mandal. “Applicability of Tool Condition Monitoring Methods Used for Conventional Milling in Micromilling: A Comparative Review”. In: *Journal of Industrial Engineering* 2014 (2014), p. 8.

[131] ME Martellotti. “An analysis of the milling process”. In: *trans. ASME* 63.8 (1941), pp. 677–700.

[132] T. Masuzawa. “State of the Art of Micromachining”. In: *CIRP Annals - Manufacturing Technology* 49.2 (2000), pp. 473 –488.

[133] George K. Mathai, Shreyes N. Melkote, and David W. Rosen. “Effect of Process Parameters on Burrs Produced in Micromilling of a Thin Nitinol Foil”. In: *Journal of Micro and Nano-Manufacturing* 1.2 (2013), p. 021005.

[134] M McCracken. “Dental implant materials: commercially pure titanium and titanium alloys.” In: *Journal of prosthodontics : official journal of the American College of Prosthodontists* 8.1 (1999), pp. 40–3.

[135] J.A. McGeough. *Micromachining of Engineering Materials*. Mechanical Engineering. Taylor & Francis, 2001.

[136] Shreyes N. Melkote et al. “Advances in material and friction data for modelling of metal machining”. In: *CIRP Annals - Manufacturing Technology* 66.2 (2017), pp. 731–754.

[137] J. C. Miao et al. “Review of dynamic issues in micro-end-milling”. In: *The International Journal of Advanced Manufacturing Technology* 31.9 (2007), pp. 897–904.

[138] M H Miguélez et al. “An efficient implementation of boundary conditions in an ALE model for orthogonal cutting”. In: *Journal of Theoretcial and Applied Mechanics* 47 (2009), pp. 599–616.

[139] Michael Miranda. “Influencia de los parámetros de corte en la vida útil de herramientas con recubrimiento usadas en operaciones de micro-fresado de Titanio Comercialmente puro para aplicaciones biomédicas”. MA thesis. Universidad del Norte, 2016, p. 103.

[140] Michael Miranda et al. “Tool edge radius wear and material removal rate performance charts for titanium micro-milling”. In: *International Journal of Precision Engineering and Manufacturing* 19.1 (2018), pp. 79–84.

[141] Michael Miranda-Giraldo et al. “Burr formation and control for polymers micro-milling: A case study with vortex tube cooling”. In: *Dyna* 84.203 (2017), pp. 150–159.

[142] Z Mohid et al. “Study on Laser Assisted Micro Milling (LAMM) Processing Characteristic Titanium Alloy (Ti6Al4V) using TiAlN coated carbide micro ball mill”. In: *Proceedings of the international conference on micro-manufacturing.* 31. 2014.

[143] Douglas C. Montgomery. *Design and Analysis of Experiments.* 8th. John Wiley & Sons, 2013.

[144] R.H. Myers, D.C. Montgomery, and C.M. Anderson-Cook. *Response Surface Methodology: Process and Product Optimization Using Designed Experiments.* Wiley Series in Probability and Statistics. John Wiley & Sons, 2016.

[145] Jung Soo Nam, Pil Ho Lee, and Sang Won Lee. “Experimental characterization of micro-drilling process using nanofluid minimum quantity lubrication”. In: *International Journal of Machine Tools and Manufacture* 51.7-8 (2011), pp. 649–652.

[146] Nanotech. “Nanotech 350UPM”. In: *Available from: http://www.nanotechsys.com/* (2017).

[147] Chandra Nath et al. “Design and evaluation of an atomization-based cutting fluid spray system in turning of titanium alloy”. In: *Journal of Manufacturing Processes* 14.4 (2012), pp. 452–459.

[148] S. Nemat-Nasser, W.G. Guo, and J.Y. Cheng. “Mechanical properties and deformation mechanisms of a commercially pure titanium”. In: *Acta Materialia* 47.13 (1999), pp. 3705 –3720.

[149] Piotr Nieslony and Wit Grzesik. “Sensitivity Analysis of the Constitutive Models in Fem-Based Simulation of the Cutting Process”. In: *Journal of Machine Engineering* 13.1 (2013), pp. 106–116.

[150] Stina Odelros. “Tool wear in titanium machining”. MA thesis. Uppsala University, 2012, p. 63.

[151] Samad Nadimi Bavil Oliaei and Yiğit Karpat. “Influence of tool wear on machining forces and tool deflections during micro milling”. In: *The International Journal of Advanced Manufacturing Technology* 84.9 (2016), pp. 1963–1980.

[152] Fábio De Oliveira et al. “Study of the cutting forces on micromilling of an aluminum alloy”. In: *Journal of the Brazilian Society of Mechanical Sciences and Engineering* (2016), pp. 1–8.

[153] Fernando Brandão de Oliveira et al. “Size effect and minimum chip thickness in micromilling”. In: *International Journal of Machine Tools and Manufacture* 89 (2015), pp. 39 –54.

[154] Tiaan Oosthuizen et al. “The effect of cutting parameters on surface integrity in milling Ti6Al4V”. In: *South African Journal of Industrial Engineering* 27.4 (2016), pp. 115–123.

[155] Tahsin Tecelli Öpöz and Xun Chen. “Chip Formation Mechanism Using Finite Element Simulation”. In: *Strojniški vestnik - Journal of Mechanical Engineering* 62.11 (2016), pp. 636–646.

[156] Yenny Marcela Orozco O, Jovanny Alejandro Pacheco B., and Jorge Bris C. “Microfresado de polímeros biocompatibles”. es. In: *Ingeniería y Desarrollo* 30 (June 2012), pp. 61 –78.

[157] Tugrul Özel. “The influence of friction models on finite element simulations of machining”. In: *International Journal of Machine Tools and Manufacture* 46.5 (2006), pp. 518 –530.

[158] Tuğrul Özel, Alaa Olleak, and Thanongsak Thepsonthi. “Micro milling of titanium alloy Ti-6Al-4V: 3-D finite element modeling for prediction of chip flow and burr formation”. In: *Production Engineering* 11.4-5 (2017), pp. 435–444.

[159] Petar Piljek, Zdenka Keran, and Miljenko Math. “Micromachining–Review of Literature from 1980 to 2010”. In: *Interdisciplinary description of complex systems* 12.1 (2014), pp. 1–27.

[160] Josep Planell and F.J. Gil. “Aplicaciones biomédicas del titanio v sus aleaciones”. In: *Biomecánica* 1.1 (1993), pp. 34–42.

[161] K B Popov et al. “Micromilling: Material microstructure effects”. In: *Proceedings of the Institution of Mechanical Engineers, Part B: Journal of Engineering Manufacture* 220.11 (2006), pp. 1807–1813.

[162] Tej Pratap, Karali Patra, and A.A. Dyakonov. “Modeling Cutting Force in Micro-Milling of Ti-6Al-4V Titanium Alloy”. In: *Procedia Engineering* 129 (2015), pp. 134 –139.

[163] H. Pérez et al. “Estimation of cutting forces in micromilling through the determination of specific cutting pressures”. In: *Journal of Materials Processing Technology* 190.1–3 (2007), pp. 18 –22.

[164] Y. Qin. *Micromanufacturing Engineering and Technology*. Micro and Nano Technologies. Elsevier Science, 2015.

[165] Foad Rahimidehgolan et al. “Determination of the Constants of GTN Damage Model Using Experiment, Polynomial Regression and Kriging Methods”. In: *Applied Sciences* 7.11 (2017), p. 1179.

[166] R. Venkata Rao and V. D. Kalyankar. “Optimization of modern machining processes using advanced optimization techniques: A review”. In: *International Journal of Advanced Manufacturing Technology* 73.5-8 (2014), pp. 1159–1188.

[167] P. Rodríguez and J.E. Labarga. “A new model for the prediction of cutting forces in micro-end-milling operations”. In: *Journal of Materials Processing Technology* 213.2 (2013), pp. 261 –268.

[168] J.B. Saedon et al. “Prediction and Optimization of Tool Life in Micromilling AISI D2 (62 HRC) Hardened Steel”. In: *Procedia Engineering* 41 (2012), pp. 1674 – 1683.

[169] M. Saez-De-Buruaga et al. “A Coupled Eulerian Lagrangian Model to Predict Fundamental Process Variables and Wear Rate on Ferrite-pearlite Steels”. In: *Procedia CIRP* 58 (2017), pp. 251–256.

[170] R. Jalili Saffar et al. “Simulation of three-dimension cutting force and tool deflection in the end milling operation based on finite element method”. In: *Simulation Modelling Practice and Theory* 16.10 (2008). The Analysis of Complex Systems, pp. 1677 –1688.

[171] Kushendarsyah Saptaji and Sathyan Subbiah. “Burr Reduction of Micro-milled Microfluidic Channels Mould Using a Tapered Tool”. In: *Procedia Engineering* 184 (2017), pp. 137–144.

[172] Kushendarsyah Saptaji, Sathyan Subbiah, and Jaspreet Singh Dhupia. “Effect of side edge angle and effective rake angle on top burrs in micro-milling”. In: *Precision Engineering* 36.3 (2012), pp. 444–450.

[173] Partchapol Sartkulvanich, Taylan Altan, and Joerg Soehner. “Flow Stress Data for Finite Element Simulation in Metal Cutting: a Progress Report on Madams”. In: *Machining Science and Technology* 9.2 (2005), pp. 271–288.

[174] F Schäfer. “Grundlagen zur Lösung von Entgratproblemen”. In: *Entgrat-Technik, Entwicklungsstand und Problemlösungen, Reihe Kontakt und Studium, Oberfläche* 392 (1992), pp. 33–42.

[175] G.M. Schueler et al. “Burr Formation and Surface Characteristics in Micro-End Milling of Titanium Alloys”. In: *Burrs - Analysis, Control and Removal: Proceedings of the CIRP International Conference on Burrs, 2nd-3rd April, 2009, University of Kaiserslautern, Germany.* Ed. by Jan C. Aurich and David Dornfeld. Berlin, Heidelberg: Springer Berlin Heidelberg, 2010, pp. 129–138.

[176] D Serje, J Pacheco, and E Diez. “Avances recientes en sistemas de lubricación/refrigeración en procesos de mecanizado”. In: *XVII Congreso Chileno de Ingeniería Mecánica.* 2017.

[177] J. Y. Sheikh-Ahmad and J. A. Bailey. “A Constitutive Model for Commercially Pure Titanium”. In: *Journal of Engineering Materials and Technology* 117.2 (Apr. 1995), pp. 139–144.

[178] Z. Y. Shi and Z. Q. Liu. “Numerical Modeling of Minimum Uncut Chip Thickness for Micromachining With Different Rake Angle”. In: *ASME 2011 International Manufacturing Science and Engineering Conference.* 44311. ASME. 2011, pp. 403–407.

[179] Zhenyu Shi et al. “Determination of minimum uncut chip thickness during micro-end milling Inconel 718 with acoustic emission signals and FEM simulation”. In: *The International Journal of Advanced Manufacturing Technology* (2017).

[180] M. S. Shunmugam. “Machining Challenges: Macro to Micro Cutting”. In: *Journal of The Institution of Engineers (India): Series C* 97.2 (2016), pp. 223–241.

[181] Mohammad Sima and Tuğrul Özel. “Modified material constitutive models for serrated chip formation simulations and experimental validation in machining of titanium alloy Ti-6Al-4V”. In: *International Journal of Machine Tools and Manufacture* 50.11 (2010), pp. 943–960.

[182] Sodick. “Sodick AZ250L”. In: *Available from: http://www.sodick.com/* (2017).

[183] Seong Min Son, Han Seok Lim, and Jung Hwan Ahn. “Effects of the friction coefficient on the minimum cutting thickness in micro cutting”. In: *International Journal of Machine Tools and Manufacture* 45.4-5 (2005), pp. 529–535.

[184] S L Soo and D K Aspinwall. “Developments in modelling of metal cutting processes”. In: *Proceedings of the Institution of Mechanical Engineers, Part L: Journal of Materials: Design and Applications* 221.4 (2007), pp. 197–211.

[185] Fabian Spreng and Peter Eberhard. “Machining Process Simulations with Smoothed Particle Hydrodynamics”. In: *Procedia CIRP* 31 (2015), pp. 94 –99.

[186] G. H. Staab and A. Gilat. “A Direct Tension Split Hopkinson Bar for High Strain Rate Testing”. In: *Experimental Mechanics* 31.3 (1991), pp. 232–235.

[187] ASTM Standard. “B265-06. Standard Specification for Titanium and Titanium Alloy Strip, Sheet, and Plate”. In: *ASTM International, West Conshohocken, PA* (2006).

[188] Xizhi Sun et al. “Multiscale simulation on nanometric cutting of single crystal copper”. In: *Proceedings of the Institution of Mechanical Engineers, Part B: Journal of Engineering Manufacture* 220.7 (2006), pp. 1217–1222.

[189] M Takács, B Verö, and I Mészáros. “Micromilling of metallic materials”. In: *Journal of Materials Processing Technology* 138.1–3 (2003). {IMCC2000}, pp. 152 – 155.

[190] Thanongsak Thepsonthi and Tugrul Ozel. “Experimental and finite element simulation based investigations on micro-milling Ti-6Al-4V titanium alloy: Effects of cBN coating on tool wear”. In: *Journal of Materials Processing Technology* 213.4 (2013), pp. 532–542.

[191] Thanongsak Thepsonthi and Tugrul Özel. “Multi-objective process optimization for micro-end milling of Ti-6Al-4V titanium alloy”. In: *International Journal of Advanced Manufacturing Technology* 63.9-12 (2012), pp. 903–914.

[192] Thanongsak Thepsonthi and Tuğrul Özel. “3-D finite element process simulation of micro-end milling Ti-6Al-4V titanium alloy: Experimental validations on chip flow and tool wear”. In: *Journal of Materials Processing Technology* 221 (2015), pp. 128 –145.

[193] Timet. *Timetal 50A: Commercially pure titanium.* 2000.

[194] L. C. Tsao et al. “Flow stress behavior of commercial pure titanium sheet during warm tensile deformation”. In: *Materials and Design* 34 (2012), pp. 179–184.

[195] İrfan Ucun, Kubilay Aslantas, and Fevzi Bedir. “Finite element modeling of micro-milling: Numerical simulation and experimental validation”. In: *Machining Science and Technology* 20.1 (2016), pp. 148–172.

[196] Deepak Rajendra Unune and Harlal Singh Mali. “Current status and applications of hybrid micro-machining processes: A review”. In: *Proceedings of the Institution of Mechanical Engineers, Part B: Journal of Engineering Manufacture* 229.10 (2015), pp. 1681–1693.

[197] L Uriarte et al. “Mechanistic modelling of the micro end milling operation”. In: *Proceedings of the Institution of Mechanical Engineers, Part B: Journal of Engineering Manufacture* 222.1 (2008), pp. 23–33.

[198] LG Uriarte et al. “Balance de incertidumbre y evaluación de la cadena de rigidez de una microfresadora dotada de herramientas de diámetro inferior a 0, 3 mm”. In: *Revista Iberoamericana de Ingeniería Mecánica* 11.1 (2007), pp. 13–36.

[199] Vijay Venkatesh et al. “Review on the machining characteristics and research prospects of conventional microscale machining operations”. In: *Materials and Manufacturing Processes* 32.3 (2017), pp. 235–262.

[200] Michael P. Vogler, Richard E. DeVor, and Shiv G. Kapoor. “Microstructure-Level Force Prediction Model for Micro-milling of Multi-Phase Materials”. In: *Journal of Manufacturing Science and Engineering* 125.2 (Apr. 2003), pp. 202–209.

[201] Michael P. Vogler, Richard E. DeVor, and Shiv G. Kapoor. “On the Modeling and Analysis of Machining Performance in Micro-Endmilling, Part I: Surface Generation”. In: *Journal of Manufacturing Science and Engineering* 126.4 (Feb. 2005), pp. 685–694.

[202] Michael P. Vogler, Shiv G. Kapoor, and Richard E. DeVor. “On the Modeling and Analysis of Machining Performance in Micro-Endmilling, Part II: Cutting Force Prediction”. In: *Journal of Manufacturing Science and Engineering* 126.4 (Feb. 2005), pp. 695–705.

[203] Jinsheng Wang et al. “Chip formation analysis in micromilling operation”. In: *International Journal of Advanced Manufacturing Technology* 45.5-6 (2009), pp. 430–447.

[204] K. Weinert et al. “Dry Machining and Minimum Quantity Lubrication”. In: *CIRP Annals - Manufacturing Technology* 53.2 (2004), pp. 511–537.

[205] H. Weule, V. Hüntrup, and H. Tritschler. “Micro-Cutting of Steel to Meet New Requirements in Miniaturization”. In: *CIRP Annals - Manufacturing Technology* 50.1 (2001), pp. 61 –64.

[206] WHO. “Visual impairment and blindness”. In: *Available from: http://www.who.int/* (2014).

[207] Jong Woo Won et al. “Integrated constitutive model for flow behavior of pure Titanium considering interstitial solute concentration”. In: *Metals and Materials International* 20.6 (2014), pp. 1017–1025.

[208] Xian Wu, Liang Li, and Ning He. "Investigation on the burr formation mechanism in micro cutting". In: *Precision Engineering* 47 (2017), pp. 191–196.

[209] Yao Xi et al. "SPH/FE modeling of cutting force and chip formation during thermally assisted machining of Ti6Al4V alloy". In: *Computational Materials Science* 84 (2014), pp. 188 –197.

[210] Amrendra K. Yadav et al. "{FE} modeling of burr size in high- speed micro-milling of Ti6Al4V". In: *Precision Engineering* 49 (2017), pp. 287 –292.

[211] M Yaich et al. "Numerical analysis of constitutive coefficients effects on FE simulation of the 2D orthogonal cutting process : application to the Ti6Al4V". In: *The International Journal of Advanced Manufacturing Technology* mm (2016).

[212] Jie Yi et al. "Surface roughness models and their experimental validation in micro milling of 6061-T6 al alloy by response surface methodology". In: *Mathematical Problems in Engineering* 2015 (2015).

[213] Z. J. Yuan, M. Zhou, and S. Dong. "Effect of diamond tool sharpness on minimum cutting thickness and cutting surface integrity in ultraprecision machining". In: *Journal of Materials Processing Technology* 62.4 (1996), pp. 327–330.

[214] G Yucesan. "An Analytic Mechanistic Cutting Force Model for Milling Operations : A Theory and Methodology". In: *Journal of Engineering for Industry* 116.August 1994 (1994), pp. 324–330.

[215] Jinyuan Zhai et al. "Modeling the ductile damage process in commercially pure titanium". In: *International Journal of Solids and Structures* 91 (2016), pp. 26–45.

[216] Tao Zhang, Zhanqiang Liu, and Chonghai Xu. "Theoretical modeling and experimental validation of specific cutting force for micro end milling". In: *The International Journal of Advanced Manufacturing Technology* 77.5 (2015), pp. 1433–1441.

[217] Xuewei Zhang, Tianbiao Yu, and Wanshan Wang. "Instantaneous uncut chip thickness modeling for micro-end milling process". In: *Machining Science and Technology* 0.0 (2017), pp. 1–21.

[218] Xuewei Zhang et al. "Cutting forces in micro-end-milling processes". In: *International Journal of Machine Tools and Manufacture* 107 (2016), pp. 21 –40.

[219] Yancheng Zhang, J C Outeiro, and Tarek Mabrouki. "On the selection of Johnson-Cook constitutive model parameters for Ti-6Al-4V using three types of numerical models of orthogonal cutting". In: *Procedia CIRP* 31 (2015), pp. 112–117.

[220] Y.C. Zhang et al. "Chip formation in orthogonal cutting considering interface limiting shear stress and damage evolution based on fracture energy approach". In: *Finite Elements in Analysis and Design* 47.7 (2011), pp. 850 –863.

[221] Xiaohu Zheng et al. "Experimental study on micro-milling of Ti6Al4V with minimum quantity lubrication". In: *International Journal of Nanomanufacturing* 9.5-6 (2013), pp. 570–582.

[222] Lin Zhou et al. “Prediction and Experimental Validation of Micro End-Milling Forces with Finite Element Method”. In: *Intelligent Robotics and Applications: 8th International Conference, ICIRA 2015, Portsmouth, UK, August 24-27, 2015, Proceedings, Part II*. Ed. by Honghai Liu et al. Cham: Springer International Publishing, 2015, pp. 664–675.

[223] NN Zorev. “Inter-relationship between shear processes occurring along tool face and shear plane in metal cutting”. In: *International research in production engineering* 49 (1963), pp. 42–49.